

U-PB AND LU-HF LA-ICP-MS DETRITAL ZIRCON AND STRUCTURAL INVESTIGATIONS
IN THE ABITIBI SUBPROVINCE, CANADA, WITH IMPLICATIONS FOR ARCHEAN
GEODYNAMIC PROCESSES AND DEFORMATION BEHAVIOR ALONG
GOLD-BEARING, CRUSTAL-SCALE FAULTS

By

Ben M. Frieman

A thesis submitted to the Faculty and Board of Trustees of the Colorado School of Mines
in partial fulfillment of the requirements for the degree of Doctor of Philosophy (Geology).

Golden, Colorado

Date: _____

Signed: _____

Ben M. Frieman

Signed: _____

Dr. Yvette D. Kuiper
Thesis Advisor

Golden, Colorado

Date: _____

Signed: _____

Dr. M. Stephen Enders
Head of Department
Department of Geology and Geological Engineering

ABSTRACT

This work presents investigations based in the south-central Abitibi subprovince of Ontario and Quebec, Canada, which place constraints on a sequence of Neoproterozoic geodynamic and structural processes, including crustal growth and amalgamation with the rest of the Superior Province, and the formation of orogenic gold deposits along regional deformation zones. Neoproterozoic geodynamic processes were primarily investigated by multi-isotope U-Pb and Lu-Hf laser ablation – inductively coupled plasma – mass spectrometry (LA-ICP-MS) analysis of detrital zircon grains from successor basins. Three temporally distinct successor basin groups are recognized: the ~2690-2685 Ma Porcupine assemblage, the ~2685-2682 Ma Pontiac subprovince, and the ~2680-2670 Ma Timiskaming assemblage. All samples contain abundant Neoproterozoic grains (~85-95% of the individual sample populations), while the remaining grains yielded Mesoproterozoic ages. The Neoproterozoic grains likely reflect predominately local sources. Since no Mesoproterozoic rocks occur in the Abitibi and Pontiac subprovinces, and based on comparison with published zircon ages from the Superior Province, Mesoproterozoic grains are interpreted as derived from an orogenic hinterland to the NNW that developed during regional amalgamation. The older Porcupine assemblage contains ~5% Mesoproterozoic zircon, while Pontiac subprovince and Timiskaming assemblage samples contain ~18% and ~13%, respectively. This suggests hinterland sources were more prevalent during the late stages of collision, probably as a result of progressive uplift and denudation of the hinterland. The paired Lu-Hf isotopic analyses support this interpretation of provenance and further indicate that the majority of grains (~96%) have compositions consistent with derivation from a modern MORB depleted mantle (mMORB-DM) reservoir. This occurrence of mMORB-DM-like signatures in detrital zircon grains that were sourced from multiple disparate crustal domains suggests that a modern-style depleted mantle reservoir was not only well established, but widely occurring by the Mesoproterozoic. The observed pattern of lateral accretion of crustal domains that grew from a mMORB-DM-like reservoir, the transport of detritus across terrane boundaries, and the progressive uplift and denudation of a hinterland are most consistent with the operation of plate tectonic processes during Neoproterozoic construction and amalgamation of the southern Superior Province. During the late stages of accretion, deformation became increasingly localized along regionally extensive, crustal-scale fault zones, including the Larder Lake Cadillac deformation zone (LLCdz) in the Kirkland Lake area of Ontario. New field mapping and map compilation indicates that a series of spaced brittle-ductile deformation zones occur in a broad, >6 km area to the north of the LLCdz. Detailed structural mapping and analysis further indicate that the location of late-stage brittle-ductile deformation, fluid flow, and

gold mineralization was likely controlled by early brittle deformation zones characterized by breccia. Therefore, undiscovered gold deposits may be hosted by deformation zones farther from the LLCdz than previously recognized and that fault-related breccia bodies may provide an indicator for nearby prospective structures in both the Kirkland Lake area and in similar structural settings of all ages, worldwide.

TABLE OF CONTENTS

ABSTRACT	iii
LIST OF FIGURES	x
LIST OF TABLES	xiii
ACKNOWLEDGEMENTS	xiv
CHAPTER 1 INTRODUCTION	1
1.1 The Abitibi subprovince	1
1.2 Thesis goals	5
1.3 Thesis organization	6
1.4 References	7
CHAPTER 2 CONSTRAINTS ON THE GEODYNAMIC EVOLUTION OF THE SOUTHERN SUPERIOR PROVINCE: U-PB LA-ICP-MS ANALYSIS OF DETRITAL ZIRCON IN SUCCESSOR BASINS OF THE ARCHEAN ABITIBI AND PONTIAC SUBPROVINCES OF ONTARIO AND QUEBEC, CANADA	10
2.1 Introduction	11
2.2 Geological background	14
2.2.1 Neoproterozoic assembly in the Superior Province	14
2.2.2 Geology of the Abitibi and Pontiac subprovinces	15
2.3 Methods	18
2.3.1 Sampling strategy	18
2.3.2 Sample preparation	18
2.3.3 U-Pb isotope data collection, reduction, and analytical methods	19
2.3.4 Compilation of U-Pb zircon data	21
2.4 Sample descriptions and U-Pb zircon LA-ICP-MS results	21
2.4.1 Porcupine assemblage samples	22
2.4.1.1 Sample P-1	22
2.4.1.2 Sample P-2	23
2.4.1.3 Sample P-3	25
2.4.1.4 Sample P-4	25

2.4.1.5	Sample P-5	25
2.4.1.6	Sample P-6	26
2.4.2	Pontiac subprovince samples	26
2.4.2.1	Sample PS-1	26
2.4.2.2	Sample PS-2	27
2.4.3	Timiskaming assemblage samples	27
2.4.3.1	Sample T-1	27
2.4.3.2	Sample T-2	28
2.4.3.3	Sample T-3	29
2.4.3.4	Sample T-4	29
2.4.3.5	Sample T-5	29
2.4.3.6	Sample T-6	30
2.4.3.7	Sample T-7	30
2.4.3.8	Sample T-8	31
2.5	Compiled regional U-Pb zircon data	31
2.5.1	Abitibi and Pontiac subprovinces	32
2.5.1.1	Igneous zircon data	32
2.5.1.2	Detrital zircon data	32
2.5.1.3	Inherited zircon data	34
2.5.2	southern Superior Province	34
2.5.2.1	The Wawa subprovince	34
2.5.2.2	The Moyen-Nord region	36
2.5.2.3	The Quetico subprovince	36
2.5.2.4	The Western Wabigoon, Winnipeg River, and Marmion subprovinces	37

2.6	Summary of detrital zircon age distributions for graywacke samples of the Abitibi and Pontiac subprovinces	37
2.7	Provenance and significance	38
2.8	Conclusions	44
2.9	Acknowledgements	45
2.10	References	45
CHAPTER 3	INSIGHT INTO ARCHEAN CRUSTAL GROWTH PROCESSES AND CRUST-MANTLE EVOLUTION FROM MULTI-ISOTOPE, U-PB AND LU-HF LA-ICP-MS ANALYSIS OF DETRITAL ZIRCON GRAINS FROM SUCCESSOR BASINS OF THE ABITIBI AND PONTIAC SUBPROVINCES, CANADA	55
3.1	Introduction	56
3.2	Regional geological framework	59
3.2.1	Eo- to Mesoproterozoic rocks of the Superior Province	59
3.2.2	Juvenile Neoproterozoic rocks of the Superior Province	61
3.2.3	Successor basin deposits in the Superior Province	62
3.2.4	Geology of the Abitibi and Pontiac subprovinces	62
3.2.4.1	Neoproterozoic volcanic-plutonic successions	63
3.2.4.2	Successor basins of the southern Abitibi and Pontiac subprovince	65
3.3	Methods	66
3.3.1	Sampling strategy, processing, and grain characteristics	66
3.3.2	U-Pb and Lu-Hf analytical techniques	66
3.4	U-Pb and Lu-Hf isotopic results	69
3.5	Lu-Hf data trends and regional correlations	72
3.6	Significance of Lu-Hf results to the record of crust-mantle reservoirs in the Superior Province	78
3.7	Significance of Lu-Hf results to Proterozoic geodynamic processes	79
3.8	Conclusions	82
3.9	Acknowledgements	83
3.10	References	83
CHAPTER 4	ACROSS-STRIKE ARCHITECTURE OF HIGH- AND LOW-STRAIN ZONES NORTH OF THE LARDER LAKE-CADILLAC DEFORMATION ZONE IN THE KIRKLAND LAKE AREA, ONTARIO, CANADA	95

4.1	Introduction	95
4.2	Geologic setting	99
4.3	Structural setting	103
4.4	Across-strike structure north of the LLCdz in Kirkland Lake, Ontario	104
4.5	Discussion	112
4.6	Implications	115
4.7	References	116
CHAPTER 5	INSIGHT INTO THE FORMATION AND EVOLUTION OF GOLD-BEARING SPREADS OF CRUSTAL-SCALE FAULT ZONES: A CASE STUDY OF THE KIRANA DEFORMATION ZONE IN THE KIRKLAND LAKE AREA OF ONTARIO, CANADA	121
5.1	Introduction	122
5.2	Geologic setting	124
5.3	Fault-associated brecciation and vein forming processes	129
5.4	Analysis of fault products by particle size distributions	130
5.5	Methods	132
	5.5.1 Field mapping	133
	5.5.2 Microstructural and petrographic characterization	133
	5.5.3 Particle size distribution theory and application	133
	5.5.4 Kinematic analysis of small-scale faults and shear veins	135
5.6	Results of km- to outcrop-scale mapping	135
	5.6.1 The Kirana East outcrop	139
5.7	Petrographic and microstructural observations	143
	5.7.1 Microstructural characteristics of breccia samples	143
	5.7.2 Kirana East (ultra)mylonite samples	147
	5.7.3 Foliated intrusive rocks	147
5.8	Particle size distributions of Kirana East breccia samples	147
5.9	Results of small-scale faults and shear vein analysis	149
5.10	Discussion and structural synthesis	149
	5.10.1 Early fault behavior and breccia-forming processes	149
	5.10.2 Early fault veins and intrusion of porphyritic rocks	152
	5.10.3 Ductile shear localization	154
	5.10.4 Renewed brittle deformation	155
	5.10.5 Timing of gold mineralization	156
5.11	Implications	156

5.12	References	157
CHAPTER 6	GENERAL CONCLUSIONS	164
6.1	Investigations into the U-Pb LA-ICP-MS age patterns of detrital zircon grains from graywacke of successor basins (Chapter 2)	164
6.2	Multi-isotope U-Pb and Lu-Hf LA-ICP-MS analysis of detrital zircon from successor basins of the Abitibi and Pontiac subprovinces (Chapter 3)	165
6.3	Across-strike architecture of the Larder Lake-Cadillac deformation zone in the Kirkland Lake area of Ontario (Chapter 4)	165
6.4	The Kirana deformation zone (Chapter 5)	166
6.5	References	167
APPENDIX A:	ADDITIONAL FIELD MAPS AND OBSERVATIONS	169
A.1	References	175
APPENDIX B:	SUPPLEMENTAL ELECTRONIC FILES	176
B.1	References	176

LIST OF FIGURES

Figure 1.1	Map of the Superior Province	2
Figure 1.2	Geological map of the south-central Abitibi subprovince	3
Figure 1.3	Schematic stratigraphic section for the south-central Abitibi subprovince	4
Figure 2.1	Geological map of the Superior Province	12
Figure 2.2	Map of the Abitibi and Pontiac subprovinces	13
Figure 2.3	Representative zircon images	20
Figure 2.4	Sample-by-sample U-Pb date results	24
Figure 2.5	Field photographs of representative sample localities	28
Figure 2.6	Compiled U-Pb zircon age data from the Abitibi and Pontiac subprovinces	33
Figure 2.7	Individual, pre-2750 Ma detrital zircon ages from published data	33
Figure 2.8	Compilation of published zircon age data for the southern Superior Province	35
Figure 2.9	Comparison of detrital zircon age data from this study to published zircon age data	39
Figure 2.10	Spatial comparison of detrital zircon age results	42
Figure 2.11	Schematic time-space diagram for the southern Superior Province	43
Figure 3.1	Geologic map of the Superior Province	58
Figure 3.2	Time-space diagram for the Superior Province	60
Figure 3.3	Map of the Abitibi and Pontiac subprovinces	64
Figure 3.4	Representative zircon images	68
Figure 3.5	Plots displaying U-Pb and Lu-Hf zircon data	70
Figure 3.6	Comparison of detrital zircon ages from this study to published zircon ages	71
Figure 3.7	Schematic diagram illustrating potential processes driving the dominant Lu-Hf data distributions presented in this study	75
Figure 3.8	U-Th-Pb assessment for the detrital zircon analyses in this study	77

Figure 4.1	Schematic illustrations of orogenic gold-bearing fault systems	96
Figure 4.2	Geological map of the south-central Abitibi subprovince	98
Figure 4.3	Simplified geological map of the Kirkland Lake study area	100
Figure 4.4	Geological map of the Kirkland Lake study area	102
Figure 4.5	Field photographs of D ₃ shear zones	105
Figure 4.6	Field photographs of primary igneous and sedimentary structures preserved in low-strain domains	106
Figure 4.7	Field photographs of the Larder Lake-Cadillac deformation zone exposed in the south of the Kirkland Lake map area	107
Figure 4.8	Structural orientation data for the Kirkland Lake area	108
Figure 4.9	Simplified map of the Kirkland Lake study area displaying the distribution of mapped faults, interpreted high-strain zones, and gold-bearing veins	110
Figure 4.10	Comparison of S ₃ /L ₃ structural data from high- and low-strain domains	113
Figure 4.11	Schematic diagram illustrating the inferred pattern of strain in the Kirkland Lake area	114
Figure 4.12	Schematic conceptual diagrams illustrating the across-strike architectural evolution of the Larder Lake-Cadillac deformation zone (LLCdz) in Kirkland Lake	116
Figure 5.1	Schematic illustrations of orogenic gold-bearing fault systems	123
Figure 5.2	Geological map of the south-central Abitibi subprovince	124
Figure 5.3	Simplified geological map of the Kirkland Lake study area	125
Figure 5.4	Geologic map of the Kirana deformation zone with new structural data	127
Figure 5.5	Schematic illustrations of the relationship between fault breccia and particle size distribution	131
Figure 5.6	Outline drawings of the breccia samples from the Kirana East outcrop area used for particle size distribution analysis	134
Figure 5.7	Schematic diagram illustrating movement plane kinematic analysis	136
Figure 5.8	S ₃ /L ₃ structural orientation data	136

Figure 5.9	Field photos of ductile structures observed along the Kirana deformation zone	137
Figure 5.10	Field photos of brittle deformation textures observed along the Kirana deformation zone	138
Figure 5.11	Field photos of quartz vein morphologies commonly observed along the Kirana deformation zone	139
Figure 5.12	Detailed geological map of the Kirana East outcrop	140
Figure 5.13	Photomicrographs of samples from the Kirana deformation zone	142
Figure 5.14	Mineralogical characteristics of sample KL-12	144
Figure 5.15	Microstructural characteristics of sample KL-26	145
Figure 5.16	Mineralogical and microstructural characteristics of sample KL-17	146
Figure 5.17	Results of the particle size distribution analysis	148
Figure 5.18	Orientation data and kinematic analysis of small-scale faults and shear veins	150
Figure 5.19	Schematic illustration of the relationship between the observed breccia textures and the fault core and associated damage zone of the Kirana deformation zone during progressive displacement through time (t_1 to t_2) and subsequent ductile localization (t_3)	153
Figure A.1	Geological map of the western Kirkland Lake area, Ontario	169
Figure A.2	Geological map of the Blake River assemblage – Timiskaming assemblage Timiskaming unconformity at Perron Lake	170
Figure A.3	Distribution of outcrops associated with the Blake River assemblage – Timiskaming assemblage unconformity in the north of Kirkland Lake	171
Figure A.4	Results of the outcrop-scale mapping conducted at the Blake River assemblage – Timiskaming assemblage in the north of Kirkland Lake	172
Figure A.5	Field photos of the Blake River assemblage – Timiskaming assemblage unconformity in the north of Kirkland Lake.	173
Figure A.6	Modal mineralogy of Kirana East breccia samples	174

LIST OF TABLES

Table 2.1 List of Porcupine assemblage, Pontiac subprovince, and Timiskaming assemblage samples for detrital zircon U-Pb LA-ICP-MS analysis. 23

Table 3.1 List of detrital zircon graywacke samples from successor basins of the Abitibi and Pontiac subprovinces investigated by U-Pb and Lu-Hf LA-ICP-MS analysis in this study 67

ACKNOWLEDGEMENTS

First and foremost, I would like to thank Dr. Yvette Kuiper. I couldn't have completed this thesis without her constant encouragement, enthusiasm, and faith in me. I appreciate her patience and how much she genuinely cares about me and my future career, wherever that may take me. She has taught me how to be a better scientist through her rigorous application of the scientific method. It has been an honor to be one of her first doctoral students.

To Dr. Thomas Monecke I will be forever indebted. I thank him for introducing me to the wonders of the Abitibi, for teaching me DCIP, and for instructing me on the ways of field work in Ontario and Quebec. He was always willing to discuss my project and provided me with support whether I asked for it or not. I would also like to thank Dr. Nigel Kelly. Nigel's insightful advice on writing, research, and life will stick with me forever. I would also like to thank Dr. Brandon Dugan for being a willing and able committee chair. I am grateful to Dr. Andrew Kylander-Clark for his dedicated work collecting thousands of LA-ICP-MS analyses, which was indispensable.

The detrital zircon isotope analyses were funded by Osisko Mining. A special thanks to Bob Wares for his support of this project and his unending exuberance for scientific understanding of the Abitibi. A special thanks to Glencore and Goldcorp for allowing access to the Hoyle Pond and Kidd Creek mines for sample collection. Further thanks goes to Eric Barr and Tom Gemmell for their on-site assistance. I would also like to thank the Society of Economic Geologist Canada Foundation and the Geological Society of America for research grants that helped make the field work possible.

Thanks to Dr. Martin Guitreau for his advice on the Lu-Hf isotopic data. Thanks to Drs. Christie Rowe and Ben Melosh for their help with PSDs and the understanding of fault processes. Thanks to Howard Poulsen for showing me around the Abitibi, even when I wasn't invited. Thanks to Dave Guindon at the Ontario Geological Survey for his help with legacy data in Kirkland Lake. Thanks to Drs. Katharina Pfaff and Heather Lowers for help with SEM imaging. Thanks to Dr. Patrick Mercier-Langevin for his help publishing with the Geological Survey of Canada and for being an invaluable resource on the Abitibi. Thanks to my many colleagues at the Colorado School of Mines such as proto-Drs. Wes Buchanan, Halley Keevil, and Alli Severson to name a few. A special thanks to everyone at Joyride Brewing Company and the members of the #CAT trivia team, without you I would have gone crazy.

Last but not least, I would like to thank all of my family and friends whom have supported me through these many years of college, especially my beautiful, talented, and loving wife, Amy Frieman.

CHAPTER 1 INTRODUCTION

This chapter outlines the general framework of investigations conducted in the Neoproterozoic south-central Abitibi subprovince of Ontario and Quebec, Canada. First, a brief overview of the geological framework is provided. Then, the general research goals are outlined, and finally the organizational structure of the thesis is discussed.

1.1 The Abitibi subprovince

The Abitibi subprovince of the southeastern Superior Province is the largest Neoproterozoic greenstone belt in the world. The belt straddles the Ontario-Quebec border and spans approximately 500 km from east to west and 350 km from north to south (Fig. 1.1). Ample glacially polished outcrop exposure and mine strippings, and the generally low metamorphic grade of the rocks have allowed for reconstruction of the primary igneous and sedimentary environments and the deformational history in great detail. The early history of the Abitibi subprovince consisted of primary volcanic construction in a submarine environment that largely occurred between ~2750 Ma and ~2695 Ma (Figs. 1.2 and 1.3; Ayer et al., 2002). Based on stratigraphic, geochemical, and geochronological data, six distinct composite volcanic assemblages are recognized (Fig. 1.2). The termination of submarine volcanism at ~2695 Ma marks the onset of regional deformation and initial collision of the Abitibi subprovince with domains to the north (Percival et al., 2012). Collision resulted in widespread shortening and coincided with the formation of primarily sedimentary successor basins. Based on structural, sedimentological, and geochronological constraints, two distinct successor basin types are distinguished: the ~2690-2685 Ma, turbidite-dominated Porcupine assemblage and the ~2679-2669 Ma, coarse, clastic dominated Timiskaming assemblage (Fig. 1.3; Ayer et al., 2002). Deformation continued through deposition of the successor basins and culminated in localized strain along regionally extensive deformation zones, in particular the >300 km long, crustal-scale Larder Lake-Cadillac and Porcupine-Destor deformation zones (Fig. 1.2).

The Abitibi subprovince is world-renowned for the abundance of economic ore deposits that it hosts. Numerous volcanogenic massive sulfide deposits occur in the belt (Fig. 1.2) that have a total endowment of over 800 million metric tonnes of polymetallic ore (Mercier-Langevin et al., 2011), are hosted by the volcanic assemblages, and formed during the early history of volcanic construction. The Abitibi subprovince also contains several world-class and many smaller, orogenic gold deposits (Fig. 1.2). These formed during the late stages of deformation during localization of strain and fluids along the major regional deformation zones. In total, orogenic gold deposits in the Abitibi subprovince contain over 6200 metric tonnes of gold

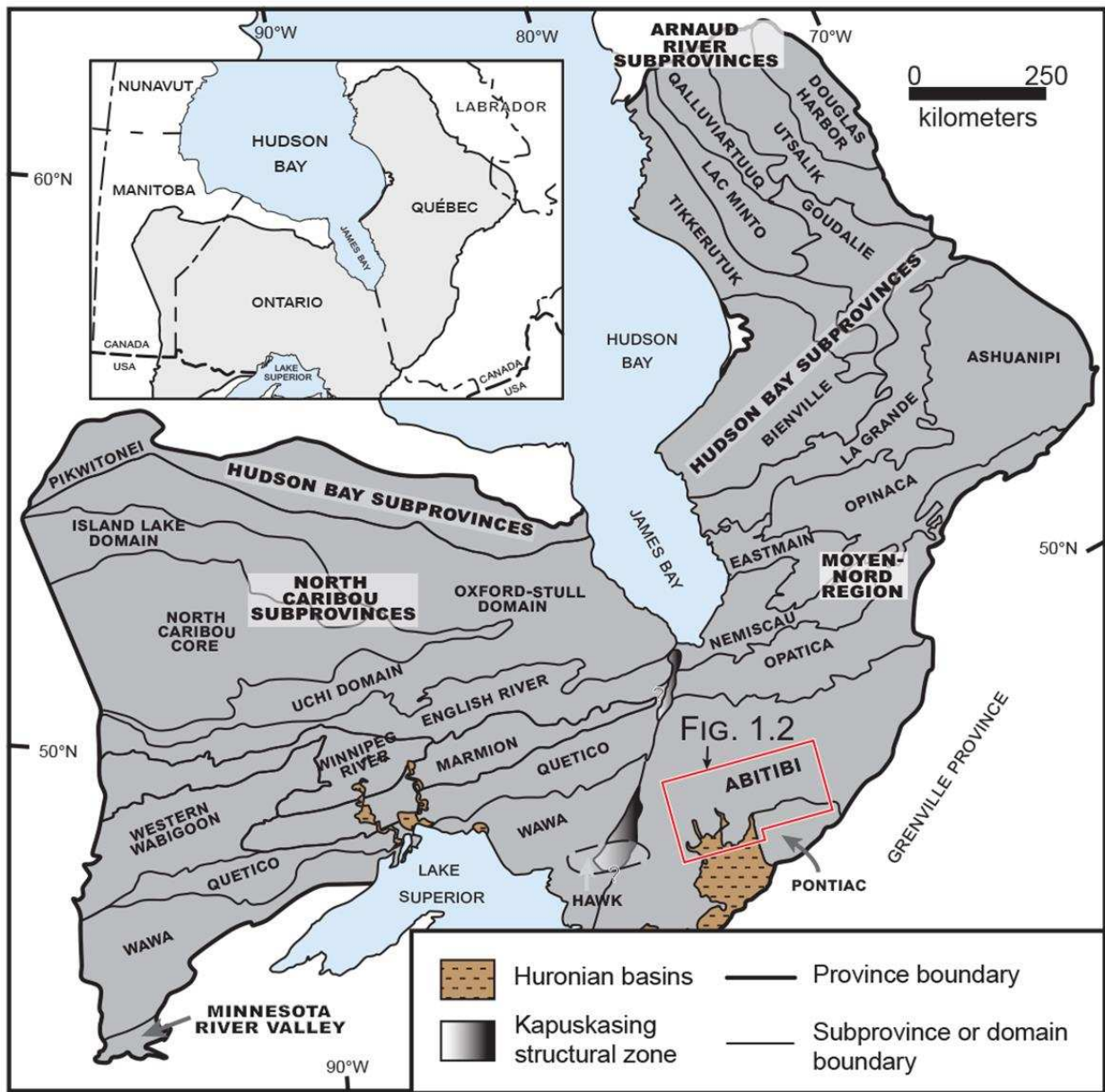


Figure 1.1 – Map of the subdivisions of the Superior Province. Modified from Stott et al. (2010).

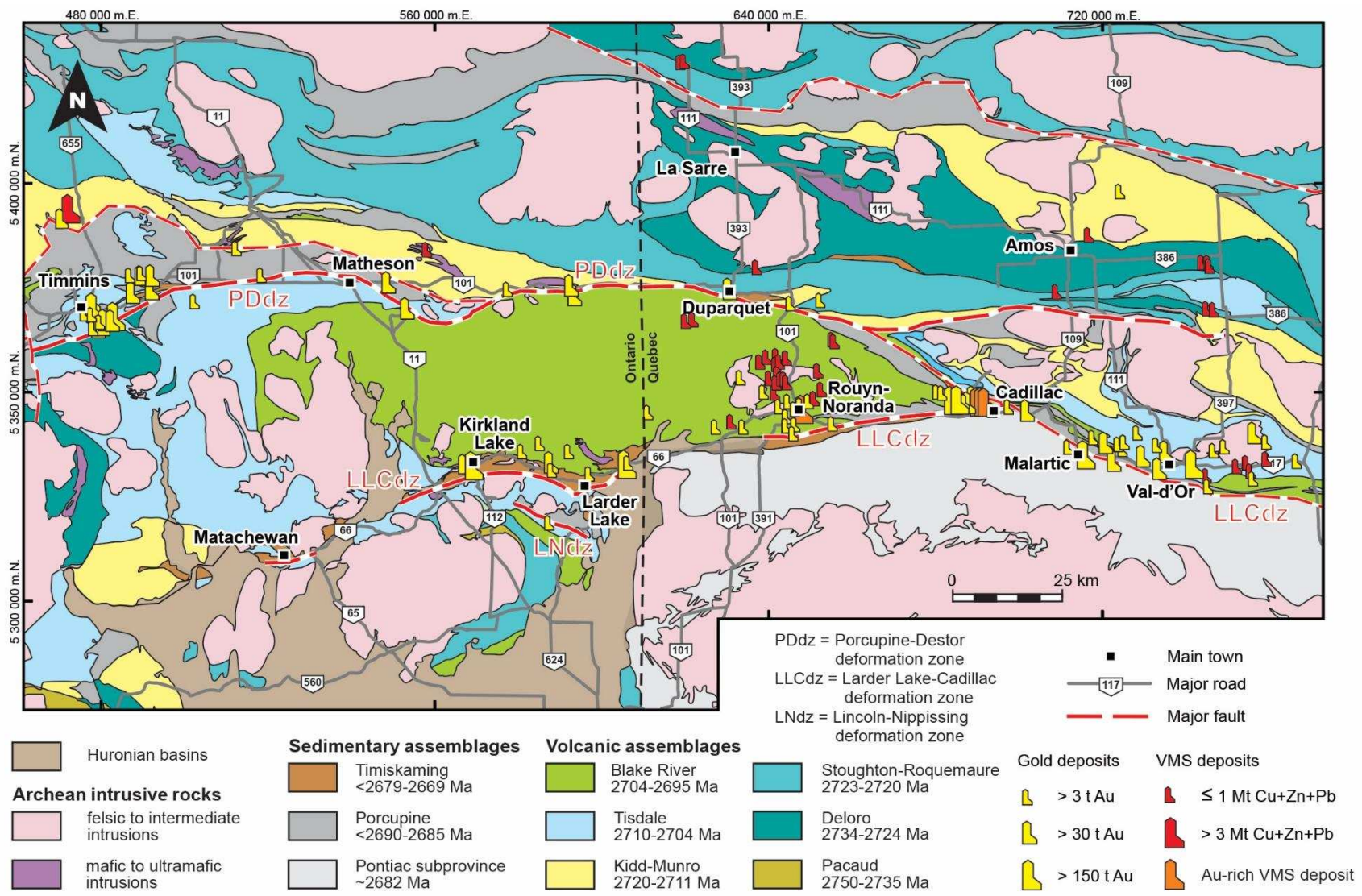


Figure 1.2 – Simplified geological map of the south-central Abitibi subprovince. Modified from Thurston et al. (2008) and Monecke et al. (2017).

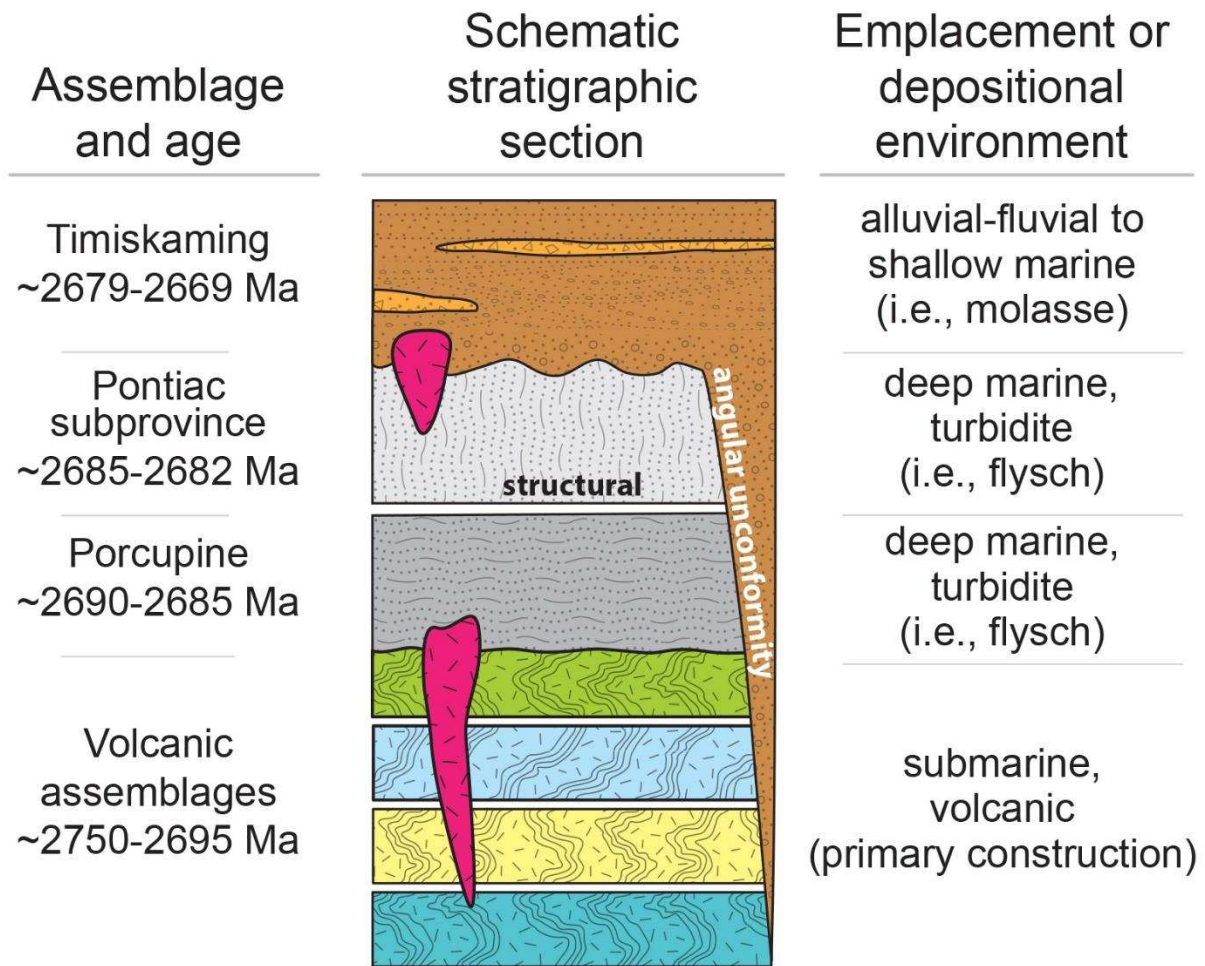


Figure 1.3 – Schematic stratigraphic section for the south-central Abitibi subprovince. Displays the relative stratigraphic position and the primary emplacement or depositional environment of volcanic greenstone assemblages and successor basin assemblages. The ages of assemblages are indicated based on U-Pb ID-TIMS zircon geochronology from Ayer et al. (2002) and Davis (2002).

(Monecke et al., 2017). Thus, the Abitibi subprovince represents one of the most economically significant terranes in the world.

Since the discovery of base and precious metal deposits over 100 years ago, the Abitibi subprovince has been the subject of hundreds of research papers, theses, private exploration, and geological surveys (see Monecke et al., 2017, for a more in-depth review). As a result, the Abitibi subprovince is exceptionally well mapped, there is abundant geochemical and geophysical data available, and the ages of lithologic units are well constrained by high-resolution U-Pb zircon geochronology. The evolution of the Abitibi subprovince (Fig. 1.3) is similar to that observed in other greenstone belts of the Superior Province and is typical of

Archean greenstone belts worldwide. This work was focused on the south-central portion of the Abitibi subprovince where these relationships are best constrained. As this brief review demonstrates, the Abitibi subprovince is an ideal location in which to investigate Archean geodynamic processes and the deformation behavior recorded in gold deposits that are associated with regional deformation zones.

1.2 Thesis goals

One of the primary goals of this thesis was to investigate Neoproterozoic geodynamic processes. Some workers have proposed that plate tectonic processes predominated (e.g., Percival et al., 2012), while others have proposed that non-plate tectonic scenarios can explain the observed lithotectonic progression (e.g., Bédard and Harris, 2014). Since the successor basins investigated were deposited coevally with regional amalgamations, they have the potential to preserve evidence that supports one interpretation or the other. While the primary age of successor basin deposits is well-constrained by high-resolution geochronology (Ayer et al., 2002; Davis, 2002), no single study has conducted a comparative statistical investigation of all the successor basin groups recognized in the south-central Abitibi subprovince. In this study, U-Pb and Lu-Hf laser ablation – inductively coupled plasma – mass spectrometry (LA-ICP-MS) analysis of detrital zircon grains was carried out on samples from the successor basins of the Abitibi and Pontiac subprovinces in order to accomplish the following:

- Statistically constrain the U-Pb age patterns of graywacke detrital zircon samples
- Compare the U-Pb age patterns between samples and among the successor basin groups to assess temporal and spatial variations
- Compare observed U-Pb and Lu-Hf isotopic signatures to published zircon age data to establish the provenance for the successor basins
- Compare the U-Pb and Lu-Hf isotopic signatures to evolution curves for the depleted mantle
- Utilize U-Pb and Lu-Hf isotopic signatures to investigate crustal growth processes in inferred source domains
- Explore how the patterns of provenance and crust-mantle growth signatures fit into the framework of regional amalgamations and related geodynamic models

The second major goal of this thesis was to investigate deformation processes along gold-bearing, regional deformation zones. During the late stages of amalgamation, localized deformation and fluid flow along regional crustal-scale deformation zones resulted in the formation of structurally controlled orogenic gold deposits. Understanding the deformation behavior along these zones is critical for interpreting the regional tectonic evolution as well as

for constraining the distribution of economically significant ore deposits and to predict prospective areas. These concepts were investigated along a segment of the Larder Lake-Cadillac deformation zone (LLCdz) in the Kirkland Lake area of Ontario (Fig. 1.2). The LLCdz is a major regional deformation zone that extends for 100s of km along strike, hosting over 100 Moz of orogenic gold deposits along its length (Fig. 1.2; Monecke et al., 2017). Mineralization was related to coupled deformation and fluid flow processes associated with mixed brittle-ductile deformation behavior (Groves et al., 1998; Cox et al., 2001). While gold deposits are hosted directly within the LLCdz, they also occur in distributed, higher-order structural networks that occur as far as 2-10 km from the primary fault zone (Robert 1994; Robert et al., 1995). The Kirkland Lake area was selected for detailed analysis, because it is known to host orogenic gold within higher-order structures (e.g., the world-class 30 Moz deposit in the Main Break; Ispolatov et al., 2008), the surface geology is well mapped (e.g., MacLean, 1944; Thomson, 1945), the regional structural framework is well established (Wilkinson et al., 1999; Lafrance, 2015; Ispolatov et al., 2008), the absolute age of lithologic units is well constrained by high-resolution U-Pb zircon geochronology (e.g., Corfu et al., 1991; Corfu, 1993; Ayer et al., 2002), and there is abundant and easily accessible outcrop exposure. Furthermore, although the structural history of the LLCdz and immediate splay is well described, little work has been done to synthesize the across-strike architecture in the Kirkland Lake area using modern structural concepts, even though these areas may be prospective for gold. The primary goals of the structural investigations along the LLCdz in the Kirkland Lake area were to:

- Compile and synthesize existing maps and structural data in the Kirkland Lake area
- Conduct new mapping to constrain the structural history and distribution of brittle-ductile structures
- Analyze and interpret the kinematics of brittle-ductile structures
- Relate patterns of alteration and gold occurrences to the structural history to investigate how localization of strain and potentially gold-bearing, hydrothermal fluids relate to brittle-ductile deformation processes

1.3 Dissertation organization

Following this introductory chapter, the thesis consists of five additional chapters. Chapter 2 is a manuscript that details the U-Pb LA-ICP-MS detrital zircon data and is already published in *Precambrian Research* (Frieman et al., 2017a). Chapter 3 is a manuscript that focuses on the multi-isotope U-Pb and Lu-Hf isotopic signatures and will be submitted to *Earth and Planetary Science Letters*. Chapter 4 discusses the across-strike architecture of the LLCdz in the Kirkland Lake area and represents a more in-depth discussion of a map and report that is

already published with the Geological Survey of Canada (Frieman et al., 2017c). Chapter 5 presents a detailed study of a higher-order, gold bearing splay of the LLCdz, the Kirana deformation zone, which will be submitted to the Journal of Structural Geology. Chapter 6 provides general conclusions to all work presented. A number of abstracts presenting various components of research related to this thesis are also included in Appendix B (Frieman et al., 2013, 2014a,b, 2015a,b, 2016,a,b,c, 2017b,d).

1.4 References

- Ayer, J., Amelin, Y., Corfu, F., Kamo, S., Ketchum, J., Kwok, K., Trowell, N., 2002. Evolution of the southern Abitibi greenstone belt based on U-Pb geochronology: Autochthonous volcanic construction followed by plutonism, regional deformation and sedimentation. *Precambrian Research* 115, 63–95.
- Bédard, J.H., Harris, L.B., 2014. Neoproterozoic disaggregation and reassembly of the Superior craton. *Geology* 42, 951–954. doi:10.1130/G35770.1
- Corfu, F., 1993. The evolution of the southern Abitibi greenstone belt in light of precise U-Pb geochronology. *Economic Geology* 88, 1323–1340.
- Corfu, F., Jackson, S.J., Sutcliffe, R.H., 1991. U-Pb ages and tectonic significance of Late Archean alkalic magmatism and nonmarine sedimentation, Timiskaming Group, southern Abitibi belt, Ontario. *Canadian Journal of Earth Sciences* 28, 489–503.
- Cox, S.F., Knackstedt, M.A., Braun, J., 2001. Principles of structural control on permeability and fluid flow in hydrothermal systems. *Reviews in Economic Geology* 14, 1–27.
- Davis, D.W., 2002. U-Pb geochronology of Archean metasedimentary rocks in the Pontiac and Abitibi subprovinces, Quebec, constraints on timing, provenance and regional tectonics. *Precambrian Research* 115, 97–117. doi:10.1016/S0301-9268(02)00007-4
- Frieman, B.M., Kuiper, Y.D., Monecke, T., Kelly, N.M., 2013. Preliminary structural analysis of Timiskaming basins along the Larder Lake-Cadillac deformation zone, Ontario and Quebec, Canada: A record of Archean deformation in the southern Abitibi greenstone belt. *Geological Society of America, Abstracts with Programs* 45, 298.
- Frieman, B.M., Kuiper, Y.D., Monecke, T., Kelly, N.M., 2014a. Evidence for early horizontal shortening in the southern Abitibi subprovince, Canada: Implications for Neoproterozoic geodynamic processes. *SEG Conference 2014: Building Exploration Capability for the 21st Century* held in Keystone, CO, USA, Abstract with Programs.
- Frieman, B.M., Kuiper, Y.D., Monecke, T., Kelly, N.M., 2014b. Pre-Timiskaming Folding in the Archean Southern Abitibi Greenstone Belt, Ontario and Québec, Canada: Structural Constraints and Conundrums. *3rd Biennial Structural Geology and Tectonics Forum, Abstracts with Programs*, p. 48.
- Frieman, B.M., Kuiper, Y.D., Monecke, T., Kelly, N.M., 2015a. Structural characteristics and distribution of strain associated with dextral transpression along the Larder Lake-Cadillac deformation zone in the southern Abitibi subprovince, Canada. *Geological Society of America, Abstracts with Programs* 47, 150.

- Frieman, B.M., Kuiper, Y.D., Kelly, N.M., Monecke, T., 2015b. Insights into Archean greenstone belt evolution: Evidence from compilation of high precision U-Pb zircon data in the southern Abitibi subprovince, Canada. AGU-GAC-MAC Joint Assembly, Abstracts with Programs, PG34A-0279.
- Frieman, B.M., Kuiper, Y.D., Kelly, N.M., Monecke, T., 2016a. Provenance and tectonic evolution recorded by successor basins in the Abitibi-Wawa terrane: Insights from new U-Pb LA-ICP-MS analyses of detrital zircon. 62nd Institute on Lake Superior Geology Proceeding 62, Part 1-Program and Abstracts, 46-47.
- Frieman, B.M., Kuiper, Y.D., Monecke, T., Kelly, N.M., 2016b. Characteristics and distribution of brittle-ductile structures associated with dextral transpression along the Larder Lake-Cadillac deformation zone in the southern Abitibi subprovince, Canada. 4th Biennial Structural Geology and Tectonics Forum, Abstracts with Programs, 36.
- Frieman, B.M., Kuiper, Y.D., Kelly, N.M., Monecke, T.M., 2016c. Provenance and tectonic evolution recorded by successor basins in the southern Abitibi subprovince: Insights from new U-Pb LA-ICP-MS analyses of detrital zircon. Geological Society of America, Abstracts with Programs 48. doi:10.1130/abs/2016AM-281904
- Frieman, B.M., Kuiper, Y.D., Kelly, N.M., Monecke, T., Kylander-Clark, A., 2017a. Constraints on the geodynamic evolution of the southern Superior Province: U-Pb LA-ICP-MS analysis of detrital zircon in successor basins of the Archean Abitibi and Pontiac subprovinces of Ontario and Quebec, Canada. Precambrian Research 292, 398–416. doi:10.1016/j.precamres.2017.01.027
- Frieman, B.M., Kuiper, Y.D., Monecke, T.M., Kelly, N.M., 2017b. Distribution, characteristics, and relationship between brittle and ductile dextral transpressive structures along the Larder Lake-Cadillac deformation zone in the Kirkland Lake area of the Abitibi subprovince, Canada. Prospectors & Developers Association of Canada, Abstracts with Programs, [www.http://cmic-footprints.ca/smc/2017](http://cmic-footprints.ca/smc/2017).
- Frieman, B.M., Kuiper, Y.D., Monecke, T., Kelly, N.M., 2017c. Precambrian geology and new structural data, Kirkland Lake area, Ontario. Geological Survey of Canada, Open File 8245, 8 p.
- Frieman, B.M., Kuiper, Y.D., Monecke, T.M., Kelly, N.M., 2017d. Field-based evidence for dilational brecciation prior to ductile localization and fault-valve behavior along a gold-bearing splay of the Archean Larder Lake-Cadillac deformation zone, Ontario, Canada. Geological Society of America, Abstracts with Programs, 49. doi:10.1130/abs/2017AM-299180
- Groves, D.I., Goldfarb, R.J., Gebre-Mariam, M., Hagemann, S.G., Robert, F., 1998. Orogenic gold deposits: A proposed classification in the context of their crustal distribution and relationship to other gold deposit types. Ore Geology Reviews 13, 7–27.
- Ispolatov, V., Lafrance, B., Dubé, B., Creaser, R., Hamilton, M., 2008. Geologic and structural setting of gold mineralization in the Kirkland Lake-Larder Lake gold belt, Ontario. Economic Geology 103, 1309–1340.

- Lafrance, B., 2015. Geology of the orogenic Cheminis gold deposit along the Larder Lake-Cadillac deformation zone, Ontario: *Canadian Journal of Earth Sciences* 52, 1093–1108.
- MacLean, A., 1944. Township of Lebel, District of Timiskaming, Ontario. Ontario Department of Mines, Map 53a, scale 1:12 000.
- Mercier-Langevin, P., Goutier, J., Ross, P.S., McNicoll, V., Monecke, T., Dion, C., Dubé, B., Thurston, P., Bécu, V., Gibson, H., Hannington, M., Galley, A., 2011. The Blake River Group of the Abitibi greenstone belt and its unique VMS and gold-rich VMS endowment. *Geological Survey of Canada Open File 6869*, 61 p.
- Monecke, T., Mercier-Langevin, P., Dubé, B., Frieman, B.M., 2017. Geology of the Abitibi greenstone belt. *Reviews in Economic Geology* 19, 7–49.
- Percival, J.A., Skulski, T., Sanborn-Barrie, M., Stott, G.M., Leclair, A.D., Corkery, M.T., Boily, M., 2012. Geology and tectonic evolution of the Superior Province, Canada. *Geological Association of Canada Special Paper 49*, 321–378.
- Robert, F., 1994. Vein fields in gold districts: The example of Val d'Or, southeastern Abitibi subprovince, Quebec. *Geological Survey of Canada Current Research 1994-C*, 295–302.
- Robert, F., Boullier, A.-M., Firdaous, K., 1995. Gold–quartz veins in metamorphic terranes and their bearing on the role of fluids in faulting. *Journal of Geophysical Research* 100, 12861–12881.
- Stott, G.M., Corkery, M.T., Percival, J.A., Simard, M., Goutier, J., 2010. A revised terrane subdivision of the Superior Province. *Ontario Geological Survey Open File Report 6260*, 20–1 to 20–10.
- Thomson, J.E., 1945. Township of Teck, district of Timiskaming, Ontario. Ontario Department of Mines, Map No. 1945-1, scale 1:12,000.
- Thurston, P.C., Ayer, J.A., Goutier, J., Hamilton, M.A., 2008. Depositional gaps in Abitibi greenstone belt stratigraphy: A key to exploration for syngenetic mineralization. *Economic Geology* 103, 1097–1134. doi:10.2113/gsecongeo.103.6.1097

CHAPTER 2

CONSTRAINTS ON THE GEODYNAMIC EVOLUTION OF THE SOUTHERN SUPERIOR PROVINCE: U-PB LA-ICP-MS ANALYSIS OF DETRITAL ZIRCON IN SUCCESSOR BASINS OF THE ARCHEAN ABITIBI AND PONTIAC SUBPROVINCES OF ONTARIO AND QUEBEC, CANADA

Modified from a paper published in the journal of *Precambrian Research*

Ben M. Frieman^a, Yvette D. Kuiper^a, Nigel M. Kelly^b,
Thomas Monecke^a, Andrew Kylander-Clark^c

To investigate the tectonic development of the southern Superior Province, new U-Pb laser ablation inductively-coupled mass-spectrometry analysis of detrital zircon was conducted on graywacke samples from successor basins of the Abitibi and Pontiac subprovinces. The three successor basin successions investigated are the <2690-2685 Ma Porcupine assemblage and the <2679-2669 Timiskaming assemblage of the Abitibi subprovince, and the ~2682 Ma sedimentary rocks of the Pontiac subprovince. Predominately Neoproterozoic zircon grains (80-95% of the total zircon population) reflect local sources in the Abitibi and Pontiac subprovinces. The successor basins were deposited within 100 Ma of the majority of the detrital zircon grains primary crystallization ages, which is consistent with patterns observed at modern convergent margin settings. Porcupine assemblage samples contain ~5% Mesoarchean zircon, while Pontiac subprovince and Timiskaming assemblage samples contain ~18% and ~13%, respectively. No local Mesoarchean sources exist in the Abitibi or Pontiac subprovinces, suggesting input from an adjacent hinterland. The higher proportion of Mesoarchean zircon in the Timiskaming assemblage relative to the Porcupine assemblage suggest that detritus from the hinterland was more prevalent during the later stages of collision, probably as a result of progressive uplift and denudation of the hinterland. The high proportion of Mesoarchean zircon in the Pontiac subprovince sedimentary rocks may reflect an additional Mesoarchean source. Compilation data for the Superior Province indicates that the hinterland was to the north and is, in part, comprised of the Winnipeg River, Marmion, and Opatoca subprovinces. Patterns of contractional deformation, successor basin formation, and felsic plutonism progressively young to the south in the southern Superior Province and are interpreted in terms of accretionary

^a Department of Geology and Geological Engineering, Colorado School of Mines, Golden, CO

^b Department of Geological Sciences, University of Colorado, Boulder, CO

^c Department of Earth Sciences, University of California, Santa Barbara, CA

processes. Detrital transport across subprovince or terrane boundaries, progressive hinterland emergence, and foreland-directed propagation of the deformational front recorded by successor basins is similar to that observed in modern style collisional or accretionary orogens.

2.1 Introduction

The Abitibi subprovince of the Superior Province is host to some of the largest and best exposed Archean greenstone belts in the world. These are composed of volcanic successions that are overlain by sedimentary rocks deposited in younger successor basins (Fig. 2.1). The successor basins developed in response to Neoproterozoic collision and assembly of the Superior Craton (Percival et al., 2012). Successor basins in the Abitibi subprovince include the <2690-2685 Ma Porcupine assemblage and the <2679-2669 Ma Timiskaming assemblage (Fig. 2.2; Ayer et al., 2002). The Porcupine assemblage deposits are dominated by up to several kilometers thick successions of turbiditic graywacke that were deposited in a deep-water environment (Ayer et al., 2002). The younger Timiskaming assemblage contains thick turbiditic graywacke successions emplaced in a deep-water environment as well as abundant conglomerate interpreted to have been deposited in a subaerial, alluvial-fluvial to shallow marine or lacustrine environment (Hyde, 1980). Sedimentary rocks of the Pontiac subprovince, bounding the Abitibi subprovince to the southeast (Fig. 2.2), were deposited at ~2682 Ma and predominately consist of turbiditic graywacke successions that were deposited in a deep-water environment, similar to the Porcupine assemblage (Mortensen and Card, 1993; Davis, 2002). The sedimentary rocks of the Pontiac subprovince have been interpreted as a foreland basin or accretionary prism (Davis, 2002). While the ages of deposition of the three successor basin types are well constrained (e.g., Ayer et al., 2002), their provenance, and potential relationships between deposition and progressive amalgamation of the Superior Province is not.

U-Pb detrital zircon analysis of syn-tectonic successor basins has been used in various tectonic settings to provide insight into the geodynamic and paleogeographic evolution of associated orogens (DeGraaff-Surpless et al., 2002; Gehrels et al., 2011; Cawood et al., 2012; LaMaskin, 2012). While existing high-resolution, U-Pb zircon data have provided constraints on the stratigraphic development of the Superior Province (Corfu and Stott, 1998; Ayer et al., 2002; Thurston et al., 2008), a comprehensive and statistically significant U-Pb detrital zircon study that directly compares the detrital zircon patterns in graywacke units of the Porcupine assemblage, Pontiac subprovince, and Timiskaming assemblage has not previously been carried out. To establish the detrital zircon age patterns in these rocks we analyzed >100 zircon grains per sample for 16 samples by U-Pb laser ablation inductively-coupled mass-spectrometry

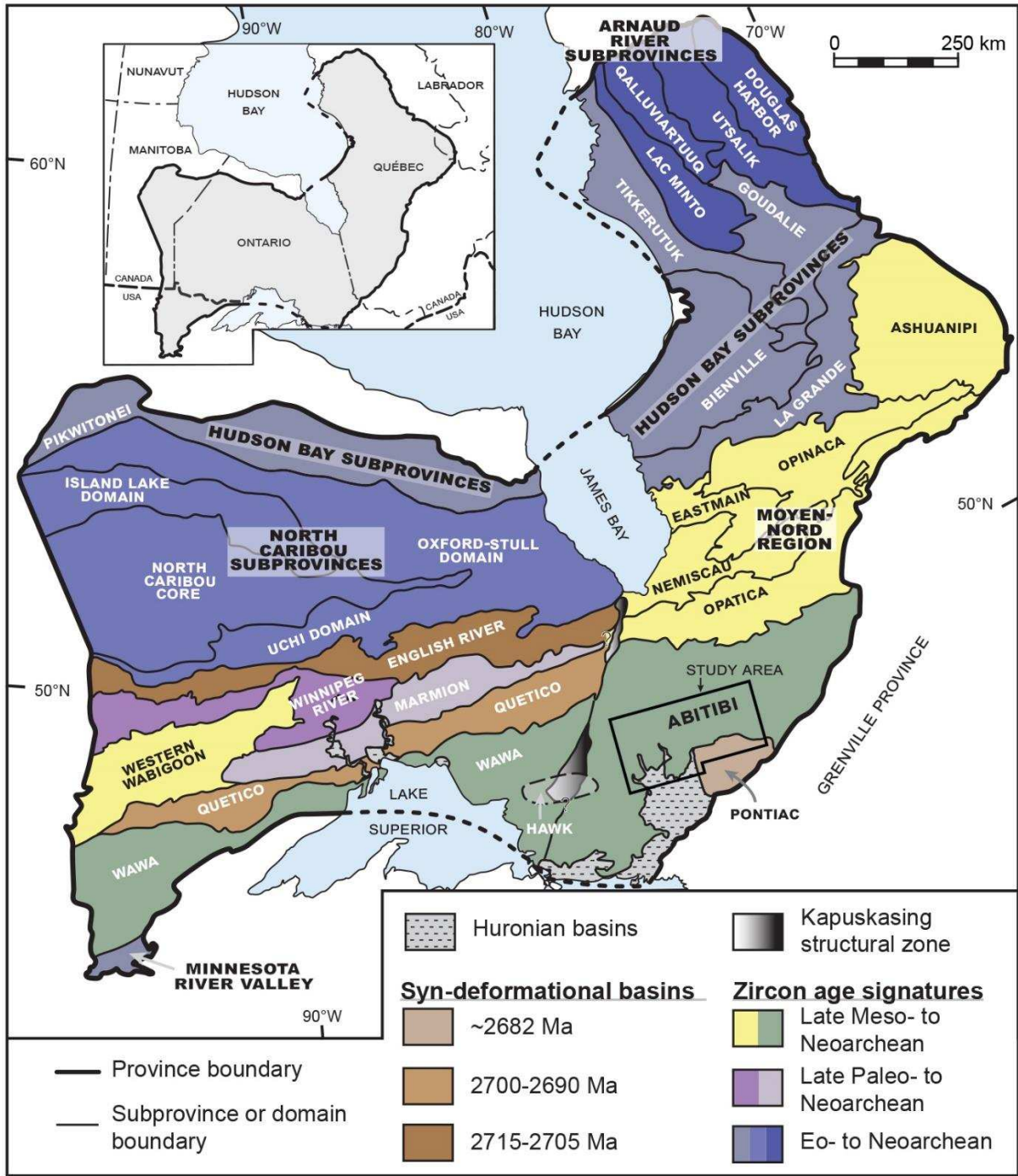


Figure 2.1 – Geological map of the Superior Province. The map displays the distribution of subprovinces or domains and syn-deformational basins colored by their relative zircon age signatures (modified from Stott et al., 2010).

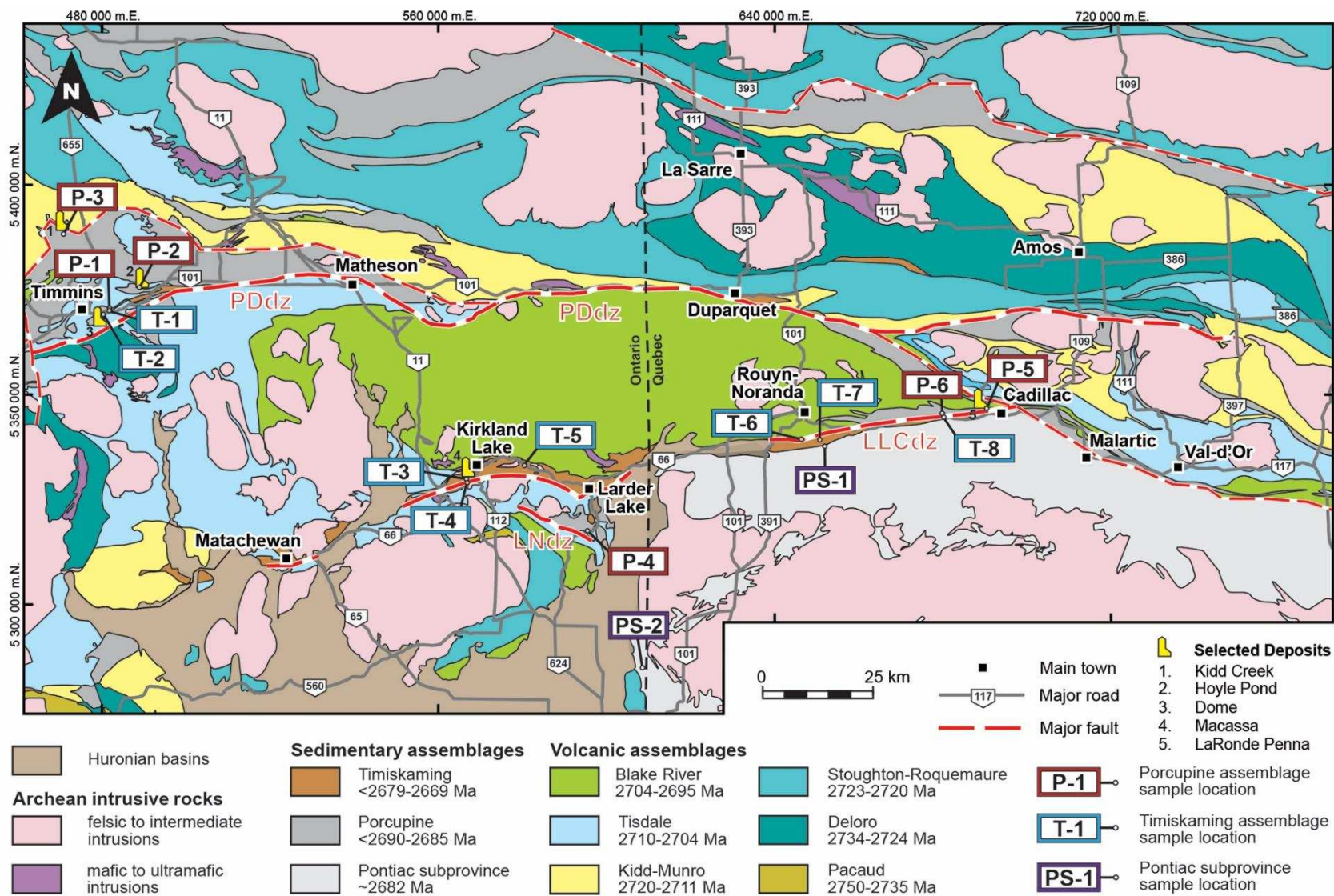


Figure 2.2 – Map of the Abitibi and Pontiac subprovinces. Map displays the distribution of volcanic assemblages and successor basins. The location of Porcupine detrital zircon samples investigated in the present study are highlighted (modified from Thurston et al., 2008).

(LA-ICP-MS). We then compared our data with new compilations of existing U-Pb zircon data from the Superior Province to relate our observed detrital zircon age patterns to progressive amalgamations of the Superior Province. The present contribution provides robust statistical constraints on the detrital zircon age patterns of graywacke in successor basins of the Abitibi and Pontiac subprovinces, which display statistical differences that are related to assembly and deformation of the southern Superior Province.

2.2 Geological background

The following sections summarize the geological context of the Abitibi and Pontiac subprovinces in relation to the Superior Province. First the regional setting is discussed, then the local geological background is reviewed.

2.2.1 Neoproterozoic assembly in the Superior Province

The Superior Province is the largest preserved area of Archean cratonic rocks on Earth. It consists of Archean crustal blocks, which largely amalgamated in the Neoproterozoic (Fig. 2.1; Bédard et al., 2003; Stott et al., 2010; Percival et al., 2012). The Superior Province is predominately composed of Eo- to Neoproterozoic granite-greenstone, gneissic, and/or metasedimentary domains (Percival and Williams, 1989; Williams et al., 1992). Domains with similar structural, magmatic, geochemical, and/or detrital zircon data populations have been grouped into subprovinces (Fig. 2.1; Percival et al., 2006, 2012; Stott et al., 2010), which have been interpreted to represent superterraces or terranes (Percival et al., 2012).

Neoproterozoic assembly began in the northern Superior Province at ~2720 Ma and involved collision of the Hudson Bay subprovinces with the North Caribou subprovinces (Fig. 2.1; Percival et al., 2012). This orogenic system is characterized by north-directed shear and the appearance of 3.9-3.5 Ga detrital zircon grains in associated successor basins (Corkery et al., 1992; Böhm et al., 2000; Skulski et al., 2000; Lin et al., 2006). At ~2720-2705 Ma, along the southern margin of the North Caribou subprovinces, north directed collision culminated in the juxtaposition of the Winnipeg River and Marmion subprovinces with the North Caribou subprovinces (Corfu et al., 1995; Percival et al., 2012). The collisional system is characterized by south-vergent structures and deposition of 2715-2705 Ma successor basins, including sedimentary rocks of the English River subprovince (Sleep, 1992; Corfu and Stone, 1998). Collision was immediately followed by post-deformational plutonism and initial retrograde metamorphism by ~2700 Ma (Sleep, 1992; Corfu and Stone, 1998). Penetrative deformation was diachronous along the boundary, but generally occurred at ~2718-2704 Ma (Corfu and Stott, 1993; Percival et al., 2006). At ~2720-2700 Ma, orogenesis had propagated into the Western Wabigoon and Winnipeg River subprovinces (Fig. 2.1). It was characterized by the

onset of penetrative deformation, intrusion of ~2710 Ma tonalite complexes, and the deposition of the 2715-2705 Ma Warclub Group successor basin sedimentary rocks (Percival et al., 2012).

The northeastern Superior Province is characterized by several composite domains, which amalgamated during ~2720-2700 Ma collision of the Hudson Bay and Arnaud River subprovinces (Fig. 2.1; Percival et al., 2001; Bédard et al., 2003; Bédard, 2006). Despite temporal correlations, links between this orogenic system and those in the western Superior Province are unclear (Percival et al., 2012). Domains in the northeastern Superior Province contain some of the oldest rocks on Earth, including supracrustal assemblages with ~4000-3200 Ma zircon crystallization ages and isotopic signatures (Skulski et al., 1996; O'Neil et al., 2008; Boily et al., 2009; Cates and Mojzsis, 2009; David et al., 2009). However, most of the supracrustal assemblages consist of 2900-2720 Ma volcanic-plutonic successions and limited 2750-2720 Ma successor basin deposits (Skulski et al., 1996; Percival et al., 2001; Simard et al., 2005; O'Neil et al., 2008; Boily et al., 2009; David et al., 2009).

At ~2695 Ma, contractional deformation had propagated to the Abitibi and Wawa subprovinces due to their collision with the subprovinces to the north (Corfu and Stott, 1998; Bateman et al., 2008). The suture zone is inferred to be below the Quetico subprovince, which is an accretionary wedge to foreland basin that formed during this collision (Fig. 2.1; Percival and Williams, 1989; Davis et al., 1990; Williams et al., 1992; Zaleski et al., 1999; Fralick et al., 2006). Progressive docking of the Abitibi and Wawa subprovinces with the subprovinces to the north is documented by ~2700-2690 transgressive sedimentary assemblages in the Quetico subprovince (Davis et al., 1990; Zaleski et al., 1999; Fralick et al., 2006). Contractional deformation continued in the Abitibi and Wawa subprovinces between 2690 Ma and 2665 Ma (Ayer et al., 2002; Bateman et al., 2008; Ispolatov et al., 2008). Late deformation in the southern Superior Province is, in part, inferred to have been related to collision and underthrusting of the Minnesota River Valley subprovince (Fig. 2.1) below the Abitibi and Wawa subprovinces along the Great Lakes tectonic zone (White et al., 2003). Structural and seismic studies indicate that the upper 10 km of crust of the Abitibi and Pontiac subprovinces is characterized by widespread fold and thrust structures and steeply dipping shear zones that relate to the 2690-2665 Ma collisional events (Dimroth et al., 1983; Camiré and Burg, 1993; Sawyer and Benn, 1993; Jackson et al., 1995; Calvert and Ludden, 1999; Snyder et al., 2008).

2.2 Geology of the Abitibi and Pontiac subprovinces

The Abitibi subprovince is bounded by the Kapuskasing structural zone to the west, the Opatoca subprovince to the north, the Grenville Province to the east, the Pontiac subprovince to the southeast, and the sedimentary deposits of the Huronian basin to the south (Fig. 2.1).

Historically, greenstone belts within the Abitibi subprovince have been subdivided into northern and southern belts based on stratigraphic criteria, the proportion and composition of intrusive rocks, and differences in metamorphic grade (Dimroth et al., 1982; Ludden et al., 1986; Chown et al., 1992). However, the age of volcanic and plutonic rocks in the northern and southern belts of the Abitibi subprovince are largely comparable (Ayer et al., 2002; 2005; David et al., 2006, 2007) and the observed differences likely relate to differences in the crustal exposure level (Benn and Moyen, 2008). The present study focuses on successor basin deposits in the Abitibi subprovince and the adjacent Pontiac subprovince, located between Timmins, Ontario in the west and Cadillac, Quebec in the east (Fig. 2.2). The area is well-mapped and the relative ages and depositional settings of syn-deformational successor basins are well-constrained (Ayer et al., 2002).

In the study area, the Abitibi subprovince is largely composed of mafic to intermediate ~2750-2695 Ma volcanic rocks (Fig. 2.2; Ayer et al., 2002, 2005; Thurston et al., 2008; McNicoll et al., 2014). The volcanic rocks are subdivided based on stratigraphic, geochemical, and geochronological data into six distinct composite volcanic assemblages, referred to as the Pacaud, Deloro, Staughton-Roquemaure, Kidd-Munro, Tisdale, and Blake River assemblages (Fig. 2.2; Ayer et al., 2002, 2005; Thurston et al., 2008). The volcanic assemblages were deposited in a subaqueous environment and display chemical signatures consistent with formation in an arc, back-arc, and/or rifted arc setting with intermittent plume influences (Ayer et al., 2002).

Several younger, primarily sedimentary, successor basins occur within the study area. Based on structural, sedimentological, and geochronological constraints, two distinct successor basin types are distinguished, namely the subaqueous, turbidite-dominated Porcupine assemblage (i.e., 'flysch' deposits) and the coarse, clastic-dominated, subaqueous to subaerial Timiskaming assemblage (i.e., 'mollase' deposits; Hyde, 1980; Mueller and Corcoran, 1998; Ayer et al., 2002; Corcoran and Mueller, 2007; Bateman et al., 2008; Ispolatov et al., 2008). The deposits of the Porcupine assemblage form laterally extensive and narrow deposits that were deposited disconformably to paraconformably on the older volcanic assemblages (Fig. 2.2; Ferguson et al., 1968). Deposits of the Timiskaming assemblage are commonly fault-bounded, are preserved as spatially restricted deposits, and unconformably overlie all older assemblages (Fig. 2.2). Both assemblages are spatially associated with major regional structures, such as the Porcupine-Destor, Larder Lake-Cadillac, and Lincoln-Nippissing deformation zones in Ontario and Quebec (Fig. 2.2). The Porcupine assemblage was deposited at <2690-2685 Ma (Mortensen, 1993a,b; Bleeker and Parrish, 1996; Heather and Shore, 1999; Ayer et al., 2002,

2005; Davis, 2002; Ropchan et al., 2002; Bleeker and van Breemen, 2011) and the Timiskaming assemblage at <2679-2669 Ma (Corfu et al., 1991; Corfu, 1993; Heather and Shore, 1999; Ropchan et al., 2002; Ayer et al., 2002, 2005; Davis, 2002; Ispolatov et al., 2008; Ayer and Chartrand, 2011; Bleeker et al., 2015).

In the southeastern portion of the study area in Quebec, rocks of the Pontiac subprovince occur south of the Larder Lake-Cadillac deformation zone (Fig. 2.2). The Pontiac subprovince is largely composed of graywacke and granitic batholiths (Gariépy et al., 1984; Camiré and Burg, 1993; Camiré et al., 1993; Mortensen and Card, 1993; Sawyer and Barnes, 1994). Graywacke deposits are predominately fine-grained, km-scale turbiditic successions and are interpreted to have been deposited in a foreland basin setting, similar to the sedimentary rocks of the Quetico subprovince (Davis, 2002; Ayer et al., 2005). The age of deposition of sedimentary rocks in the Pontiac subprovince is ~2682 Ma, based on the ~2683 Ma U-Pb age of the youngest detrital zircon populations and the ~2682 Ma zircon crystallization age of a cross-cutting pluton (Mortensen and Card, 1993; Davis, 2002). Deposition in the Pontiac subprovince may have been partially coeval with the Porcupine assemblage and may represent a distal or transitional equivalent (Davis, 2002). Seismic evidence indicates that the Pontiac subprovince is juxtaposed with the Abitibi subprovince along a north dipping, south-vergent thrust zone that emplaced the Abitibi subprovince over the Pontiac subprovince (Benn et al., 1994). Based on geophysical surveys, the western contact of the Pontiac subprovince with the Abitibi subprovince, along the Ontario-Quebec border, is interpreted as a structural discontinuity (Kalliokoski, 1987). Along their contact in Quebec, where strain is low, bedding in the Pontiac subprovince displays subvertical dips, while bedding in adjacent Timiskaming assemblage units is moderate. Thus, the contact between them is inferred to be an angular unconformity (Holubec, 1972).

Plutonic rocks in the Abitibi and Pontiac subprovinces can be subdivided into syn-volcanic, syn-deformational, and post-deformational intrusions (Chown et al., 1992; Heather and Shore, 1999; Ayer et al., 2002). Syn-volcanic intrusions are ~2750-2695 Ma and display compositions similar to coeval volcanic units (Corfu, 1993; Mortensen, 1993a,b; Heather and Shore, 1999; Ayer et al., 2005). Many syn-volcanic intrusions occur as large, spatially restricted batholithic complexes (Fig. 2.2). These complexes were typically constructed over a protracted period by multiple intrusive events (Mortensen, 1993a,b; Heather and Shore, 1999; Davis et al., 2000). Syn-deformational intrusions are ~2695-2670 Ma (Corfu, 1993; Mortensen, 1993a,b; Ayer et al., 2005; David et al., 2006, 2007; Galley and Lafrance, 2014; McNicoll et al., 2014). These intrusions are broadly distributed throughout the Abitibi and the Pontiac subprovinces.

They are hosted in volcanic rocks, batholithic complexes, and sedimentary assemblages. Early syn-deformational intrusions (2695-2685 Ma) consist mainly of tonalite and granodiorite, while late syn-deformational (2685-2670 Ma) intrusions are commonly more potassic (i.e., granite, monzonite, and syenite) with lesser mafic phases consisting of diorite, hornblendite, and lamprophyre (Ayer et al., 2002). Syn-deformational intrusions range from undeformed to strongly foliated, depending on their location and proximity to the major deformation zones. Lastly, ~2670-2650 Ma post-deformational intrusions are typically massive, non-foliated, and commonly occur as relatively small intrusions within or close to large batholithic complexes (Heather and Shore, 1999; Davis et al., 2000).

2.3 Methods

The following sections summarize the methods used to investigate the U-Pb age patterns of detrital zircon graywacke samples from the Abitibi and Pontiac subprovinces. First, the sampling strategy is discussed. Then, the methods used for sampling processing through LA-ICP-MS analysis are discussed

2.3.1 Sampling strategy

To establish the detrital zircon pattern of sedimentary rocks in the Abitibi and Pontiac subprovinces, a representative set of 16 graywacke samples was collected (Fig. 2.2; Table 2.1). Graywacke is ubiquitous in the Porcupine assemblage and sedimentary rocks of the Pontiac subprovince. In contrast, the Timiskaming assemblage contains less graywacke and is commonly dominated by conglomerate and alkaline volcanic rocks. Graywacke units were sampled, because (1) reasonable sample volumes of the fine-grained graywacke provide representative detrital zircon populations, and (2) graywacke is a shared lithologic unit in the three basin groups, providing zircon data from equivalent facies or sedimentary environments.

2.3.2 Sample preparation

Fourteen samples were collected from outcrops throughout the Abitibi and Pontiac subprovinces. At each sample location ~20-30 kg of material was collected. Two additional samples (P-2 and P-3) were obtained from drill core provided by Goldcorp and Glencore and consisted of 15-25 kg of material. All samples were processed at the mineral separation laboratory of the Department of Geology and Geological Engineering, Colorado School of Mines. Sample preparation included sample crushing using a Boyd jaw crusher, grinding using a Bico disc mill grinder, weight separation using a Wilfley 'wet shaking' table, magnetic separations using a Frantz Barrier separator, and heavy liquid (lithium metatungstate, ~2.95 g/cm³) density separation. A representative split of 150-400 zircon grains was hand-picked for

each sample and mounted in 2.7 cm epoxy plugs by size fractions (short axis diameters of <50 μm , 50-75 μm , and >75 μm).

Polished grain mounts were imaged using plane polarized and reflected light microscopy. Subsequent back-scattered electron (BSE), secondary electron (SE), and cathodoluminescence (CL) imaging was conducted at the Denver Microbeam Laboratory, U.S. Geological Survey in Lakewood, Colorado on a JOEL 5800LV scanning electron microscope. Analysis was conducted under high vacuum, using a 15 kV operating voltage, and 5 nA beam current. Additional SE and BSE imaging of selected samples was conducted at the Department of Geology and Geological Engineering, Colorado School of Mines, using a TESCAN MIRA3 field emission-scanning electron microscope. The instrument was operated at 15 kV, with a beam current of 11 nA.

For each sample, at least 100 grains were selected for analysis. These grains were randomly selected from a digital grid imposed on images of the grain mounts. The number of grains selected per size fraction was proportional to the number of grains in that size fraction relative to the number of grains in the total sample population. Spot analysis locations within the selected grains were based on the CL images to avoid overlap of the spot with more than one age or compositional domain (as determined from SEM images; Fig. 2.3). A limited number of grains was selected for multiple spot analyses to evaluate reproducibility and/or potential age differences between compositional or morphological domains. Prior to analysis, plane polarized, reflected light, SEM images were cross-referenced to ensure selected portions of the zircon grains contained no visible inclusions or fractures.

2.3.3 U-Pb isotope data collection, reduction, and analytical methods

Isotopic analyses were conducted by LA-ICP-MS at the University of California Santa Barbara, using a *Nu Plasma* multi-collector system coupled to a *Photon Machines Excite* 193 nm laser ablation system, following the analytical procedures of Kylander-Clark et al. (2013). The 91500 zircon (Wiedenbeck et al., 1995) was used as a primary reference material. Secondary reference materials included the GJ-1, Plešovice, and SL1 zircon standards (Wiedenbeck et al., 1995, 2004; Woodhead and Hergt, 2005; Blichert-Toft, 2008; Morel et al., 2008; Sláma et al., 2008), which were interspersed throughout the analytical session to evaluate accuracy. All secondary reference materials yielded ratios within 2% of their accepted values. Data was reduced using *lolyte v2.5* (Paton et al., 2011), and 2% uncertainty was added in quadrature to each ratio to account for the long-term reproducibility of the secondary reference materials. Limited data from metamict grains and/or grains that contained high common lead contents were rejected during data acquisition and/or reduction. The majority of the U-Pb



Figure 2.3 – Representative zircon images. Cathodoluminescence images of detrital zircon grains analyzed from graywacke samples collected in the Abitibi and Pontiac subprovinces organized by age from youngest to oldest. The analysis location, sample number, spot reference number, and $^{207}\text{Pb}/^{206}\text{Pb}$ age with 2σ uncertainty for each zircon grain are indicated.

isotope data was filtered following the method proposed by Gehrels et al. (2011); all U-Pb data that was >5% discordant was rejected, including that used for statistical comparisons (Appendix B).

Accepted U-Pb data are plotted on Wetherill Concordia diagrams, frequency histograms, probability density function (PDF) plots, and cumulative distribution function (CDF) plots. The Wetherill Concordia, frequency histogram, and PDF plots were calculated and plotted using Isoplot 4.1 (Ludwig, 2012). Frequency histograms were binned into 40 bins over the age distribution for each sample set. The PDF curves are calculated by summing the normal distribution curves defined by each U-Pb zircon age and its 2σ uncertainty, following standard Isoplot procedures. The CDF curves were calculated including 1σ uncertainty using standard routines from the Arizona LaserChron Center at the University of Arizona (<http://www.laserchron.org>). The CDF curves are calculated by summing the probability distributions with increasing age and are useful for determining the probability that a zircon in the sample population will be younger or older than a certain age. Binned histograms of the accepted $^{207}\text{Pb}/^{206}\text{Pb}$ age data are included with the calculated PDF and CDF curves to display the number and distribution of data from which these curves were derived.

2.3.4 Compilation of U-Pb zircon data

To better assess the patterns of detrital zircon age populations in the samples investigated, existing U-Pb zircon data from the southern Superior Province were compiled. The data compiled were derived from the Canadian Geochronology Knowledge Base (2013) and supplemented by selected data from several publications (Ayer et al., 2005; Lafrance et al., 2005; David et al., 2006, 2007; Ayer and Chartrand, 2011; Appendix B). Only data with a 2σ error of <10 Ma was included. The database contains >1500 U-Pb zircon ages that are mainly isotope dilution - thermal ionization mass spectroscopy (ID-TIMS) data, but also include secondary ionization mass spectroscopy (SIMS) and LA-ICP-MS data (Appendix B). The compiled dataset includes U-Pb ages interpreted from single grain, multiple spot, and multiple grain analyses. The compilation data were subdivided by reported geological subprovince, rock type, and zircon type (i.e., igneous, detrital, inherited, or metamorphic).

2.4 Sample descriptions and U-Pb zircon LA-ICP-MS results

Detrital zircon grain sizes for all samples range from <50 μm to >200 μm in length (aspect ratios of 2:1 to 8:1) with grain shapes that are euhedral to subhedral, commonly with minor rounding from detrital abrasion of grain tips. Grains range from clear to pale pink to brown in color. Figure 2.3 displays a representative set of zircon grains with analysis locations and $^{207}\text{Pb}/^{206}\text{Pb}$ ages (uncertainties at 2σ) indicated. Grains display low to intermediate CL

intensities with lesser bright CL responses. The majority of zircon grains display textures consistent with crystallization in an igneous environment. Textures identified in CL range from simple oscillatory or sector zoning (e.g., Fig. 2.3; P-2, spot 4-2; T-3, spot 1-25), to complex, patchy, and/or cryptic CL textures (e.g., Fig. 2.3; P-1, spot 8B-1). Some grains display multiple growth domains characterized by oscillatory zoning (e.g., Fig. 2.3; T-7, spot 5-10), which are interpreted to be successive stages of magmatic growth. A limited number of analyses was performed in successive growth zones observed within a single grain (e.g., Fig. 2.3; P-6, spots 3-11 and 3-12). These results most commonly yielded $^{207}\text{Pb}/^{206}\text{Pb}$ ages that are within uncertainty of one another, although a limited number of grains yielded data indicative of differing age domains. In general, there is no clear relationship between $^{207}\text{Pb}/^{206}\text{Pb}$ age, CL intensity, textural variations, and/or inferred growth domain (Figs. 2.3 and 2.4). Of all concordant analyses, <3% yield Th/U ratios ~0.05-0.3 and ~95% yield ratios of 0.3-2.0 (Appendix B). Rare, <15 μm , presumably metamorphic rims are present and were not targeted for detrital zircon analysis.

2.4.1 Porcupine assemblage samples

Sedimentological studies in Timmins (Born, 1995), Larder Lake (Hyde, 1980), Rouyn-Noranda (Rocheleau, 1980), and LaRonde Penna (Lafrance et al., 2003) all indicate that Porcupine assemblage deposits are characterized by deposition of turbiditic graywacke in a deep-water setting. Graywacke and mudstone beds are commonly arranged into Bouma sequences or amalgamated graywacke beds.

2.4.1.1 Sample P-1

Sample P-1 was collected east of Timmins, Ontario at an outcrop exposing the Timiskaming-Porcupine angular unconformity (Fig. 2.2; Table 2.1). Porcupine assemblage rocks at this location close to Crawford Avenue in South Porcupine (Ayer et al. 1999) are part of the Beatty Formation and are comprised of laterally continuous graywacke beds with and interbedded mudstone. Sample P-1 was collected from one of the laterally continuous graywacke beds. The maximum age of the Beatty Formation is 2687.2 ± 1.6 Ma based on the youngest detrital zircon age populations in these rocks (Table 2.1; Ayer et al., 2005).

Of a total of 178 zircon analyses, 150 were concordant and 28 were rejected due to discordance (Fig. 2.4; Appendix B). The principal group of $^{207}\text{Pb}/^{206}\text{Pb}$ ages occurs between ~2760-2680 Ma and comprises ~92% of total analyses. Seven zircon analyses yielded dates at ~2800 Ma, two at ~2900 Ma, and one at ~3030 Ma.

2.4.1.2 Sample P-2

Sample P-2 was obtained from Goldcorp from the Hoyle Pond deposit northeast of Timmins (Fig. 2.2; Table 2.1). The Porcupine assemblage graywacke at this location is interpreted to belong to the Hoyle Formation. The sample was collected from drill core (DDH 20178; 129 m to 180 m interval) and represented a composite of several graywacke beds. Ayer et al. (2005) analyzed detrital zircon grains from this formation and interpreted the maximum age of deposition, based on the date of the youngest zircon fractions in these rocks, to be 2688 ± 2 Ma (Table 2.1).

Of 189 zircon analyses, 7 analyses were rejected due to discordance (Fig. 2.4; Appendix B). A principal group of $^{207}\text{Pb}/^{206}\text{Pb}$ ages occur between ~ 2680 Ma and ~ 2750 Ma and comprises $\sim 95\%$ of the total sample population, in addition to three grains yielded ages at ~ 2800 - 2780 Ma.

Table 2.1 – List of Porcupine assemblage, Pontiac subprovince, and Timiskaming assemblage samples for detrital zircon U-Pb LA-ICP-MS analysis. Ages of deposition constrained by previous studies are indicated.

	Sample #	Location	Rock type	UTM zone (NAD83)	Northing (m)	Easting (m)	Youngest U-Pb detrital zircon ages		
Porcupine assemblage	P-1	Timmins	graywacke	17U	5371274	484261	2687 ± 2 Ma (Ayer et al., 2005)	2690-2685 Ma	GENERALIZED DEPOSITIONAL AGES
	P-2	Timmins	graywacke	17U	5377126	493189	2688 ± 2 Ma (Ayer et al., 2005)		
	P-3	Timmins	graywacke	17U	5393390	473340	2685 ± 6 Ma (Bleeker et al., 1999)		
	P-4	Larder Lake	graywacke	17U	5318272	597448	2695 ± 3 Ma (Ayer et al., 2005)		
	P-5	LaRonde Penna	graywacke	17U	5346548	690224	2687 ± 3 Ma (Davis, 2002)		
	P-6	LaRonde Penna	graywacke	17U	5345265	680339	2687 ± 3 Ma (Davis, 2002)		
Pontiac subprovince	PS-1	Rouyn-Noranda	graywacke	17U	5337608	651829	2683 ± 1 Ma (Mortensen and Card, 1993)	~ 2682 Ma	
	PS-2	western Pontiac subprovince	biotite schist	17T	5285124	610613	2683 ± 1 Ma (Mortensen and Card, 1993)		
Timiskaming assemblage	T-1	Timmins	graywacke	17U	5371207	484998	2679 ± 4 Ma; 2674 ± 2 Ma (Ayer et al., 2003)	2679-2669 Ma	
	T-2	Timmins	graywacke	17U	5369513	483540	2669 ± 1 Ma; 2674 ± 2 Ma (Bleeker et al., 1999; Ayer et al., 2003)		
	T-3	Kirkland Lake	graywacke	17U	5331699	569426	2680 ± 3 Ma (Corfu et al., 1991)		
	T-4	Kirkland Lake	graywacke	17U	5330831	570190	2680 ± 3 Ma (Corfu et al., 1991)		
	T-5	Morris-Kirkland	graywacke	17U	5333712	580331	2678 ± 3 Ma; 2670 ± 1 Ma (Ayer et al., 2005)		
	T-6	Rouyn-Noranda	graywacke	17U	5339898	646428	2673 ± 2 Ma (Davis, 2002)		
	T-7	Rouyn-Noranda	graywacke	17U	5340052	650339	2673 ± 2 Ma (Davis, 2002)		
	T-8	LaRonde Penna	graywacke to conglomerate	17U	5344928	680437	no proximal detrital zircon data		

2.4.1.3 Sample P-3

Sample P-3 was obtained from Glencore from the Kidd Creek deposit north of Timmins (Fig. 2.2; Table 2.1). Porcupine assemblage rocks at the Kidd Creek deposit are predominately comprised of turbidite successions of graywacke, mudstone, and graphitic mudstone (Bleeker et al., 1999). Sample P-3 was collected from a graywacke bed exposed underground at the 9000 feet level (2410 m below sea level). Bleeker et al. (1999) interpreted the maximum age of deposition of Porcupine assemblage graywacke at the Kidd Creek deposit to be 2684.7 ± 6.3 Ma, based on the youngest detrital zircon analysis of several samples (Table 2.1).

Analysis of zircon grains from sample P-3 yielded 65 concordant analyses from a total of 70 (Fig. 2.4; Appendix B). The concordant data, although limited in number relative to the other samples, define a principal group of $^{207}\text{Pb}/^{206}\text{Pb}$ ages between ~ 2680 Ma and ~ 2780 Ma, with one analysis yielding a $^{207}\text{Pb}/^{206}\text{Pb}$ date at ~ 2880 Ma (Fig. 2.4).

2.4.1.4 Sample P-4

Sample P-4 was collected from an outcrop of graywacke exposed along Highway 624 south of Larder Lake, Ontario (Fig. 2.2; Table 2.1). The Porcupine assemblage in this area is primarily comprised of graywacke. Ayer et al. (2005) analyzed detrital zircon grains from the same outcrop where sample P-4 was collected. They interpreted the maximum age of deposition of these rocks as 2695 ± 3 Ma, based on the youngest detrital zircon grain populations (Table 2.1).

The sample yielded 154 concordant and 17 discordant analyses (Fig. 2.4; Appendix B). The principal ~ 2800 - 2690 Ma $^{207}\text{Pb}/^{206}\text{Pb}$ age grouping is centered at ~ 2740 Ma. Two analyses yielded $^{207}\text{Pb}/^{206}\text{Pb}$ ages of ~ 2915 Ma and 2940 Ma.

2.4.1.5 Sample P-5

Sample P-5 was collected from ~ 1 km south of the LaRonde Penna deposit in Quebec (Fig. 2.2; Table 2.1). Porcupine assemblage rocks, termed the Cadillac Group in Quebec, at the sampling site comprise graywacke and mudstone arranged into Bouma sequences (Fig. 2.5A). Sample P-5 was collected from a single graywacke bed. The maximum age of deposition of these rocks, based on the youngest detrital zircon grains of a sample collected at LaRonde Penna, is 2687 ± 3 (Table 2.1; Davis, 2002).

Of a total of 172 zircon analyses, the sample yielded 145 concordant analyses (Fig. 2.4; Appendix B). The principal group of $^{207}\text{Pb}/^{206}\text{Pb}$ ages is ~ 2775 - 2670 Ma, with the maximum of the relative probability curve centered on ~ 2720 Ma. The principal data group comprises $\sim 83\%$ of the total analyses from this sample. The remaining $\sim 17\%$ of analyses are composed of pre-

2775 Ma ages; twelve ages between 2840 and 2775 Ma, five ages at ~2900 Ma, one age at ~3000 Ma, and one age at ~3100 Ma.

2.4.1.6 Sample P-6

Sample P-6 was collected ~7km west-southwest of the LaRonde Penna deposit to the west of Cadillac, Quebec (Fig. 2.2; Table 2.1). The sample was obtained from a single graywacke bed. The youngest detrital zircon grains from the Porcupine assemblage at the LaRonde Penna deposit constrain the maximum age of deposition of these rocks to 2687 ± 3 Ma (Table 2.1; Davis, 2002).

Sample P-6 yielded a total of 107 concordant zircon analyses out of a total of 142 spot analyses (Fig. 2.4; Appendix B). The principal ~2775-2680 Ma $^{207}\text{Pb}/^{206}\text{Pb}$ age grouping is centered on ~2740 Ma and comprises ~85% of the total analyses. A prominent tail on the principal population is defined by a set of older dates between ~2880-2775 Ma and one date at ~3200 Ma.

2.4.2 Pontiac subprovince samples

Sedimentary rocks in the Pontiac subprovince are dominated by monotonous successions of graywacke and mudstone arranged in Bouma sequences (Camiré et al., 1993), interpreted to have been deposited in a deep-water environment below storm-wave-base by turbidity currents. Despite metamorphic overprint, primary structures are commonly observed including grading, ripple cross-laminations, load-casts, and flame structures allowing for identification of primary stratigraphic facing (Camiré and Burg, 1993).

2.4.2.1 Sample PS-1

Sample PS-1 was collected from the northern Pontiac subprovince south of Rouyn-Noranda, Quebec (Fig. 2.2; Table 2.1). Sample PS-1 was collected from several thinly bedded (<15 cm) graywacke beds. The age of deposition of Pontiac subprovince sedimentary rocks is well-constrained to ~2682 Ma in the northern portion of the subprovince by the ~2683 Ma youngest age of detrital zircon grains and by the ~2682 Ma zircon crystallization age in cross-cutting plutonic rocks (Table 2.1; Mortensen, 1993b; Davis, 2002).

Sample PS-1 yielded 157 concordant analyses out of a total of 172 analyses (Fig. 2.4; Appendix B). The principal $^{207}\text{Pb}/^{206}\text{Pb}$ age group is between ~2775 Ma and ~2680 Ma and the relative probability curve for these data is centered on ~2720 Ma. It comprises ~80% of the total analyses. The remaining analyses are composed of pre-2775 Ma ages; scattered ages from ~2775 Ma to ~2935 Ma (12 analyses) and three ages at ~3050, ~3075, and ~3160 Ma.

2.4.2.2 Sample PS-2

Sample PS-2 was collected from the western Pontiac subprovince along the Ontario-Quebec border (Fig. 2.2; Table 2.1). The sedimentary rocks in this area are metamorphosed to amphibolite facies and are garnet- and biotite-rich. However, primary compositional layering is preserved. Sample PS-2 was collected from a laterally continuous, normally graded graywacke bed that is penetratively foliated (Fig. 2.5B). The maximum age of deposition of Pontiac subprovince sedimentary rocks in the area of the Ontario-Quebec border is poorly constrained. However, the youngest detrital zircon grains from a sample ~30 km to the southwest yielded ages of 2687.5 ± 2.0 Ma and 2688.3 ± 1.8 Ma (Davis, 2002).

Sample PS-2 yielded 152 concordant analyses out of a total of 190 (Fig. 2.4; Appendix B). The principal group of $^{207}\text{Pb}/^{206}\text{Pb}$ ages is between ~2800 and ~2680 Ma and is centered on ~2730 Ma. The remaining analyses (~21%) yielded pre-2750 Ma dates, which define a prominent tail on the principal population group between ~2925 and ~2800 Ma.

2.4.3 Timiskaming assemblage samples

Sedimentary rocks of the Timiskaming assemblage in the Timmins (Born, 1995), Kirkland Lake (Hyde, 1980; Mueller and Corcoran, 1998), Larder Lake (Hyde, 1980; Jackson et al., 1994), Rouyn-Noranda (Rocheleau, 1980), and LaRonde Penna areas (Lafrance et al., 2003) were largely deposited as alluvial fans or in braided streams or floodplains in a subaerial environment (Hyde, 1980; Born, 1995). However, at least locally, deposition occurred in a deep subaqueous environment below the storm-wave-base in submarine fan systems (Hyde, 1980; Rocheleau, 1980; Born, 1995).

2.4.3.1 Sample T-1

Sample T-1 was collected from the so-called Shovel outcrop (Ayer et al., 1999) on Government Road in South Porcupine, east of Timmins (Fig. 2.2; Table 2.1). The Timiskaming assemblage at this location is part of the Dome Formation (Ayer et al., 1999) and is predominately comprised of graywacke and mudstone arranged into Bouma sequences. Sample T-1 represents a composite of several graywacke beds. The age of deposition of the Dome Formation in Timmins is constrained by the youngest detrital zircon populations to be $<2674 \pm 2$ Ma (Table 2.1; Ayer et al., 2003).

Out of a total of 120 analyses, sample T-1 yielded 107 concordant ages (Fig. 2.4; Appendix B). The ~2775-2660 Ma principal data group comprises ~82% of the total sample. A tail on the principal group is defined by ages at ~2825-2775 Ma, which comprises ~12% of the total sample population. A further five concordant ages occur at ~2870 Ma, ~2922 Ma, ~2931 Ma, ~2935 Ma, and ~2980 Ma.

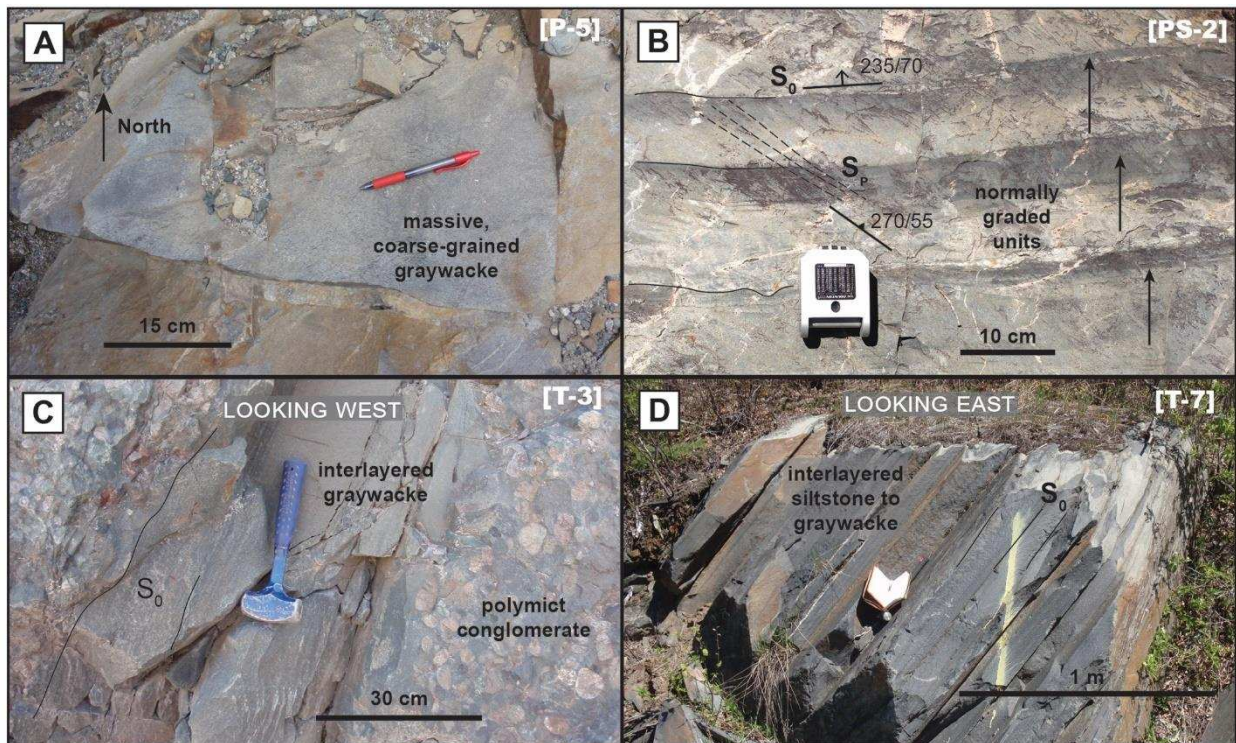


Figure 2.5 – Field photographs of representative sample localities. (A) Coarse-grained, massive graywacke sample P-5 (Porcupine assemblage). (B) Fining upward sequences in turbiditic graywacke units that are characteristic at the location of sample PS-2 (Pontiac subprovince). The orientation of bedding (S_0) and an oblique foliation (S_p) are indicated using dip direction/dip notation. (C) Sample T-3, from graywacke interlayered with pebble conglomerate in the Timiskaming assemblage (Kirkland Lake area). (D) Sample T-7 from interbedded siltstone and graywacke in the Timiskaming assemblage (Rouyn-Noranda area).

2.4.3.2 Sample T-2

Sample T-2 was collected from a roadside outcrop on Bruce Avenue near the Dome mine at south Porcupine, east of Timmins (Fig. 2.2; Table 2.1). The Timiskaming assemblage rocks at this location are assigned to the Dome Formation. The sample was taken from a single graywacke bed that is interbedded with mudstone. The maximum age of deposition of the Dome Formation is constrained by the youngest detrital zircon populations to be 2674 ± 2 Ma (Ayer et al., 2003).

Analysis of zircon grains from sample T-2 yielded 105 concordant analyses out of a total of 134 (Fig. 2.4; Appendix B). The principal ~ 2775 - 2680 Ma group of ages comprises $\sim 85\%$ of the total sample population. A set of ten ages define a ~ 2850 - 2775 Ma tail on the principal $^{207}\text{Pb}/^{206}\text{Pb}$ age group ($\sim 9\%$ of the total sample population), and a further five ages are scattered between ~ 3050 and 2900 Ma ($\sim 5\%$ of the sample population).

2.4.3.3 Sample T-3

Sample T-3 was collected at a roadside outcrop on Highway 66 in Chaput Hughes (Ayer et al., 1999), west of Kirkland Lake, Ontario (Fig. 2.2; Table 2.1). The outcrops display relatively thick (up to 15 m) units of conglomerate with intervening graywacke lenses that are parallel-laminated or show cross-stratification (Fig. 2.4C). Sample T-3 was obtained from a coarse graywacke unit (Fig. 2.5C). Timiskaming assemblage units at this location are interpreted to have been deposited in an alluvial-fluvial environment (Hyde, 1980; Ayer et al., 1999; Corcoran and Mueller, 2007). Corfu et al. (1991) interpreted the age of deposition of these units from the age of the youngest detrital zircon fractions in these rocks to be $<2680 \pm 3$ Ma (Table 2.1).

The sample yielded 205 concordant analyses out of a total of 224 analyses (Fig. 2.4; Appendix B). The principal group of $^{207}\text{Pb}/^{206}\text{Pb}$ ages is between ~ 2680 Ma and ~ 2775 Ma, and comprises $\sim 85\%$ of total analyses. Ages between 2775 and 2800 Ma comprise $\sim 12\%$ of the total sample population and the remaining ages ($\sim 3\%$) are between ~ 2850 and 2890 Ma.

2.4.3.4 Sample T-4

Sample T-4 was collected from a higher stratigraphic level within the Timiskaming assemblage, ~ 1.2 km to the southeast of sample T-3 in the southwest of Kirkland Lake (Fig. 2.2; Table 2.1). Similar to the sample T-3 locality, this area displays a series of interbedded graywacke and conglomerate units. Sample T-4 was collected from a graywacke unit. The Timiskaming assemblage at this locality is interpreted to have been deposited in an alluvial-fluvial environment (Hyde, 1980; Mueller and Corcoran, 1998) with a maximum depositional age of 2680 ± 3 Ma (Corfu et al., 1991).

Sample T-4 yielded 125 concordant analyses out of a total of 144 (Fig. 2.4; Appendix B). The principal group of $^{207}\text{Pb}/^{206}\text{Pb}$ ages occurs at ~ 2760 - 2680 Ma and comprises $\sim 65\%$ of the sample population. A prominent tail on the principal population is defined by ages between ~ 2900 and ~ 2800 Ma ($\sim 35\%$ of the sample population), and one zircon grain yielded a concordant $^{207}\text{Pb}/^{206}\text{Pb}$ age at ~ 3100 Ma.

2.4.3.5 Sample T-5

Sample T-5 was collected near the Morris-Kirkland gold deposit at King Kirkland, east of Kirkland Lake, Ontario (Fig. 2.2; Table 2.1). This locality preserves a succession of predominately graywacke and mudstone. Pebble conglomerate units and trachytic alkaline lava flows occur in the stratigraphic hanging wall of the graywacke and mudstone units. The graywacke and mudstone units at this location are interpreted to have been deposited in a subaqueous environment by turbidity currents as they are arranged in Bouma sequences

(Hyde, 1980). The youngest detrital zircon grains from samples in this area are interpreted to constrain the age of deposition to $<2678 \pm 3$ Ma (Table 2.1; Ayer et al., 2005). Additionally, stratigraphically above this sample location, intercalated trachytic lava flows have yielded zircon crystallization ages of 2670 ± 1 Ma (Ayer et al., 2005). Thus, the relative timing of deposition of the Timiskaming assemblage east of Kirkland Lake is ~ 2670 Ma, consistent with the <2679 - 2669 Ma range observed throughout the study area (Table 2.1).

Out of a total of 116 analyses, sample T-5 yielded 104 concordant ages (Fig. 2.4; Appendix B). The principal ~ 2750 - 2670 Ma $^{207}\text{Pb}/^{206}\text{Pb}$ age grouping comprises $\sim 90\%$ of the sample population. A subordinate set of the analyses ($\sim 10\%$) yielded ages between ~ 2750 and ~ 2850 Ma.

2.4.3.6 Sample T-6

Sample T-6 was collected at the Astoria property near Granada, south of Rouyn-Noranda area (Fig. 2.2; Table 2.1). The Timiskaming assemblage at this location is predominately comprised of polymict, pebble conglomerate and interbedded graywacke. Sample T-6 was collected from a graywacke unit. Due to close proximity to the Larder Lake-Cadillac deformation zone, Timiskaming deposits in the area are strongly deformed. Therefore, the primary sedimentological features are poorly preserved and the depositional environment of the Timiskaming assemblage at this location is unresolved (Rocheleau, 1980). The youngest detrital zircon age populations from samples in this area constrain the age of deposition to $<2674 \pm 1$ Ma (Table 2.1; Davis, 2002). Furthermore, zircon from an intercalated volcanoclastic yielded an age of 2673 ± 2 Ma and porphyritic intrusions that cross-cut the Timiskaming assemblage in Rouyn-Noranda yielded a zircon crystallization age of 2672 ± 1 Ma (Davis, 2002). Therefore, the Timiskaming assemblage in the Rouyn-Noranda area was deposited at <2674 - 2672 Ma, similar to the Timiskaming assemblage in Ontario.

From sample T-6, 145 concordant analyses were obtained from a total of 167 analyses (Fig. 2.4; Appendix B). The principal ~ 2750 - 2660 Ma $^{207}\text{Pb}/^{206}\text{Pb}$ date grouping comprises $\sim 70\%$ of the sample population. The remaining analyses ($\sim 30\%$) correspond to ages between ~ 2750 and ~ 2900 Ma. Two additional concordant ages occur at ~ 3035 Ma and ~ 3080 Ma.

2.4.3.7 Sample T-7

Sample T-7 was collected south of Rouyn-Noranda on Route des Pionniers, immediately south of the Larder Lake-Cadillac deformation zone in Quebec (Fig. 2.2; Table 2.1). Timiskaming assemblage rocks at this location are dominated by graywacke (Fig. 2.5D). Sample T-7 was collected from a laterally continuous unit of normally graded graywacke. Primary sedimentary features in these rocks include Bouma sequences and slump features.

The Timiskaming units are interpreted to have been deposited in a submarine fan system (Rocheleau, 1980). The timing of deposition of the Timiskaming assemblage in Rouyn-Noranda is constrained to <2674-2672 Ma, based on the youngest detrital zircon populations and the age of cross-cutting intrusive rock (Table 2.1; Davis 2002).

Sample T-7 yielded 155 concordant analyses out of a total of 169 zircon analyses (Fig. 2.4; Appendix B). The principal ~2775-2680 Ma $^{207}\text{Pb}/^{206}\text{Pb}$ age grouping comprises ~78% of the sample population. A subordinate set of $^{207}\text{Pb}/^{206}\text{Pb}$ ages (~15%) define a tail on the principal group from ~2900 to 2775 Ma. Eight grains yielded pre-2900 Ma ages including three grains at ~2970 Ma, three grains at ~3100 Ma, and two grains at ~3200 Ma.

2.4.3.8 Sample T-8

Sample T-8 was collected from south of the Larder Lake-Cadillac deformation zone ~7 km southwest of the LaRonde Penna deposit in Quebec (Fig. 2.2; Table 2.1). The Timiskaming assemblage at this location is comprised of interbedded pebble conglomerate and 10-20 cm thick graywacke beds. Sample T-8 was collected from a one of the graywacke beds. The rocks in the area are strongly tectonized due to their proximity to the Larder Lake-Cadillac deformation zone. Thus, the primary depositional setting is poorly constrained (Lafrance et al., 2003). Furthermore, no detrital or igneous geochronology has been conducted on the Timiskaming assemblage rocks in the vicinity of the LaRonde Penna deposit. However, based on lithologic similarities and map patterns, these rocks are correlated to units in the Rouyn-Noranda area and, thus, were likely deposited at <2674-2672 Ma (Davis, 2002).

Sample T-8 yielded 122 concordant analyses out of a total of 132 zircon analyses (Fig. 2.4; Appendix B). The principal ~2780-2680 Ma $^{207}\text{Pb}/^{206}\text{Pb}$ age grouping contains ~73% of the total number of analyses. The remaining ~27% of analyses are defined by scattered results between ~2800 and 2950 Ma.

2.5 Compiled regional U-Pb zircon data

To relate the detrital zircon signature of samples from the Abitibi and Pontiac subprovinces to potential source domains, existing U-Pb zircon data from throughout the Superior Province were compiled. These comparisons are used to make inferences about the relative spatial relationships of subprovinces and their potential crustal architecture during Neoproterozoic assembly. Results from the northern Superior Province (the North Caribou, Hudson Bay, and Arnaud River subprovinces) or the southern extent of the Province (Minnesota River Valley subprovince) were not included as these subprovinces contain ancient Eo- to Mesoarchean igneous rocks, detrital zircon, and isotopic signatures (Skulski et al., 1996, 2000; Böhm et al., 2000; Lin et al., 2006; O'Neil et al., 2008; Boily et al., 2009; David et al., 2009;

Percival et al., 2012), which are not observed in the detrital zircon samples investigated in the present study (Fig. 2.4).

2.5.1 Abitibi and Pontiac subprovinces

U-Pb zircon data for the Abitibi and Pontiac subprovinces include zircon ages derived from both igneous and sedimentary rocks (Figs. 2.6 and 2.7; Appendix B). The detrital zircon data from the sedimentary samples provide an indication of the existing constraints on the age patterns in these rocks. The igneous data constrain the age distributions of the local supracrustal rocks, which were likely major sources of zircon for the investigated successor basins. An alternative source for zircon within the Abitibi and Pontiac subprovinces, from inherited underlying crust, is also discussed.

2.5.1.1 Igneous zircon data

The igneous data are subdivided into zircon grains from samples of volcanic or plutonic rocks (Fig. 2.6A, B). The zircon data from volcanic rocks display ages from ~2750 Ma to ~2680 Ma, which correspond to the established age ranges of the volcanic assemblages in the Abitibi subprovince (Figs. 2.2 and 2.6A; Ayer et al., 2002; Thurston et al., 2008). The plutonic rocks display ages ranging from ~2740 Ma to 2660 Ma (Fig. 2.6B). The ~2740-2700 Ma ages corresponds to syn-volcanic plutonic rocks, which form spatially restricted tonalite-trondjemite-granodiorite (TTG) intrusions (Ayer et al., 2002; Appendix B). The ~2700-2680 Ma plutonic rocks are dominated by TTGs, reflecting ongoing plutonism during the onset of regional collision (Feng and Kerrich, 1992; Ayer et al., 2005). The youngest plutonic rocks (2680-2660 Ma) are dominated by alkaline, calc-alkaline, syenitic, and granitoid compositions (Ayer et al., 2005; Appendix B). In some cases, these intrusions cross-cut the sedimentary assemblages and have been used to constrain the minimum ages of sedimentation (Heather and Shore, 1999; Ayer et al., 2002, 2005; Davis, 2002; Ispolatov et al., 2008).

2.5.1.2 Detrital zircon data

Several important trends can be identified from the compiled detrital zircon data for successor basin sedimentary rocks of the Abitibi and Pontiac subprovinces (Figs. 2.6C-E and 2.7; Appendix B). The detrital zircon analyses for samples from the Porcupine assemblage, Pontiac subprovince, and Timiskaming assemblage all display principal age populations between ~2750 Ma and ~2670 Ma, similar to the age of the local igneous rocks (Fig. 2.6). In general, the largest proportion of data for the three successor basin groups clusters around the youngest age range (i.e., <2700 Ma; Fig. 2.6C, D, and E). While this may in part reflect zircon picking bias (e.g., the clearest zircons are typically picked for ID-TIMS), the presence of a large <2700 Ma zircon population is consistent with our own data. Potential proximal sources for

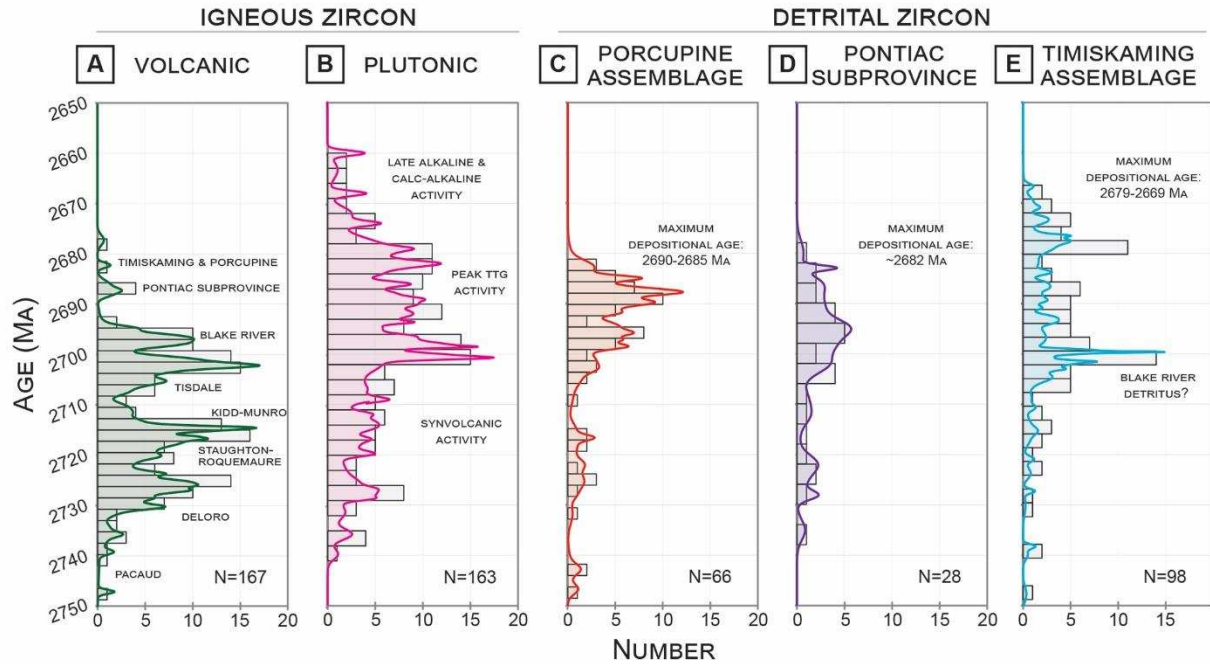


Figure 2.6 – Compiled U-Pb zircon age data from the Abitibi and Pontiac subprovince. Probability density function curves (filled solid lines) and frequency histograms (rectangles) for zircon age data (<2750 Ma) compiled from published data for the Abitibi and Pontiac subprovinces. $^{207}\text{Pb}/^{206}\text{Pb}$ age data derived from igneous rocks are subdivided into volcanic (A) and plutonic (B). The detrital zircon age data are subdivided into the Porcupine assemblage (C), Pontiac subprovince (D), and Timiskaming assemblage (E).

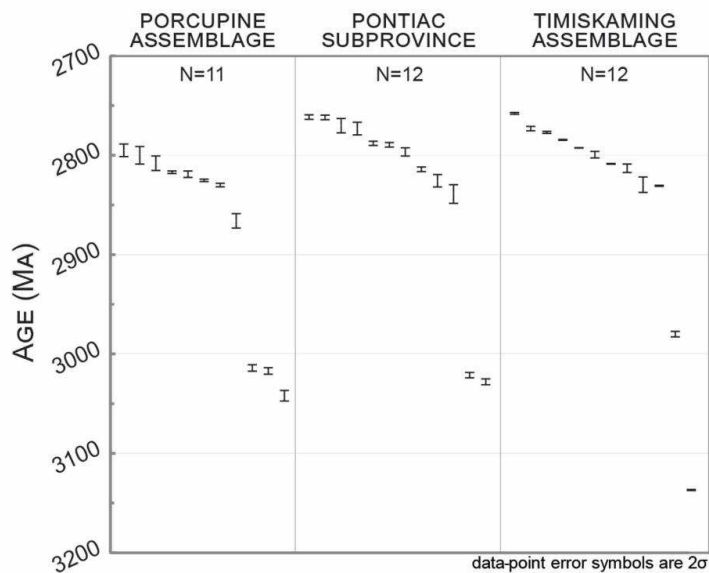


Figure 2.7 – Individual, pre-2750 Ma detrital zircon ages from published data. Ages were derived from isotope dilution - thermal ionization mass spectroscopy and include data for the Porcupine assemblage, Pontiac subprovince, and Timiskaming assemblage.

these grains are the <2700 Ma predominately felsic intrusions and to a lesser extent volcanic rocks (Fig. 2.6A, B; Feng and Kerrich, 1992; Ayer et al., 2002). These plutonic rocks may have been exhumed soon after crystallization, providing detritus to successor basins in the Abitibi and Pontiac subprovinces. This is comparable to the 'Timiskaming-type' Midway sequence, Cross Lake Group, and Crowduck basin successions elsewhere in the Superior Province (Jirsa, 2000; Corcoran and Mueller, 2007). Pre-2750 Ma data include 2850-2750 Ma and more rare ~3200-3000 Ma detrital zircon grains (Fig. 2.7). The majority of these pre-2750 Ma grains were reported in samples from the Quebec portion of the study area (Gariépy et al., 1984; Feng and Kerrich, 1991; Davis, 2002; David et al., 2006; Mercier-Langevin et al., 2007), while a limited number of the data were from samples from Ontario (Ayer et al., 2002; Ayer and Chartrand, 2011; Appendix B). However, due to the limited number of grains per sample analyzed in these studies, it is difficult to characterize any differences and similarities from these data.

2.5.1.3 Inherited zircon data

An alternative detrital zircon source may be inherited zircon in igneous rocks sourced from a potential basement below the Abitibi subprovince. The presence of an older crustal component in the Abitibi subprovince has been recognized previously based on whole-rock isotopic signatures and inherited zircon grains in igneous rocks. For example, in the western part of the Abitibi subprovince, Hf, Nd, and Pb isotopic signatures in volcanic rocks are consistent with contamination by older, 2900-2800 Ma crust (Barrie and Shirey, 1991; Ketchum et al., 2008). Furthermore, inherited ~2925 Ma and ~2860-2850 Ma zircon grains have been documented in volcanic rocks and ~2740-2700 Ma syn-volcanic plutonic rocks in the western Abitibi subprovince (Ayer et al., 2002, 2005; Ketchum et al., 2008). Thus, a 2900-2800 Ma crustal substrate may underlie portions of the Abitibi subprovince (Ketchum et al., 2008).

2.5.2 Southern Superior Province

To assess potential source regions for the Mesoarchean zircon grains observed in the graywacke samples from the Abitibi and Pontiac subprovinces, we compiled published U-Pb zircon geochronology for the southern Superior Province. The following sections contain a brief geologic background for each region to contextualize the compilation data.

2.5.2.1 The Wawa subprovince

The Wawa subprovince occurs to the west of the Kapuskasing structural zone (Fig. 2.1). It is composed of greenstone belts, plutonic complexes, and gneissic domains that are of comparable age to supracrustal rocks in the Abitibi subprovince (Fig. 2.8A; Moser et al., 1996; Corfu and Stott, 1998; Stott et al., 2010; Lodge et al., 2013; Lodge, 2016). Greenstone belts in the northern Wawa subprovince largely consist of ~2720 Ma volcanic rocks, which are

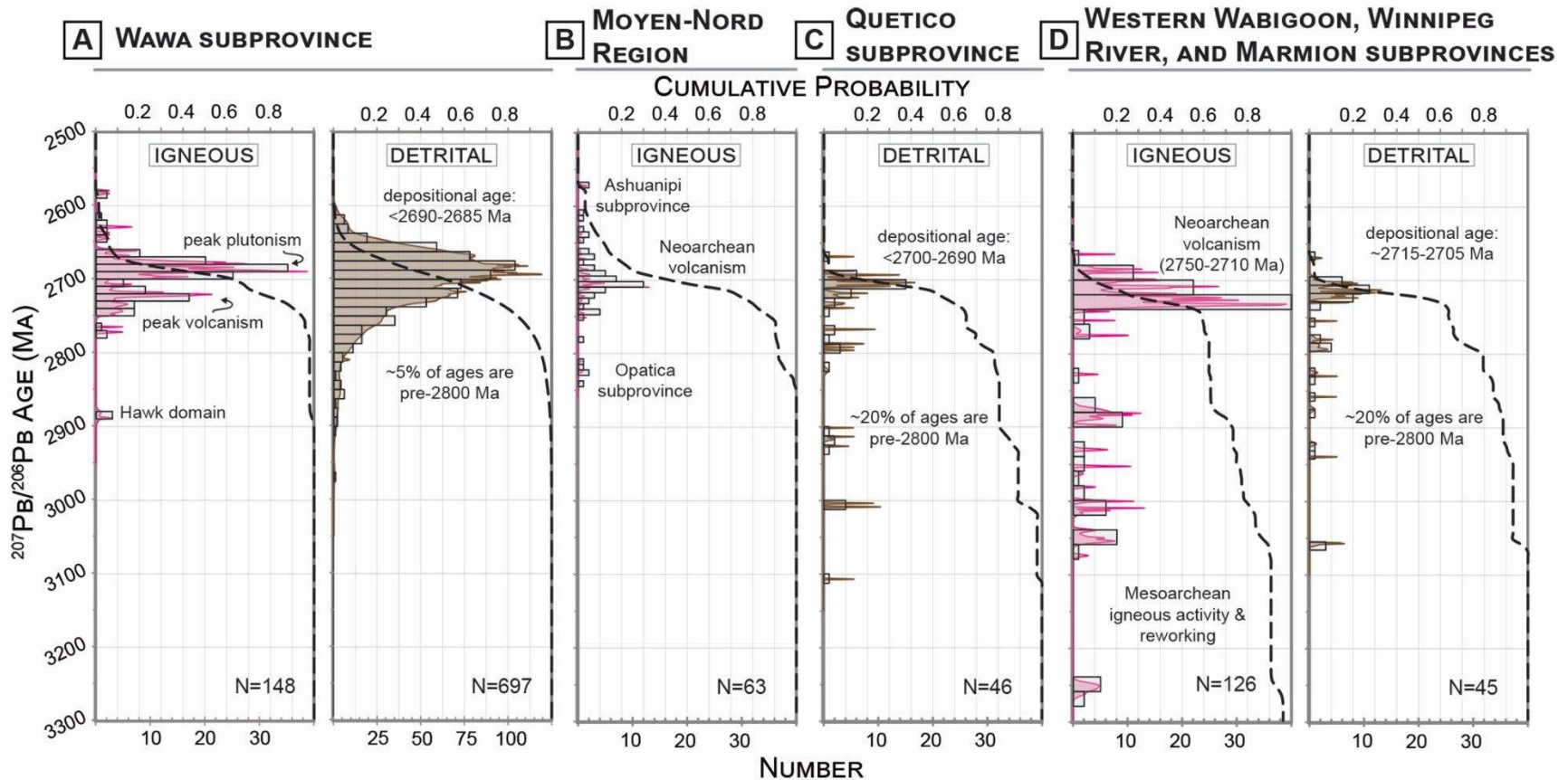


Figure 2.8 – Compilation of published zircon age data for the southern Superior Province. Probability density function curves (filled solid color lines), cumulative distribution function curves (dashed black lines), and frequency histograms (rectangles) for U-Pb zircon data compiled from the southern Superior Province. Data are divided based on reported subprovince or domain: Wawa subprovince (A), Moyen-Nord region (B), Quetico subprovince (C), and Western Wabigoon, Winnipeg River, and Marmion subprovinces (D). The data are further subdivided into zircon grains analyzed from igneous rocks and detrital grains from sedimentary rocks.

interpreted as having formed in an arc to fore- or back-arc setting (Fig. 2.8A; Lodge, 2016). Peak plutonism in the Wawa subprovince occurred at ~2700-2690 Ma and was broadly coeval with the onset of collision and the formation of successor basin successions at 2690-2685 Ma (Fig. 2.8A; Corfu and Stott, 1998; Appendix B). These successor basins are coeval with the Porcupine assemblage in the Abitibi subprovince. The principal detrital zircon population (~95%) in the compiled data is made up of ~2750-2650 Ma ages with the remaining 5% of these ages between 2800 and 2900 Ma (Fig. 2.8A). The majority of these data are LA-ICP-MS analyses with >100 grains per sample (Lodge et al., 2013), and are statistically comparable with this study. The Wawa subprovince also contains limited exposures of ~2900 Ma volcanic-plutonic rocks that are attributed to the Hawk domain (Figs. 2.1 and 2.8A; Turek et al., 1992). This domain is only exposed in a <100 km² large area, but is thought to underlie portions of the southeastern Wawa subprovince and western portions of the Abitibi subprovince (Fig. 2.1; Turek et al., 1992; Moser et al., 1996; Ketchum et al., 2008).

2.5.2.2 The Moyen-Nord region

The Moyen-Nord region occurs to the north of the Abitibi subprovince and is defined here to include the Opatoca, Nemiscau, Opinaca, Ashuanipi, and Eastmain subprovinces (Fig. 2.1). The Opatoca subprovince occurs immediately to the north of the Abitibi subprovince and is composed of ~2820 Ma tonalite, 2770-2700 Ma tonalite-granodiorite, and 2680 Ma granite units (Fig. 2.8B; Sawyer and Benn, 1993; Davis et al., 1994). The poorly understood and exposed Nemiscau and Opinaca subprovinces (Fig. 2.1) are primarily composed of metasedimentary rocks and granites that have been metamorphosed at amphibolite to granulite facies conditions with localized formation of migmatite (Simard and Gosselin, 1999; Goutier et al., 2002) and may be correlative to the English River subprovince in the western Superior Province (Percival et al., 2012). The Ashuanipi subprovince (Fig. 2.1) is a 300 x 300 km domain of largely high-grade, ~2680-2570 Ma metamorphic and plutonic rocks that represent some of the youngest Neoproterozoic igneous rocks in the Superior Province (Fig 2.9B; Percival et al., 1992). Lastly, the Eastmain subprovince (Fig. 2.1) is a domain of largely juvenile, ~2720-2700 Ma volcanic rocks (Fig. 2.8B; Goutier et al., 1999) that may correlate with the Oxford-Stull and Uchi domains to the west (Fig. 2.1; Percival et al., 2012).

2.5.2.3 The Quetico subprovince

The Quetico subprovince (Fig. 2.1) is an ENE-trending narrow domain of primarily metasedimentary rocks between the Wawa subprovince to the south, and the Western Wabigoon and Marmion subprovinces to the north. All are truncated by the Kapuskasing structural zone to the east. The Quetico subprovince is primarily comprised of complexly

deformed metagraywacke with associated migmatite and granite (Percival, 1989; Davis et al., 1990). The age of deposition of graywacke successions of the Quetico subprovince is bracketed to ~2700-2695 Ma in the north (Davis et al., 1990) and as young as ~2692-2690 Ma in the south (Zaleski et al., 1999; Fralick et al., 2006) based on the age of the youngest detrital zircon populations and the age of cross-cutting plutonic rocks (Fig. 2.8C). Detrital zircon data principally include ~2750-2700 Ma zircon (~65%; Fig. 2.8C), with some ~2950-2750 Ma and rare 3050 Ma zircon (Fig. 2.8C). This is consistent with provenance from the Western Wabigoon, Winnipeg River, and Marmion subprovinces (Davis et al., 1990; Fralick et al., 2006).

2.5.2.4 The Western Wabigoon, Winnipeg River, and Marmion subprovinces

The Western Wabigoon subprovince (Fig. 2.1) is composed of largely juvenile volcanic and plutonic rocks formed at ~2750-2710 Ma (Fig. 2.8D; Ayer and Davis, 1997). Similarly aged volcanic successions occur in the Winnipeg River and Marmion subprovinces (Fig. 2.1), where they overlie older gneissic-plutonic rocks with zircon ages of ~3250 Ma and 3100-2800 Ma (Fig 2.9D; Corfu, 1996; Stott et al., 2002; Tomlinson et al., 2004; Davis et al., 2005; Melnyk et al., 2006). These Paleo- to Mesoarchean crustal components record ~2920 Ma amalgamation of the Winnipeg River and Marmion subprovinces (Tomlinson et al., 2004), and, in part, may represent rifted components of a Paleoproterozoic Superior Craton (Davis et al., 2005; Bédard and Harris, 2014).

The Western Wabigoon, Winnipeg River, and Marmion subprovinces all contain successor basin deposits that unconformably overlie deformed Paleo- to Neoproterozoic volcanic-plutonic rocks. These basins formed in response to the initiation of collisional deformation at <2715-2705 Ma (Fig. 2.8D; Ayer and Davis, 1997; Stott et al., 2002; Corcoran and Mueller, 2007). Detrital zircon data are ~80% Neoproterozoic, with the remaining ages forming groupings at 2900-2800 Ma, ~2950 Ma, and ~3050 Ma (Fig. 2.8D). This pattern is similar to that observed in the Quetico subprovince (e.g., Fig. 2.8C), potentially indicative of a shared provenance.

2.6 Summary of detrital zircon age distributions for graywacke samples of the Abitibi and Pontiac subprovinces

All graywacke samples from the Abitibi and Pontiac subprovinces display a principal ~2775-2680 Ma age group that comprises ~80-95% of the individual sample populations (Fig. 2.4). The youngest dates in all samples are consistent with published ID-TIMS data for the youngest zircon populations in the assemblages from which they were sampled (Supplemental Table 2.1; Corfu et al., 1991; Bleeker et al., 1999; Davis, 2002; Ayer et al., 2002, 2003, 2005). However, proportions of older, Mesoarchean (3200-2800 Ma) ages vary between samples: Porcupine assemblage samples yielded <1-10% Mesoarchean ages, while Pontiac subprovince

samples contain 15-21% and Timiskaming assemblage samples contain 5-20% Mesoarchean ages (Fig. 2.4). Across all samples analyzed, the largest proportion of the Mesoarchean ages occur between ~2950 Ma and ~2800 Ma (Figs. 2.4 and 2.9), with minor (<1%) clusters or individual ages at ~3000 Ma, ~3100 Ma, and ~3200 Ma (Fig. 2.4). Figure 2.9 displays the aggregate results in this study grouped into Porcupine assemblage, Pontiac subprovince, and Timiskaming assemblage samples. The Porcupine assemblage data consists of ~95% 2800-2685 Ma and ~5% 3200-2800 Ma ages. In contrast, the Pontiac subprovince samples consist of ~82% 2800-2680 Ma, ~15% 2900-2800 Ma, and ~3% 3200-2900 Ma ages. Lastly, the Timiskaming assemblage data consists of ~87% 2800-2670 Ma, ~10% 2900-2800 Ma, and ~3% 3200-2900 Ma ages.

To assess potential spatial variations in the sample set we compared the CDF curves for each sub-region of the study area (Fig. 2.10). In the Rouyn-LaRonde area, the Porcupine and Timiskaming assemblages contain similar proportions of data in all age ranges, and are characterized by ~89-90% Neoproterozoic ages and 10-11% Mesoarchean ages (Fig. 2.10). The Pontiac subprovince sample from the Rouyn-Noranda area contains a similar distribution of age data, but displays a higher proportion (~15%) of Mesoarchean zircon ages. The western Pontiac subprovince sample displays a relatively high proportion of Mesoarchean data (~21%) with the remaining results corresponding to Neoproterozoic ages. In the Kirkland-Larder Lakes area the Porcupine assemblage contains ~5% Mesoarchean data, while the Timiskaming assemblage contains ~9% Mesoarchean data. The Porcupine and Timiskaming assemblage samples from the Timmins area display significantly different proportions of Mesoarchean detrital zircon. In this area, the Porcupine assemblage samples contain ~2% Mesoarchean ages, while the Timiskaming assemblage samples contain ~17%.

2.7 Provenance and tectonic significance

Statistical analysis of the U-Pb detrital zircon LA-ICP-MS results reveals that the successor basins in the Abitibi and Pontiac subprovinces contain between 80 and 95% Neoproterozoic and between 5 and 20% Mesoarchean detrital zircon grains (Fig. 2.4). Neoproterozoic igneous sources are ubiquitous in the Abitibi subprovince and Neoproterozoic zircon was therefore probably locally derived. The fact that the cumulative proportion of detrital zircon grains that crystallized within 100 Ma of their depositional age is 75-95% of each sample (Fig. 2.4) is consistent with deposition at a convergent plate margin (cf. Cawood et al., 2012). A convergent margin setting is consistent with seismic and structural data, which indicate that structures related to folding, thrusting, and ductile transpression dominate the boundary between the Abitibi and Pontiac subprovinces (Dimroth et al., 1983; Camiré and Burg., 1993; Jackson et al.,

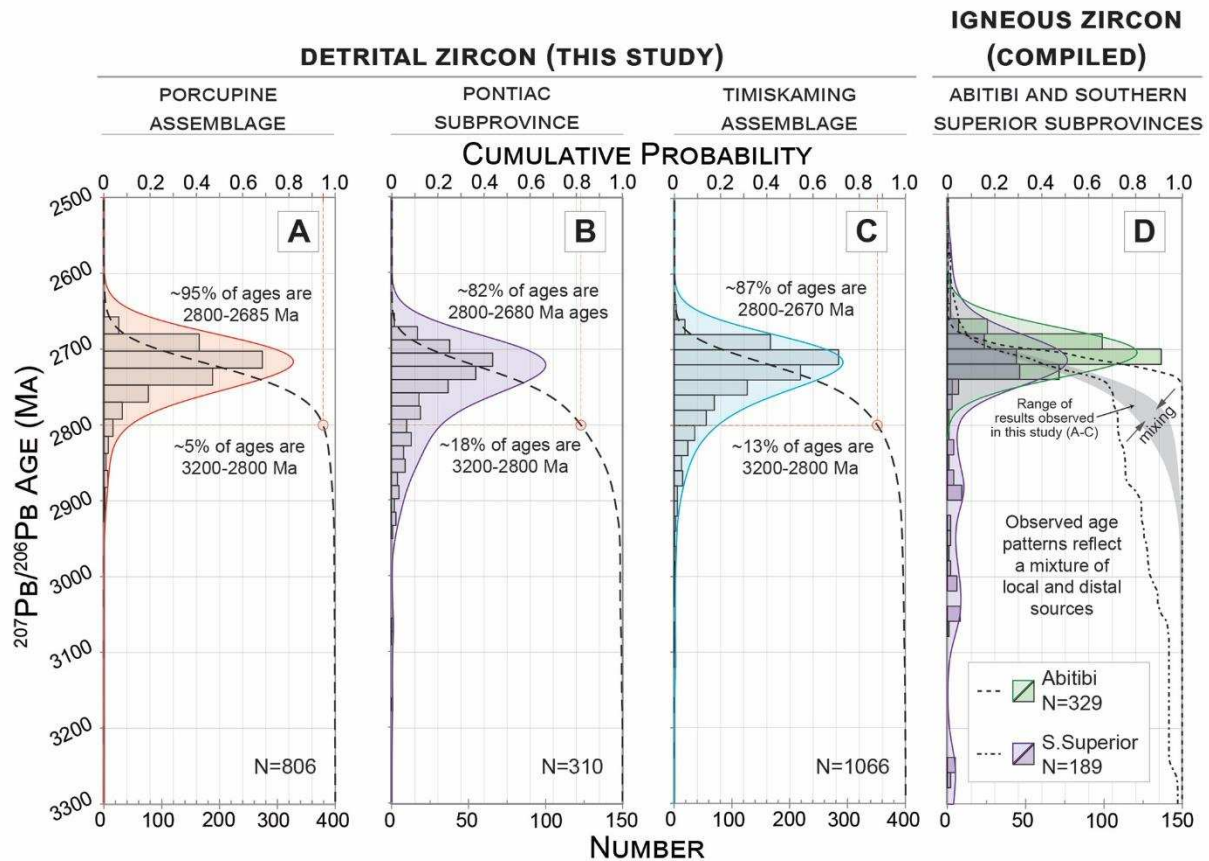


Figure 2.9 – Comparison of detrital zircon age results from this study to published zircon age data. Probability density function curves (filled solid color lines), cumulative distribution function curves (dashed black lines), and frequency histograms (rectangles) showing the aggregate detrital zircon age data for the Porcupine assemblage (A), Pontiac subprovince (B), and Timiskaming assemblage (C) graywacke samples investigated in this study.

1994; Ayer et al., 2002, 2005; Percival et al., 2012). These studies also indicated that the Abitibi and Pontiac subprovinces were structurally juxtaposed. However, the general similarity between detrital zircon signatures in the graywacke samples from the Abitibi and Pontiac subprovinces supports the conclusion by Davis (2002) that the Pontiac subprovince formed proximal to, and has had a largely shared history with, the Abitibi subprovince.

A potential source for Mesoproterozoic zircon may be underlying crust in portions of the Abitibi and Wawa subprovinces (sections 2.5.1.3 and 2.5.2.1). However, the present day exposure of 2900-2800 Ma rocks is rare in the Wawa subprovince and absent in the Abitibi subprovince. Furthermore, exposure of these rocks was probably minimal at the time of the deposition of the successor basins, due to prior formation of extensive Neoproterozoic volcanic successions. Lastly, there is no indication that pre-2900 Ma crust underlies portions of the Abitibi and Wawa subprovinces. Thus, inherited zircon components cannot explain the detrital

zircon age patterns observed, and it is unlikely that zircon from these sources significantly contributed to the detrital zircon record in the successor basins investigated.

Our data display predominately local detrital zircon signatures in the Porcupine assemblage samples (<5% Mesoarchean zircon), but larger proportions of 'exotic' zircon in Porcupine subprovince and Timiskaming assemblage samples (>13% Mesoarchean zircon). Furthermore, successor basin rocks in the Wawa subprovince, which are coeval with the Porcupine assemblage (~2690-2685 Ma; Corfu and Stott, 1998), also contain <5% Mesoarchean zircon (Fig. 2.8A; Lodge et al., 2013). Prior to ~2690 Ma, detritus derived from the north was most likely to have been deposited in the Quetico subprovince (Fralick et al., 2006). However, by ~2685 Ma, progressive uplift and erosion of the Quetico subprovince occurred (Fralick et al., 2006), which would have allowed for greater inputs of distally derived zircon to the successor basins in the Abitibi and Pontiac subprovinces. This is consistent with conclusions based on whole-rock geochemical data. Porcupine assemblage rocks in the Abitibi subprovince display a 'mafic enriched' signature, consistent with derivation from the local supracrustal rocks (Feng and Kerrich, 1990). In contrast, Pontiac subprovince and Timiskaming assemblage sedimentary rocks have been documented to display 'low mafic' signatures, consistent with derivation from a distal, deeply eroded greenstone belt (Feng and Kerrich, 1990; Camiré et al., 1993; Feng et al., 1993).

Since Mesoarchean zircon was unlikely to have been derived from within the Abitibi, Pontiac, and Wawa subprovinces, these zircon grains must have been transported across subprovince or terrane boundaries from a developing hinterland. Only a limited number of terranes have potential sources for Mesoarchean zircon but are devoid of older, Eo- to Paleoproterozoic zircon (section 2.5; Figs. 2.1, 2.6, and 2.8). The Marmion, Winnipeg River, and Opatca subprovinces contain rocks with ~3200-2800 Ma zircon crystallization ages (Fig. 2.8). These subprovinces have been interpreted as significant sources for Quetico subprovince sedimentary rocks (Fralick et al., 2006), were actively deforming at the time of deposition in the Abitibi and Pontiac subprovinces (Corfu and Stott, 1993; Percival et al., 2006; Sanborn-Barrie and Skulski, 2006), and are interpreted as the most likely source hinterland for the Mesoarchean detrital zircon observed in this study (Figs. 2.4, 2.7, and 2.9). The larger proportion of Mesoarchean zircon in Pontiac subprovince and Timiskaming assemblage graywacke versus Porcupine assemblage graywacke may reflect progressive uplift and exhumation of this hinterland. Similarly aged sources in the North Caribou subprovinces have been interpreted as the source for sedimentary rocks of the English River subprovince (Davis et al., 1990; Davis, 1996). However, contractional deformation in these subprovinces culminated at

~2700 Ma and the active deformational front had propagated south of the North Caribou subprovinces by ~2690 Ma (Sleep, 1992; Corfu and Stone, 1998). It is, therefore, most likely that the Winnipeg River, Marmion, and Opatoca subprovinces were the principal source for the ~3200-2800 Ma detrital zircon observed in this study.

The difference in the proportion of Mesoarchean zircon between the Porcupine and Timiskaming assemblages varies across the study area (Fig. 2.10). The increase in Mesoarchean zircon from Porcupine assemblage to Timiskaming assemblage samples is best developed in the Timmins area and to a lesser extent in the Kirkland Lake-Larder Lake area (Fig. 2.10). In contrast, the Porcupine assemblage samples in the Rouyn-LaRonde area contain similar proportions of Mesoarchean zircon (~10%) as the Timiskaming assemblage samples in the same area (Fig. 2.10). It is possible that Porcupine assemblage basins in the Rouyn-LaRonde area had different sources from similarly aged basins in the Timmins area. In contrast to the Porcupine assemblage samples, in which Mesoarchean input increases from west to east, Mesoarchean input to Timiskaming assemblage samples decreases to the east (Fig. 2.10). If this is indeed reflective of exposure in source regions, it suggests that the source for Mesoarchean zircon changed with time from a north-easterly location to a north-westerly location. The two Pontiac subprovince samples contain more Mesoarchean zircon grains than the adjacent Porcupine and Timiskaming assemblages (Fig. 2.9). These samples display an increase in Mesoarchean zircon towards the west from 15% to 21% (Fig. 2.10), in a pattern similar to the Timiskaming assemblage, suggesting a westerly source. The fact that the Pontiac subprovince sedimentary rocks contain more Mesoarchean zircon grains than the Porcupine and Timiskaming assemblages, may suggest they received additional input from a separate Mesoarchean source, perhaps in addition to the Quetico subprovince.

The data presented here, integrated with regional scale understanding of the Superior Province constrain patterns characterized by (1) southward younging of Neoproterozoic volcanism, felsic plutonism, and associated successor basin formation, (2) southward migration of contractional deformation and subprovince assembly and (3) progressive uplift of the hinterland with time (Fig. 2.11). The detrital zircon record in successor basins in the Abitibi and Pontiac subprovinces record the <2690 Ma portion of this evolution. These patterns can be explained by several geodynamic models. The first model is that of modern-style accretionary orogenic processes. In this model the observed patterns predominately relate to successive subprovince or terrane docking and oblique collision from north to south between ~2720 and ~2665 Ma (Percival et al., 2012). In comparison, the northern Appalachians, display a northwestward younging of plutons, contractional deformation, and formation of foreland basins that is

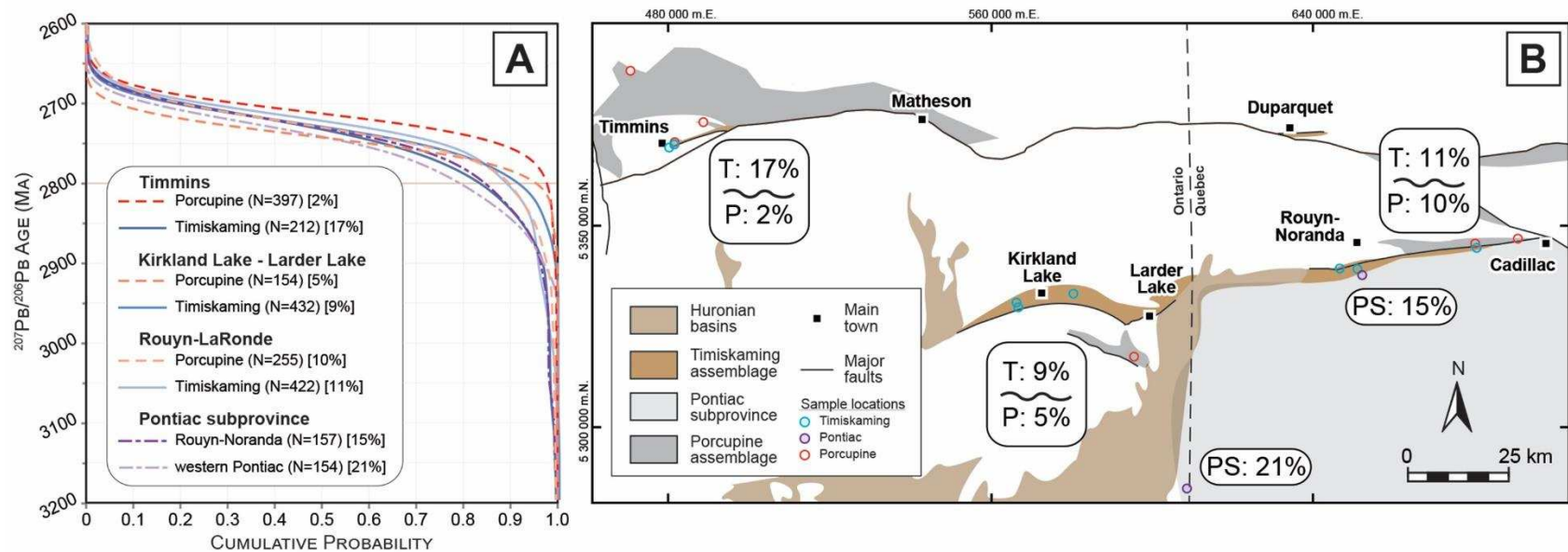


Figure 2.10 – Spatial comparison of detrital zircon age results. (A) Cumulative distribution function curves of the detrital zircon $^{207}\text{Pb}/^{206}\text{Pb}$ age data from the Abitibi and Pontiac subprovinces grouped by relative geographic distribution. The number of U-Pb ages included in each group are indicated in parentheses. The percentages of 3200-2800 Ma zircon in each group are indicated in brackets. (B) Schematic map displaying the distribution of Porcupine assemblage, Pontiac subprovince, and Timiskaming assemblage sedimentary rocks relative to major faults. The proportion of Mesoarchean zircon in graywacke samples for each portion of the study area are indicated. P=Porcupine assemblage, PS= Pontiac subprovince, and T=Timiskaming assemblage.

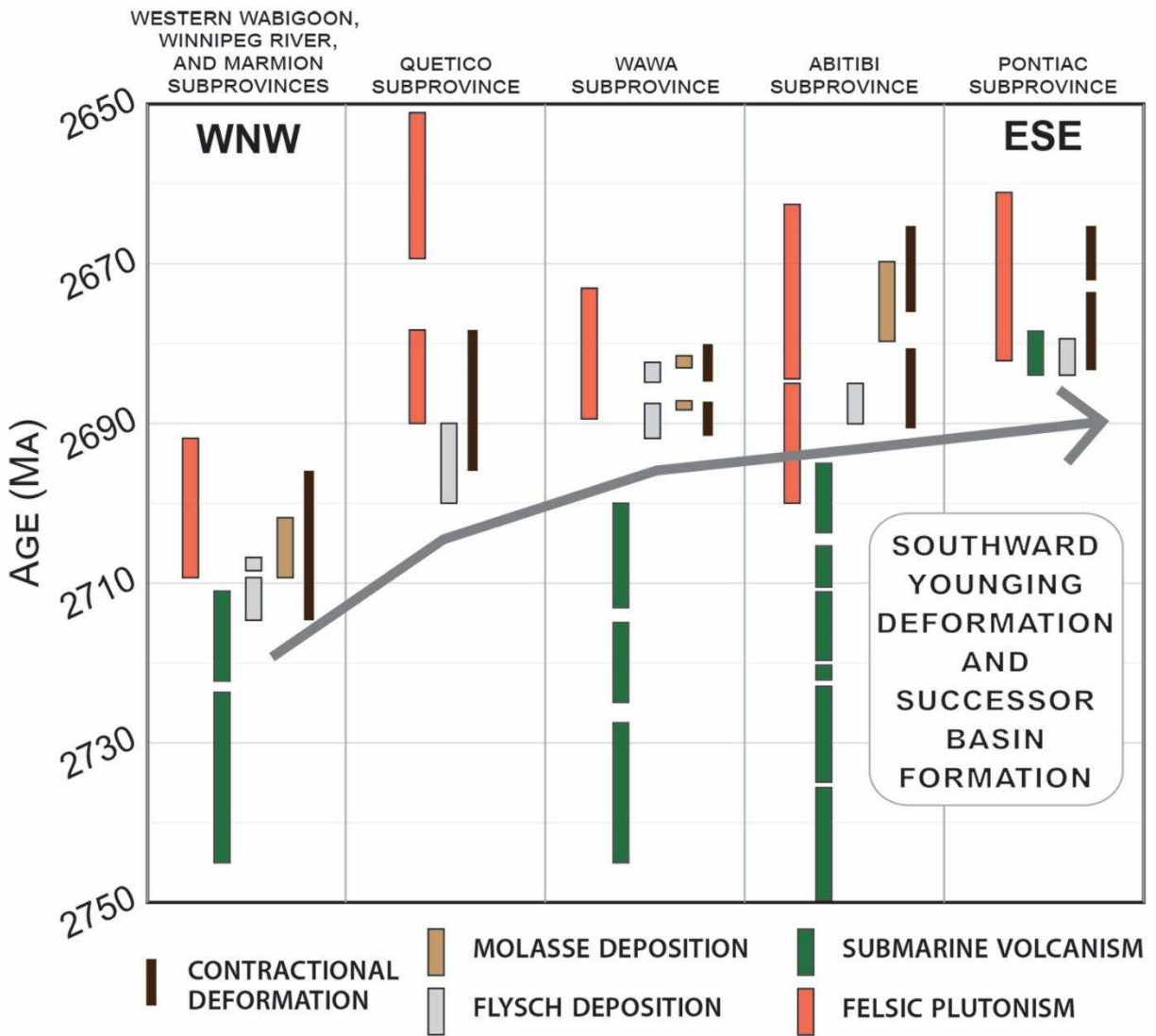


Figure 2.11 – Schematic time-space diagram for the southern Superior Province. The diagram displays the relative timing of deformation, successor basin formation, submarine volcanism, and felsic plutonism for the regions affected by progressive Neoproterozoic tectonism in the southern Superior Province

interpreted as a result of accretion of terranes during the mid-Paleozoic Acadian orogeny (Bradley et al., 2000). The similarity of the patterns observed in the southern Superior Province to those observed in the northern Appalachians suggests that modern-style plate tectonic driven accretionary processes may have operated in the Neoproterozoic. The second model, based on the geology of the Superior Province, is that the formation of ribbon continents and oceanic, Neoproterozoic volcanic subprovinces occurred during disaggregation of older, pre-2800 Ma cratonic components, as a result of radial outflow of upwelling mantle during a mantle overturn event that started at ~2780 Ma (Bédard and Harris, 2014). In this model, a shift in mantle flow at ~2720 Ma differentially pushed the northern Superior Province to the south, resulting in the <2720 Ma contractional deformation and reassembly of the craton (Bédard and Harris, 2014). Discriminating between the plate tectonic and mantle overturn models is difficult from the detrital zircon record alone and the data can be interpreted as broadly compatible with both. However, given the diverse ages (Eo- to Neoproterozoic) and independent pre-juxtaposition histories of subprovinces or terranes, as well as the spatial and temporal patterns of contractional deformation, magmatism, and provenance outlined above, we consider that a form of plate tectonic processes operated during Neoproterozoic assembly of the Superior Province. These interpretations are consistent with the inference that subduction-accretion plate tectonic processes initiated prior to 2.7 Ga (Smithies et al., 2003; O'Neill et al., 2007; Wyman et al., 2008).

2.8 Conclusions

LA-ICP-MS U-Pb analysis of detrital zircon from syn-deformational sedimentary deposits in the Abitibi and Pontiac subprovinces indicates that all graywacke samples contain large proportions (75-95%) of Neoproterozoic zircon grains with subordinate (5-25%) Mesoproterozoic zircon grains. The fact that 75-95% of the detrital zircon grains crystallized within <100 Ma of their depositional age is consistent with deposition at a convergent plate margin (cf. Cawood et al., 2012). The occurrence of Mesoproterozoic zircon requires a source from an older hinterland. The hinterland, in part, likely consisted of the Winnipeg River, Marmion, and Opatica subprovinces. The <2690-2685 Ma Porcupine assemblage graywacke samples contain a lower proportion of Mesoproterozoic zircon than the <2679-2669 Ma Timiskaming assemblage graywacke samples, which likely indicates progressive uplift of the orogenic hinterland and shedding of sedimentary material into the subaqueous successor basins. This interpretation is consistent with southward migration of deformation and successor basin formation in the southern Superior Province. Sediment transport across subprovince or terrane boundaries, foreland-directed propagation of the orogenic front, and progressive hinterland emergence,

recorded by successor basins of the Abitibi and Pontiac subprovinces, is similar to trends observed in modern-style collisional or accretionary orogens.

2.9 Acknowledgements

Sample collection at Hoyle Pond and Kidd Creek was logistically supported by Goldcorp and Glencore. We are indebted to E. Barr and T. Gemmell for help provided on site. Field work was in part financially supported by Geological Society of America and Society of Economic Geologists Canada Foundation graduate student research grants to BMF and Colorado School of Mines Professional Development funds to YDK. The analytical research would not have been possible without the generous financial support by Osisko Mining. We thank B. Wares for his continuous interest in the progress of this research and his helpful comments on the geology of the Abitibi subprovince.

2.10 References

- Ayer, J.A., Chartrand, J.E., 2011. Geological compilation of the Abitibi greenstone belt. Ontario Geological Survey Miscellaneous Release – Data 282.
- Ayer, J.A., Davis, D.W., 1997. Neoproterozoic evolution of differing convergent margin assemblages in the Wabigoon Subprovince: Geochemical and geochronological evidence from the Lake of the Woods greenstone belt, Superior Province, northwestern Ontario. *Precambrian Research* 81, 155–178.
- Ayer, J., Berger, B., Johns, G., Trowell, N., Born, P., and Mueller, W.U., 1999, Late Archean rock types and controls on gold mineralization in the southern Abitibi greenstone belt of Ontario: Geological Association of Canada – Mineralogical Association of Canada Joint Annual Meeting, Sudbury, Canada, 1999, Field Trip B3 Guidebook, 73 p.
- Ayer, J., Amelin, Y., Corfu, F., Kamo, S., Ketchum, J., Kwok, K., Trowell, N., 2002. Evolution of the southern Abitibi greenstone belt based on U-Pb geochronology: Autochthonous volcanic construction followed by plutonism, regional deformation and sedimentation. *Precambrian Research* 115, 63–95. doi:10.1016/S0301-9268(02)00006-2
- Ayer, J.A., Barr, E., Bleeker, W., Creaser, R.A., Hall, G., Ketchum, J.W.F., Powers, D., Salier, B., Still, A., Trowell, N.F., 2003. New geochronological results from the Timmins area: Implications for the timing of late-tectonic stratigraphy, magmatism and gold mineralization. Ontario Geological Survey Open File Report 6120, 33–1 to 33–11.
- Ayer, J.A., Thurston, P.C., Bateman, R., Dubé, B., Gibson, H.L., Hamilton, M.A., Hathway, B., Hocker, S.M., Houlié, M.G., Hudak, G., Ispolatov, V.O., Lafrance, B., Leshner, C.M., MacDonald, P.J., Pélouquin, A.S., Piercey, S.J., Reed, L.E., Thomson, P.H., 2005. Overview of results from the greenstone architecture project: Discover Abitibi Initiative, Open File Report 6154, 146 p.
- Barrie, C.T., Shirey, S.B., 1991. Nd- and Sr-isotope systematics for the Kamiskotia-Montcalm area: Implications for the formation of the late Archean crust in the western Abitibi subprovince, Canada. *Canadian Journal of Earth Sciences* 28, 58–76.
- Bateman, R., Ayer, J.A., Dubé, B., 2008. The Timmins-Porcupine gold camp, Ontario: Anatomy

- of an Archean greenstone belt and ontogeny of gold mineralization. *Economic Geology* 103, 1285–1308. doi:10.2113/gsecongeo.103.6.1285
- Bédard, J.H., 2006. A catalytic delamination-driven model for coupled genesis of Archaean crust and sub-continental lithospheric mantle. *Geochimica et Cosmochimica Acta* 70, 1188–1214. doi:10.1016/j.gca.2005.11.008
- Bédard, J.H., Harris, L.B., 2014. Neoproterozoic disaggregation and reassembly of the Superior craton. *Geology* 42, 951–954. doi:10.1130/G35770.1
- Bédard, J.H., Brouillette, P., Madore, L., Berclaz, A., 2003. Archaean cratonization and deformation in the northern Superior Province, Canada: An evaluation of plate tectonic versus vertical tectonic models. *Precambrian Research* 127, 61–87. doi:10.1016/S0301-9268(03)00181-5
- Benn, K., Moyen, J.-F., 2008. The late Archean Abitibi-Opatika terrane, Superior Province: A modified oceanic plateau. *The Geological Society of America Special Paper* 440, 173–197.
- Benn, K., Miles, W., Ghassemi, M.R., Gillett, J., 1994. Crustal structure and kinematic framework of the northwestern Pontiac subprovince, Quebec: An integrated structural and geophysical study. *Canadian Journal of Earth Sciences* 31, 271–281.
- Bleeker, W., Parrish, R.R., 1996. Stratigraphy and U-Pb zircon geochronology of Kidd Creek: Implications for the formation of giant volcanogenic massive sulphide deposits and the tectonic history of the Abitibi greenstone belt. *Canadian Journal of Earth Sciences* 33, 1213–1231.
- Bleeker, W., van Breemen, O., 2011. New geochronological, stratigraphic, and structural observations on the Kidd-Munro assemblage and the terrane architecture of the south-central Abitibi greenstone belt, Superior Craton, Canada. *Ontario Geological Survey Open File Report* 6258, 35 p.
- Bleeker, W., Parrish, R.R., Sager-Kinsman, S., 1999. High-precision U-Pb geochronology of the late Archean Kidd Creek deposit and surrounding Kidd volcanic complex. *Economic Geology Monograph* 10, 43–70.
- Bleeker, W., Kamo, S.L., Atkinson, B.T., Stalker, M., 2015. Constraining the age of synorogenic conglomerate and sandstone in Penhorwood Township, northern Swayze greenstone belt. *Ontario Geological Survey Open File Report* 6313, 40–1 to 40–10.
- Blichert-Toft, J., 2008. The Hf isotopic composition of zircon reference material 91500. *Chemical Geology* 253, 252–257. doi:10.1016/j.chemgeo.2008.05.014
- Böhm, C.O., Heaman, L.M., Creaser, R.A., Corkery, M.T., 2000. Discovery of pre-3.5 Ga exotic crust at the northwestern Superior Province margin, Manitoba. *Geology* 28, 75–78. Doi:10.1130/0091-7613(2000)28<75:DOPGEC>2.0.CO;2
- Boily, M., Leclair, A., Maurice, C., Bédard, J.H., David, J., 2009. Paleo- to Mesoproterozoic basement recycling and terrane definition in the northeastern Superior Province, Québec, Canada. *Precambrian Research* 168, 23–44. doi:10.1016/j.precamres.2008.07.009

- Born, P., 1995. A sedimentary basin analysis of the Abitibi greenstone belt in the Timmins area, northern Ontario, Canada. Unpublished Ph.D. thesis, Carleton University, Ottawa, Ontario, 489 p.
- Bradley, D.C., Tucker, R.D., Lux, D.R., Harris, A.G., McGregor, D.C., 2000. Migration of the Acadian orogen and foreland basin across the northern Appalachians of Maine and adjacent areas. U.S. Geological Survey Professional Paper 1624, 49 p.
- Calvert, A.J., Ludden, J.N., 1999. Archean continental assembly in the southeastern Superior Province of Canada. *Tectonics* 18, 412–429.
- Camiré, G.E., Burg, J.-P., 1993. Late Archean thrusting in the northwestern Pontiac Subprovince, Canadian Shield. *Precambrian Research* 61, 51–66. doi:10.1016/0301-9268(93)90057-9
- Camiré, G.E., Laflèche, M.R., Ludden, J.N., 1993. Archean metasedimentary rocks from the northwestern Pontiac Subprovince of the Canadian Shield: Chemical characterization, weathering and modelling of the source areas. *Precambrian Research* 62, 285–305. doi:10.1016/0301-9268(93)90026-X
- Canadian Geochronology Knowledgebase, 2013. Geological Survey of Canada, Earth Science Sector, Natural Resources Canada.
- Cates, N.L., Mojzsis, S.J., 2009. Metamorphic zircon, trace elements and Neoproterozoic metamorphism in the ca. 3.75 Ga Nuvvuagittuq supracrustal belt, Québec (Canada). *Chemical Geology* 261, 99–114. doi:10.1016/j.chemgeo.2009.01.023
- Cawood, P.A., Hawkesworth, C.J., Dhuime, B., 2012. Detrital zircon record and tectonic setting. *Geology* 40, 875–878. doi:10.1130/G32945.1
- Chown, E.H., Daigneault, R., Mueller, W., Mortensen, J.K., 1992. Tectonic evolution of the Northern Volcanic Zone, Abitibi belt, Quebec. *Canadian Journal of Earth Sciences* 29, 2211–2225.
- Corcoran, P.L., Mueller, W.U., 2007. Time-transgressive Archean unconformities underlying molasse basin-fill successions of dissected oceanic arcs, Superior Province, Canada. *Journal of Geology* 115, 655–674. doi:10.1086/521609
- Corfu, F., 1993. The evolution of the southern Abitibi greenstone belt in light of precise U-Pb geochronology. *Economic Geology* 88, 1323–1340.
- Corfu, F., 1996. Multistage zircon and titanite growth and inheritance in an Archean gneiss complex, Winnipeg River subprovince, Ontario. *Earth Planetary Science Letters* 141, 175–186.
- Corfu, F., Stone, D., 1998. Age structure and orogenic significance of the Berens River composite batholiths, western Superior Province. *Canadian Journal of Earth Sciences* 35, 1089–1109. doi:10.1139/e98-056
- Corfu, F., Stott, G.M., 1993. U-Pb geochronology of the central Uchi subprovince, Superior Province. *Canadian Journal of Earth Sciences* 30, 1179–1196.
- Corfu, F., Stott, G.M., 1998. Shebandowan greenstone belt, western Superior Province: U-Pb ages, tectonic implications, and correlations. *GSA Bulletin* 110, 1467–1484.

doi:10.1130/0016-7606(1998)110<1467:SGBWSP>2.3.CO;2

- Corfu, F., Jackson, S.L., Sutcliffe, R.H., 1991. U–Pb ages and tectonic significance of late Archean alkalic magmatism and nonmarine sedimentation: Timiskaming Group, southern Abitibi belt, Ontario. *Canadian Journal of Earth Sciences* 28, 489–503. doi:10.1139/e91-043
- Corfu, F., Stott, G.M., Breaks, F.W., 1995. U-Pb geochronology and evolution of the English River subprovince, an Archean low P-high T metasedimentary belt in the Superior Province. *Tectonics* 14, 1220–1233.
- Corkery, M.T., Davis, D.W., Lenton, P.G., 1992. Geochronological constraints on the development of the Cross Lake greenstone belt, northwest Superior Province, Manitoba. *Canadian Journal of Earth Sciences* 29, 2171–2185.
- David, J., Dion, C., Goutier, J., Roy, P., Bandyayera, D., Legault, M., Rhéaume, P., 2006. Datations U-Pb effectuées dans la Sous-province de l’Abitibi à la suite des travaux de 2004-2005. Ministère des Ressources naturelles et de la Faune du Québec, RP 2006-04, 22 p.
- David, J., Davis, D.W., Dion, C., Goutier, J., Legault, M., Roy, P., 2007. Datations U-Pb effectuées dans la Sous-province de l’Abitibi en 2005-2006. Ministère des Ressources naturelles et de la Faune du Québec, RP 2007-01, 17 p.
- David, J., Godin, L., Stevenson, R., O’Neil, J., Francis, D., 2009. U-Pb ages (3.8-2.7 Ga) and Nd isotope data from the newly identified Eoarchean Nuvvuagittuq supracrustal belt, superior Craton, Canada. *GSA Bulletin* 121, 150–163. doi:10.1130/B26369.1
- Davis, D.W., 2002. U-Pb geochronology of Archean metasedimentary rocks in the Pontiac and Abitibi subprovinces, Quebec, constraints on timing, provenance and regional tectonics. *Precambrian Research* 115, 97–117. doi:10.1016/S0301-9268(02)00007-4
- Davis, D.W., Pezzutto, F., Ojakangas, R.W., 1990. The age and provenance of metasedimentary rocks in the Quetico subprovince, Ontario, from single zircon analyses: Implications for Archean sedimentation and tectonics in the Superior Province. *Earth Planetary Science Letters* 99, 195–205. doi:10.1016/0012-821X(90)90110-J
- Davis, W.J., Gariépy, C., Sawyer, E.W., 1994. Pre-2.8 Ga crust in the Opatoca gneiss belt: A potential source of detrital zircons in the Abitibi and Pontiac subprovinces, Superior Province, Canada. *Geology* 22, 1111–1114. doi:10.1130/0091-7613(1994)022<1111:PGCITO>2.3.CO;2
- Davis, W.J., Lacroix, S., Gariépy, C., Machado, N., 2000. Geochronology and radiogenic isotope geochemistry of plutonic rocks from the central Abitibi subprovince: Significance to the internal subdivision and plutono-tectonic evolution of the Abitibi belt. *Canadian Journal of Earth Sciences* 37, 117–133. doi:10.1139/e99-093
- Davis, D.W., Amelin, Y., Nowell, G.M., Parrish, R.R., 2005. Hf isotopes in zircon from the western Superior province, Canada: Implications for Archean crustal development and evolution of the depleted mantle reservoir. *Precambrian Research* 140, 132–156. doi:10.1016/j.precamres.2005.07.005
- DeGraaff-Surpless, K., Graham, S.A., Wooden, J.L., McWilliams, M.O., 2002. Detrital zircon

- provenance analysis of the Great Valley Group, California: Evolution of an arc-forearc system. *GSA Bulletin* 114, 1564–1580. doi:10.1130/0016-7606(2002)114<1564:DZPAOT>2.0.CO;2
- Dimroth, E., Imreh, L., Rocheleau, M., Goulet, N., 1982. Evolution of the south-central part of the Archean Abitibi belt, Quebec. Part I: Stratigraphy and paleogeographic model. *Canadian Journal of Earth Sciences* 19, 1729–1758.
- Dimroth, E., Imreh, L., Goulet, N., Rocheleau, M., 1983. Evolution of the south-central segment of the Archean Abitibi belt, Quebec. Part II: Tectonic evolution and geomechanical model. *Canadian Journal of Earth Sciences* 20, 1355–1373.
- Feng, R., Kerrich, R., 1990. Geochemistry of fine-grained clastic sediments in the Archean Abitibi greenstone belt, Canada: Implications for provenance and tectonic setting. *Geochimica et Cosmochimica Acta* 54, 1061–1081. doi:10.1016/0016-7037(90)90439-R
- Feng, R., Kerrich, R., 1991. Single zircon age constraints on the tectonic juxtaposition of the Archean Abitibi greenstone belt and Pontiac subprovince, Quebec, Canada. *Geochimica et Cosmochimica Acta* 55, 3437–3441. doi:10.1016/0016-7037(91)90502-V
- Feng, R., Kerrich, R., 1992. Geodynamic evolution of the southern Abitibi and Pontiac terranes: Evidence from geochemistry of granitoid magma series (2700–2630 Ma). *Canadian Journal of Earth Sciences* 29, 2266–2286.
- Feng, R., Kerrich, R., Maas, R., 1993. Geochemical, oxygen, and neodymium isotope compositions of metasediments from the Abitibi greenstone belt and Pontiac subprovince, Canada: Evidence for ancient crust and Archean terrane juxtaposition. *Geochimica et Cosmochimica Acta* 57, 641–658. doi:10.1016/0016-7037(93)90375-7
- Ferguson, S.A., Buffam, B.S.W., Carter, O.F., Griffis, A.T., Holmes, T.C., Hurst, M.E., Jones, W.A., Lane, H.C., Longley, C.S., 1968. Geology and ore deposits of Tisdale Township, District of Cochrane. Ontario Department of Mines Geological Report 58, 177 p.
- Fralick, P., Purdon, R.H., Davis, D.W., 2006. Neoproterozoic trans-subprovince sediment transport in southwestern Superior Province: Sedimentological, geochemical, and geochronological evidence. *Canadian Journal of Earth Sciences* 43, 1055–1070. doi:10.1139/e06-059
- Galley, A.G., Lafrance, B., 2014. Setting and evolution of the Archean synvolcanic Mooshla intrusive complex, Doyon-Bousquet-LaRonde mining camp, Abitibi greenstone belt: Emplacement history, petrogenesis, and implications for Au metallogenesis. *Economic Geology* 109, 205–229.
- Gariépy, C., Allègre, C.J., Lajoie, J., 1984. U-Pb systematics in single zircons from the Pontiac sediments, Abitibi greenstone belt. *Canadian Journal of Earth Sciences* 21, 1296–1304.
- Gehrels, G.E., Blakey, R., Karlstrom, K.E., Timmons, J.M., Dickinson, B., Pecha, M., 2011. Detrital zircon U-Pb geochronology of Paleozoic strata in the Grand Canyon, Arizona. *Lithosphere* 3, 183–200. doi:10.1130/L121.1
- Goutier, J., Dion, C., David, J., Dion, D.-J., 1999. Géologie de la région de la passe Shimusuminu et du lac Vion (33F/11 et 33F/12). Ministère des Ressources naturelles du

- Québec, RG 98-17, 41 p.
- Goutier, J., Dion, C., Oullet, M.-C., Davis, D.W., David, J., Parent, M., 2002. Géologie de la région du lac Guyer (33G/05, 33G/06, 33G/11). Ministère des Ressources naturelles du Québec, RG 2001-15, 53 p.
- Heather, K.B., Shore, G.T., 1999. Geology, Swayze greenstone belt, Ontario. Geological Survey of Canada Open File 3384, scale 1:50,000.
- Holubec, J., 1972. Lithostratigraphy, structure and deep crustal relations of Archean rocks of the Canadian Shield, Rouyn-Noranda area, Quebec. *Krystalinikum* 9, 63-88.
- Hyde, R.S., 1980. Sedimentary facies in the Archean Timiskaming Group and their tectonic implications, Abitibi greenstone belt, northeastern Ontario, Canada. *Precambrian Research* 12, 161–195.
- Ispolatov, V., Lafrance, B., Dubé, B., Creaser, R., Hamilton, M., 2008. Geologic and structural setting of gold mineralization in the Kirkland Lake-Larder Lake gold belt, Ontario. *Economic Geology* 103, 1309–1340. doi:10.2113/gsecongeo.103.6.1309
- Jackson, S.L., Fyon, J.A., Corfu, F., 1994. Review of Archean supracrustal assemblages of the southern Abitibi greenstone belt in Ontario, Canada: Products of microplate interaction within a large-scale plate-tectonic setting. *Precambrian Research* 65, 183–205. doi:10.1016/0301-9268(94)90105-8
- Jackson, S.L., Cruden, A.R., White, D., Milkereit, B., 1995. A seismic-reflection-based regional cross section of the southern Abitibi greenstone belt. *Canadian Journal of Earth Sciences* 32, 135–148.
- Jirsa, M.A., 2000. The Midway sequence: A Timiskaming-type, pull-apart basin deposit in the western Wawa subprovince, Minnesota. *Canadian Journal of Earth Sciences* 37, 1–15.
- Kalliokoski, J., 1987. The Pontiac problem, Quebec-Ontario, in the light of gravity data. *Canadian Journal of Earth Sciences* 24, 1916–1919.
- Ketchum, J.W.F., Ayer, J.A., van Breemen, O., Pearson, N.J., Becker, J.K., 2008. Pericontinental crustal growth of the southwestern Abitibi subprovince, Canada - U-Pb, Hf, and Nd isotope evidence. *Economic Geology* 103, 1151–1184. doi:10.2113/gsecongeo.103.6.1151
- Kylander-Clark, A.R.C., Hacker, B.R., Cottle, J.M., 2013. Laser-ablation split-stream ICP petrochronology. *Chemical Geology* 345, 99–112. doi:10.1016/j.chemgeo.2013.02.019
- Lafrance, B., Moorhead, J., Davis, D.W., 2003. Cadre géologique du camp minier de Doyon-Bousquet-LaRonde. Ministère des Ressources naturelles du Québec, ET 2002-07, 43 p.
- Lafrance, B., Davis, D.W., Goutier, J., Moorhead, J., Pilote, P., Mercier-Langevin, P., Dubé, B., Galley, A.G., Mueller, W.U., 2005. Nouvelles datations isotopiques dans la portion québécoise du Groupe de Blake River et des unités adjacentes. Ministère des Ressources naturelles et de la Faune du Québec, RP 2005-01(a), 15 p.
- LaMaskin, T.A., 2012. Detrital zircon facies of Cordilleran terranes in western North America. *GSA Today* 22, 4–11. doi:10.1130/GSATG142A.1

- Lin, S., Davis, D.W., Rotenberg, E., Corkery, M.T., Bailes, A.H., 2006. Geological evolution of the northwestern Superior Province: Clues from geology, kinematics, and geochronology in the Gods Lake Narrows area, Oxford – Stull terrane, Manitoba. *Canadian Journal of Earth Sciences* 43, 749–765. doi:10.1139/E06-068
- Lodge, R.W.D., 2016. Petrogenesis of intermediate volcanic assemblages from the Shebandowan greenstone belt, Superior Province: Evidence for subduction during the Neoproterozoic. *Precambrian Research* 272, 150–167. doi:10.1016/j.precamres.2015.10.018
- Lodge, R.W.D., Gibson, H.L., Stott, G.M., Hudak, G.J., Jirsa, M.A., Hamilton, M.A., 2013. New U–Pb geochronology from Timiskaming-type assemblages in the Shebandowan and Vermilion greenstone belts, Wawa subprovince, Superior Craton: Implications for the Neoproterozoic development of the southwestern Superior Province. *Precambrian Research* 235, 264–277. doi:10.1016/j.precamres.2013.06.011
- Ludden, J., Hubert, C., Gariépy, C., 1986. The tectonic evolution of the Abitibi greenstone belt of Canada. *Geological Magazine* 123, 153–166.
- Ludwig, K.R., 2012. User's manual for Isoplot 4.15: A geochronological toolkit for Microsoft Excel. Berkeley Geochronology Center, Special Publication 4, 75 p.
- McNicoll, V., Goutier, J., Dubé, B., Mercier-Langevin, P., Ross, P.-S., Dion, C., Monecke, T., Legault, M., Percival, J., Gibson, H., 2014. U-Pb geochronology of the Blake River Group, Abitibi greenstone belt, Quebec, and implications for base metal exploration. *Economic Geology* 109, 27–59.
- Melnyk, M., Davis, D.W., Cruden, A.R., Stern, R.A., 2006. U-Pb ages constraining structural development of an Archean terrane boundary in the Lake of the Woods area, western Superior Province, Canada. *Canadian Journal of Earth Sciences* 43, 967–993. doi:10.1139/E06-35
- Mercier-Langevin, P., Dubé, B., Hannington, M.D., Davis, D.W., Lafrance, B., Gosselin, G., 2007. The LaRonde Penna Au-rich volcanogenic massive sulfide deposit, Abitibi greenstone belt, Quebec: Part I. Geology and geochronology. *Economic Geology* 102, 585–609.
- Morel, M.L.A., Nebel, O., Nebel-Jacobsen, Y.J., Miller, J.S., Vroon, P.Z., 2008. Hafnium isotope characterization of the GJ-1 zircon reference material by solution and laser-ablation MC-ICPMS. *Chemical Geology* 255, 231–235. doi:10.1016/j.chemgeo.2008.06.040
- Mortensen, J.K., 1993a. U-Pb geochronology of the eastern Abitibi subprovince. Part 1: Chibougamau-Matagami-Joutel region. *Canadian Journal of Earth Sciences* 30, 11–28.
- Mortensen, J.K., 1993b. U-Pb geochronology of the eastern Abitibi subprovince. Part 2: Noranda-Kirkland Lake area. *Canadian Journal of Earth Sciences* 30, 29–41.
- Mortensen, J.K., Card, K.D., 1993. U-Pb age constraints for the magmatic and tectonic evolution of the Pontiac subprovince, Quebec. *Canadian Journal of Earth Sciences* 30, 1970–1980.
- Moser, D.E., Heaman, L.M., Krogh, T.E., Hanes, J.A., 1996. Intracrustal extension of an Archean orogen revealed using single-grain U-Pb zircon geochronology. *Tectonics* 15,

1093–1109.

- Mueller, W.U., Corcoran, P.L., 1998. Late-orogenic basins in the Archaean Superior Province, Canada: Characteristics and inferences. *Sedimentary Geology* 120, 177–203.
- O'Neill, C., Lenardic, A., Moresi, L., Torsvik, T.H., Lee, C.-T.A., 2007. Episodic Precambrian subduction. *Earth Planetary Science Letters* 262, 552–562. doi:10.1016/j.epsl.2007.04.056
- O'Neil, J., Carlson, R.W., Francis, D., Stevenson, R.K., 2008. Neodymium-142 evidence for Hadean mafic crust. *Science* 321, 1828–1831.
- Paton, C., Hellstrom, J., Paul, B., Woodhead, J., Hergt, J., 2011. Lolite: Freeware for the visualization and processing of mass spectrometer data. *Journal of Analytical Atomic Spectrometry* 26, 2508–2518.
- Percival, J.A., 1989. A regional perspective of the Quetico metasedimentary belt, Superior Province, Canada. *Canadian Journal of Earth Sciences* 26, 677–693.
- Percival, J.A., Williams, H.R., 1989. Late Archean Quetico accretionary complex, Superior Province, Canada. *Geology* 17, 23–25. doi:10.1130/0091-7613(1989)017<0023:LAQACS>2.3.CO;2
- Percival, J.A., Mortensen, J.K., Stern, R.A., Card, K.D., Bégin, N.J., 1992. Giant granulite terranes of northeastern Superior Province: The Ashuanipi complex and Minto block. *Canadian Journal of Earth Sciences* 29, 2287–2308.
- Percival, J.A., Stern, R.A., Skulski, T., 2001. Crustal growth through successive arc magmatism: Reconnaissance U-Pb SHRIMP data from the northeastern Superior Province, Canada. *Precambrian Research* 109, 203–238. doi:10.1016/S0301-9268(01)00148-6
- Percival, J.A., Sanborn-Barrie, M., Skulski, T., Stott, G.M., Helmstaedt, H., White, D.J., 2006. Tectonic evolution of the western Superior Province from NATMAP and Lithoprobe studies. *Canadian Journal of Earth Sciences* 43, 1085–1117. doi:10.1139/e06-062
- Percival, J.A., Skulski, T., Sanborn-Barrie, M., Stott, G.M., Leclair, A.D., Corkery, M.T., Boily, M., 2012. Geology and tectonic evolution of the Superior Province, Canada. *Geological Association of Canada Special Paper* 49, 321–378.
- Rocheleau, M., 1980. Stratigraphie et sédimentologie de l'Archéen dans la région de Rouyn, Abitibi, Québec. Unpublished Ph.D. thesis, University de Montréal, Québec, 313 p.
- Ropchan, J.R., Luinstra, B., Fowler, A.D., Benn, K., Ayer, J., Berger, B., Dahn, R., Labine, R., Amelin, Y., 2002. Host-rock and structural controls on the nature and timing of gold mineralization at the Holloway mine, Abitibi subprovince, Ontario. *Economic Geology* 97, 291–309. doi:10.2113/gsecongeo.97.2.291
- Sanborn-Barrie, M., Skulski, T., 2006. Sedimentary and structural evidence for 2.7 Ga continental arc-oceanic-arc collision in the Savant-Sturgeon greenstone belt, western Superior Province, Canada. *Canadian Journal of Earth Sciences* 43, 995–1030. doi:10.1139/E06-060
- Sawyer, E.W., Barnes, S.-J., 1994. Thrusting, magmatic intraplating, and metamorphic core complex development in the Archaean Belleterre-Angliers greenstone belt, Superior

- Province, Quebec, Canada. *Precambrian Research* 68, 183–200. doi:10.1016/0301-9268(94)90029-9
- Sawyer, E.W., Benn, K., 1993. Structure of the high-grade Opatoca belt and adjacent low-grade Abitibi subprovince, Canada: An Archaean mountain front. *Journal of Structural Geology* 15, 1443–1458.
- Simard, M., Gosselin, C., 1999. Géologie de la région du Lac Lichteneger (SNRC 33B). Ministère des Ressources naturelles du Québec, RG 98-15, 25 p.
- Simard, M., Chev , S., David, J., Labb , J.-Y., Sharma, K.N.M., 2005. G ologie de la r gion du Lac Minto (34F et 34G). Ministère des Ressources naturelles, de la Faune et des Parcs du Qu bec, RG 2004-04, 25 p.
- Skulski, T., Percival, J.A., Stern, R.A., 1996. Archean crustal evolution in the central Minto block, northern Quebec. *Geological Survey of Canada Current Research 1995-F*, 17–31.
- Skulski, T., Corkery, M.T., Stone, D., Whalen, J.B., Stern, R.A., 2000. Geological and geochronological investigations in the Stull Lake – Edmund Lake greenstone belt and granitoid rocks of the northwestern Superior Province. Manitoba Geological Survey, Report of Activities 2000, 117–128.
- Sl ma, J., Ko ler, J., Condon, D.J., Crowley, J.L., Gerdes, A., Hanchar, J.M., Horstwood, M.S.A., Morris, G.A., Nasdala, L., Norberg, N., Schaltegger, U., Schoene, B., Tubrett, M.N., Whitehouse, M.J., 2008. Ple ovice zircon — A new natural reference material for U – Pb and Hf isotopic microanalysis. *Chemical Geology* 249, 1–35. doi:10.1016/j.chemgeo.2007.11.005
- Sleep, N.H., 1992. Archean plate tectonics: What can be learned from continental geology? *Canadian Journal of Earth Sciences* 29, 2066–2071. doi:10.1139/e92-164
- Smithies, R.H., Champion, D.C., Cassidy, K.F., 2003. Formation of Earth’s early Archaean continental crust. *Precambrian Research* 127, 89–101. doi:10.1016/S0301-9268(03)00182-7
- Snyder, D.B., Bleeker, W., Reed, L.E., Ayer, J.A., Houl , M.G., Bateman, R., 2008. Tectonic and metallogenic implications of regional seismic profiles in the Timmins mining camp. *Economic Geology* 103, 1135–1150.
- Stott, G.M., Davis, D.W., Parker, J.R., Straub, K.J., Tomlinson, K.Y., 2002. Geology and tectonostratigraphic assemblages, eastern Wabigoon subprovince, Ontario. Geological Survey of Canada Open File 4285, scale 1:250,000.
- Stott, G.M., Corkery, M.T., Percival, J.A., Simard, M., Goutier, J., 2010. A revised terrane subdivision of the Superior Province. Ontario Geological Survey Open File Report 6260, 20–1 to 20–10.
- Thurston, P.C., Ayer, J.A., Goutier, J., Hamilton, M.A., 2008. Depositional gaps in Abitibi greenstone belt stratigraphy: A key to exploration for syngenetic mineralization. *Economic Geology* 103, 1097–1134. doi:10.2113/gsecongeo.103.6.1097
- Tomlinson, K.Y., Stott, G.M., Percival, J.A., Stone, D., 2004. Basement terrane correlations and crustal recycling in the western Superior Province: Nd isotopic character of granitoid and

- felsic volcanic rocks in the Wabigoon subprovince, N. Ontario, Canada. *Precambrian Research* 132, 245–274. doi:10.1016/j.precamres.2003.12.017
- Turek, A., Sage, R.P., Van Schmus, W.R., 1992. Advances in the U-Pb zircon geochronology of the Michipicoten greenstone belt, Superior Province, Ontario. *Canadian Journal of Earth Sciences* 29, 1154–1165.
- White, D.J., Musacchio, G., Helmstaedt, H.H., Harrap, R.M., Thurston, P.C., van der Velden, A., Hall, K., 2003. Images of a lower-crustal oceanic slab: Direct evidence for tectonic accretion in the Archean western Superior Province. *Geology* 31, 997–1000. doi:10.1130/G20014.1
- Wiedenbeck, M., Allé, P., Corfu, F., Griffin, W.L., Meier, M., Oberli, F., von Quadt, A., Roddick, J.C. and Spiegel, W., 1995. Three natural zircon standards for U-Th-Pb, Lu-Hf, trace element and REE analyses. *Geostandards Newsletter* 19, 1-23.
- Wiedenbeck, M., Hanchar, J.M., Peck, W.H., Sylvester, P., Valley, J., Whitehouse, M., Kronz, A., Morishita, Y., Nasdala, L., Fiebig, J., Franchi, I., Girard, J.-P., Greenwood, R.C., Hinton, R., Kita, N., Mason, P.R.D., Norman, M., Ogasawara, M., Piccoli, P.M., Rhede, D., Satoh, H., Schulz-Dobrick, B., Skår, Ø., Spicuzza, M.J., Terada, K., Tindle, A., Togashi, S., Vennemann, T., Xie, Q. and Zheng, Y.-F., 2004. Further characterization of the 91500 zircon crystal. *Geostandards and Geoanalytical Research* 28, 9-39.
- Williams, H.R., Stott, G.M., Thurston, P.C., Sutcliffe, R.H., Bennett, G., Easton, R.M., Armstrong, D.K., 1992. Tectonic evolution of Ontario: Summary and synthesis. Ontario Geological Survey Special Volume 4, 1255–1332.
- Woodhead, J.D., Hergt, J.M., 2005. A preliminary appraisal of seven natural zircon reference materials for *in situ* Hf isotope determination. *Geostandards and Geoanalytical Research* 29, 183–195.
- Wyman, D.A., O'Neill, C., Ayer, J.A., 2008. Evidence for modern-style subduction to 3.1 Ga: A plateau – adakite – gold (diamond) association. *Geological Society of America Special Paper* 440, 129–148. doi:10.1130/2008.2440(06)
- Zaleski, E., van Breemen, O., Peterson, V.L., 1999. Geological evolution of the Manitouwadge greenstone belt and Wawa-Quetico subprovince boundary, Superior Province, Ontario, constrained by U-Pb zircon dates of supracrustal and plutonic rocks. *Canadian Journal of Earth Sciences* 36, 945–966. doi:10.1139/e99-016

CHAPTER 3
INSIGHT INTO ARCHEAN CRUSTAL GROWTH PROCESSES AND CRUST-MANTLE
EVOLUTION FROM MULTI-ISOTOPE, U-PB AND LU-HF LA-ICP-MS ANALYSIS OF
DETRITAL ZIRCON GRAINS FROM SUCCESSOR BASINS OF THE
ABITIBI AND PONTIAC SUBPROVINCES, CANADA

A manuscript to be submitted to the journal of *Earth and Planetary Science Letters*

Ben M. Frieman^a, Nigel M. Kelly^b, Yvette D. Kuiper^a,
Thomas Monecke^a, Andrew Kylander-Clark^c

This study reports on the results of a U-Pb and Lu-Hf isotopic study of detrital zircon grains from successor basins of the Archean Abitibi and Pontiac subprovinces of Ontario and Quebec, Canada. Results consist of ~1800 paired analyses making it the most comprehensive multi-isotope detrital zircon data set reported for the region. These were used to constrain the isotopic character of magmatic source domains to establish their provenance and to provide constraints on terrane configurations during regional amalgamations at the time of ~2690-2670 Ma successor basin formation, thus affording insight into crustal generation processes in the Neoproterozoic. The majority of results (~96%) yielded ϵ_{Hf} values of +1 to +10 in the ~3000-2675 Ma age range, and cluster along projections from modern MORB depleted mantle (mMORB-DM) compositions into the Archean. Subordinate results, comprising ~4% of the data set, yielded ϵ_{Hf} values of $>+10$ or are CHUR-like and lower and correspond to either anomalously radiogenic or evolved magmas. These are best explained by sources with multi-stage melt histories, reworking after short-lived crustal residence, and/or local melting from or mixing with magmas derived from older crust.

While Neoproterozoic grains dominate our data set (~88%), the remaining grains (~12%) are Mesoproterozoic in age. The absence of Mesoproterozoic rocks in the Abitibi and Pontiac subprovinces suggests that they must have come from domains juxtaposed during ~2690-2670 Ma amalgamation. Comparison of our data with published U-Pb age and Lu-Hf zircon isotope results indicate that probable source regions are represented by the Winnipeg River, Marmion, and Quetico subprovinces, supporting earlier interpretations based in the zircon age spectra.

^a Department of Geology and Geological Engineering, Colorado School of Mines, Golden, CO

^b Department of Geological Sciences, University of Colorado, Boulder, CO

^c Department of Earth Sciences, University of California, Santa Barbara, CA

Since mMORB-DM-like compositions are characteristic of both age groups, and since sources include local and distal domains that were likely separated by many 100s of kilometers prior to amalgamation, we infer that a modern-style depleted upper mantle reservoir was not only well-established, but prevalent in the mantle below each of these areas during their construction. Since enriched (negative) data are not common and thought to be a result of mixing with older, crustal material, and our data do not display trends indicative of progressive differentiation from a CHUR-like reservoir, it is interpreted that no complementary enriched reservoir is represented. We consider that the development of the observed mMORB-DM reservoir occurred by pre-3000 Ma geodynamic processes.

3.1 Introduction

The Archean Eon is a critical time in Earth history during which a large proportion (40-60%) of preserved continental crust formed (Taylor and McLennan, 1995). Archean crustal components, which form the core of continental interiors, represent the nuclei on which additional crust was accreted during the subsequent Eons. The growth of continental crust in the Phanerozoic is generally accepted to have been driven by plate tectonic processes where volumetrically dominant proportions of new continental crust are produced by partial melting at subduction zones. In this environment, arc melts are produced by extraction from a mantle with a time-integrated depletion history (Griffin et al., 2002; Dhuime et al., 2012), reflecting prior segregation of crust from the mantle (Hofmann, 1988). Therefore, constraining the secular evolution of the mantle is critical for indirectly constraining the development of crustal growth through time. How applicable these processes and implied geodynamic settings are to the timing and processes of craton growth in the Archean and earlier history (Hamilton, 1998; Van Kranendonk et al., 2013; Bédard and Harris, 2014), is unclear. The earliest evidence for Hadean to Eoarchean crust from the zircon record suggests derivation from a primitive, chondritic uniform reservoir (CHUR; Amelin et al., 1999; Harrison et al., 2008; Kemp et al., 2010). Where Hadean to Archean depleted signatures are observed, processes such as the formation of mafic protocrust by differentiation from a magma ocean have been invoked (Amelin et al., 2000; Caro et al., 2003; Boyet and Carlson, 2005, 2006). By the Neoproterozoic depleted mantle signatures were more common (Guitreau et al., 2012), however how widely developed this reservoir was and how it may relate to the construction of Archean cratons is uncertain.

To assess if modern-style crust-mantle differentiation processes are recorded in the isotopic signature of Archean crust we compared the Hf-isotope compositions of zircon grains to projected compositions of the modern MORB depleted mantle (mMORB-DM). Hafnium isotopic studies in single mineral grains such as zircon are one of the most useful tools for investigating

the chemical differentiation of crust and mantle (Kinny and Maas, 2003). Hafnium isotope studies in zircon have been widely applied to investigate crust-mantle interactions (Amelin et al., 1999, 2000), supercontinent cycles and the preservation potential of continental crust (Condie et al., 2011), and Hadean crustal growth in the presence of water (Harrison et al., 2005, 2008). Zircon is uniquely suited for these types of investigations due to the fact that it incorporates high Hf and low Lu concentrations, thereby preserving an initial Hf ratio close to that of its parent magma at the time of crystallization. The timing of crystallization can be independently constrained using the U-Pb isotopic system, which also provides a means to independently assess for post-crystallization isotopic perturbations. The refractory nature of zircon leads to enrichment in clastic sedimentary rocks. While the primary context of the host rocks is lost, analysis of detrital zircon grains allows for access to broader source regions with the context of a smaller sample set. Where their provenance is constrained, the magmatic evolution of the various contributing terrains can be elucidated. Consequently, the detrital zircon record has become an integral tool for investigating the Hf isotope evolution of the crust and mantle (Condie et al., 2011).

We investigated the record of Archean crustal growth of the southern Superior Province using the detrital zircon record of graywacke samples of successor basins deposited in the Abitibi and Pontiac subprovinces during their amalgamation with the rest of Superior Province. The Superior Province represents the largest preserved area of Archean crust on Earth, and was primarily constructed by periodic igneous processes in the Eo- to Neoproterozoic (Percival et al., 2012 and references therein). The present-day configuration of the Superior Province (Fig. 3.1) largely reflects progressive amalgamation of disparate crustal blocks between ~2720 Ma and ~2670 Ma, generally from north to south (Percival et al., 2012). Although igneous rocks predominate, younger, primarily sedimentary rocks were deposited in so-called successor basins that formed coeval with amalgamation of the various crustal components (Corcoran and Mueller, 2007). Detrital zircon grains from successor basin deposits were used in this study, because they record the isotopic characteristics of hinterland sources where uplift and denudation was driven by amalgamations (Frieman et al., 2017). Therefore, the detrital zircon record may provide insight into the crustal growth histories of the hinterland areas. This study presents U-Pb and Lu-Hf laser ablation – inductively coupled plasma – mass spectrometry (LA-ICP-MS) analyses of detrital zircon from successor basins of the Abitibi and Pontiac subprovinces. These basins formed between ~2690 and ~2670 Ma during the latter stages of regional amalgamation (Ayer et al., 2002) and the provenance of these basins can be interpreted within the well-understood geological framework of the Superior Province (Davis,

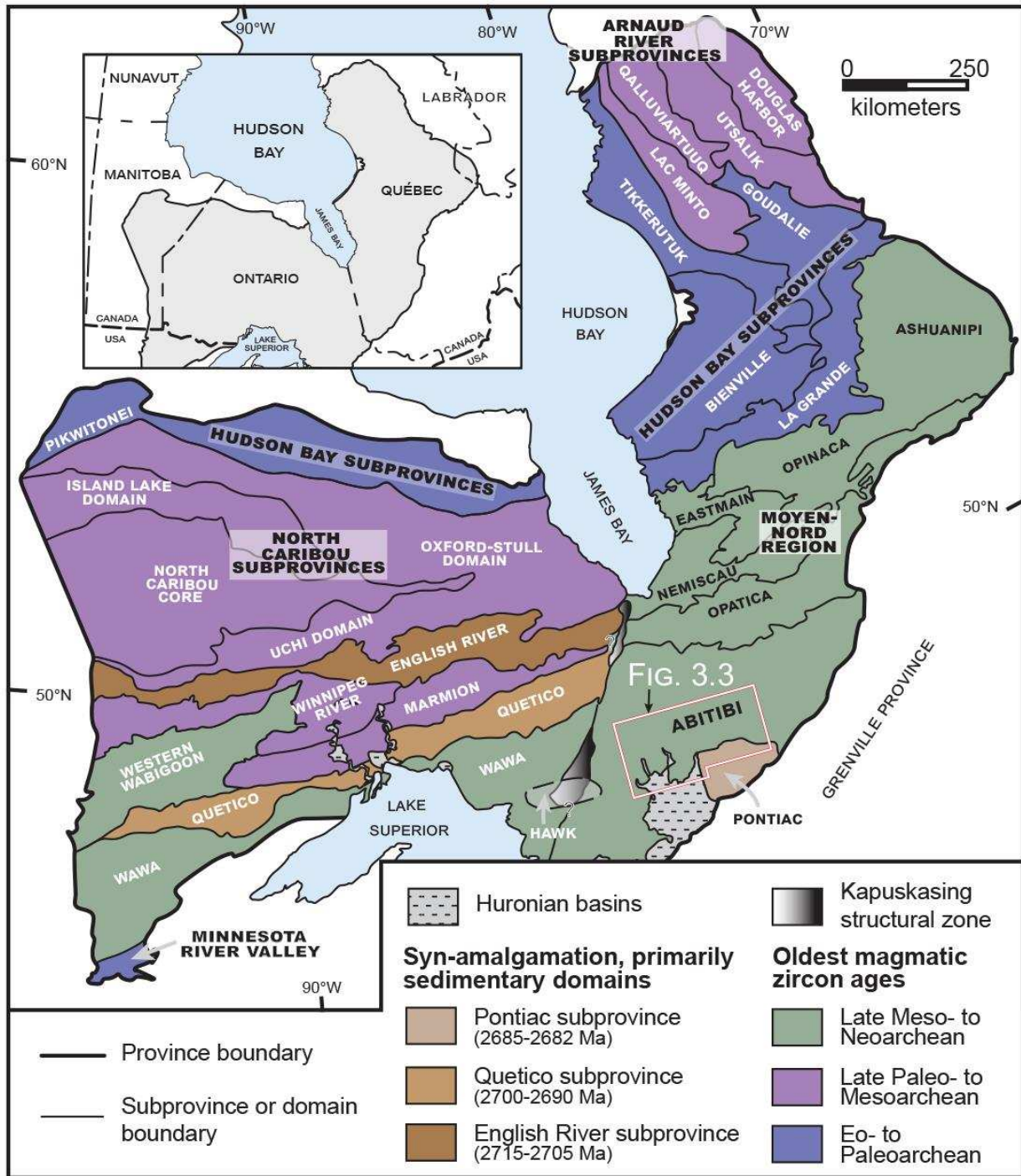


Figure 3.1 – Geologic map of the Superior Province. Map displays the distribution of predominantly magmatic subprovinces or domains colored by their oldest magmatic zircon ages and of primarily sedimentary subprovinces with depositional ages given in parentheses (modified from Stott et al., 2010).

2002; Frieman et al., 2017). Our data set of ~1800 paired isotopic analyses provides statistically significant constraints on the isotopic characteristics of source rocks to these basins. Results indicate that a mMORB-DM-like reservoir was regionally extensive beneath the different components of the southern Superior Province throughout protracted construction of juvenile arc terrains during the Meso- to Neoarchean.

3.2 Regional geological framework

The Superior Province contains an extensive record of crustal growth spanning the Eo- to Neoarchean. The Superior Province has been subdivided into subprovinces and/or domains with distinct pre-amalgamation histories (Fig. 3.1; Card and Ciesielski, 1986; Stott et al., 2010; Percival et al., 2012). These subprovinces or domains have been further grouped where shared structural, magmatic, and/or depositional histories have been identified, and are interpreted to represent terranes or superterranes (Fig. 3.1; Percival et al., 2012). Below, we briefly review the distribution, age, and isotopic character of crustal components in the Superior Province in order to provide a comparative framework for the interpretation of detrital zircon isotope results.

3.2.1 Eo- to Mesoarchean rocks of the Superior Province

Domains that preserve rocks with Eo- to Mesoarchean ages are interspersed throughout the Superior Province (Figs. 3.1 and 3.2). Older crustal components occur as a continental substrate on which Neoarchean crust was emplaced, and/or as structurally interleaved panels that were integrated during amalgamation.

The oldest rocks are Eo- to Paleoproterozoic (>3800-3200 Ma) and occur in the Hudson Bay subprovinces (northern Superior Province) and the Minnesota River Valley subprovince (southern Superior; Figs. 3.1 and 3.2). The Hudson Bay subprovinces contain gneissic-plutonic rocks with U-Pb magmatic zircon crystallization ages of ~3800-3400 Ma (Cates and Mojzsis, 2007; O'Neil et al., 2008, 2013; David et al., 2009; Cates et al., 2013; Darling et al., 2013) that display Nd and Hf isotopic signatures indicative of derivation from primitive mantle sources. Neodymium isotope anomalies suggest localized mixing with source rocks aged ~4300-3800 Ma (Böhm et al., 2000; O'Neil et al., 2012, 2013; Guitreau et al., 2013; Augland and David, 2015; Caro et al., 2017; O'Neil and Carlson, 2017), indicating the potential for a preserved Hadean history. Gneissic-plutonic rocks of the Minnesota River Valley subprovince yield younger, ~3500-3100 Ma U-Pb magmatic zircon crystallization ages (Fig. 3.2; Bickford et al., 2006; Schmitz et al., 2006) in rocks with mantle extraction (Hf model) ages of ~3750-3500 Ma (Satkoski et al., 2013).

While Eoarchean rocks are not aurally extensive, many domains contain a record of Paleo- to Mesoarchean (~3600-2800 Ma) crustal genesis (Figs. 3.1 and 3.2). These include the

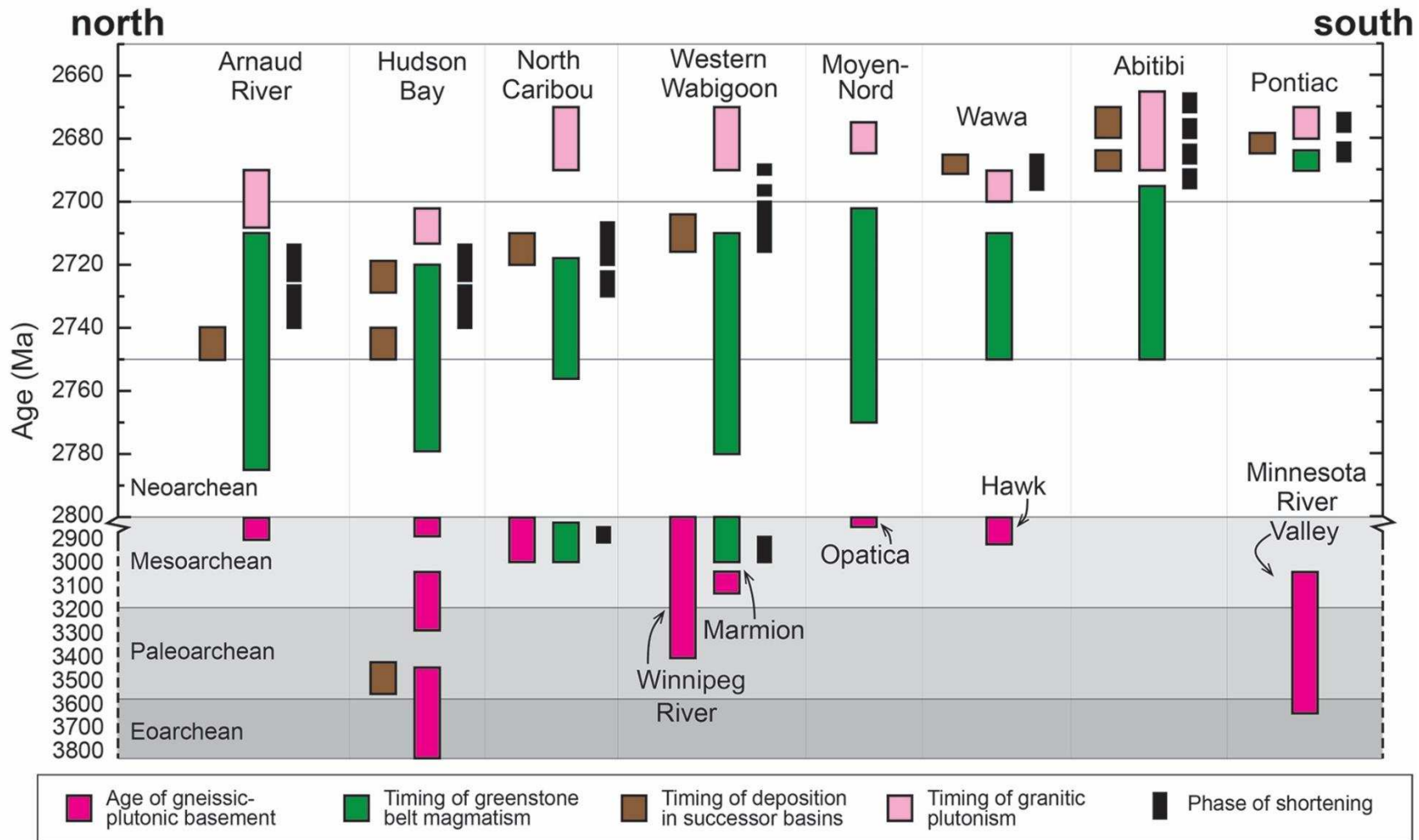


Figure 3.2 – Time-space diagram for the Superior Province. Diagram illustrates the relative temporal and spatial relationships between gneissic-plutonic basement rocks, greenstone belt magmatism, granitic plutonism, deposition of successor basins, and phases of shortening deformation from north to south in the Superior Province.

Arnaud River, North Caribou, Winnipeg River, and Marmion subprovinces, the Hawk domain, and occurrences in the Moyen-Nord region (Fig. 3.1). The Arnaud River subprovinces contain inherited zircon and Nd model ages of ~2920-2800 Ma (Fig. 3.2; Percival et al., 2012 and references therein). The North Caribou subprovinces comprise the majority of the northwestern Superior Province, forming the core of a Mesoarchean superterrane (Davis et al., 2005). These subprovinces are characterized by the widespread occurrence of 3000-2800 Ma volcanic-plutonic rocks with juvenile Nd signatures (Percival et al., 2012 and references therein). The Winnipeg River subprovince is cored by ~3325-2825 Ma tonalitic rocks that yield evolved Nd and Hf isotopic signatures with model ages up to ~3500 Ma (Fig. 3.2; Henry et al., 2000; Davis et al., 2005; Lu et al., 2013), potentially representing a rifted component of the North Caribou superterrane (Davis et al., 2005). The Marmion subprovince, which contains ~3000-2900 Ma volcanic-plutonic rocks (Tomlinson et al., 2004; Melnyk et al., 2006) with juvenile, depleted mantle Hf and Nd signatures (Tomlinson et al., 2004; Davis et al., 2005; Lu et al., 2013), amalgamated with the Winnipeg River subprovince at ~2920 Ma (Tomlinson et al., 2004). In the Opatoca subprovince (Moyen-Nord region), restricted domains of ~2820 Ma tonalitic rocks occur as enclaves within younger plutonic rocks (Davis et al., 1994). The Hawk domain (southern Superior Province) is a poorly exposed area of ~2900-2800 Ma gneissic-plutonic rocks, forming an isolated fragment of juvenile Mesoarchean crust (Figs. 3.1 and 3.2; Turek et al., 1992; Moser et al., 1996; Ketchum et al., 2008).

3.2.2 Juvenile Neoproterozoic rocks of the Superior Province

Neoproterozoic (<2800 Ma) crustal genesis was widespread in the Superior Province (Fig. 3.2). Neoproterozoic volcanic-plutonic successions may unconformably overlie and/or be structurally interleaved with Eo- to Mesoarchean rocks (Percival et al., 2012). However, many domains contain no older components and represent Neoproterozoic juvenile crust. These now comprise large proportions of the central to southern Superior Province, including the majority of the Moyen-Nord region, and the Western Wabigoon, Wawa, and Abitibi subprovinces (Figs. 3.1 and 3.2). In these domains, magmatic construction included both juvenile greenstone belt formation and the intrusion of tonalite-trondjemite-granodiorite (TTG) rocks. The onset of deformation coincided with deposition of successor basins, and culminated with post-deformational granitic plutonism (Fig. 3.2; Percival et al., 2012 and references therein). Formation of greenstone belts occurred at ~2795-2755 Ma in the Opatoca (Sawyer and Benn, 1993; Davis et al., 1994; Boily and Dion, 2002), ~2775-2720 Ma in the Wabigoon subprovince (Davis et al., 2005), ~2720-2700 Ma in the Eastmain subprovince (Goutier et al., 1999), ~2720 Ma in the Wawa subprovince (Corfu and Stott, 1998; Lodge et al., 2013), and ~2795-2695 Ma in

the Abitibi subprovince (Mortensen, 1993a; Ayer et al., 2002, 2005; Thurston et al., 2008; Leclerc et al., 2011, 2012). Whole-rock and single mineral isotopic (Hf and Nd) and geochemical analyses indicate that greenstone belts were primarily derived from juvenile, depleted mantle sources, and are variably interpreted to represent arc to back-arc complexes formed in an oceanic setting (Smith et al., 1987; Henry et al., 2000; Ayer et al., 2002; Davis et al., 2005; Lu et al., 2013; Lodge, 2016).

3.2.3 Successor basin deposits in the Superior Province

The occurrence of primarily sedimentary successor basin deposits is common throughout the Superior Province. These form regional (100s of km) to local (10s of km) sedimentary basins that range in age from >2750 Ma to as young as ~2670 Ma (Fig. 3.2; Percival et al., 2012). In each location, basin formation postdates primary igneous construction by millions of years and is temporally associated with the local onset of deformation driven by amalgamations. The timing of deposition in the successor basins has been constrained by their youngest detrital zircon populations (i.e., the maximum depositional age) and/or by the age of cross-cutting or intercalated igneous rocks, with current estimates of ~2720-2705 Ma in the English River and North Caribou subprovinces (Corfu et al., 1995; Davis, 1998), ~2715-2705 Ma in the Western Wabigoon, Winnipeg River, and Marmion subprovinces (Stott et al., 2002; Sanborn-Barrie and Skulski, 2006), ~2700-2690 Ma in the Quetico and northern Abitibi subprovinces (Davis et al., 1990; Zaleski et al., 1999; David et al., 2006, 2007), and ~2690-2670 Ma in the Wawa, southern Abitibi, and Pontiac subprovinces (Mortensen and Card, 1993; Corfu and Stott, 1998; Ayer et al., 2002, 2005; Davis, 2002; Lodge et al., 2013). Successor basin deposits are progressively younger from north to south, reflecting propagation of the regional deformation front during Neoproterozoic amalgamation.

3.2.4 Geology of the Abitibi and Pontiac subprovinces

The Abitibi greenstone belt in southeastern Superior Province is one of the largest and best-preserved greenstone belts in the world (Fig. 3.1). Volcanic and plutonic rocks are similarly-aged across the Abitibi subprovince (Ayer et al., 2002, 2005; David et al., 2006, 2007; Thurston et al., 2008). However, metamorphic grades are highest (amphibolite facies) in the northern portion of the Abitibi subprovince, where proportionally more plutonic rocks are exposed (Dimroth et al., 1982). In the southern Abitibi subprovince rocks are primarily metamorphosed to greenschist facies conditions or below (Dimroth et al., 1982, 1983; Powell et al., 1995). This potentially reflects different crustal exposure levels (Benn and Moyen, 2008). This study is focused on successor basin deposits that occur in the southern Abitibi greenstone

belt, where the distribution and relative age of volcanic-plutonic and successor basin deposits is best-constrained (Fig. 3.3).

3.2.4.1 Neoproterozoic volcanic-plutonic successions

Supracrustal rocks of the Abitibi subprovince mainly consist of submarine mafic to felsic volcanic successions erupted between ~2795 Ma and ~2695 Ma (Figs. 3.2 and 3.3; Mortensen, 1993a; Ayer et al., 2002, 2005; Thurston et al., 2008; McNicoll et al., 2014; Leclerc et al., 2011, 2012). The volcanic successions consist of tholeiitic to calc-alkaline basalt-rhyolite or tholeiitic basalt-komatiite associations that may have formed in an arc-related settings with minor, intermittent plume influences (Dostal and Mueller, 1996, 1997; Polat and Kerrich, 2001; Ayer et al., 2002, 2005; Sproule et al., 2002).

Plutonic rocks occur as syn-volcanic, syn-deformational, and post-deformational intrusions (Chown et al., 1992; Heather and Shore, 1999, Ayer et al., 2002). Syn-volcanic intrusions display compositions similar to coeval volcanic units (ultramafic to felsic), are ~2750-2695 Ma in age, and occur as spatially restricted complexes that were constructed by multiple magmatic pulses (Corfu, 1993; Mortensen, 1993a,b; Heather and Shore, 1999; Ayer et al., 2005). Syn-deformational intrusions are ~2690-2670 Ma in age and variably hosted in the volcanic successions, batholithic complexes, or successor basin deposits. These display a range of compositions including TTG, monzonite, syenite, granite, and diorite (Corfu, 1993; Mortensen, 1993a,b; Ayer et al., 2005; McNicoll et al., 2014). Post-deformational intrusions are ~2670-2650 Ma in age, dominated by granitic compositions, and occur as relatively small intrusions adjacent to or within the larger batholiths (Heather and Shore, 1999; Davis et al., 2000).

Whole-rock and single mineral isotopic, Nd and Hf studies indicate that magma sources to the volcanic-plutonic rocks underwent no significant interaction with older crustal material (Corfu and Noble, 1992; Kerrich et al., 1999; Ayer et al., 2002; Wyman et al., 2002). This has led to the interpretation that they formed in an oceanic basin setting prior to accretion with the rest of the Superior Province (Ludden et al., 1986; Jackson and Fyon, 1991; Desrochers et al., 1993; Jackson et al., 1994; Wyman et al., 1999; Polat et al., 2017). In contrast, rare ~2900-2800 Ma inherited xenocrystic zircon grains have been documented (Ayer et al., 2002, 2005; Ketchum et al., 2008). The Hf isotopic signatures of some zircon grains may be suggestive of limited mixing with Mesoarchean crustal melts (Ketchum et al., 2008). These observations have led some workers to propose that the Abitibi subprovince formed proximal to a Mesoarchean crustal fragment (Ketchum et al., 2008). In part, the presence of Mesoarchean crust has remained ambiguous, because no known exposures exist in the Abitibi subprovince. Moreover, given the

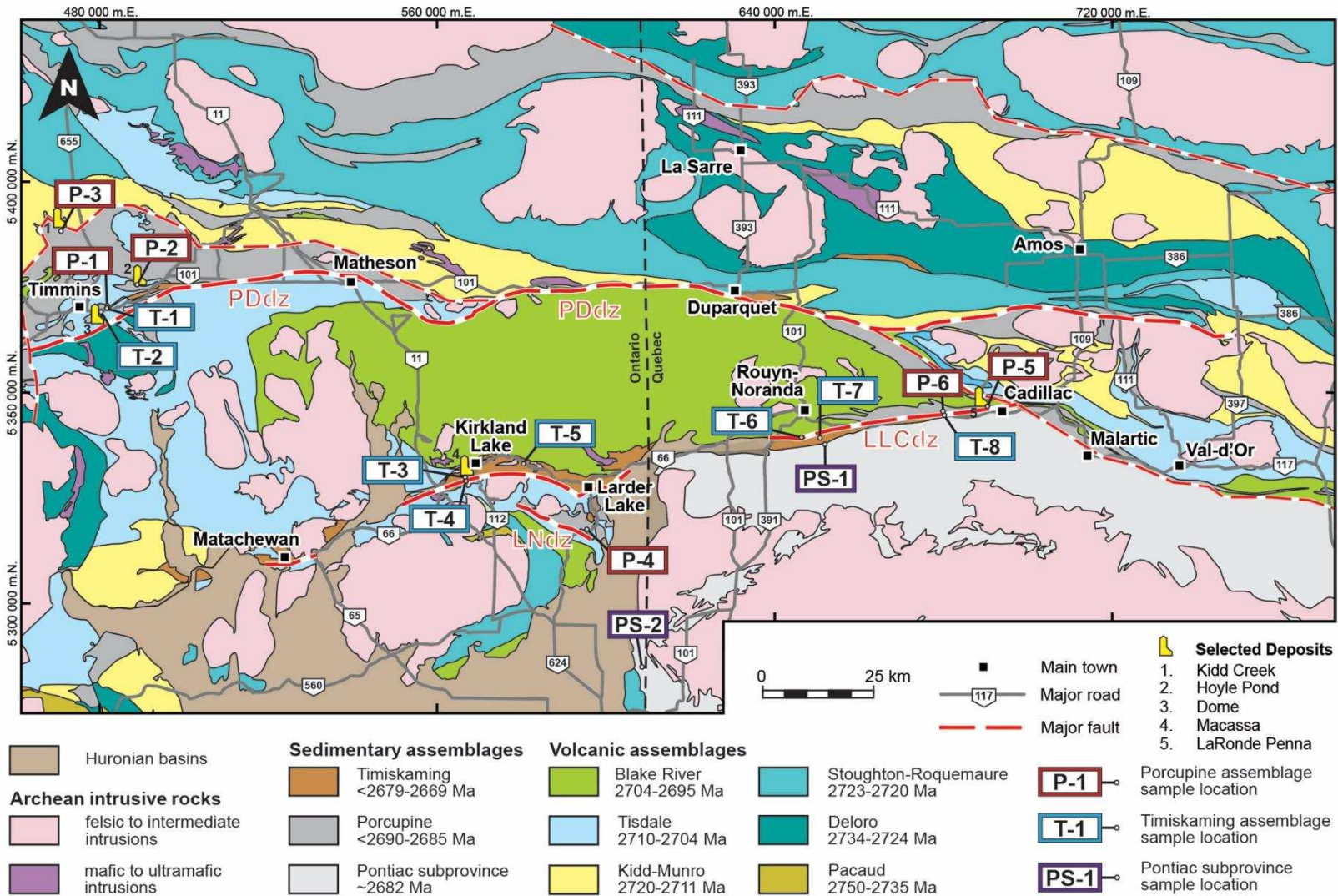


Figure 3.3 – Map of the Abitibi and Pontiac subprovinces. Map displays the distribution of volcanic assemblages, mafic and felsic to intermediate intrusions, and primary sedimentary assemblages. The location of detrital zircon samples investigated in the present study are highlighted. Modified from Thurston et al. (2008) and Monecke et al. (2017).

uncertainty on the geochemical data, interactions with crust that was not significantly older (i.e., ~2900-2800 Ma) would be difficult to recognize (Bleeker, 2002).

3.2.4.2 Successor basins of the southern Abitibi and Pontiac subprovinces

Two distinct successor basin successions are recognized in the southern Abitibi subprovince, which are interpreted to have formed in response to progressive deformation driven by collision of the Abitibi subprovince with Superior Province domains to the north between ~2690 Ma and ~2670 Ma (Ayer et al., 2002; Davis, 2002; Bleeker, 2012; Percival et al., 2012). The Porcupine assemblage, a subaqueous, turbidite-dominated sedimentary succession, was deposited at ~2690-2685 Ma (Ayer et al., 2002, 2005; Davis, 2002; Ropchan et al., 2002) during the initial phases of deformation, while the Timiskaming assemblage, a subaqueous to subaerial, coarse clastic-dominated sedimentary succession, was deposited at ~2679-2669 Ma (Corfu et al., 1991; Corfu, 1993; Ropchan et al., 2002; Ayer et al., 2002, 2005; Davis, 2002), during a later stage of deformation. The Porcupine assemblage disconformably overlies, while the Timiskaming assemblage unconformably overlies the ~2750-2695 Ma volcanic assemblages, and both are spatially associated with regional fault zones (Fig. 3.2).

Sedimentary rocks of the Pontiac subprovince consist of extensive turbidite successions deposited at ~2685-2682 Ma (Mortensen and Card 1993; Davis, 2002; De Souza et al., 2017), displaying similar sedimentological characteristics to the Porcupine assemblage. They were intruded by post-deformational (2660-2640 Ma) granitic batholiths (Fig. 3.2; Mortensen and Card, 1993; Davis, 2002; De Souza et al., 2017). The subprovince may represent a distinct crustal block (Feng et al., 1993). However, sedimentary rocks of the Pontiac subprovince have been interpreted to unconformably overlain by Abitibi subprovince rocks (Holubec, 1972) indicating it formed proximal to the Abitibi subprovince, and has a largely shared history with it (Davis, 2002; Frieman et al., 2017).

Samples from successor basins of the Abitibi and Pontiac subprovinces display broadly similar detrital zircon age patterns (Davis, 2002; Frieman et al., 2017), defined by a majority (80-95%) of Neoproterozoic and subordinate amount (5-15%) of Mesoproterozoic aged grains (Frieman et al., 2017). Similarities are interpreted to reflect the persistence of relatively local and shared provenance domains throughout their deposition from ~2690 Ma to ~2670 Ma. Although broadly similar, statistically significant differences between the detrital age spectra are present, including a higher proportion of Mesoproterozoic zircon grains in the Timiskaming assemblage deposits relative to the Porcupine and Pontiac successor basins. These differences have been interpreted to reflect greater inputs from a distal hinterland sources as regional amalgamation and hinterland emergence progressed (Frieman et al. 2017).

3.3 Methods

Below the methods associated with the detrital zircon LA-ICP-MS analysis are discussed. First, the sampling strategy and processing techniques are reviewed, then the grain characteristics and analytical techniques associated with data collection and processing are discussed.

3.3.1 Sampling strategy, processing, and grain characteristics

To constrain the U-Pb and Lu-Hf isotopic record of detrital zircon grains from the Abitibi and Pontiac subprovinces, a set of 16 graywacke samples was collected (Fig. 3.2; Table 3.1). These consist of six Porcupine assemblage, two Pontiac subprovince, and eight Timiskaming assemblage samples (Fig. 3.2; Table 3.1). Detailed sample descriptions, sampling methodology, zircon separation techniques, and sample-by-sample comparisons of U-Pb age patterns are given in Frieman et al. (2017). All samples yielded heavy mineral separates from which a >125 zircon grains were mounted in epoxy plugs and polished to half depth. Back-scattered electron (BSE), secondary electron (SE), and cathodoluminescence (CL) images were collected for each grain mount at the Denver Microbeam Laboratory, U.S. Geological Survey in Lakewood, Colorado on a JOEL 5800LV scanning electron microscope. Analysis was conducted under high vacuum, using a 15 kV operating voltage, and 5 nA beam current. Additional SE and BSE imaging of selected samples was conducted at the Department of Geology and Geological Engineering, Colorado School of Mines, using a TESCAN MIRA3 field emission-scanning electron microscope using a voltage of 15 kV and a beam current of 11 nA. Analysis locations within the selected grains were chosen by cross-referencing the CL, BSE, and SE imagery to ensure spot analyses were placed in domains with similar textural characteristics that contained no visible inclusions or cracks. Where possible, analyses were limited to zones that displayed textural characteristics interpreted to represent magmatic growth such as simple oscillatory or sector zoning (Fig. 3.4).

3.3.2 U-Pb and Lu-Hf analytical techniques

Isotopic analyses were conducted by LA-ICP-MS at the University of California Santa Barbara, using a *Nu Plasma* multi-collector system coupled to a *Photon Machines Excite* 193 nm laser ablation system, following the analytical procedures of Kylander-Clark et al. (2013). The U-Pb and Lu-Hf isotopes were measured during separate analytical sessions. Initially, the U-Pb laser spots (~15 μm) were placed and then the Lu-Hf spots (~40–50 μm) were overlain or placed directly adjacent within the same textural domain identified from SEM images (Fig. 3.4).

The U-Pb analyses used here are a subset of those reported by Frieman et al. (2017) on which Lu-Hf analyses were performed. For U-Pb analyses the 91500 zircon (Wiedenbeck et al.,

Table 3.1 – List of detrital zircon graywacke samples from successor basins of the Abitibi and Pontiac subprovinces investigated by U-Pb and Lu-Hf LA-ICP-MS analysis in this study.

	Sample #	Location	UTM zone (NAD83)	Northing (m)	Easting (m)
Porcupine assemblage	P-1	Timmins	17U	5371274	484261
	P-2	Timmins	17U	5377126	493189
	P-3	Timmins	17U	5393390	473340
	P-4	Larder Lake	17U	5318272	597448
	P-5	LaRonde Penna	17U	5346548	690224
	P-6	LaRonde Penna	17U	5345265	680339
Pontiac subprovince	PS-1	Rouyn-Noranda	17U	5337608	651829
	PS-2	western Pontiac subprovince	17T	5285124	610613
Timiskaming assemblage	T-1	Timmins	17U	5371207	484998
	T-2	Timmins	17U	5369513	483540
	T-3	Kirkland Lake	17U	5331699	569426
	T-4	Kirkland Lake	17U	5330831	570190
	T-5	Morris-Kirkland	17U	5333712	580331
	T-6	Rouyn-Noranda	17U	5339898	646428
	T-7	Rouyn-Noranda	17U	5340052	650339
	T-8	LaRonde Penna	17U	5344928	680437

1995, 2004) was used as a primary reference material, while secondary reference materials included the GJ-1, Plešovice, and Peixe zircons (Jackson et al., 2004; Sláma et al., 2008; Dickinson and Gehrels, 2003). Secondary reference materials were interspersed throughout the analytical sessions to evaluate accuracy. They yielded U-Pb ratios within 2% of their accepted

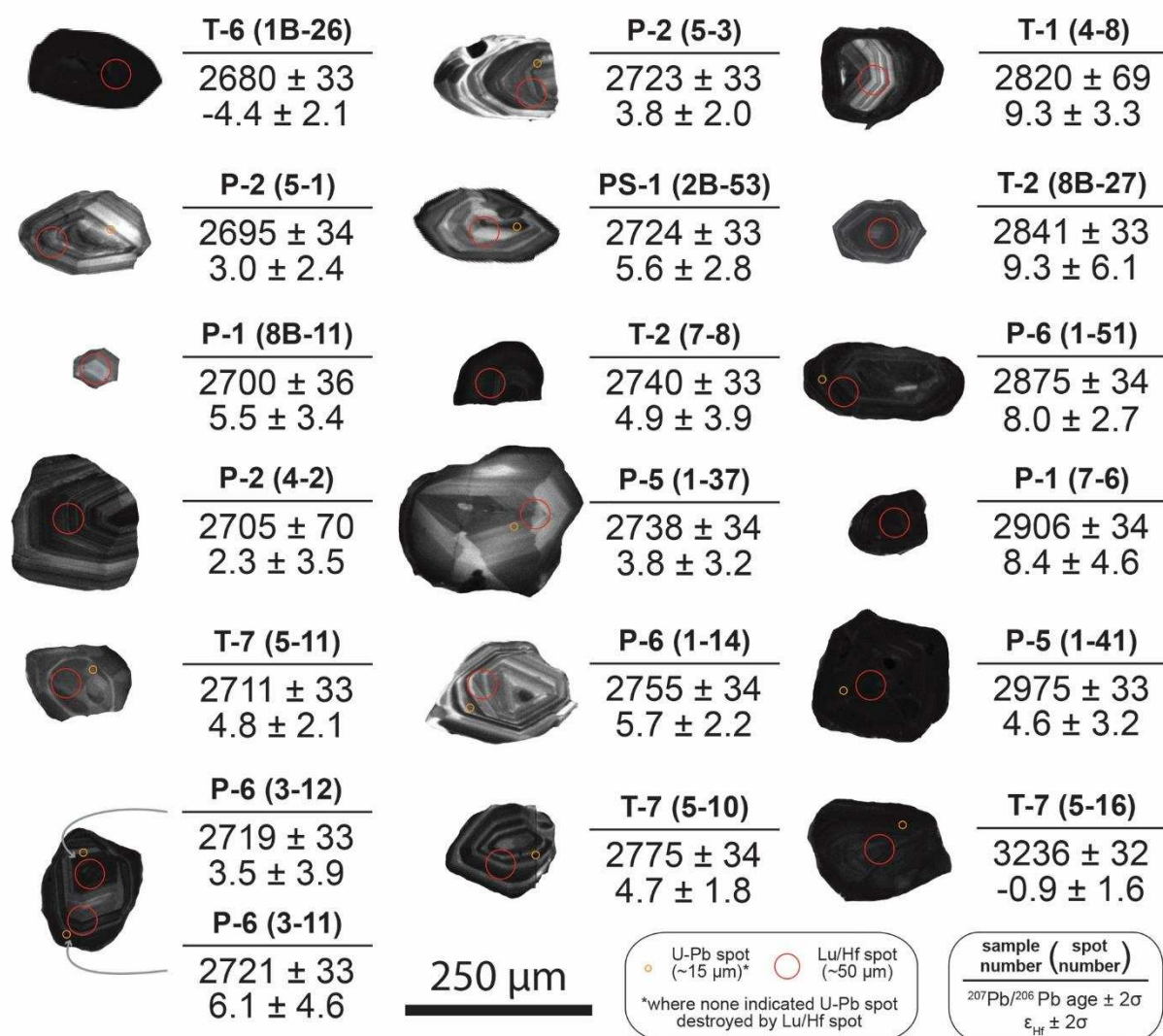


Figure 3.4 – Representative zircon images. Cathodoluminescence images of detrital zircon grains analyzed from successor basin rocks of the Abitibi and Pontiac subprovinces organized by age from youngest to oldest. The analysis location, sample/spot reference number, $^{207}\text{Pb}/^{206}\text{Pb}$ age, and ϵ_{Hf} value for each grain are labeled. Indicated uncertainty for all analyses is 2σ .

values. The U-Pb data was reduced using *Iolite v2.5* (Paton et al., 2011), and 2% uncertainty was added in quadrature to each ratio to account for the long-term reproducibility of the secondary reference materials. Where U-Pb analyses were more than >5% discordant, the U-Pb and corresponding Lu-Hf data were rejected from further analysis (method after Gehrels et al., 2011). The data are provided in Appendix B. Uncertainties on all reported data are 2σ , unless stated otherwise.

The hafnium isotope data were normalized using an exponential mass bias correction and a natural $^{179}\text{Hf}/^{177}\text{Hf}$ ratio of 0.7325. Isobaric interferences of ^{176}Lu and ^{176}Yb on ^{176}Hf were corrected by measuring $^{171}\text{Yb}/^{173}\text{Yb}$ and assuming $^{171}\text{Yb}/^{173}\text{Yb}$, $^{171}\text{Yb}/^{173}\text{Yb}$, $^{176}\text{Lu}/^{175}\text{Lu}$ ratios of 1.123575, 0.786847, and 0.02655, respectively (Thirwall and Anczkiewicz, 2004; Vervoort et al., 2004). Secondary reference materials analyzed for quality control were zircon reference materials 91500, GJ-1, Plešovice, Mud Tank, and Mun-3 and Mun-4 (Wiedenbeck et al., 1995; Sláma et al., 2008; Morel et al., 2008; Fisher et al., 2011). Each reference material yielded weighted-mean $^{176}\text{Hf}/^{177}\text{Hf}$ ratios within 50 ppm of the accepted value. The mass-corrected $^{176}\text{Lu}/^{177}\text{Hf}$ isotopic ratios were used to calculate the initial $^{176}\text{Hf}/^{177}\text{Hf}$ ratios and ϵ_{Hf} values at the time of crystallization (i.e., at the measured $^{207}\text{Pb}/^{206}\text{Pb}$ age; Appendix B). The reported uncertainty on the initial $^{176}\text{Hf}/^{177}\text{Hf}$ ratios and ϵ_{Hf} values includes propagation of the 2σ uncertainty on: (1) the measured $^{176}\text{Lu}/^{177}\text{Hf}$ ratios, (2) the calculated $^{207}\text{Pb}/^{206}\text{Pb}$ dates, and (3) the ^{176}Lu decay constant. Propagation of these internal and external uncertainties was calculated using the Model 2 algorithms of Ickert (2013). We utilized the ^{176}Lu decay constant of Söderlund et al. (2004) ($1.867 \pm 8 \times 10^{-11}$) and the values for the chondritic uniform reservoir (CHUR) of Bouvier et al. (2008) ($^{176}\text{Lu}/^{177}\text{Hf} = 0.0336$ and $^{176}\text{Hf}/^{177}\text{Hf} = 0.282785$). The resultant initial $^{176}\text{Hf}/^{177}\text{Hf}$ ratios and ϵ_{Hf} values are plotted against the isotope evolution curve for the depleted mantle and CHUR (Fig. 3.5). The depleted mantle curve was calculated based on the modern-day MORB values of $^{176}\text{Lu}/^{177}\text{Hf} = 0.0384$ and $^{176}\text{Hf}/^{177}\text{Hf} = 0.283250$ (Griffin et al., 2002), hereafter referred to as mMORB-DM (Fig. 3.5). To better visualize the high density of data, the $\epsilon_{\text{Hf}} - ^{207}\text{Pb}/^{206}\text{Pb}$ age results are also presented as a bivariate histogram plot, which was constructed using standard Matlab routines with 10 Ma and 0.5 ϵ_{Hf} unit bin spacing (Fig. 5D).

3.4 U-Pb and Lu-Hf isotopic results

The U-Pb age discussed in this study are from zircon grains analyzed by Frieman et al. (2017) for which paired Lu-Hf spot analyses were obtained. These consist of 1792 U-Pb determinations that met the filtering criterion discussed above. The U-Pb age data consist of ~12% Mesoarchean and ~88% Neoarchean ages (Fig. 3.6A), which is representative of the age

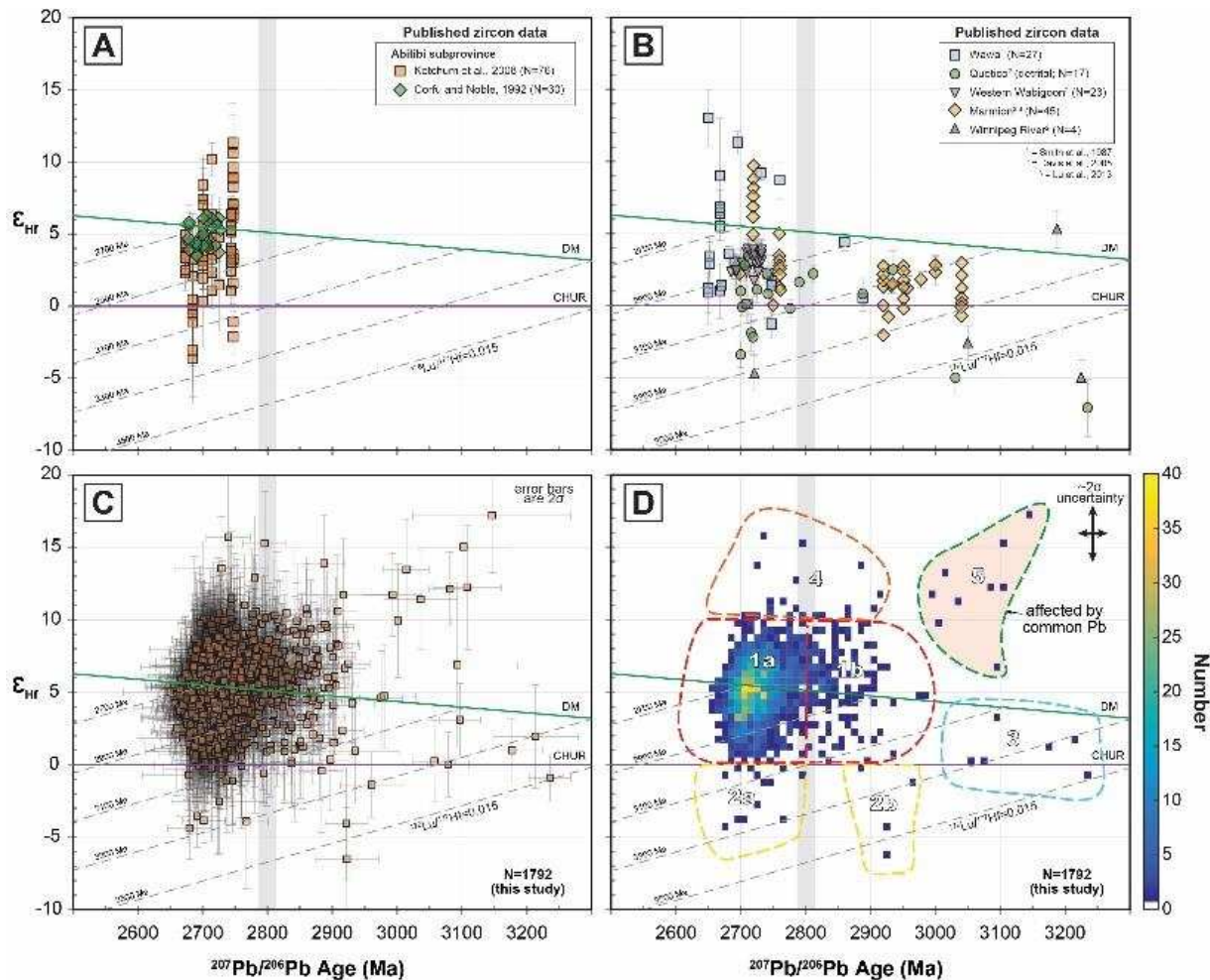


Figure 3.5 – Plots displaying U-Pb and Lu-Hf zircon data. (A) Previously published U-Pb and Lu-Hf zircon data from the Abitibi subprovince. (B) Previously published U-Pb and Lu-Hf zircon data from the Wawa, Quetico, Western Wabigoon, Marmion, and Winnipeg River subprovinces. (C) The $\epsilon_{\text{Hf}} - {}^{207}\text{Pb}/{}^{206}\text{Pb}$ age results from LA-ICP-MS analysis of detrital zircon grains from Abitibi and Pontiac subprovince successor basin samples in this study. Error bars in A-C are 2σ uncertainty (note: no uncertainty was reported by Lu et al., 2013). (D) A bivariate histogram plot of the data displayed in (C) using 10 Ma and 0.5 ϵ_{Hf} unit bin spacing, approximate average 2σ uncertainty is indicated, and data groups with similar distributions are outlined. Vertical gray bars represent the approximate age threshold between Abitibi (younger) and non-Abitibi (older) ages. Green line represents the evolution of depleted mantle (DM) compositions as calculated from modern MORB values of Griffin et al. (2002). Purple line corresponds to compositions of the chondritic uniform reservoir (CHUR). Gray dashed lines represent ϵ_{Hf} growth curves calculated using ${}^{176}\text{Lu}/{}^{177}\text{Hf} = 0.015$, which is the approximate mid-point between reported end-member values for crustal mafic rocks (0.022; Amelin et al., 1999) and Precambrian granitoid rocks (0.0093; Vervoort and Patchett, 1996). This value also coincides with the average crustal composition of the Superior Province as derived from whole-rock geochemical analyses of sedimentary rocks (Stevenson and Patchett, 1990).

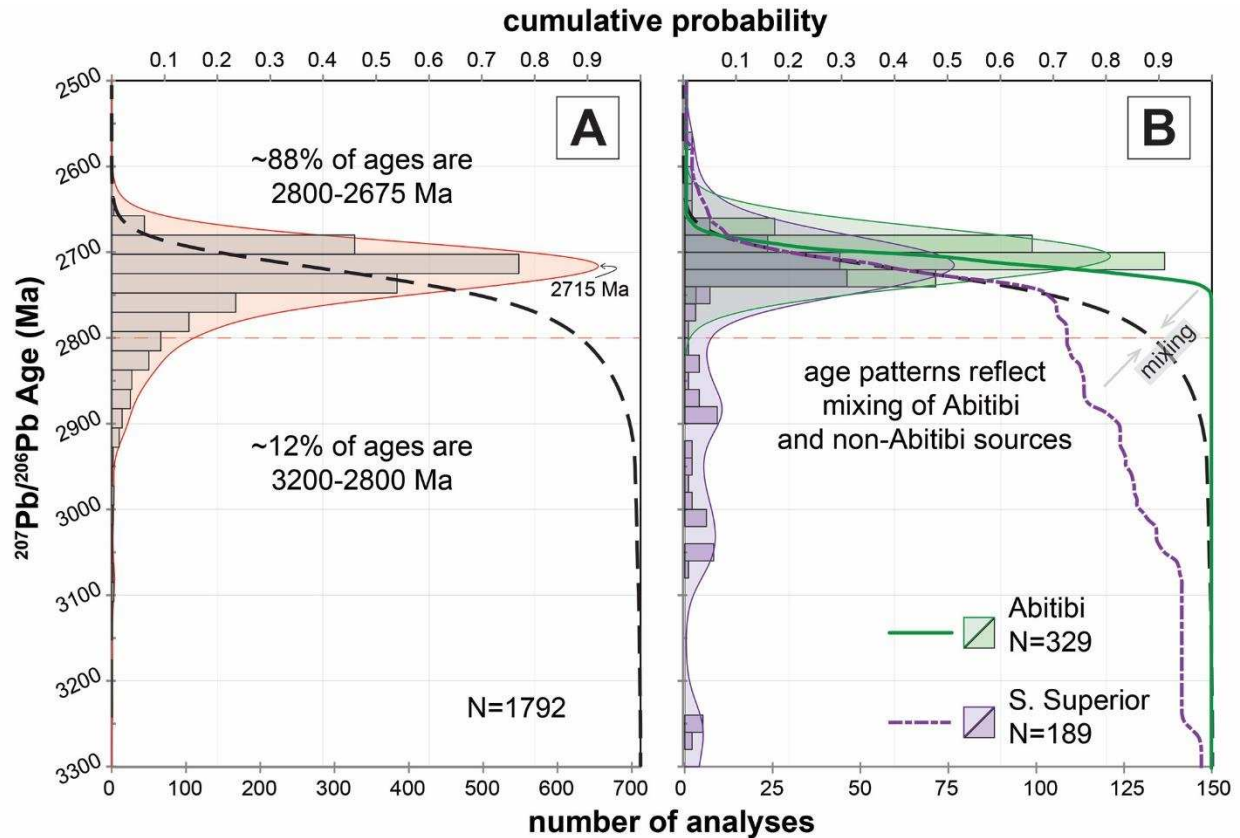


Figure 3.6 – Comparison of detrital zircon ages from this study to published zircon ages. Frequency histograms (rectangles), probability density function curves (filled solid colored lines), and cumulative distribution function curves (solid and dashed lines) for U-Pb zircon data in the study region. (A) Selected concordant $^{207}\text{Pb}/^{206}\text{Pb}$ ages of detrital zircon grains from the Abitibi and Pontiac subprovinces from Frieman et al. (2017) on which Lu-Hf analyses were performed. (B) Compilation of published U-Pb age data for volcanic-plutonic rocks of the Abitibi subprovince and adjacent domains in the southern Superior Province (Winnipeg River, Marmion, and Opatca subprovinces) (modified from Frieman et al., 2017). The published age data for volcanic-plutonic rocks of the Abitibi subprovince (solid green line) do not match the detrital zircon age pattern observed in successor basin samples of the Abitibi and Pontiac subprovinces (black dashed line). However, the observed distribution of ages in our samples can be explained by a component of mixing between Abitibi and older source rocks (southern Superior; purple irregular dashed line).

distributions in successor basin samples from the Abitibi and Pontiac subprovinces (Frieman et al., 2017).

The initial $^{176}\text{Hf}/^{177}\text{Hf}$ ratios for all analyses are between 0.280667 and 0.281464 with an average uncertainty of ± 0.000093 (Appendix B). They correspond to ϵ_{Hf} values between -6.5 to +17.2, although the majority of the data (~86%) fall between +1 and +10 ϵ_{Hf} units (Fig. 3.5C and D; Appendix B). The 2σ uncertainty on the ϵ_{Hf} data, including covariance on all parameters, ranges from 1.7 to 9.1 ϵ_{Hf} units with a mean uncertainty of 3.5 (Appendix B).

For the purposes of discussion, data have been qualitatively subdivided into five data groups based on distribution in U-Pb age and ϵ_{Hf} space (Fig. 3.5D). Data group 1 is composed of the largest proportion of results (~96%; ~1724 analyses) and is defined by ages spanning from ~2675 Ma to ~3000 Ma and ϵ_{Hf} values between 0 and +10 (Fig. 3.5C and D). Group 1 is further subdivided into group 1a (~1580 analyses), which corresponds to zircon grains with ages <2800 Ma, and group 1b (~144 analyses), which contains ~3000-2800 Ma zircon (Fig. 3.5C and D). The division between groups 1a and 1b is based on the approximate maximum possible age (including measured age uncertainty, ~2800 Ma) of magmatic zircon associated with Abitibi subprovince volcanic-plutonic rocks (e.g., Fig. 3.6B). Data group 2 is defined by a set of 17 analyses with ages between 2675 Ma and 2950 Ma and ϵ_{Hf} values between 0 and -6.5 (Fig. 3.5D). This data group represents zircon grains with ages similar to those observed in data group 1 (3000-2675 Ma), but with ϵ_{Hf} compositions that are CHUR-like or negative. Data group 2 has been subdivided into subgroups with ages <2800 Ma (group 2a: 13 analyses) and those with ages of 2950-2800 Ma (group 2b: 4 analyses; Fig. 3.5D). Data group 3 is defined by a set of 6 analyses with U-Pb ages of 3250-3000 Ma and ϵ_{Hf} values of +4 to -1 (Fig. 3.5D). Data groups 4 and 5 are defined by clusters of data that yielded relatively high ϵ_{Hf} values of $> +10$ (Fig. 3.5D), with data group 4 (~30 analyses) composed of zircon grains with U-Pb ages between 2700 Ma and 2950 Ma, and data group 5 (8 analyses) composed of zircon grains with ages between ~2950 and 3150 Ma (Fig. 3.5D).

3.5 Lu-Hf data trends and regional correlations

Newly acquired, coupled LA-ICP-MS U-Pb and Lu-Hf analyses of zircon grains from successor basins of the Abitibi and Pontiac subprovinces represent the largest and most comprehensive multi-isotope detrital zircon data set compiled to date for the Superior Province. These data (Fig. 3.5C and D) provide constraints on the isotopic character of source rocks to these successor basin sedimentary rocks. We will first compare these results to previously published U-Pb and Lu-Hf data, using regional geological constraints to determine probable

source domains, to develop insights into the amalgamation history of the Abitibi subprovince and growth of the Superior Province.

The U-Pb age patterns of successor basin detrital zircon grains from the Abitibi and Pontiac subprovinces indicate that these rocks were derived from a mixture of both local and distal sources (Fig. 6; Davis, 2002; Frieman et al., 2017). In part, this interpretation is based on the presence of Mesoarchean zircon grains in the successor basin sedimentary rocks and the absence of volcanic-plutonic rocks of this age in the Abitibi and Pontiac subprovinces (Figs. 3.5A and 3.6B). Zircon grains with U-Pb ages that are ≥ 2800 Ma account for $\sim 12\%$ of the total data set (~ 215 analyses; Fig. 3.6A), requiring a substantial component of mixing between local, < 2800 Ma and older, > 2800 Ma sources to produce the observed age spectra in our samples (Fig. 3.6B). Statistical comparisons with published zircon age data from the southern Superior Province suggest that the occurrence of 'exotic' Mesoarchean zircon grains are best explained by sources from areas juxtaposed during amalgamation at ~ 2690 - 2670 Ma, such as the Winnipeg River, Marmion, and Opatica subprovinces (Fig. 3.6B; Frieman et al., 2017). The absence of any Eo- to Paleoproterozoic components in the Abitibi successor basin sediments suggests that source regions did not include terranes in the northern Superior Province (Frieman et al., 2017). These conclusions are supported by our new paired U-Pb and Lu-Hf isotopic data, as domains from the southern Superior Province display similar Hf-isotope / age patterns (compare Figs. 3.5B and C). Hence, our data provide insight into the isotopic characteristics of a significant portion of the southern Superior Province. A notable exception to this interpretation is the data observed in group 5 (Fig. 3.5D), which do not compare with any previously reported analyses (Fig. 3.5A and B).

Data group 1 (~ 3000 - 2675 Ma) represents the majority of results obtained in this study ($\sim 96\%$) and the population cluster centers on mMORB-DM compositions (Fig. 3.5C and D). The statistical dominance of data group 1a (88%; Fig. 3.4D) is interpreted to reflect local derivation from the Neoproterozoic igneous source rocks that make up the Abitibi subprovince (Figs. 3.4A and 3.6B; Davis, 2002; Frieman et al., 2017). Volcanic-plutonic rocks of the Abitibi subprovince are largely ~ 2750 - 2695 Ma in age (see compilation in Fig. 3.6B) and previously published zircon data display ϵ_{Hf} values of +2 to +7 (Fig. 3.5A; Corfu and Noble, 1992; Ketchum et al., 2008). This is comparable to the range we observe in our group 1a (Fig. 3.5C and D). Neoproterozoic igneous rocks with similar mMORB-DM Hf or Nd isotopic compositions are also abundant in the Wawa (Smith et al., 1987; Henry et al., 2000), Western Wabigoon (Henry et al., 2000; Davis et al., 2005; Lu et al., 2013), and Marmion (Tomlinson et al., 2004; Davis et al., 2005; Lu et al., 2013) subprovinces (Fig. 3.5B). Consequently, some of the zircon grains in group 1a may well

have been derived from domains juxtaposed during regional amalgamation, as has been interpreted from the U-Pb age patterns in our samples (Frieman et al., 2017).

The ~2950-2800 Ma aged grains observed in group 1b (Fig. 3.5C and D) are likely to have been sourced from juxtaposed domains that also contain a history of Mesoarchean crustal genesis. We suggest that the Marmion subprovince is the probable source for these grains (Fig. 3.5B), because volcanic-plutonic rocks of the Marmion subprovince contain abundant evidence for crustal growth at ~3000-2900 Ma with mMORB-DM-like Hf and Nd isotopic signatures (Tomlinson et al., 2004, Davis et al., 2005; Melnyk et al., 2006; Lu et al., 2013), consistent with our group 1b results (compare Fig. 3.5B and D). Alternatively, inherited zircon grains that have ages of ~2925 Ma and ~2860-2850 Ma have been reported from ~2740-2700 Ma volcanic-plutonic rocks of the Abitibi subprovince (Ayer et al., 2002, 2005; Ketchum et al., 2008). These are interpreted to have been incorporated into Neoproterozoic magmas from a fragment of Mesoarchean crust in the middle to lower crust (Ketchum et al., 2008). The extent of this fragment is poorly constrained, but is interpreted to extend from the western Abitibi subprovince (Ketchum et al., 2008) through the Paleoproterozoic Kapuskasing uplift (Moser et al., 1996) to present-day exposures of ~3000-2900 Ma gneissic-plutonic rocks in the eastern Wawa subprovince (Turek et al., 1992). These are collectively referred to as the Hawk domain (Fig. 3.1; Turek et al., 1992). While the zircon grains from the Hawk domain may have been incorporated as inherited components during Neoproterozoic magmatism, it is unlikely that it contributed detritus to our samples, since these rocks were probably not extensively exposed at the time of successor basin formation in the Abitibi and Pontiac subprovinces (Frieman et al., 2017). Accordingly, we consider that group 1b principally reflects derivation from the Marmion subprovince.

The presence of Mesoarchean and older crust may also explain the more evolved (negative) ϵ_{Hf} values we document (data groups 2 and 3; Fig. 3.5D). Based on comparison to ϵ_{Hf} growth curves for Superior Province crust ($^{176}\text{Lu}/^{177}\text{Hf} = 0.015$; Stevenson and Patchett, 1990), data groups 2 and 3 may have crystallized from magmas either derived directly from older sources or from Neoproterozoic mantle melts that partially mixed with magmas derived from older crust (Fig. 3.7). Data group 2a plots in a region roughly bracketed by the 2900 Ma and 3300 Ma evolution lines, while data groups 2b and 3 approximately correspond to the region between the 3100 Ma and 3500 Ma lines (Fig. 3.5B and C). These associations suggest that rocks from which these zircon grains were derived contain a late Paleo- to Mesoarchean crustal component. This supports our interpretation that the Marmion subprovince was a prominent

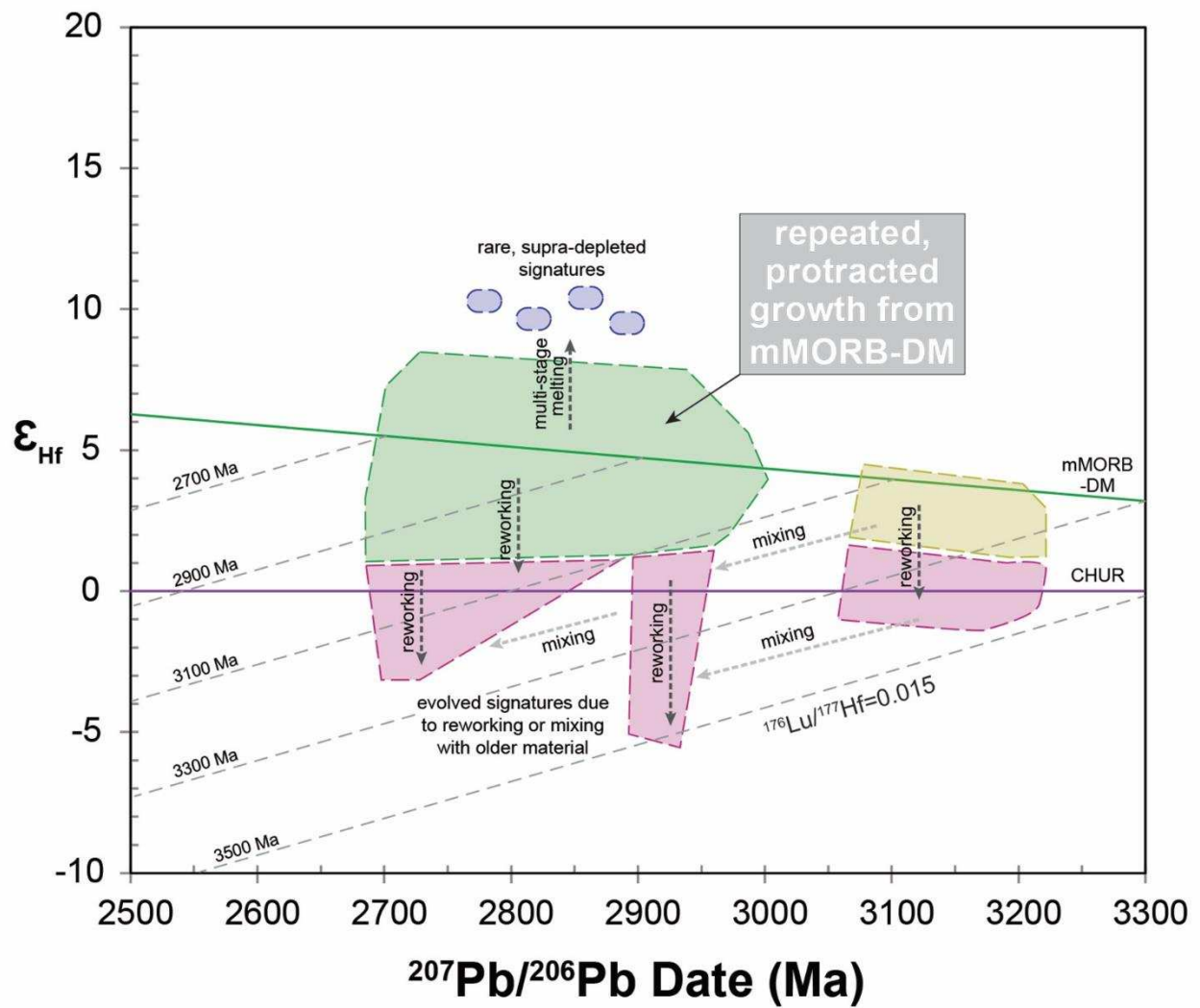


Figure 3.7 – Schematic diagram illustrating potential processes driving the dominant Lu-Hf data distributions presented in this study.

source and further suggests that older (~3300-3000 Ma) basement in Winnipeg River subprovince (Fig. 3.5B; Davis et al., 2005; Lu et al., 2013) are represented in our detrital zircon samples (groups 2b and 3; Fig. 3.5D).

Detrital zircon grains with low to negative ϵ_{Hf} values at ~3200-2900 Ma and ~2700 Ma, similar to groups 2 and 3, are also observed in sedimentary rocks of the intervening Quetico subprovince (Fig. 3.5B; Davis et al., 2005). The Marmion and Winnipeg River subprovinces are interpreted to have been the primary sources for detritus in the Quetico subprovince during deposition in the basin at ~2700-2690 Ma (Fralick et al., 2006). However, due to its impingement between the Wawa and Marmion / Western Wabigoon subprovinces, sedimentation in the Quetico subprovince ceased at <2690 Ma as it began to experience deformation, uplift, and erosion (Corfu and Stott, 1998; Percival et al., 2006; Sanborn-Barrie and Skulski, 2006). Thus, at <2690 Ma, following initiation of deposition in the Abitibi subprovince successor basins, evolved Meso- to Neoproterozoic detrital zircon grains were more likely to have been directly or indirectly (eroded Quetico subprovince) derived from the Winnipeg River and Marmion subprovinces, which could be represented by data groups 2 and 3 in our samples (Fig. 3.5).

While statistically minor (<2%), the high, > +10 ϵ_{Hf} values documented in this study (e.g., group 4; Fig. 3.5C and D) are enigmatic as anomalously depleted signatures are rare in Meso- to Neoproterozoic rocks worldwide (Guitreau et al., 2012). However, elevated ϵ_{Hf} signatures have been reported in the Superior Province, including ϵ_{Hf} values as high as +8 to +12 from whole-rock and zircon samples from the Wawa and Abitibi subprovinces (Fig. 3.5A and B; Smith et al., 1987; Ketchum et al., 2008, respectively). It has been proposed that these ϵ_{Hf} values reflect derivation from melt sources in the lower crust or upper mantle that experienced prior melt histories (Smith et al., 1987). For example, melts sourced from garnet-rich residues, which would have elevated Lu-Hf ratios, may inherit anomalously high ϵ_{Hf} (e.g., Zheng et al., 2005). Therefore, we interpret the ϵ_{Hf} values > +10 to reflect derivation from volumetrically minor crustal or mantle regions that retained multi-stage melt histories.

While data groups 1-4 can be interpreted within the framework of the published isotopic data and geological history of the southern Superior Province (Fig. 3.5A), data from group 5 does not fit this model. It is possible that they may correlate to undocumented lithologies, reflect multi-stage melt processes, and/or represent artifacts of data reduction. An assessment of U-Th-Pb data following the method outlined in Pidgeon et al. (2017), compared measured $^{232}\text{Th}/^{238}\text{U}$ ratios to those predicted based on measured Th/U and $^{208}\text{Pb}/^{232}\text{Th}$ ratios, and $^{207}\text{Pb}/^{206}\text{Pb}$ age (Fig. 3.8). While rare in other data groups (Fig. 3.8A and B), analyses in data

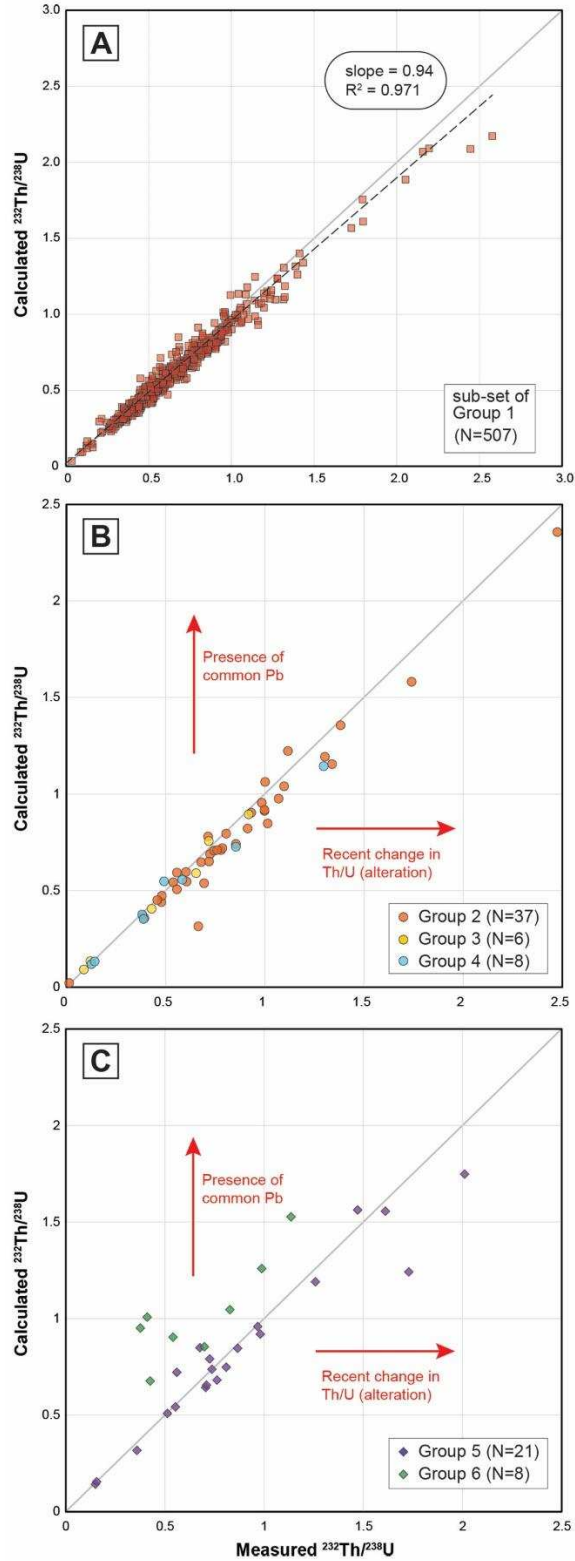


Figure 3.8 – U-Th-Pb assessment for the detrital zircon analyses in this study. Measured $^{232}\text{Th}/^{238}\text{U}$ ratios versus $^{232}\text{Th}/^{238}\text{U}$ ratios calculated from measured $^{208}\text{Pb}/^{206}\text{Pb}$ ratios for a representative subset of analyses from data group 1 (A), data groups 2, 3, and 4 (B), and data groups 4 and 5 (C) (2σ uncertainty is less than symbol size).

group 5 display high calculated $^{232}\text{Th}/^{238}\text{U}$ relative to measured ratios, suggesting that these results are likely affected by common Pb contamination (Fig. 3.8C). Therefore, the U-Pb ages for these grains are likely overestimated and may be correlative to similarly elevated ϵ_{Hf} values in data group 4.

3.6 Significance of Lu-Hf results to the record of crust-mantle reservoirs in the Superior Province

Our data set is dominated by zircon grains with ϵ_{Hf} signatures that are centered on the mMORB-DM composition projected to ~2750-2700 Ma (Fig. 3.5C and D). As discussed above, these zircon grains were likely derived from a combination of local, Abitibi subprovince sources, and distal, non-Abitibi subprovince domains in the southern Superior Province (Figs. 3.5 and 3.6). Non-Abitibi sources represent domains that were juxtaposed during regional amalgamation prior to and during development of the Abitibi successor basins. Each of these domains – e.g., the Wawa and Marmion subprovinces – contain Neoproterozoic and, locally, Mesoproterozoic zircon with ϵ_{Hf} signatures equivalent to mMORB-DM compositions (Fig. 3.5). The magnitudes of separation of these domains prior to their amalgamation in the Neoproterozoic are unknown (Percival et al., 2012). However, based on the present day configuration, the proportion of shortening recorded (50-100%), and a >25 Myr record of convergence (assuming conservative rates of 60 km/Myr) defined by amalgamation events from ~2715 Ma in the Winnipeg River and Western Wabigoon subprovince to ~2690 Ma in the Abitibi and Wawa subprovinces (Percival et al., 2012 and references therein), they likely represent horizontal dimensions of 100s to potentially several 1000 kilometers. There is no evidence for a temporal progression from CHUR towards DM compositions during volcano-plutonic construction and no coeval complementary enriched reservoir is observed (Fig. 3.5). Thus, it is unlikely that the observed mMORB-DM-like signature developed beneath these domains by direct differentiation from a chondritic source during synchronous magmatism, suggesting that it developed by the activity of pre-3000 Ma geodynamic processes. Based on this interpretation and the broad area of provenance observed, we suggest that a mMORB-DM-like reservoir was not only well-established within the Meso- to Neoproterozoic mantle beneath each of the domains within the southern Superior Province when they formed, but was pervasive in the mantle by this time.

While mMORB-DM-like ϵ_{Hf} signatures dominate in our results (e.g., group 1), it is less apparent that progressively younger grains spread towards CHUR-like values (Fig. 3.5C and D). This trend can be explained by reworking of juvenile crust after short-lived residence (Fig. 3.7), which is well-documented in the region. In the Abitibi and Wawa subprovinces, younger, syn- to post-deformational intrusions display $\epsilon_{\text{Hf}} \approx 0$ to +2.5, while older, volcanic assemblage host

rocks display ϵ_{Hf} values of +4 to +7 (Fig. 3.5A and B; Smith et al., 1987; Corfu and Noble, 1992), which is also well-described by whole-rock Nd isotopic data (Ayer et al., 2002; Lodge, 2016). A comparable temporal trend is observed in juvenile arcs associated with the Proterozoic Svecofennian orogeny in Sweden (Guitreau et al., 2014). In these arcs, decreasing ϵ_{Hf} with time is interpreted to reflect initial arc growth by extraction from a depleted reservoir and subsequent lowering of ϵ_{Hf} in magmatically-derived zircon grains by internal reworking and/or arc accretion. It is important to note that isotopic differentiation in juvenile terrains may be difficult to recognize. Newly formed juvenile terrains tend to display a strongly depleted signature, whereas the magnitude of temporal changes in ϵ_{Hf} values are relatively small (1-5 units), particularly when no older crust is involved. Therefore, given the minimum uncertainty on ϵ_{Hf} measurements ($2\sigma = 1-4$ units; Guitreau et al., 2012), recognizing the first-cycle of reworking can be problematic (e.g., Bleeker, 2002; Lodge, 2016). To adequately distinguish reworking of juvenile crust, more accurate solution methods, targeted lithological analysis, oxygen isotopes, and/or trace element trends may be required (e.g., Guitreau et al., 2012, 2014).

3.7 Significance of Lu-Hf results to Archean geodynamic processes

Our results indicate that a mMORB-DM was well-established and repeatedly tapped in the mantle associated with construction of the southern Superior Province (Fig. 3.7). However, the exact geodynamic mechanism responsible for depletion of the upper mantle reservoir is unclear. Since the modern compositions of the depleted mantle and the continental crust are complementary (Hofmann, 1988), any prospective geodynamic mechanism must account for the production of both. Previous interpretations include transient episodes of subduction (Moyen and van Hunen, 2012), or more sustained subduction through plate tectonics (Shirey et al., 2008), which achieve a depleted mantle by progressive sequestration of material into volcanic arcs and into the deep mantle by foundering of slabs. Alternative interpretations include whole mantle-scale overturn/upwelling events (Stein and Hofmann, 1994; Bédard, 2006, 2018; Bédard and Harris, 2014) with intervening periods of stagnant-lid behavior (O'Neil et al., 2007, 2013; Piper, 2013; Bédard, 2018). Discriminating between these processes from the isotopic record is difficult. However, some of the models predict specific temporal trends and isotopic or geochemical signatures.

The mantle overturn/upwelling model can explain the formation of a depleted upper mantle, but does not explain its time-integrated evolution and the isotopic signatures recorded in the juvenile crust produced by it. This is due to the fact that mantle overturn upwelling zones (OUZOs) transport primitive lower mantle material to the upper mantle, effectively homogenizing geochemical signatures and producing CHUR-like upper mantle compositions (Bédard, 2018).

Consequently, OUZO-derived juvenile crust is predicted to have a primitive mantle (CHUR-like) isotopic signature, with minimal depleted mantle signatures. Extraction of OUZO-derived melts would leave behind a depleted upper mantle residue, which may persist during intervening stagnant-lid episodes. However, stagnant-lid episodes are inferred to represent quiescent periods with no crustal growth (Piper, 2013), leaving this reservoir effectively untapped. The overturn/upwelling model has been used to explain Neoproterozoic crustal genesis and amalgamation of the Superior Province (Bédard, 2006, 2018; Bédard and Harris, 2014). In this model, an OUZO drives disaggregation of older, pre-2800 Ma crust and melting in the intervening regions, forming the juvenile Neoproterozoic magmatic domains such as the Abitibi subprovince (Bédard and Harris, 2014; Bédard, 2018). Our observations are inconsistent with this model, since strongly depleted signatures dominate our results and no accompanying data with enriched signatures are observed. Our data combined with previously published data, form a regionally extensive and record of repeated extraction of crustal material from a mMORB-DM-like reservoir from ~3000 Ma to ~2700 Ma (Fig. 3.5). In addition, the primitive (CHUR-like) signatures are a minor component of our data set and are more easily explained by secondary processes such as mixing of juvenile magmas with those derived from older crust or by crustal reworking during amalgamation (Fig. 3.7; see below). Thus, while an OUZO event may explain the formation of the depleted mantle prior to late Meso- to Neoproterozoic crustal genesis, it is inconsistent with the dominant mMORB-DM-like signature that characterizes crust of that age in the southern Superior Province.

An alternative model involves a hybrid, two-stage process with an early stage of plume upwelling and a later history of subduction-driven geodynamic behavior (after Guitreau et al., 2012). In the first stage, upper mantle depletion is accomplished through the build-up of refractory melt residues by the transit of deeply sourced mantle plumes, similar to the mantle overturn/upwelling model. Our data indicate that derivation from a depleted upper mantle reservoir repeatedly occurred from ~3000 Ma (Fig. 3.5C and D), suggesting that plume residues would have had formed this reservoir by this time. In part, melting at plume heads may have contributed to the formation of juvenile crust, although, in this model, the majority of growth occurred at subduction zones by partial melting of the newly formed depleted upper mantle. The Abitibi subprovince has previously been proposed to represent an oceanic plateau that also records subduction signatures (Benn and Moyen, 2008), comparable to predictions made in the hybrid model. In the older volcanic successions (~2750-2704 Ma) of the Abitibi subprovince, plume influences are inferred based on the presence of komatiite rocks (Dostal and Mueller, 1996, 1997; Wyman et al., 1999, 2002; Sproule et al., 2002), which are absent in the younger

volcanic successions (~2704-2695 Ma; Blake River assemblage). Instead, bimodal volcanic associations (basalt-rhyolite) and subduction-like geochemical trends are dominant in the younger successions (Polat and Kerrich, 2001, 2006; Ayer et al., 2002; Benn and Moyen, 2008; Polat et al., 2017). Thus, we suggest that the Abitibi (and other) juvenile subprovinces formed in an arc-like setting by crustal growth through direct derivation from a modern-style depleted mantle reservoir (i.e., the mMORB-DM). This type of mixed geodynamic signal is well-documented in modern settings. For example, they exist along Circum-Pacific plate boundaries, where hot spot-derived, oceanic plateaus are being subducted along continental margins (e.g., the Carnegie ridge in Ecuador; the Cocos ridge, Costa Rica; the Hikurangi ridge in New Zealand, and the Palau-Kyushu ridge in Japan; Martin et al., 2014 and references therein). At these locations, subduction of oceanic plateaus is associated with elevated magma production rates and the trace element geochemistry compositions are comparable to those observed in Archean TTGs (Martin et al., 2014), which suggest a similar process may have been in operation during the Archean. Subduction of oceanic plateaus may explain the large volume of crustal production observed in the Neoproterozoic juvenile subprovinces of the southern Superior Province and is consistent with the mMORB-DM-like signatures we observe. We acknowledge that conditions, such as higher ambient mantle temperatures (Korenaga, 2008a,b; Herzberg et al., 2010) or thicker oceanic lithosphere (Herzberg and Rudnick, 2012) were likely in the Archean, but consider that subduction-accretion geodynamic systems broadly similar to modern environments were well-established by the late Meso- to Neoproterozoic.

The depleted mantle evolution curve we utilize (mMORB-DM) was calculated by projecting modern day values (Griffin et al., 2002) into the Archean. This curve intersects CHUR compositions at ~4100 Ma, which is proposed to be a transitional period in Earth geodynamics (Martin, 1993). Some have suggested that this is when sustained plate tectonic processes began (Blichert-Toft and Albarède, 2008; Hopkins et al., 2008; Shirey et al., 2008), which, if correct, suggests that the mMORB-DM curve reflects more or less continuous operation of subduction-tectonic systems since the late Hadean. However, coupled continental growth and mantle depletion may have been episodic (Condie, 1998), gradual (Dhuime et al., 2012), rapid (Armstrong, 1981), and/or nonlinear (Fyfe, 1978; Campbell, 2003) early in Earth's history, making these types of broad projections problematic. Despite complications, our data support the presence of a long-lived mMORB-DM reservoir in the southern Superior Province and the operation of subduction-tectonic processes since at least ~3000 Ma (Fig. 3.7). This time in Earth history has been recognized as a point when geodynamic systems shifted towards a plate tectonic-dominated system (Shirey and Richardson, 2011; Dhuime et al., 2012; Næraa et al.,

2012; Satkoski et al., 2013). Based on Nd and Os isotopic compositions of inclusions in diamonds from kimberlites, a change from peridotite to eclogite mantle components at ~3000 Ma is interpreted to reflect hydration of the upper mantle due to initiation of plate tectonic processes (Shirey and Richardson, 2011). Similarly, Hf isotopes in gneissic-plutonic rocks from west Greenland and the Minnesota River Valley subprovince display closed-system behavior, governed by internal reworking, prior to ~3200 Ma and open-system behavior, with mixing between juvenile material and recycled older crust, at ~3200 Ma that has been interpreted to reflect the transition to plate tectonic-dominated dynamics (Næraa et al., 2012; Satkoski et al., 2013). Our data support these inferences and are consistent with the operation of modern-style plate tectonic processes since at least the late-Mesoarchean.

3.8 Conclusions

This study presents ~1800 paired U-Pb and Lu-Hf LA-ICP-MS analysis of detrital zircon grains from successor basins of the Abitibi and Pontiac subprovinces. These results represent the most comprehensive multi-isotope detrital zircon data set in the region, providing a robust view of the isotopic character of magmatic source regions. The majority of analyses (96%) yielded ϵ_{Hf} values of +1 to +10 in the ~3000-2675 Ma age range (data group 1), while a relatively minor component (<4%) of the results yielded evolved (negative) or anomalously radiogenic ϵ_{Hf} values (data groups 2-4). The dominant portion of our results (data group 1) plot along modern MORB-DM compositions projected into the Archean, indicating that crustal genesis repeatedly occurred by derivation from this reservoir. The subordinate CHUR-like or more evolved results (data groups 2 and 3) are best explained by a combination of reworking after short-lived crustal residence and local derivation from or mixing with magmas derived from domains with older, Mesoarchean crustal components. The anomalously radiogenic results (data group 4) are interpreted in terms of volumetrically minor crustal or mantle sources that retained multi-stage melt histories.

These results were compared to the well-established geological framework and published multi-isotope zircon data from the southern Superior Province to provide insight into the provenance of the successor basins and the regional configuration during their deposition at ~2690-2670 Ma. This comparison indicates that, while local Neoproterozoic sources predominate, a significant component (>200 analyses) display Mesoarchean ages with mMORB-DM-like signatures that cannot have been derived from within the Abitibi and Pontiac subprovinces as no comparable rocks are documented within them. Viable source domains, with correlative U-Pb age and Lu-Hf signatures, include the Winnipeg River, Marmion, and Quetico subprovinces, similar to interpretations made from the U-Pb age patterns (Davis, 2002; Frieman et al., 2017).

Based on these regional correlations, we suggest that the dominant mMORB-DM signature in these crustal blocks, originally separated by 100s of kilometers, reflects a well-established and regionally extensive modern-style depleted upper mantle. Since no temporal progression from CHUR-like values or a coeval complementary enriched reservoir is observed, we suggest that pre-3000 Ma geodynamic processes must be responsible for the formation of this reservoir.

To assess which geodynamic processes could explain our observations, we compared to the isotopic, geochemical, and temporal trends predicted by a variety of proposed models. Geodynamic scenarios investigated included stagnant-lid behavior with intermittent mantle-scale overturn/upwelling events and modern style subduction-accretion plate tectonics. While the overturn/upwelling model can explain the formation of a depleted upper mantle reservoir prior to ~3000 Ma, it cannot explain protracted growth from this reservoir during widespread crustal genesis from ~3000 Ma to ~2700 Ma. This is due to the fact that upwelling primitive material results in the homogenization of the upper mantle and predicts that CHUR-like signatures will be observed in associated magmatic domains, which is inconsistent with the statistical dominance of mMORB-DM-like values in our results. We favor a hybrid model where pre-3000 Ma mantle upwelling or plume activity resulted in the initial development of the depleted upper mantle and post-3000 Ma tectonic processes resulted in a time-integrated evolution along predicted mMORB-DM compositions, supporting the onset of modern-style plate tectonic processes from at least the late-Mesoarchean.

3.9 Acknowledgments

Sample collection at Hoyle Pond and Kidd Creek was logistically supported by Goldcorp and Glencore. Onsite support from E. Barr and T. Gemmell was invaluable. The analytical work would not have been possible without the generous financial support of Osisko Mining. We thank B. Wares for his helpful comments of the geology of the Abitibi subprovince and ongoing interest in the results of this research. We thank M. Guitreau for fruitful discussions and helpful comments. In part, field work was supported by graduate student research grants from the Society of Economic Geologists Canada Foundation and the Geological Society of America awarded to B. Frieman and Colorado School of Mines Professional Development Funds to Y. Kuiper.

3.10 References

- Amelin, Y., Lee, D.C., Halliday, A.N., Pidgeon, R.T., 1999. Nature of the Earth's earliest crust from hafnium isotopes in single zircons. *Nature* 399, 252–255.
- Amelin, Y., Lee, D.C., Halliday, A.N., 2000. Early-middle Archaean crustal evolution deduced from Lu-Hf and U-Pb isotopic studies of single zircon grains. *Geochimica et Cosmochimica Acta* 64, 4205–4225. doi:10.1016/S00167037(00)00493-2.

- Armstrong, R.L., 1981. Radiogenic isotopes: the case for crustal recycling on a near-steady-state no-continental-growth Earth. *Royal Society of London Philosophical Transactions A* 301, 443–472.
- Augland, L.E., David, J., 2015. Protocrustal evolution of the Nuvvuagittuq Supracrustal Belt as determined by high precision zircon Lu-Hf and U-Pb isotope data. *Earth and Planetary Science Letters* 428, 162–171. doi:10.1016/j.epsl.2015.07.039
- Ayer, J., Amelin, Y., Corfu, F., Kamo, S., Ketchum, J., Kwok, K., Trowell, N., 2002. Evolution of the southern Abitibi greenstone belt based on U-Pb geochronology: Autochthonous volcanic construction followed by plutonism, regional deformation and sedimentation. *Precambrian Research* 115, 63–95. doi:10.1016/S0301-9268(02)00006-2
- Ayer, J.A., Thurston, P.C., Bateman, R., Dubé, B., Gibson, H.L., Hamilton, M.A., Hathway, B., Hocker, S.M., Houlié, M.G., Hudak, G., Ispolatov, V.O., Lafrance, B., Leshner, C.M., MacDonald, P.J., Pélouquin, A.S., Piercey, S.J., Reed, L.E., Thomson, P.H., 2005. Overview of results from the Greenstone Architecture Project: Discover Abitibi Initiative. Ontario Geological Survey Open File Report 6154, 146 p.
- Bédard, J.H., 2006. A catalytic delamination-driven model for coupled genesis of Archaean crust and sub-continental lithospheric mantle. *Geochimica et Cosmochimica Acta* 70, 1188–1214. doi:10.1016/j.gca.2005.11.008
- Bédard, J.H., 2018. Stagnant lids and mantle overturns: Implications for Archaean tectonics, magmagenesis, crustal growth, mantle evolution, and the start of plate tectonics. *Geoscience Frontiers* 9, 19–49.
- Bédard, J.H., Harris, L.B., 2014. Neoproterozoic disaggregation and reassembly of the Superior craton. *Geology* 42, 951–954. doi:10.1130/G35770.1
- Benn, K., Moyen, J.F., 2008. The late Archean Abitibi-Opatika terrane, Superior Province: A modified oceanic plateau. *Geologic Society of America Special Paper* 440, 173–197.
- Bickford, M.E., Wooden, J.L., Bauer, R.L., 2006. SHRIMP study of zircons from Early Archean rocks in the Minnesota River Valley: implications for the tectonic history of the Superior Province. *Geological Society of America Bulletin* 118, 94–108.
- Bleeker, W., 2002. Archaean tectonics: A review, with illustrations from the Slave craton. *Geological Society of London Special Publication* 199, 151–181.
- Bleeker, W., 2012. Lode gold deposits in ancient deformed and metamorphosed terranes: The role of extension in the formation of Timiskaming basins and large gold deposits, Abitibi greenstone belt—a discussion. Ontario Geological Survey Open File Report 6280, 47-1–47-12.
- Blichert-Toft, J., Albarède, F., 2008. Hafnium isotopes in Jack Hills zircons and the formation of the Hadean crust. *Earth and Planetary Science Letters* 265, 686–702.
- Böhm, C.O., Heaman, L.M., Creaser, R.A., Corkery, M.T., 2000. Discovery of pre-3.5 Ga exotic crust at the northwestern Superior Province margin, Manitoba. *Geology* 28, 75–78. doi:10.1130/0091-7613(2000)28<75:DOPGEC>2.0.CO;2
- Boily, M., Dion, C., 2002. Geochemistry of boninite-type volcanic rocks in the Frotet-Evans greenstone belt, Opatika subprovince, Quebec: implications for the evolution of Archaean greenstone belts. *Precambrian Research* 115, 349–371.

- Bouvier, A., Vervoort, J.D., Patchett, P.J., 2008. The Lu–Hf and Sm–Nd isotopic composition of CHUR: Constraints from unequilibrated chondrites and implications for the bulk composition of terrestrial planets. *Earth and Planetary Science Letters* 273, 48–57.
- Boyet, M., Carlson, R.W., 2005. ^{142}Nd evidence for early (>4.53 Ga) global differentiation of the silicate Earth. *Science* 309, 567–581. doi:10.1126/science.1113634
- Boyet, M., Carlson, R.W., 2006. A new geochemical model for the Earth's mantle inferred from ^{146}Sm – ^{142}Nd systematics. *Earth and Planetary Science Letters* 250, 254–268. doi:10.1016/j.epsl.2006.07.046.
- Campbell, I.H., 2003. Constraints on continental growth models from Nb/U ratios in the 3.5 Ga Barberton and other Archaean basalt-komatiite suites. *American Journal of Science* 303, 319–351.
- Card, K.D., Ciesielski, A., 1986. Subdivisions of the Superior Province of the Canadian Shield. *Geoscience Canada* 13, 5–13.
- Caro, G., Bourdon, B., Birck, J.L., Moorbath, S., 2003. ^{146}Sm – ^{142}Nd evidence from Isua metamorphosed sediments for early differentiation of the Earth's mantle. *Nature* 423, 428–432.
- Caro, G., Morino, P., Mojzsis, S.J., Cates, N.L., Bleeker, W., 2017. Sluggish Hadean geodynamics: Evidence from coupled $^{146,147}\text{Sm}$ – $^{142,143}\text{Nd}$ systematics in Eoarchean supracrustal rocks of the Inukjuak domain (Québec). *Earth and Planetary Science Letters* 457, 23–37.
- Cates, N.L., Mojzsis, S.J., 2007. Pre-3750 Ma supracrustal rocks from the Nuvvuagittuq supracrustal belt, northern Québec. *Earth and Planetary Science Letters* 255, 9–21.
- Cates, N.L., Ziegler, K., Schmitt, A.K., Mojzsis, S.J., 2013. Reduced, reused and recycled: detrital zircons of the 3780 Myr-old Nuvvuagittuq supracrustal belt (Quebec, Canada). *Earth and Planetary Science Letters* 316, 283–293.
- Chown, E.H., Daigneault, R., Mueller, W., Mortensen, J.K., 1992. Tectonic evolution of the Northern volcanic zone, Abitibi belt, Quebec. *Canadian Journal of Earth Sciences* 29, 2211–2225.
- Condie, K.C., 1998. Episodic continental growth and supercontinents: a mantle avalanche connection? *Earth and Planetary Science Letters* 163, 97–108.
- Condie, K.C., Bickford, M.E., Aster, R.C., Belousova, E., Scholl, D.W., 2011. Episodic zircon ages, Hf isotopic compositions, and the preservation rate of continental crust. *Geological Society of America Bulletin* 123, 951–957.
- Corcoran, P.L., Mueller, W.U., 2007. Time-transgressive Archean unconformities underlying molasse basin-fill successions of dissected oceanic arcs, Superior province, Canada. *Journal of Geology* 115, 655–674.
- Corfu, F., 1993. The evolution of the southern Abitibi greenstone belt in light of precise U–Pb geochronology. *Economic Geology* 88, 1323–1340.
- Corfu, F., Noble, S.R., 1992. Genesis of the southern Abitibi greenstone belt, Superior Province, Canada: Evidence from zircon Hf isotope analyses using a single filament technique. *Geochimica et Cosmochimica Acta* 56, 2081–2097.

- Corfu, F., Stott, G.M., 1998. Shebandowan greenstone belt, western Superior Province: U-Pb ages, tectonic implications, and correlations. *Geological Society of America Bulletin* 110, 1467–1484. doi:10.1130/0016-7606(1998)110<1467:SGBWSP>2.3.CO;2
- Corfu, F., Jackson, S.L., Sutcliffe, R.H., 1991. U–Pb ages and tectonic significance of late Archean alkalic magmatism and nonmarine sedimentation: Timiskaming Group, southern Abitibi belt, Ontario. *Canadian Journal of Earth Sciences* 28, 489–503. doi:10.1139/e91-043
- Corfu, F., Stott, G.M., Breaks, F.W., 1995. U-Pb geochronology and evolution of the English River subprovince, an Archean low P-high T metasedimentary belt in the Superior Province. *Tectonics* 14, 1220–1233.
- Darling, J.R., Moser, D.E., Heaman, L., Davis, W.J., O’Neil, J., Carlson, R., 2013. Eoarchean to Neoproterozoic evolution of the Nuvvuagittuq greenstone belt: new insights from U–Pb zircon geochronology. *American Journal of Science* 313, 844–876.
- David, J., Dion, C., Goutier, J., Roy, P., Bandyayera, D., Legault, M., Rhéaume, P., 2006. Datations U-Pb effectuées dans la Sous-province de l’Abitibi à la suite des travaux de 2004-2005. Ministère des Ressources naturelles et de la Faune du Québec, RP 2006-04, 22 p.
- David, J., Davis, D.W., Dion, C., Goutier, J., Legault, M., Roy, P., 2007. Datations U-Pb effectuées dans la Sous-province de l’Abitibi en 2005-2006. Ministère des Ressources naturelles et de la Faune du Québec, RP 2007-01, 17 p.
- David, J., Godin, L., Stevenson, R., O’Neil, J., Francis, D., 2009. U–Pb ages (3.8–2.7 Ga) and Nd isotope data from the newly identified Eoarchean Nuvvuagittuq supracrustal belt, Superior craton, Canada. *Geological Society of America Bulletin* 121, 150–163.
- Davis, D.W., 1998. Speculations on the formation and crustal structure of the Superior province from U-Pb geochronology. In: Harrap, R.M., Helmstaedt, H.H. (Eds.), *Western Superior Transect Fourth Annual Workshop*. Lithoprobe Report 65, 21–28, Lithoprobe Secretariat, University of British Columbia.
- Davis, D.W., 2002. U-Pb geochronology of Archean metasedimentary rocks in the Pontiac and Abitibi subprovinces, Quebec, constraints on timing, provenance and regional tectonics. *Precambrian Research* 115, 97–117. doi:10.1016/S0301-9268(02)00007-4
- Davis, D.W., Pezzutto, F., Ojakangas, R.W., 1990. The age and provenance of metasedimentary rocks in the Quetico subprovince, Ontario, from single zircon analyses: implications for Archean sedimentation and tectonics in the Superior Province. *Earth and Planetary Science Letters* 99, 195–205. doi:10.1016/0012-821X(90)90110-J
- Davis, W.J., Gariépy, C., Sawyer, E.W., 1994. Pre-2.8 Ga crust in the Opatoca gneiss belt: A potential source of detrital zircons in the Abitibi and Pontiac subprovinces, Superior Province, Canada. *Geology* 22, 1111–1114.
- Davis, D.W., Amelin, Y., Nowell, G.M., Parrish, R.R., 2005. Hf isotopes in zircon from the western Superior province, Canada: Implications for Archean crustal development and evolution of the depleted mantle reservoir. *Precambrian Research* 140, 132–156. doi:10.1016/j.precamres.2005.07.005
- Davis, W.J., Lacroix, S., Gariépy, C., Machado, N., 2000. Geochronology and radiogenic isotope geochemistry of plutonic rocks from the central Abitibi subprovince: Significance

- to the internal subdivision and plutono-tectonic evolution of the Abitibi belt. *Canadian Journal of Earth Sciences* 37, 117–133.
- De Souza, S., Dubé, B., McNicoll, V.J., Dupuis, C., Mercier-Langevin, P., Creaser, R.A., Kjarsgaard, I.M., 2017. Geology and hydrothermal alteration of the world-class Canadian Malartic gold deposit: Genesis of an Archean stockwork-disseminated gold deposit in the Abitibi greenstone belt. *Reviews in Economic Geology* 19, 263–291.
- Desrochers, J.P., Hubert, C., Ludden, J.N., Pilote, P., 1993. Accretion of Archean oceanic plateau fragments in the Abitibi greenstone belt, Canada. *Geology* 21, 451–454.
- Dhuime, B., Hawkesworth, C.J., Cawood, P.A., Storey, C.D., 2012. A change in geodynamics of continental growth 3 billion years ago. *Science* 335, 1334–1336.
- Dickinson, W.R., Gehrels, G.E., 2003. U–Pb ages of detrital zircons from Permian and Jurassic eolian sandstones of the Colorado Plateau, USA: paleogeographic implications. *Sedimentary Geology* 163, 29–66.
- Dimroth, E., Imreh, L., Rocheleau, M., Goulet, N., 1982. Evolution of the south-central part of the Archean Abitibi belt, Quebec. Part I: Stratigraphy and paleogeographic model. *Canadian Journal of Earth Sciences* 19, 1729–1758.
- Dimroth, E., Imreh, L., Goulet, N., Rocheleau, M., 1983. Evolution of the south-central segment of the Archean Abitibi belt, Quebec. Part III: Plutonic and metamorphic evolution and geotectonic model. *Canadian Journal of Earth Sciences* 20, 1374–1388.
- Dostal, J., Mueller, W., 1996. An Archean oceanic felsic dyke swarm in a nascent arc: The Hunter Mine Group, Abitibi greenstone Belt, Canada. *Journal of Volcanology and Geothermal Research* 72, 37–57.
- Dostal, J., Mueller, W., 1997. Komatiite flooding of a rifted Archean rhyolite complex: Geochemical signature and tectonic significance of the Stoughton-Roquemaure Group, Abitibi greenstone belt, Canada. *Journal of Geology* 105, 545–563.
- Feng, R., Kerrich, R., Maas, R., 1993. Geochemical, oxygen, and neodymium isotope compositions of metasediments from the Abitibi greenstone belt and Pontiac Subprovince, Canada: Evidence for ancient crust and Archean terrane juxtaposition. *Geochimica et Cosmochimica Acta* 57, 641–658.
- Fisher, C.M., Hanchar, J.M., Samson, S.D., Dhuime, B., Blichert-Toft, J., Vervoort, J.D., Lam, R., 2011. Synthetic zircon doped with hafnium and rare earth elements: a reference material for in situ hafnium isotope analysis. *Chemical Geology* 286, 32–47.
- Fralick, P., Purdon, R.H., Davis, D.W., 2006. Neoproterozoic trans-subprovince sediment transports in the southwestern Superior Province: Sedimentological, geochemical, and geochronological evidence. *Canadian Journal of Earth Sciences* 43, 1055–1070.
- Frieman, B.M., Kuiper, Y.D., Kelly N.M., Monecke, T., Kylander-Clark, A., 2017. Constraints on the geodynamic evolution of the southern Superior province: U–Pb LA-ICP-MS analysis of detrital zircon in successor basins of the Archean Abitibi and Pontiac subprovinces of Ontario and Quebec, Canada. *Precambrian Research* 292, 398–416.
- Fyfe, W.S., 1978. The evolution of the Earth's crust: Modern plate tectonics to ancient hot spot tectonics? *Chemical Geology* 23, 89–114.

- Gehrels, G.E., Blakey, R., Karlstrom, K.E., Timmons, J.M., Dickinson, B., Pecha, M., 2011. Detrital zircon U-Pb geochronology of Paleozoic strata in the Grand Canyon, Arizona. *Lithosphere* 3, 183–200. doi:10.1130/L121.1
- Goutier, J., Dion, C., David, J., Dion, D.J., 1999. Géologie de la région de la passe Shimusuminu et du lac Vion (33F/11 et 33F/12). Ministère des Ressources naturelles du Québec, RG 98-17, 41 p.
- Griffin, W.L., Wang, X., Jackson, S.E., Pearson, N.J., O'Reilly, S.Y., Xu, X., Zhou, X., 2002. Zircon chemistry and magma mixing, SE China: in-situ analysis of Hf isotopes, Tonglu and Pingtan igneous complexes. *Lithos* 61, 237–269.
- Guitreau, M., Blichert-Toft, J., Martin, H., Mojzsis, S.J., Albarède, F., 2012. Hafnium isotope evidence from Archean granitic rocks for deep-mantle origin of continental crust. *Earth and Planetary Science Letters* 337-338, 211–223.
- Guitreau, M., Blichert-Toft, J., Mojzsis, S.J., Roth, A.S.G., Bourdon, B., 2013. A legacy of Hadean silicate differentiation inferred from Hf isotopes in Eoarchean rocks of the Nuvvuagittuq supracrustal belt (Québec, Canada). *Earth and Planetary Science Letters* 362, 171–181.
- Guitreau, M., Blichert-Toft, J., Billström, K., 2014. Hafnium isotope evidence from early-Proterozoic volcanic arc reworking in the Skellefte district (northern Sweden) and implications for the Svecofennian orogeny. *Precambrian Research* 252, 39–52.
- Hamilton, W.B., 1998. Archean magmatism and deformation were not the products of plate tectonics. *Precambrian Research* 91, 143–179.
- Harrison, T.M., Blichert-Toft, J., Mueller, W., Albarède, F., Holden, P., Mojzsis, S.J., 2005. Heterogeneous Hadean hafnium: Evidence of continental crust at 4.4 to 4.5 Ga. *Science* 310, 1947–1950.
- Harrison, T.M., Schmitt, A.K., McCulloch, M.T., Lovera, O.M., 2008. Early (≥ 4.5 Ga) formation of terrestrial crust: Lu–Hf, $\delta^{18}\text{O}$, and Ti thermometry results for Hadean zircons. *Earth and Planetary Science Letters* 268, 476–486.
- Heather, K.B., Shore, G.T., 1999. Geology, Swayze greenstone belt, Ontario. Geological Survey of Canada Open File 3384a, scale 1:50,000.
- Henry, P., Stevenson, R., Larbi, Y., Gariépy, C. 2000. Nd isotopic evidence for Early to Late Archean (3.4- 2.7 Ga) crustal growth in the Western Superior Province (Ontario, Canada). *Tectonophysics* 322, 135–151.
- Herzberg, C., Rudnick, R., 2012. Formation of cratonic lithosphere: An integrated thermal and petrological model. *Lithos* 149, 4–15.
- Herzberg C., Condie K., Korenaga, J., 2010. Thermal history of the Earth and its petrological expression. *Earth and Planetary Science Letters* 292, 79–88.
- Hofmann, A.W., 1988. Chemical differentiation of the Earth: The relationship between mantle, continental crust, and oceanic crust. *Earth and Planetary Science Letters* 90, 297–314.
- Holubec, J., 1972. Lithostratigraphy, structure and deep crustal relations of Archean rocks of the Canadian Shield, Rouyn-Noranda area, Quebec. *Krystalinikum* 9, 63–88.

- Hopkins, M., Harrison, T.M., Manning, C.E., 2008. Low heat flow inferred from >4 Gyr zircons suggests Hadean plate boundary interactions. *Nature* 456, 493–496.
- Ickert, R.B., 2013. Algorithms for estimating uncertainties in initial radiogenic isotope ratios and model ages. *Chemical Geology* 340, 131–138.
- Jackson, S.L., Fyon, A.J., 1991. The western Abitibi subprovince in Ontario. *Ontario Geological Survey Special Volume 4/1*, 405–482.
- Jackson, S.L., Fyon, J.A., Corfu, F., 1994. Review of Archean supracrustal assemblages of the southern Abitibi greenstone belt in Ontario, Canada: Products of microplate interaction within a large-scale plate-tectonic setting. *Precambrian Research* 65, 183–205. doi:10.1016/0301-9268(94)90105-8
- Jackson, S.E., Pearson, N.J., Griffin, W.L., Belousova, E.A., 2004. The application of laser-ablation-inductively coupled plasma-mass spectrometry to in situ U/Pb zircon geochronology. *Chemical Geology* 211, 47–69.
- Kemp, A.I.S., Wilde, S.A., Hawkesworth, C.J., Coath, C.D., Nemchin, A., Pidgeon, R.T., Vervoort, J.D., DuFrane, S.A., 2010. Hadean crustal evolution revisited: New constraints from Pb-Hf isotope systematics of the Jack Hills zircons. *Earth and Planetary Science Letters* 296, 45–56.
- Kerrick, R., Polat, A., Wyman, D.A., Hollings, P., 1999. Trace element systematics of Mg- to Fe-tholeiitic basalt suites of the Superior province: Implications for Archean mantle reservoirs and greenstone belt genesis. *Lithos* 46, 163–187.
- Ketchum, J.W.F., Ayer, J.A., van Breemen, O., Pearson, N.J., Becker, J.K., 2008. Pericontinental crustal growth of the southwestern Abitibi subprovince, Canada - U-Pb, Hf, and Nd isotope evidence. *Economic Geology* 103, 1151–1184. doi:10.2113/gsecongeo.103.6.1151
- Kinny, P.D., Maas, R., 2003. Lu–Hf and Sm–Nd isotope systems in zircon. *Reviews in Mineralogy and Geochemistry* 53, 327–341.
- Korenaga, J., 2008a. Plate tectonics, flood basalts, and the evolution of Earth’s oceans. *Terra Nova* 20, 419–39.
- Korenaga, J., 2008b. Urey ratio and the structure and evolution of Earth’s mantle. *Reviews of Geophysics* 46, RG2007.
- Kylander-Clark, A.R.C., Hacker, B.R., Cottle, J.M., 2013. Laser-ablation split-stream ICP petrochronology. *Chemical Geology* 345, 99–112. doi:10.1016/j.chemgeo.2013.02.019
- Leclerc, F., Houlié, P., Rogers, R., 2011. Géologie de la région de Chapais (32G15-200-0101). Ministère des Ressources naturelles, de la Faune et des Parcs du Québec, report RP 2010-09, 19 p.
- Leclerc, F., Harris, L.B., Bédard, J.H., van Breemen, O., Goulet, N., 2012. Structural and stratigraphic controls on magmatic, volcanogenic, and shear zone-hosted mineralization in the Chapais-Chibougamau mining camp, northeastern Abitibi, Canada. *Economic Geology* 107, 963–989.
- Lodge, R.W.D., 2016. Petrogenesis of intermediate volcanic assemblages from the Shebandowan greenstone belt, Superior Province: Evidence for subduction during the

- Neoproterozoic. *Precambrian Research* 272, 150–167.
doi:10.1016/j.precamres.2015.10.018
- Lodge, R.W.D., Gibson, H.L., Stott, G.M., Hudak, G.J., Jirsa, M.A., Hamilton, M.A., 2013. New U–Pb geochronology from Timiskaming-type assemblages in the Shebandowan and Vermilion greenstone belts, Wawa subprovince, Superior Craton: Implications for the Neoproterozoic development of the southwestern Superior Province. *Precambrian Research* 235, 264–277. doi:10.1016/j.precamres.2013.06.011
- Lu, Y., McCuaig, T.C., Hollings, P., Ketchum, K., Kerrich, R., Smyk, M., Cliff, J., Bagas, L., 2013. Zircon multi-isotopic mapping in Wabigoon Subprovince, western Superior Craton: Implications for lithospheric architecture and controls on orogenic gold mineral systems. *Proceedings, 12th Biennial Meeting, Society For Geology Applied To Mineral Deposits* 3, 1148–1151.
- Ludden, J., Hubert, C., Gariépy, C., 1986. The tectonic evolution of the Abitibi greenstone belt of Canada. *Geological Magazine* 123, 153–166.
- Martin, H., 1993. The mechanisms of petrogenesis of the Archean continental crust – Comparison with modern processes. *Lithos* 30, 373–388.
- Martin, H., Moyen, J.-F., Guitreau, M., Blichert-Toft, J., Le Pennec, J.-L., 2014. Why Archean TTG cannot be generated by MORB melting in subduction zones. *Lithos* 198-199, 1–13.
- McNicoll, V., Goutier, J., Dubé, B., Mercier-Langevin, P., Ross, P.S., Dion, C., Monecke, T., Legault, M., Percival, J., Gibson, H., 2014. U-Pb geochronology of the Blake River Group, Abitibi greenstone belt, Quebec, and implications for base metal exploration. *Economic Geology* 109, 27–59.
- Melnyk, M., Davis, D.W., Cruden, A.R., Stern, R.A., 2006. U-Pb ages constraining structural development of an Archean terrane boundary in the Lake of the Woods area, western Superior Province, Canada. *Canadian Journal of Earth Sciences* 43, 967–993.
doi:10.1139/E06-35
- Monecke, T., Mercier-Langevin, P., Dubé, B., Frieman, B.M., 2017. Geology of the Abitibi greenstone belt. *Reviews in Economic Geology* 19, 7–49.
- Morel, M.L.A., Nebel, O., Nebel-Jacobsen, Y.J., Miller, J.S., Vroon, P.Z., 2008. Hafnium isotope characterization of the GJ-1 zircon reference material by solution and laser-ablation MC-ICPMS. *Chemical Geology* 255, 231–235. doi:10.1016/j.chemgeo.2008.06.040
- Mortensen, J.K., Card, K.D., 1993. U-Pb age constraints for the magmatic and tectonic evolution of the Pontiac subprovince, Quebec. *Canadian Journal of Earth Sciences* 30, 1970–1980.
- Mortensen, J.K., 1993a. U-Pb geochronology of the eastern Abitibi subprovince. Part 1: Chibougamau-Matagami-Joutel region. *Canadian Journal of Earth Sciences* 30, 11–28.
- Mortensen, J.K., 1993b. U-Pb geochronology of the eastern Abitibi subprovince. Part 2: Noranda-Kirkland Lake area. *Canadian Journal of Earth Sciences* 30, 29–41.
- Moser, D.E., Heaman, L.M., Krogh, T.E., Hanes, J.A., 1996. Intracrustal extension of an Archean orogen revealed using single-grain U-Pb zircon geochronology. *Tectonics* 15, 1093–1109.

- Moyen, J.F., van Hunen, J., 2012. Short-term episodicity of Archean plate tectonics. *Geology* 40, 451–454.
- Næraa, T., Scherstén, A., Rosing, M.T., Kemp, A.I.S., Hoffmann, J.E., Kokfelt, T.F., Whitehouse, M.J., 2012. Hafnium isotope evidence for a transition in the dynamics of continental growth 3.2 Ga ago. *Nature* 485, 627–631.
- O’Neil, J., Carlson, R.W., 2017. Building Archean cratons from Hadean mafic crust. *Science* 355, 1199–1202.
- O’Neil, J., Carlson, R.W., Francis, D., Stevenson, R.K., 2008. Neodymium-142 evidence for Hadean mafic crust. *Science* 321, 1828–1831.
- O’Neil, J., Carlson, R.W., Paquette, J.L., Francis, D., 2012. Formation age and metamorphic history of the Nuvvuagittuq Greenstone Belt. *Precambrian Research* 220–221, 23–44.
- O’Neil, J., Boyet, M., Carlson, R.W., Paquette, J.L., 2013. Half a billion years of re-working of Hadean mafic crust to produce the Nuvvuagittuq Eoarchean felsic crust. *Earth and Planetary Science Letters* 379, 13–25.
- O’Neill, C., Lenardic, A., Moresi, L., Torsvik, T.H., Lee, C.T.A., 2007. Episodic Precambrian subduction. *Earth and Planetary Science Letters* 262, 552–562.
- O’Neill, C., Debaille, V., Griffin, W., 2013. Deep Earth recycling in the Hadean and constraints on surface tectonics. *American Journal of Science* 313, 912–932.
- Paton, C., Hellstrom, J., Paul, B., Woodhead, J., Hergt, J., 2011. Iolite: Freeware for the visualization and processing of mass spectrometer data. *Journal of Analytical Atomic Spectrometry* 26, 2508–2518.
- Percival, J.A., Sanborn-Barrie, M., Skulski, T., Stott, G.M., Helmstaedt, H., White, D.J., 2006. Tectonic evolution of the western Superior Province from NATMAP and Lithoprobe studies. *Canadian Journal of Earth Sciences* 43, 1085–1117.
- Percival, J.A., Skulski, T., Sanborn-Barrie, M., Stott, G.M., Leclair, A.D., Corkery, M.T., Boily, M., 2012. Geology and tectonic evolution of the Superior Province, Canada. *Geological Association of Canada Special Paper* 49, 321–378.
- Pidgeon, R.T., Nemchin, A.A., Whitehouse, M.J., 2017. The effect of weathering on the U-Th-Pb and oxygen isotope systems of ancient zircons from the Jack Hills, Western Australia. *Geochimica et Cosmochimica Acta* 197, 142–166.
- Piper, J.D.A., 2013. A planetary perspective on Earth evolution: lid tectonics before plate tectonics. *Tectonophysics* 589, 44–56.
- Polat, A., Kerrich, R., 2001. Geodynamic processes, continental growth, and mantle evolution recorded in late Archean greenstone belts of the southern Superior Province, Canada. *Precambrian Research* 112, 5–25.
- Polat, A., Kerrich, R., 2006. Regarding the geochemical fingerprints of Archean hot subduction volcanic rocks: evidence for accretion and crustal recycling in a mobile tectonic regime. *American Geophysical Union Monograph* 164, 189–213.
- Polat, A., Frei, R., Longstaffe, F.J., Woods, R., 2017. Petrogenetic and geodynamic origin of the Neoproterozoic Doré Lake Complex, Abitibi subprovince, Superior Province, Canada. *International Journal of Earth Sciences* (published online), 33 p.

- Powell, W.G., Carmichael, D.M., Hodgson, C.J., 1995. Conditions and timing of metamorphism in the southern Abitibi greenstone belt, Quebec. *Canadian Journal of Earth Sciences* 32, 787–805.
- Ropchan, J.R., Luinstra, B., Fowler, A.D., Benn, K., Ayer, J., Berger, B., Dahn, R., Labine, R., Amelin, Y., 2002. Host-rock and structural controls on the nature and timing of gold mineralization at the Holloway mine, Abitibi subprovince, Ontario. *Economic Geology* 97, 291–309. doi:10.2113/gsecongeo.97.2.291
- Sanborn-Barrie, M., Skulski, T., 2006. Sedimentary and structural evidence for 2.7 Ga continental arc-oceanic-arc collision in the Savant-Sturgeon greenstone belt, western Superior Province, Canada. *Canadian Journal of Earth Sciences* 43, 995–1030. doi:10.1139/E06-060
- Satkoski, A.M., Bickford, M.E., Samson, S.D., Bauer, R.L., Mueller, P.A., Kamenov, G.D., 2013. Geochemical and Hf-Nd isotopic constraints on the crustal evolution of the Archean rocks from the Minnesota River Valley, USA. *Precambrian Research* 224, 36–50.
- Sawyer, E.W., Benn, K., 1993. Structure of the high-grade Opatoca belt and adjacent low-grade Abitibi subprovince, Canada: An Archean mountain front. *Journal of Structural Geology* 15, 1443–1458.
- Schmitz, M.D., Bowring, S.A., Southwick, D.L., Boerboom, T.J., Wirth, K.R., 2006. High-precision U–Pb geochronology in the Minnesota River Valley subprovince and its bearing on the Neoproterozoic to Paleoproterozoic evolution of the southern Superior Province. *Geological Society of America Bulletin* 118, 82–93.
- Shirey, S.B., Richardson, S.H., 2011. Start of the Wilson cycle at 3 Ga shown by diamond from subcontinental mantle. *Science* 333, 434–436.
- Shirey, S.B., Kamber, B.S., Whitehouse, M.J., Mueller, P.A., Basu, A.R., 2008. A review of the isotopic and trace element evidence for mantle and crustal processes in the Hadean and Archean: Implications for the onset of plate tectonic subduction. *Geologic Society of America Special Paper* 440, 1–29.
- Sláma, J., Košler, J., Condon, D.J., Crowley, J.L., Gerdes, A., Hanchar, J.M., Horstwood, M.S.A., Morris, G.A., Nasdala, L., Norberg, N., Schaltegger, U., Schoene, B., Tubrett, M.N., Whitehouse, M.J., 2008. Plešovice zircon — A new natural reference material for U–Pb and Hf isotopic microanalysis. *Chemical Geology* 249, 1–35. doi:10.1016/j.chemgeo.2007.11.005
- Smith, P.E., Tatsumoto, M., Faarquhar, R.M., 1987. Zircon Lu–Hf Systematics and the evolution of the Archean crust in the southern Superior Province, Canada. *Contributions to Mineralogy and Petrology* 97, 93–104.
- Söderlund, U., Patchett, P.J., Vervoort, J.D., Isachsen, C.E., 2004. The ^{176}Lu decay constant determined by Lu-Hf and U-Pb isotope systematics of Precambrian mafic intrusions. *Earth and Planetary Science Letters* 219, 311–324.
- Sproule, R.A., Leshar, C.M., Ayer, J.A., Thurston, P.C., Herzberg, C.T., 2002. Spatial and temporal variations in the geochemistry of komatiites and komatiitic basalts in the Abitibi greenstone belts. *Precambrian Research* 115, 153–186.
- Stein, M., Hofmann, A.W., 1994. Mantle plumes and episodic crustal growth. *Nature* 372, 63–68.

- Stevenson, R.K., Patchett, P.J., 1990. Implications for the evolution of continental crust from Hf isotopes of Archean detrital zircons. *Geochimica et Cosmochimica Acta* 54, 1683–1697.
- Stott, G.M., Davis, D.W., Parker, J.R., Straub, K.J., Tomlinson, K.Y., 2002. Geology and tectonostratigraphic assemblages, eastern Wabigoon subprovince, Ontario. Geological Survey of Canada Open File 4285, scale 1:250,000.
- Stott, G.M., Corkery, M.T., Percival, J.A., Simard, M., Goutier, J., 2010. A revised terrane subdivision of the Superior Province. Ontario Geological Survey Open File Report 6260, 20–1 to 20–10.
- Taylor, S.R., McLennan, S.M., 1995. The geochemical evolution of the continental crust. *Reviews of Geophysics* 33, 241–265.
- Thirwall, M.F., Anczkiewicz, R., 2004. Multidynamic isotope ratio analysis using MC-ICP-MS and the causes of secular drift in Hf, Nd and Pb isotope ratios. *International Journal of Mass Spectrometry* 235, 59–81.
- Thurston, P.C., Ayer, J.A., Goutier, J., Hamilton, M.A., 2008. Depositional gaps in Abitibi greenstone belt stratigraphy: A key to exploration for syngenetic mineralization. *Economic Geology* 103, 1097–1134. doi:10.2113/gsecongeo.103.6.1097
- Tomlinson, K.Y., Stott, G.M., Percival, J.A., Stone, D., 2004. Basement terrane correlations and crustal recycling in the western Superior Province: Nd isotopic character of granitoid and felsic volcanic rocks in the Wabigoon subprovince, N. Ontario, Canada. *Precambrian Research* 132, 245–274. doi:10.1016/j.precamres.2003.12.017
- Turek, A., Sage, R.P., Van Schmus, W.R., 1992. Advances in the U-Pb zircon geochronology of the Michipicoten greenstone belt, Superior Province, Ontario. *Canadian Journal of Earth Sciences* 29, 1154–1165.
- Van Kranendonk, M.J., Ivanic, T.J., Wingate, M.T.D., Kirkland, C.L., Wyche, S., 2013. Long-lived, autochthonous development of the Archean Murchison Domain, and implications for Yilgarn Craton tectonics. *Precambrian Research* 229, 49–92.
- Vervoort, J.D., Patchett, P.J., 1996. Behavior of hafnium and neodymium isotopes in the crust: Constraints from Precambrian crustally derived granites. *Geochimica et Cosmochimica Acta* 60, 3717–3733.
- Vervoort, J.D., Patchett, P.J., Söderlund, U., Baker, M., 2004. Isotopic composition of Yb and the determination of Lu concentrations and Lu/Hf ratios by isotope dilution using MC-ICPMS. *Geochemistry Geophysics Geosystems* 5, 15 p.
- Wiedenbeck, M., Allé, P., Corfu, F., Griffin, W.L., Meier, M., Oberli, F., von Quadt, A., Roddick, J.C., Spiegel, W., 1995. Three natural zircon standards for U-Th-Pb, Lu-Hf, trace element and REE analyses. *Geostandards Newsletter* 19, 1–23.
- Wiedenbeck, M., Hanchar, J.M., Peck, W.H., Sylvester, P., Valley, J., Whitehouse, M., Kronz, A., Morishita, Y., Nasdala, L., Fiebig, J., Franchi, I., Girard, J.-P., Greenwood, R.C., Hinton, R., Kita, N., Mason, P.R.D., Norman, M., Ogasawara, M., Piccoli, P.M., Rhede, D., Satoh, H., Schulz-Dobrick, B., Skår, Ø., Spicuzza, M.J., Terada, K., Tindle, A., Togashi, S., Vennemann, T., Xie, Q., Zheng, Y.F., 2004. Further characterization of the 91500 zircon crystal. *Geostandards and Geoanalytical Research* 28, 9–39.
- Wyman, D.A., Kerrich, R., Groves, D.I., 1999. Lode gold deposits and Archean mantle-plume-island arc interaction, Abitibi subprovince, Canada. *Journal of Geology* 107, 715–725.

- Wyman, D.A., Kerrich, R., Polat, A., 2002. Assembly of Archean cratonic mantle lithosphere and crust: Plume-arc interaction in the Abitibi-Wawa subduction-accretion complex. *Precambrian Research* 115, 37–62.
- Zaleski, E., van Breemen, O., Peterson, V.L., 1999. Geological evolution of the Manitouwadge greenstone belt and Wawa-Quetico subprovince boundary, Superior Province, Ontario, constrained by U-Pb zircon dates of supracrustal and plutonic rocks. *Canadian Journal of Earth Sciences* 36, 945–966. doi:10.1139/e99-016
- Zheng, Y.F., Wu, Y.B., Zhao, Z.F., Zhang, S.B., Xu, P., Wu, F.Y., 2005. Metamorphic effect on zircon Lu-Hf and U-Pb isotope systems in ultrahigh-pressure eclogite-facies metagranite and metabasite. *Earth and Planetary Science Letters* 240, 378–400.

CHAPTER 4

ACROSS-STRIKE ARCHITECTURE OF HIGH- AND LOW-STRAIN ZONES NORTH OF THE LARDER LAKE-CADILLAC DEFORMATION ZONE IN THE KIRKLAND LAKE AREA, ONTARIO, CANADA

Crustal-scale fault zones and their higher-order structural networks may be host to economically significant orogenic gold deposits in mountain belts of all ages. While the first-order fault is the primary conduit for gold-bearing fluids, distributed across-strike, higher-order structural networks also accommodate fluid flow, making them principal sites for ore deposition. Consequently, understanding the distribution and brittle-ductile deformation history of the higher-order structural networks is key for constraining the architecture of crustal-scale fault systems, the distribution of potential fluid conduits, and probable sites for gold mineralization. This study presents constraints on the across-strike distribution of high- and low-strain domains associated with the crustal-scale Larder Lake-Cadillac deformation zone (LLCdz) in the Archean southern Abitibi greenstone belt in the Kirkland Lake area of Ontario. High-strain zones form spaced (500-1000 m) domains in a >6 km area to the north of the LLCdz. The high-strain zones are characterized by a penetrative east-northeast-trending subvertical foliation with a moderately to steeply northeast-plunging stretching lineation, and dextral shear sense indicators on horizontal erosional surfaces. These fabric relationships are interpreted to reflect a pure shear-dominated (i.e., a low kinematic vorticity number) dextral transpressional strain regime with a steeply inclined extension direction. The high-strain zones are spatially associated with earlier formed fault zones, and form the location for carbonate alteration and gold occurrences. The ductile high-strain zones separate zones of low-strain where primary sedimentary or igneous structures are well preserved, the foliation is weakly developed and subparallel to that in the high-strain domains, and alteration is generally weak. The low-strain domains show no shear sense indicators and are interpreted as predominantly pure-shear domains that formed coevally with the high-strain zones. These observations suggest that a series of distributed brittle-ductile high-strain zones may have localized the upflow of hydrothermal fluids in the Kirkland Lake district. Undiscovered deposits may be hosted by these type of structures, providing a new framework for exploration in the area.

4.1 Introduction

Coupled deformation and fluid flow processes may contribute to the formation of orogenic gold deposits along crustal-scale fault zones in mountain belts, both ancient and modern (Goldfarb et al., 2001). Examples of orogenic gold deposits associated with crustal-

scale fault systems include the Mesozoic and presently active systems in the south island of New Zealand (Craw, 1992; Cox et al., 1997; Craw et al., 2006), the Jurassic to Cretaceous systems along the west coast of North America (Goldfarb et al., 1997; Goldfarb et al., 2008), and Archean systems in greenstone belts of the Yilgarn and Superior cratons (Robert et al., 2005; Bateman and Bierlein, 2007). Regardless of age, in these systems, the crustal-scale fault represents the primary fluid conduit that transports metamorphic, gold-bearing fluids from the middle to lower crust to depositional sites in the middle to upper crust (Fig. 4.1A; Groves et al., 1998; Phillips and Powell, 2010). Above the brittle-ductile transition, in the upper crust, in addition to the main crustal-scale fault, other major sites for gold emplacement are higher-order fault splays (Fig. 4.1B; Robert, 1994; Robert et al., 1995).

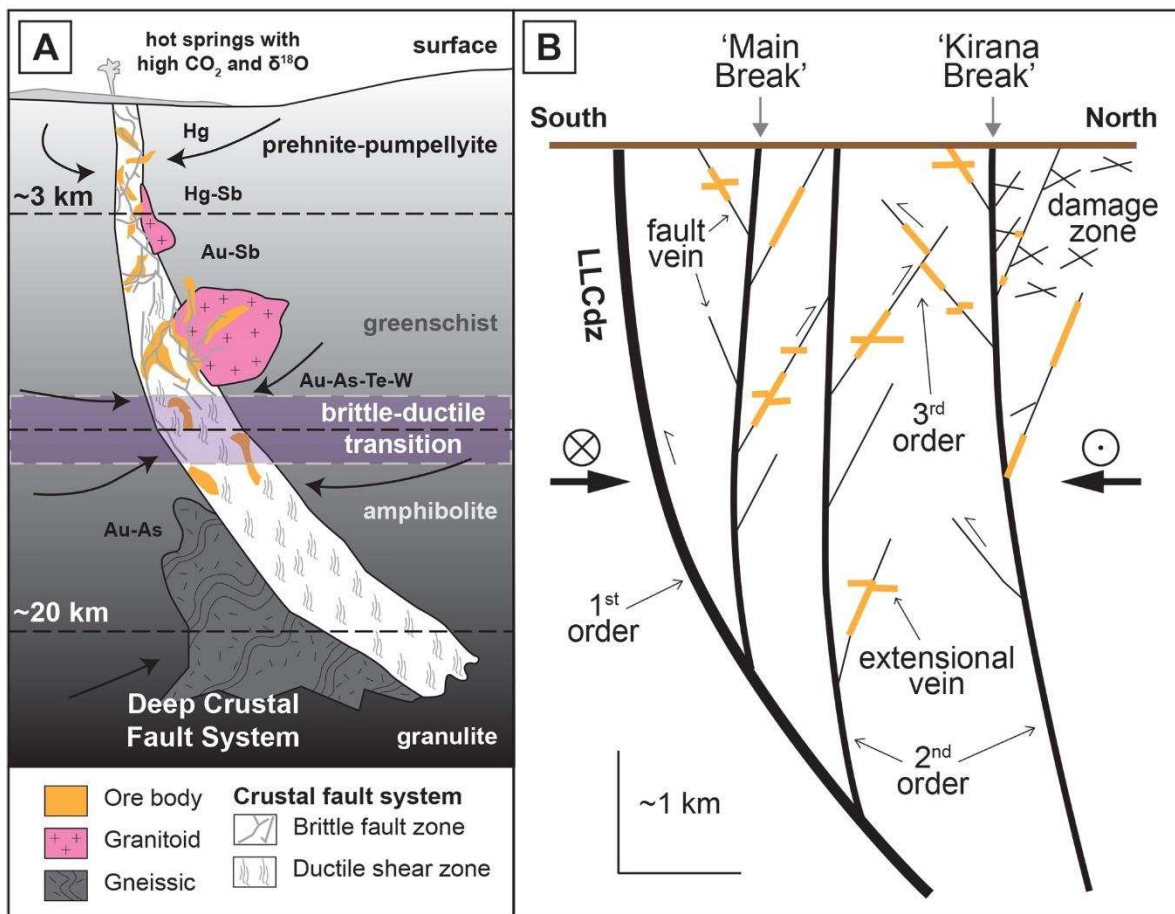


Figure 4.1 – Schematic illustrations of orogenic gold-bearing fault systems. (A) Schematic diagram illustrating the characteristics of crustal-scale deformation zones with associated orogenic gold deposits. The vertical scale varies. Modified from Groves et al. (1998). (B) Schematic illustration of the relationship between the primary, first-order fault zone (LLCdz – Larder Lake Cadillac deformation zone) and higher-order structures such as gold-bearing faults, shear zones, damage zones, and gold-bearing veins. Modified from Robert et al. (1995).

These higher-order structures can form distributed, 2-15 km structural networks splaying off the primary fault zone (Fig. 4.1B; Robert, 1994; Robert et al., 1995). Cyclic fault-valve behavior may be accommodated by all of these structures, where the overpressure of fluid reservoirs at depth induces failure, resulting in the emplacement of vein arrays along them (Sibson et al., 1988; Robert and Poulsen, 2001). During interseismic periods, both first- and higher-order structural zones commonly record ductile shear strain localization (Hodgson, 1989; Robert, 1989; Robert et al., 1995) and, based on the alteration assemblages that define dynamic recrystallization features, can provide evidence for syn-deformational fluid infiltration (Böhlke, 1989). Therefore, understanding the processes of mixed, brittle-ductile deformation along gold-bearing structures is key to understanding how they accommodated fluid flow (Colvine et al., 1988) and, potentially, form gold deposits. The purpose of this study was to investigate the across-strike pattern of brittle-ductile deformation along a gold-bearing segment of a crustal-scale fault zone. The pattern of strain partitioning revealed in this study helps to understand the locations of past fluid infiltration, alteration, and gold occurrences, not only in the southern Abitibi greenstone belt, but within crustal-scale fault systems in general.

The crustal-scale fault system investigated was the Archean Larder Lake-Cadillac deformation zone (LLCdz) in the southern Abitibi greenstone belt of the Superior Province, Canada (Fig. 4.2). The LLCdz is a major, ~east-trending fault zone that extends for 100s of km along strike, hosting over 100 Moz of gold along its length (Fig. 4.2; Monecke et al., 2017). Due to this economic significance, the structural history of the LLCdz and its immediate splays is well constrained (Wilkinson et al., 1999; Ispolatov et al., 2008; Lafrance, 2015; Bedeaux et al., 2017; Poulsen, 2017). This includes the primary gold-hosting structure in Kirkland Lake, the 'Main Break', which has been the focus of numerous studies (Fig. 4.3; Todd, 1928; Thomson et al., 1950; Charlewood, 1964; Kerrich and Watson, 1983; Watson, 1984; Still, 2001; Ispolatov et al., 2008). The Main Break is a second-order splay that occurs ~2 km to the north of the LLCdz from which over 30 Moz of gold has been recovered (Fig. 4.3; Ispolatov et al., 2008). In the Kirkland Lake area the distribution of lithologies and faults are well constrained by district-scale mapping (Figs. 4.3 and 4.4; MacLean, 1944; Thomson, 1945; Rupert and Lovell, 1970; Ispolatov et al., 2005) and the ages of the lithologic units in the area are well constrained by U-Pb ID-TIMS zircon geochronology (Corfu et al., 1991; Corfu, 1993; Wilkinson et al., 1999; Ayer et al., 2002, 2005). However, the distribution of brittle and ductile strain is poorly constrained beyond the LLCdz and Main Break. The Kirkland Lake district represents an ideal location to synthesize existing information and integrate new structural analysis to constrain the across-strike distribution and kinematic history of brittle-ductile structures in greater detail, because the

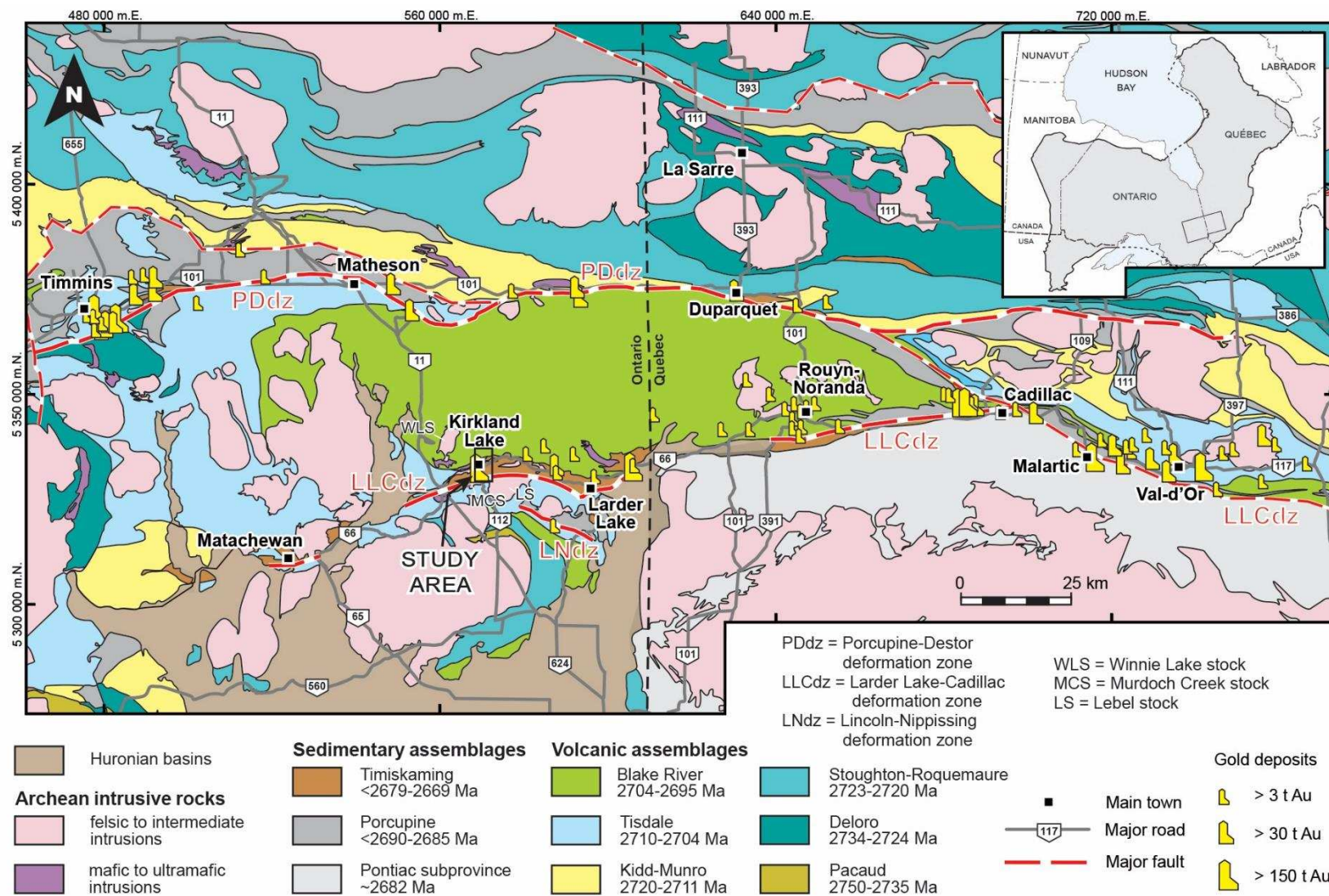


Figure 4.2 – Geological map of the south-central Abitibi subprovince. Map displays volcanic assemblages, sedimentary assemblages and intrusive rocks, the major crustal-scale deformation zones, and orogenic gold deposits (modified from Thurston et al., 2008 and Monecke et al., 2017).

generalized structural and stratigraphic framework is well established and outcrops are abundant and easily accessible. This study presents map compilations and structural analysis within a 3.5 km by 7.0 km area to the north of the LLCdz in Kirkland Lake, Ontario (Figs. 4.3 and 4.4) and discusses the potential for undiscovered gold deposits in the district.

4.2 Geologic setting

In the study area, the LLCdz forms an ENE-trending, 10-500 m wide zone of penetrative, steeply-dipping foliation and a steeply-plunging stretching lineation with dextral shear sense indicators (S-C fabrics, Z-folds, and σ -clasts), both within the LLCdz and in adjacent host rocks (Wilkinson et al., 1999; Ispolatov et al., 2008; Poulsen, 2017). Lithoprobe seismic reflection profiles indicate that the LLCdz dips steeply towards the south and extends to at least 15 km depth (Jackson et al., 1995). The LLCdz is further characterized by pervasive carbonate alteration and abundant quartz-carbonate fault veins, providing an indication of its role in the localization of fluid flow (Poulsen, 2017). The present-day exposure of the LLCdz is marked by juxtaposition of the older Tisdale assemblage with the younger Timiskaming assemblage and/or by fuchsite-bearing ultramafic rocks of unknown stratigraphic affinity (Figs. 4.3 and 4.4).

Rocks hosting the LLCdz and associated structures are supracrustal exposures dominated by the ~2710-2704 Ma Tisdale assemblage in the south, the ~2704-2695 Ma Blake River assemblage in the north, and the ~2679-2669 Ma Timiskaming assemblage in the central portion (Figs. 4.3 and 4.4; Corfu et al., 1991; Corfu, 1993, Ayer et al., 2002, 2005; Thurston et al., 2008). The Tisdale assemblage primarily consists of interstratified tholeiitic basalt and komatiite, while the Blake River assemblage consists of tholeiitic to calc-alkaline basalt with minor rhyolite and andesite (Ayer et al., 2002). The Tisdale and Blake River assemblages are kilometers-thick, composite volcanic successions that were deposited in a submarine environment and have been interpreted to represent juvenile arc to back-arc sequences (Ayer et al., 2002).

The Timiskaming assemblage in the study area forms a 3-4 kilometers thick, south-facing, and moderately to steeply south-dipping package that is truncated to the south by the LLCdz (Fig. 4.3). To the north, the Timiskaming assemblage is in unconformable contact with the Blake River assemblage (Figs. 4.3 and 4.4). The Timiskaming assemblage consists of conglomerate, sandstone, and mudstone units that are intercalated with alkaline volcanic units

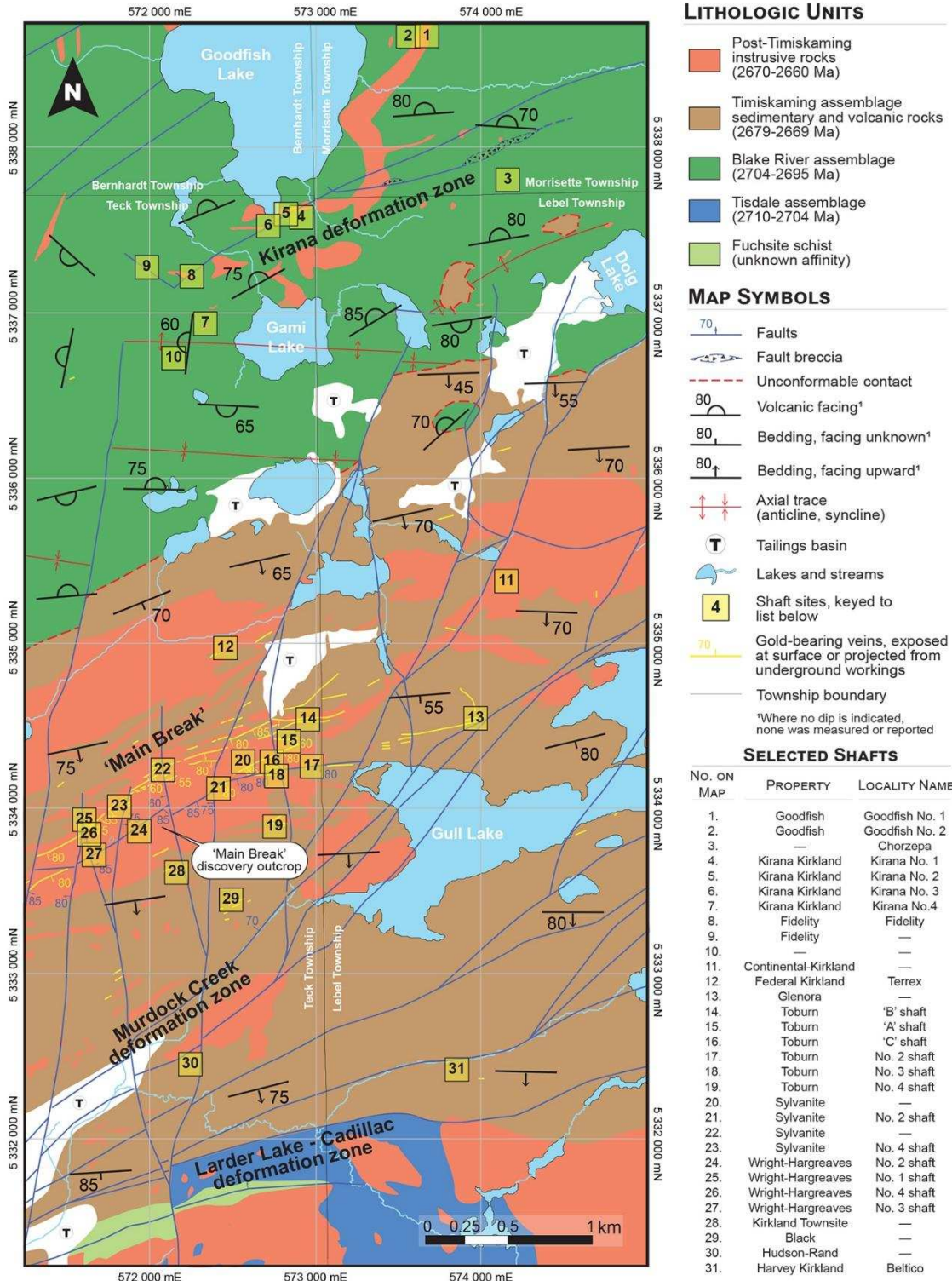


Figure 4.3 – Simplified geological map of the Kirkland Lake study area. Map displays the orientation of primary sedimentary and volcanic stratigraphy. The major named deformation zones, gold-bearing veins, and selected shafts are labeled (modified from Frieman et al., 2017).

such as tuffs and volcanoclastic deposits (Hyde, 1980; Mueller et al., 1994). The sedimentary units are interpreted to have been deposited in a subaerial, alluvial-fluvial to lacustrine or shallow marine environments in a fault-controlled basin associated with the LLCdz (Hyde, 1980; Mueller et al., 1994).

The Tisdale, Blake River, and Timiskaming assemblages are variably intruded by voluminous alkaline intrusive rocks (Fig. 4.4). Based on mineralogical, textural, and bulk rock geochemical constraints, the intrusive rocks include, from oldest to youngest: mafic (augite) syenite, syenite, and porphyritic syenite (Hattori and Hodgson, 1990; Wilkinson et al., 1999; Ispolatov et al., 2008). The intrusive rocks crosscut the sedimentary units of the Timiskaming assemblage or are intruded along bedding surfaces. Major and trace element geochemistry indicates that they are compositionally similar to volcanic rocks that comprise portions of the Timiskaming assemblage (Hattori and Hodgson, 1990), suggesting that they are broadly cogenetic. The porphyritic syenite rocks form sill to dike-like intrusions that crosscut both the mafic (augite) syenite and syenite intrusive rocks, indicating that they are the youngest of the intrusive rocks (Ispolatov et al., 2008). Along the LLCdz, magmatic zircon from porphyritic syenite rocks of the Murdoch Creek and Lebel stocks yielded U-Pb ID-TIMS ages of 2672 ± 2 and 2673 ± 2 , respectively (Wilkinson et al., 1999). Zircon from porphyritic syenite rocks of the Winnie Lake stock ~7 km to the WNW of the study area yielded a U-Pb ID-TIMS age of 2677 ± 3 Ma (Corfu, 1993), supporting the interpretation that these intrusive rocks are syn- to post-Timiskaming in age.

The Timiskaming assemblage and intrusive rocks are host to the mineralized zones of the Main Break (Fig. 4.3). The Main Break forms a structural zone defined by a series of parallel and/or branching, steeply south-dipping, faults, shear zones, and associated veins (Todd, 1928; Thomson et al., 1950; Charlewood, 1964; Kerrich and Watson, 1983; Watson, 1984; Still, 2001; Ispolatov et al., 2008). These form a nearly continuous zone that extends for >5 km along strike and to a depth of >2.5 km (Todd, 1928; Thomson et al., 1950; Charlewood, 1964; Watson and Kerrich, 1984; Still, 2001; Ispolatov et al., 2008). Mineralization in the Main Break is associated with sulfide-poor, Te-rich mineral assemblages and penetrative, foliation surfaces that are reactivated as chlorite-bearing fault slip surfaces (Ispolatov et al., 2008). Thus, gold deposited along the Main Break is interpreted to have been broadly coeval with the late stages of deformation (Ispolatov et al., 2008).

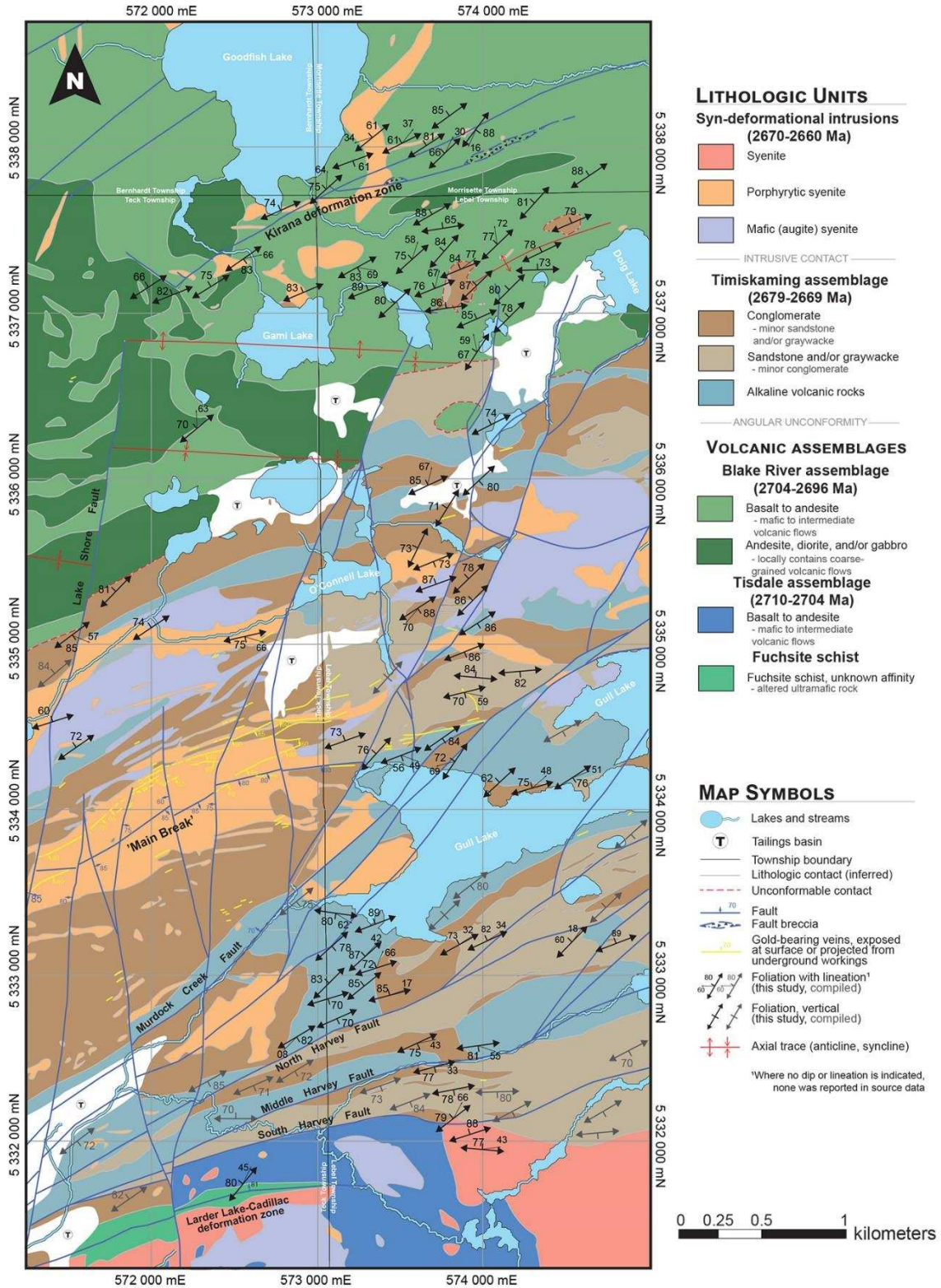


Figure 4.4 – Geologic map of the Kirkland Lake study area. The map displays compiled and new structural data from this study (modified from Frieman et al., 2017).

4.3 Structural setting

In the study area, three deformation events have been identified based on contact relationships and the development of successive, overprinting structural relationships. D_1 is characterized by folds in volcanic rocks of the Blake River assemblage that are truncated by basal conglomerate of the Timiskaming assemblage (Figs. 4.3 and A.2 to A.5; Thomson, 1946; Hewitt, 1963; Frieman et al., 2017; Poulsen, 2017). No penetrative structural fabrics are associated with the folds, potentially indicating flexural-slip (Dimroth et al., 1983). Mapping and subsurface seismic imaging indicate that the Tisdale and Blake River assemblages are folded tightly in proximity (<5-10 km) to the LLCdz (Jackson et al., 1995; Ispolatov et al., 2008; Poulsen, 2017), while openly farther from the LLCdz (Dimroth et al., 1983). This suggests that some of the shortening recorded by these folds may reflect post-Timiskaming deformation. The D_1 folds are truncated at a high angle by the base of the Timiskaming assemblage (Thomson, 1946; Hewitt, 1963, Poulsen, 2017), suggesting that they were uplifted and partially eroded during or after D_1 shortening, but prior to the deposition of the Timiskaming assemblage at ~2679 Ma (Monecke et al., 2017).

Deposition of the Timiskaming assemblage is generally interpreted as having occurred in fault-controlled basins along the major regional fault zones, although the structural setting of the basins and kinematics along the fault zones at the time of deposition is debated (Dimroth et al., 1982; Cameron, 1993; Mueller et al., 1994; Daignault et al., 2002; Bleeker, 2012). Cameron (1993) argued for deposition in an extensional setting based on the presence of deeply sourced alkaline igneous rocks within the Timiskaming stratigraphy and sedimentary successions indicative of rapid basin deepening. Based on the presence of gneissic clasts in the Timiskaming assemblage that may have been sourced from an area exposed by extensional unroofing in a proximal hinterland, Bleeker (2012) suggested that extension was regional. Alternatively, deposition of the Timiskaming assemblage may have occurred in localized pull-apart basins that formed at bends along the fault zones during oblique convergence (Dimroth et al., 1982; Daignault et al., 2002). The early kinematic histories of the fault zones has remained difficult to unravel due to pervasive post-Timiskaming deformational overprint (Poulsen, 2017).

Post-Timiskaming deformation along the LLCdz primarily has been interpreted as a result of progressive north-south to northwest-southeast shortening and dextral transpression (Wilkinson et al., 1999; Ispolatov et al., 2008). These deformation events resulted in several generations of folds, thrusts, and localized ductile shear (Wilkinson et al., 1999; Ispolatov et al., 2008; Lafrance, 2015; Poulsen, 2017) that, in this work, are referred to as D_2 and D_3 . Faults and foliations associated with both deformation events are well developed in Timiskaming

assemblage and younger intrusive rocks indicating their post-Timiskaming ages (e.g., Wilkinson et al., 1999). D₂ structures include an east-trending, subvertical foliation that is axial planar to upright folds in the Timiskaming assemblage (Wilkinson et al., 1999; Ispolatov et al., 2008; Lafrance, 2015). The S₂ foliation is well developed regionally, but poorly preserved in the Kirkland Lake area (Ispolatov et al., 2008; Frieman et al., 2017). Based on the emplacement of the older Tisdale assemblage in the south over the younger Timiskaming assemblage rocks to the north, D₂ thrusting along the LLCdz has been regarded as north-directed (Thomson, 1948; Wilkinson et al., 1999; Lafrance, 2015). In contrast, D₃ faults commonly display north-side-up as well as south-side-up reverse to oblique-reverse displacements (Ispolatov et al., 2008), indicating both north- and south-directed thrusting. The S₃ foliation is the dominant fabric preserved in the Kirkland Lake area and is associated with a moderately to steeply east-northeast-plunging lineation and with dextral sense shear indicators on horizontal erosional surfaces, including S-C fabrics, σ -clasts, and Z-folds (Robin and Cruden, 1994; Wilkinson et al., 1999; Ispolatov et al., 2008; this study). These have been interpreted to reflect a transition to NW-SE shortening and dextral transpression during D₃ deformation (Wilkinson et al., 1999; Lafrance, 2015; Ispolatov et al., 2008). S₃ is well documented within a 10-50 m wide zone LLCdz (Wilkinson et al., 1999) and within high-strain zones associated with the Main Break (Ispolatov et al., 2008). However, S₃ has also been recognized outside the high-strain zones (Ispolatov et al., 2008).

4.4 Across-strike structure north of the LLCdz in Kirkland Lake, Ontario

The geology of the Kirkland Lake area was compiled in portions of the Teck (Thomson, 1945; Ispolatov et al., 2005), Lebel (MacLean, 1944; Ispolatov et al., 2005), Bernhardt (Rupert and Lovell, 1970), and Morrisette (Rupert and Lovell, 1970) townships. These were combined with new structural investigations that constrain the distribution and intensity of ductile shear zones relative to known fault zones (Figs. 4.3 and 4.4; Frieman et al., 2017).

The angular unconformity between Blake River and Timiskaming assemblage rocks is well exposed in the study area (Figs. 4.3 and 4.4). The contact in the western portion of the study area is strongly overprinted by D₃ shear zones. However, in the northeastern portion of the study area, where strain is low, the Timiskaming assemblage dips moderately to the south proximal to the contact and steeper in the south farther from the contact (Fig. 4.3). The map pattern of the unconformable contact is complex in the Lebel township (Figs. 4.3 and 4.4), due to the presence of erosional outliers of the Timiskaming assemblage. The erosional outliers of the Timiskaming assemblage north of the main Blake River assemblage – Timiskaming assemblage contact are comprised of poorly stratified basal conglomerate containing abundant,

angular mafic volcanic clasts and/or felsic volcanoclastic material (Figs. A.3 to A.5). South of the main contact, in an erosional window of the Timiskaming assemblage, Blake River assemblage basaltic flows that are subvertical and north facing are exposed (Fig. 4.3). However, within a few hundred meters to the north, volcanic facing in the Blake River assemblage is towards the south, indicating the occurrence of tight folds (Fig. 4.3). These observations suggest that the contact between these assemblages is an angular unconformity and that tight, km-scale folds in Blake River assemblage are truncated at a high angle by the base of the shallowly- to moderately-dipping Timiskaming assemblage.

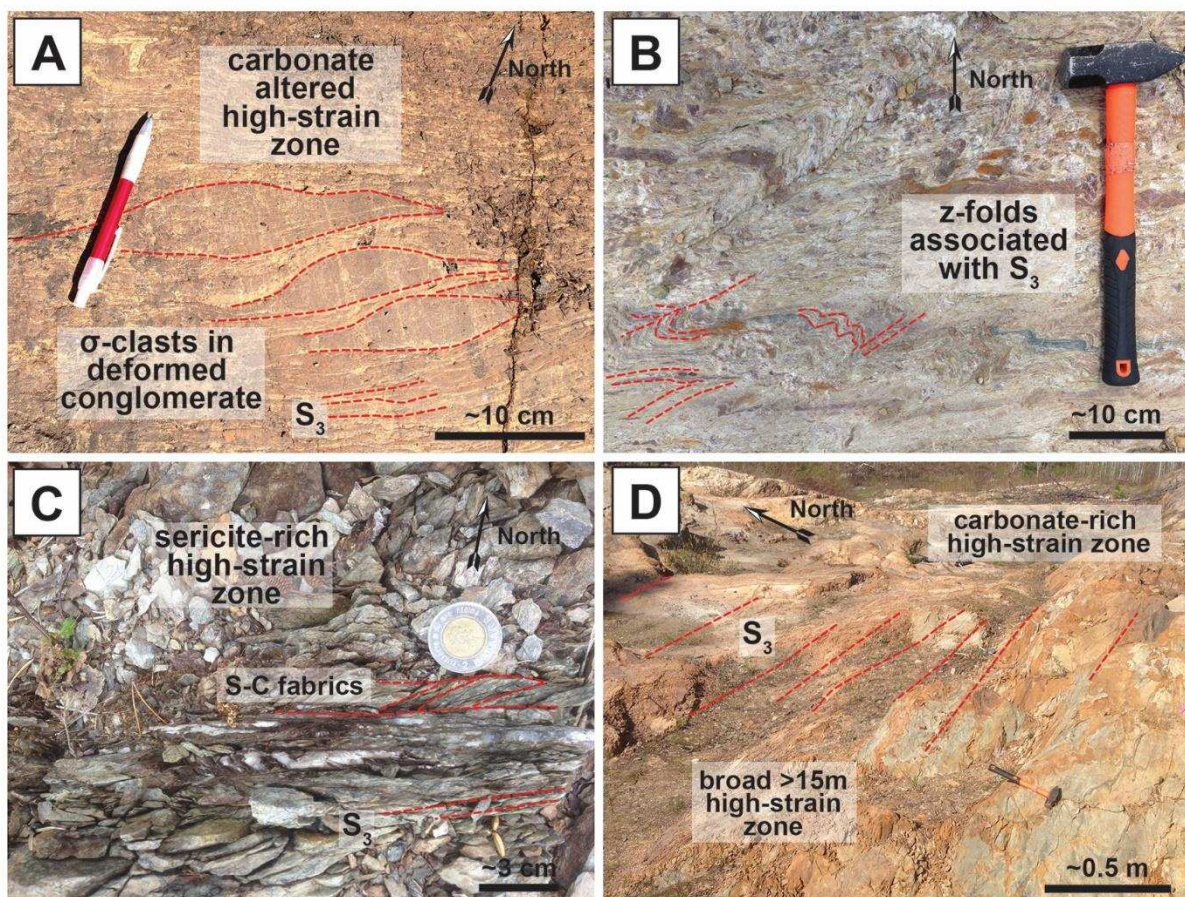


Figure 4.5 – Field photographs of D₃ high-strain zones. (A) A high-strain zone in carbonate-altered Timiskaming assemblage rocks within the Murdock Creek deformation zone (Figs 4.3 and 4.4) with σ -clasts and a well-developed S₃ foliation. (B) Z-folds associated with a D₃ high-strain zone developed in fine-grained sedimentary rocks of the Timiskaming assemblage in the Murdock Creek deformation zone. (C) A sericite-rich high-strain zone associated with the Kirana deformation zone displaying well-developed S-C fabrics. (D) A wide, >15 m pervasive carbonate-altered D₃ high-strain zone associated with the western extension of the Kirana deformation zone.

Mapping of the volcanic facing in the Blake River assemblage, including areas to the north and northwest of Kirkland Lake (Fig. A.1), indicates that the folds are km scale and have northwest-trending, subvertical axial planes and steeply northeast-plunging to subvertical hinge lines.

Post-Timiskaming high- and low-strain zones were investigated by across-strike structural investigations from the LLCdz in the south to ~6.5 km to the north (Fig. 4.4). This work focused on defining high- and low-strain zones relative to known fault zones, alteration zones, and documented gold occurrences. In this work, high-strain zones are defined as strongly foliated and generally lineated rocks, commonly displaying shear sense indicators (Fig. 4.5). The high-strain zones are further characterized by pervasively altered rock and contain foliation planes defined by chlorite, sericite, and/or carbonate mineral-rich domains (Fig. 4.5).

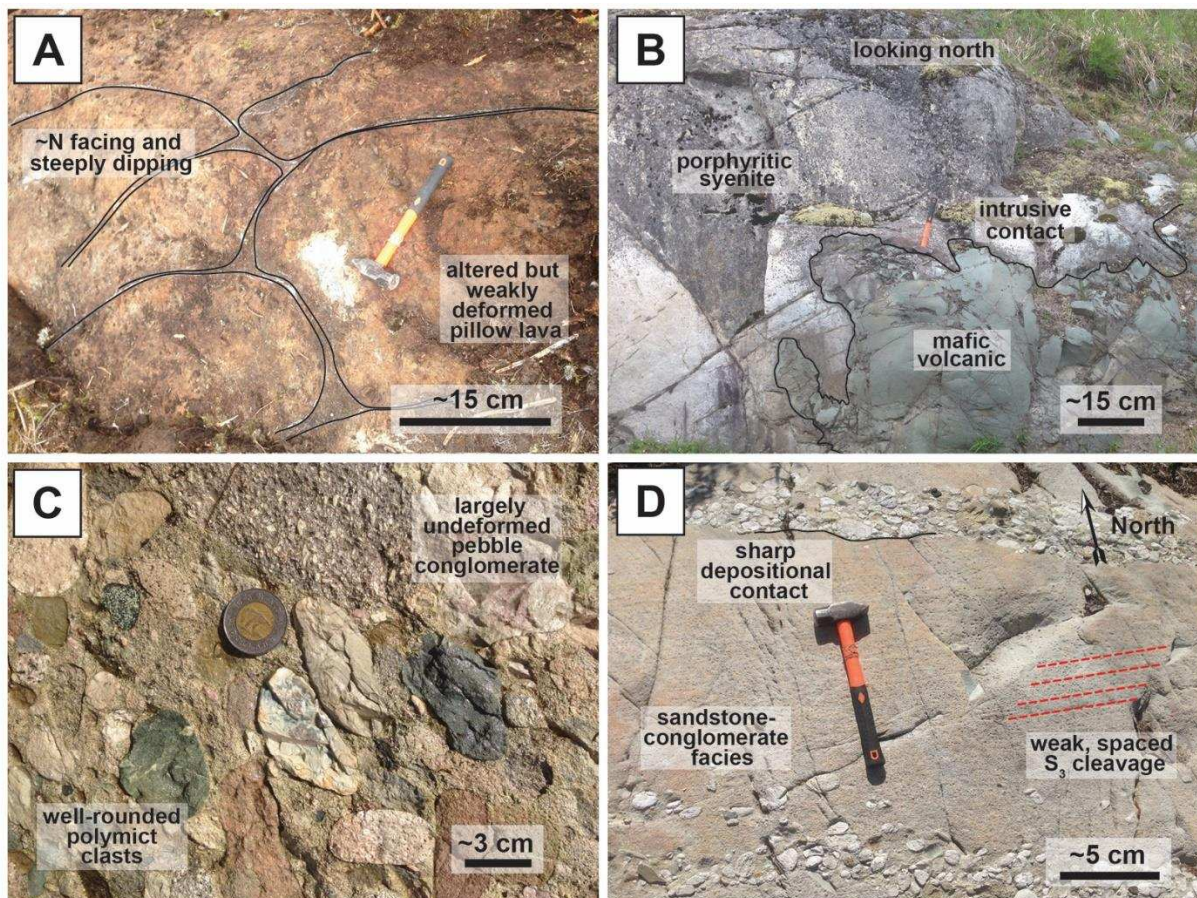


Figure 4.6 – Field photographs of primary igneous and sedimentary structures preserved in low-strain domains. (A) Carbonate-altered but largely undeformed pillow basalt adjacent to the Kirana deformation zone. (B) An undeformed intrusive contact between porphyritic syenite and mafic volcanic rocks adjacent to the Kirana deformation zone. (C) Undeformed polymict conglomerate of the Timiskaming assemblage north of the ‘Main Break’. (D) Interbedded sandstone and conglomerate of the Timiskaming assemblage displaying a spaced S_3 cleavage adjacent to the Murdock Creek deformation zone.

Low-strain zones are characterized by locations where primary sedimentary or igneous structures are well preserved and the foliation is a spaced, weakly-developed cleavage (Fig. 4.6). Low-strain zones typically display minimal amounts of host rock alteration (Fig 4.6B-D), although where directly adjacent to high-strain zones alteration may be pervasive (Fig. 4.6A). The distribution and characteristics of post-Timiskaming high- and low-strain zones are described from south to north below.



Figure 4.7 – Field photographs of the Larder Lake-Cadillac deformation zone exposed in the south of the Kirkland Lake map area. (A) Foliated fuchsite to talc schist crosscut by a curvilinear reverse fault. (B) Planar quartz veins containing carbonate-altered wall rock clasts. (C) Deformed quartz-carbonate vein arrays in hosted in fuchsite schist.

The LLCdz is well exposed in the south of Kirkland Lake area (Fig. 4.4) consisting primarily of fuchsite or talc schist (Fig. 4.7). Schists of the LLCdz display a well-developed penetrative S_3 fabric that is northeast-trending and steeply dipping (Fig. 4.8C). S_3 foliation surfaces contain a well-developed mineral lineation that plunges moderately to steeply towards

the east-northeast (Fig. 4.8D). S_3 fabrics are locally crosscut by prominent fault-slip surfaces defined by polished slip planes with slickenfibers, asymmetric steps, and observable offsets (Fig. 4.7A). These indicate reverse to reverse-oblique kinematics and north-side-up displacements. Zones with abundant quartz-carbonate veins are common, forming cm- to m-scale planar, banded, and/or stockwork vein networks that, locally, contain clasts of carbonate altered ultramafic wall rock (Fig. 4.7B and C). Earlier veins are overprinted by S_3 foliation and may be affected by D_3 deformation (Fig. 4.7C), while late veins are parallel to the foliation and are weakly to undeformed (Fig. 4.7B). All vein generations are texturally associated with carbonate alteration in their host rocks.

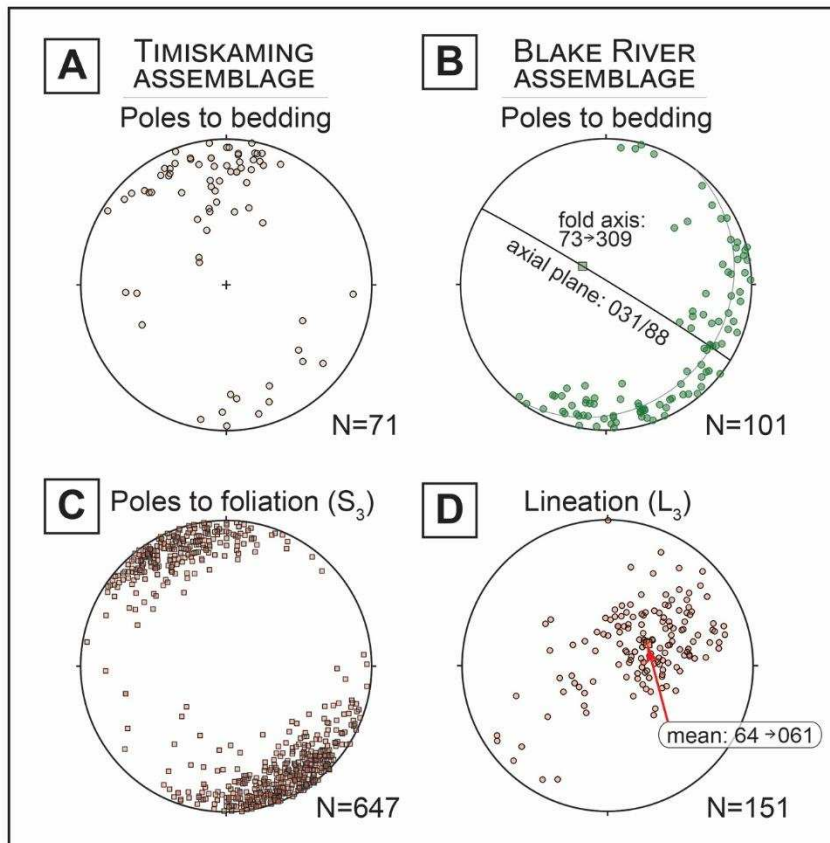


Figure 4.8 – Structural orientation data for the Kirkland Lake area. Poles to bedding of the Timiskaming assemblage (A), volcanic bedding in the Blake River assemblage (B), and S_3 foliation (C) from the Kirkland Lake area with the orientation of L_3 lineation (D) displayed as equal-area lower-hemisphere projections.

Immediately north of the LLCdz, the Timiskaming assemblage is variably faulted by the Harvey and Murdock Creek fault zones (Figs. 4.4 and 4.9). In this area, the Timiskaming assemblage is poorly exposed, intensely carbonate altered, and sheared, typically displaying a

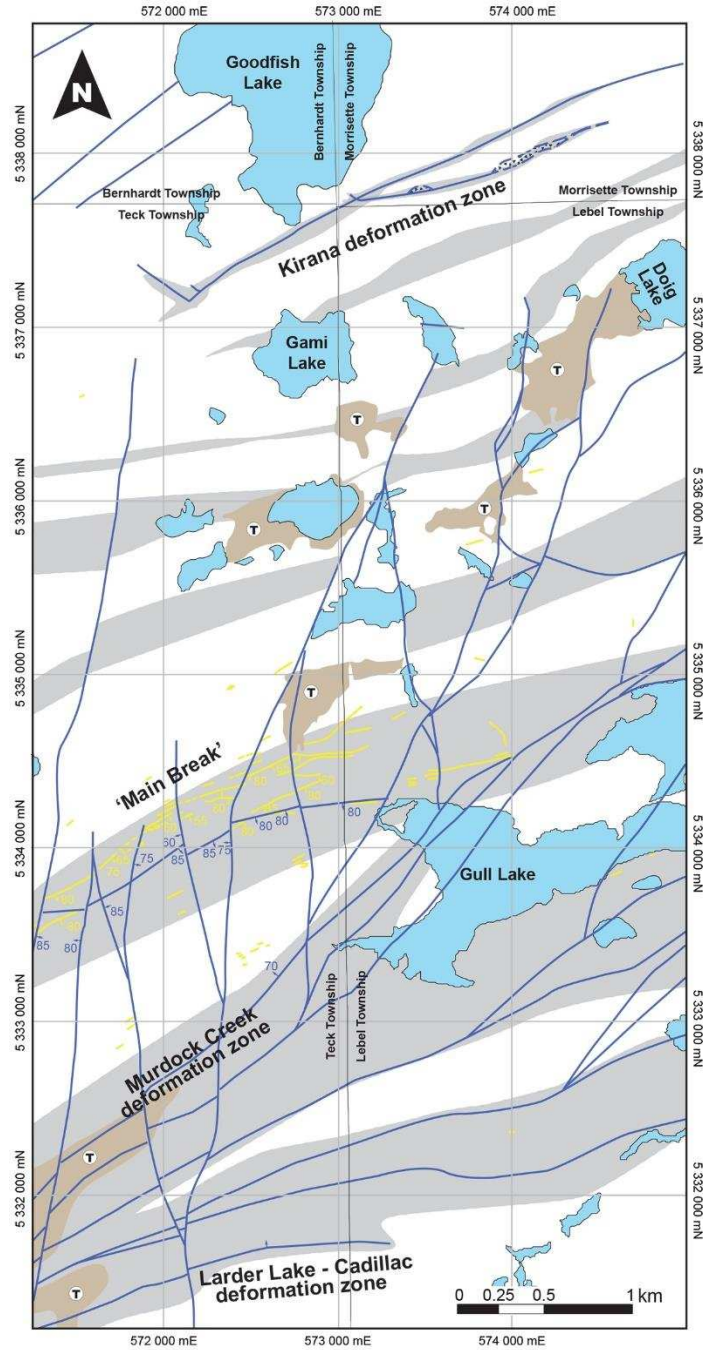
well-developed penetrative S_3 foliation with dextral shear sense indicators such as σ -clasts (Fig. 4.5A) and Z-folds (Fig. 4.5B).

In the area between the Harvey and Murdock Creek fault zones and the Main Break, the Timiskaming assemblage locally displays low-strain and the S_3 foliation is a weakly-developed spaced (cm-scale) cleavage (Fig. 4.6C and D). In these zones primary sedimentary structures are well preserved. The bedding dips 70-80° south and is locally overturned due to D_2 deformation (Figs. 4.2 and 4.8A). Younging indicators such as cross-bedding or fining upward sequences consistently indicate it is south-facing.

Approximately ~2 km north of the LLCdz the Main Break is exposed, as a ~10 m zone of alteration and penetrative S_3 foliation that is cored by a ~2 cm, gold-bearing fault vein (Ispolatov et al., 2008; Poulsen, 2017). The foliation overprints the fault vein and dextral shear sense indicators are lacking. Other high-strain zones are heterogeneously distributed in the vicinity of the Main Break. They are narrow, <1 m zones, or wider, 5-10 m zones showing penetrative foliation, well developed dextral shear sense indicators, and pervasive carbonate alteration (Ispolatov et al., 2008). Brecciation and early generations of quartz-carbonate veins are commonly overprinted by the S_3 foliation, while late vein generations display little D_3 overprint (Ispolatov et al., 2008). For the purposes of the km-scale mapping transect, the Main Break, including associated distributed zones, is considered as a single ~500 m wide zone of high-strain (Fig. 4.9).

North of the Main Break, additional, spaced high-strain zones occur (Fig. 4.9). These form 1-100 m wide zones of penetrative S_3 foliation with well-formed L_3 lineation and dextral shear sense indicators (Fig. 4.8C and D). These zones contain variable carbonate alteration and well-foliated zones rich in sericite or chlorite minerals. The high-strain zones separate low-strain zones where foliation is a weakly-formed, spaced cleavage and primary sedimentary structures easily recognizable (Fig. 4.6C), similar to low-strain domains to the south. Discrete fault zones were observed in this region, defined by slip surfaces with observable offsets with north-side-up and south-up-up displacements. Map-scale continuity of these structures was difficult to constrain.

Approximately 1.5 km to the north of the Blake River-Timiskaming assemblage contact, brittle-ductile structures of the east-northeast-trending >3 km long and 5-10 m wide Kirana deformation zone (Kdz; Figs. 4.3 and 4.4) occur. The center of the Kdz is marked by a penetrative S_3 foliation, pervasive carbonate alteration, and abundant quartz-carbonate veins. Southwest of Goodfish Lake (Fig. 4.4), the Kdz forms a >15 meter shear zone with pervasive



LEGEND




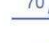


- | | | | | |
|---|----------------------------|---|----|--------------------|
|  | Inferred high-strain zones |  | 70 | Gold-bearing veins |
|  | Tailings basin |  | 70 | Faults |
|  | Lakes and streams |  | | Fault breccia |

Figure 4.9 – Simplified map of the Kirkland Lake study area displaying the distribution of mapped faults, interpreted high-strain zones, and gold-bearing veins.

carbonate alteration and foliated composite quartz-carbonate vein sets (Fig. 4.5D). Southeast of Goodfish Lake (Fig. 4.4), the Kdz forms multiple narrow, <1-5 m wide shear zones (Fig. 4.5C), similar to the Main Break to the south. The high-strain zones of the Kdz show a northeast-trending, subvertical, S_3 foliation and associated dextral shear sense indicators on horizontal erosional surfaces, including S-C fabrics and σ -clasts (Figs. 4.5C and 4.8C). Mineral lineations associated with S_3 (L_3) plunge moderately to steeply towards the east-northeast (Fig. 4.8D). S_3 overprints breccia zones and composite quartz-carbonate faults veins. Late moderately- to shallowly-dipping conjugate vein sets crosscutting foliated and brecciated domains are common. Breccia bodies form small local pods as well as 10s of meter wide damage zones. Low-strain zones adjacent to the Kdz preserve primary igneous structures, including sharp, irregular intrusive contacts between porphyritic syenite rocks and mafic volcanic rocks (Fig. 4.6B) as well as pervasively altered but weakly deformed pillow basalt (Fig. 4.6A).

Throughout the study area, the major east-northeast-trending deformation zones as well as ore-controlling faults in the Main Break (Ispolatov et al., 2008) are crosscut by younger, north- to north-northeast-trending faults (e.g., the Lake Shore fault; Figs. 4.3 and 4.4). Therefore, these are post- D_3 structures.

In summary, post-Timiskaming structures are heterogeneously distributed in a broad, >6 km area extending north from the LLCdz (Fig. 4.9). Observed D_2 structures include a monocline in the Timiskaming assemblage rocks that is defined by steeply-dipping and south-facing exposures and brittle fault zones hosted by the assemblage that are strongly overprinted by S_3 shear zones. S_2 fabrics are not well preserved and were not observed. East-northeast-trending fault zones occur at regular 500-1000 m intervals and are marked by discrete fault zones, domains with abundant quartz-carbonate veins, local cataclasite, and/or pervasive carbonate alteration. These may have formed during D_2 , as direct timing constraints are lacking. The majority of the fault zones are strongly overprinted by northeast-trending, D_3 shear zones, characterized by penetrative S_3 foliation and associated dextral shear fabrics (Figs. 4.5 and 4.8C). While there is a spatial association between D_3 shear zones and brittle fault zones, some D_3 shear zones display no association to earlier brittle faults and are coincident with rheological boundaries such as the contact between massive Blake River assemblage volcanic rocks and fine-grained sedimentary units of the Timiskaming assemblage (Fig. 4.9). Together the brittle-ductile structures define the major high-strain zones throughout the study area, which include the LLCdz, Murdock Creek, Main Break, and Kirana deformation zones (Figs. 4.4 and 4.9). Zones of high-strain are separated by low-strain zones in which primary sedimentary or igneous structures are well preserved, S_3 foliations are weakly developed, and carbonate alteration is

generally absent (Fig. 4.6). While better developed in the high-strain zones, the orientations of S_3 and L_3 is similar in low- and high-strain domains (Fig. 4.10). No crosscutting relationships between the fabrics in the low- and high-strain zones was documented, suggesting they formed at the same time.

4.5 Discussion

The Kirkland Lake district preserves evidence for north-south shortening followed by dextral transpression. Km-scale folds with northwest-trending axial planes and subvertical to steeply west-northwest-plunging hinge lines in the Blake River assemblage (Fig. 4.8B) suggest northeast-directed D_1 shortening. Based on facing relationships in the Blake River assemblage, and high angle truncations of the Blake River assemblage by the base of the Timiskaming assemblage, at least part of this folding occurred prior to deposition of the Timiskaming assemblage (Figs. A.2, A.4, and A.5; Thomson, 1946; Hewitt, 1963; Poulsen, 2017; this study).

Tilting and folding of the Timiskaming assemblage about an ~east-trending axis, and the formation of an ~east-trending axial planar cleavage reflect further shortening during D_2 (Fig. 4.3; Wilkinson et al., 1999; Ispolatov et al., 2008). There is also evidence for localized, south directed thrusting along the LLCdz at this time (Wilkinson et al., 1999; Lafrance, 2015; Ispolatov et al., 2008). It is unclear if the second-order faults, such as the Main Break or Kirana deformation zone formed during D_2 . Many of these fault zones display cataclasite, gouge, or discrete fault slip surfaces with observable north-side-up dextral oblique-reverse displacements (Fig. 4.7A), suggesting that they may be associated with D_3 dextral transpression. Locally, it is difficult to distinguish between S_2 and S_3 where no crosscutting relationships exist, or where S_2 is strongly overprinted by D_3 structures. Regardless, it is clear that the east-northeast-trending faults zones are widely overprinted by D_3 shear zones.

Ductile high-strain zones in the Kirkland Lake area typically show a northeast-trending, steeply-dipping foliation (S_3) defined by sericite, chlorite, or carbonate mineral-rich folia with millimeter- to sub-millimeter scale spacing (Figs 4.5 and 4.10A). The occurrence of fabric-forming alteration assemblages indicates that dynamic recrystallization within these zones was coeval with the migration of hydrothermal fluids at greenschist facies conditions. Dynamic recrystallization and grain-size reduction within these shear zones resulted in reaction softening (Wilkinson et al., 1999), which likely led to further ductile localization. In the high-strain zones identified in this study, S_3 commonly overprints zones of prior brittle deformation, marked by the occurrence of cataclasite, fault gouge, fault veins, and/or discrete fault planes with observable offsets (Fig. 4.9; Ispolatov et al., 2008; Chapter 5), suggesting that early brittle deformation produced favorable zones for later ductile localization. Faults overprinted by S_3 fabrics include

gold-bearing fault veins of the Main Break (see section 4.3; Ispolatov et al., 2008; Poulsen, 2017), indicating an early phase of fluid infiltration. The majority of gold deposits and occurrences in the Kirkland Lake area are spatially associated with the major deformation zones (Fig. 4.3) and each displays sericite or chlorite mineral-rich domains and/or pervasive carbonate alteration (Fig. 4.5). Early formed fault veins that are overprinted by D_3 shear zones are also commonly associated with carbonate alteration halos. This suggests that the brittle-ductile deformation zones were exploited as fluid conduits during both early brittle development and later ductile shear localization.

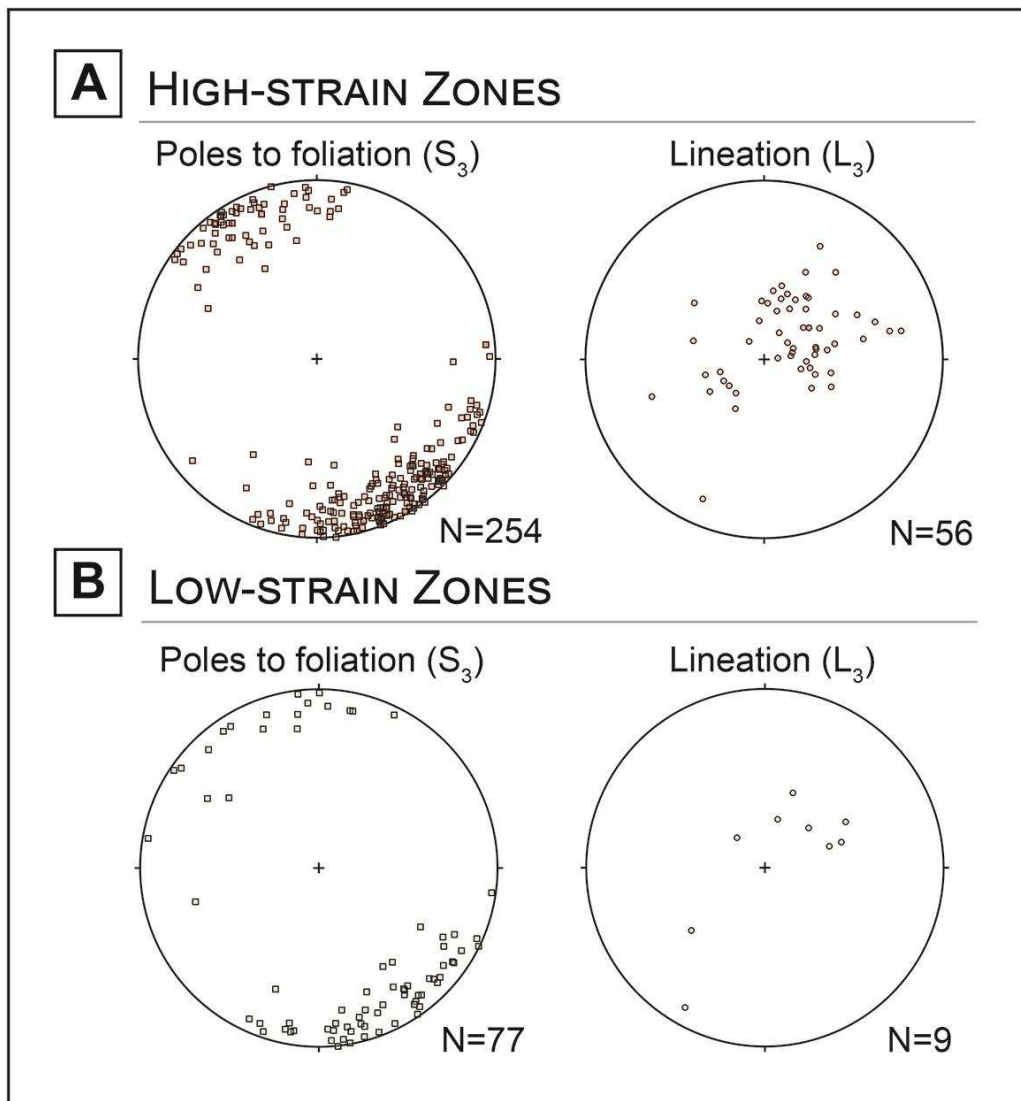


Figure 4.10 – Comparison of S_3/L_3 structural data from high- and low-strain domains. Poles to foliation (S_3) and lineation (L_3) orientation data from high-strain zones (A) and intervening low-strain zones (B) shown in equal-area lower-hemisphere projections.

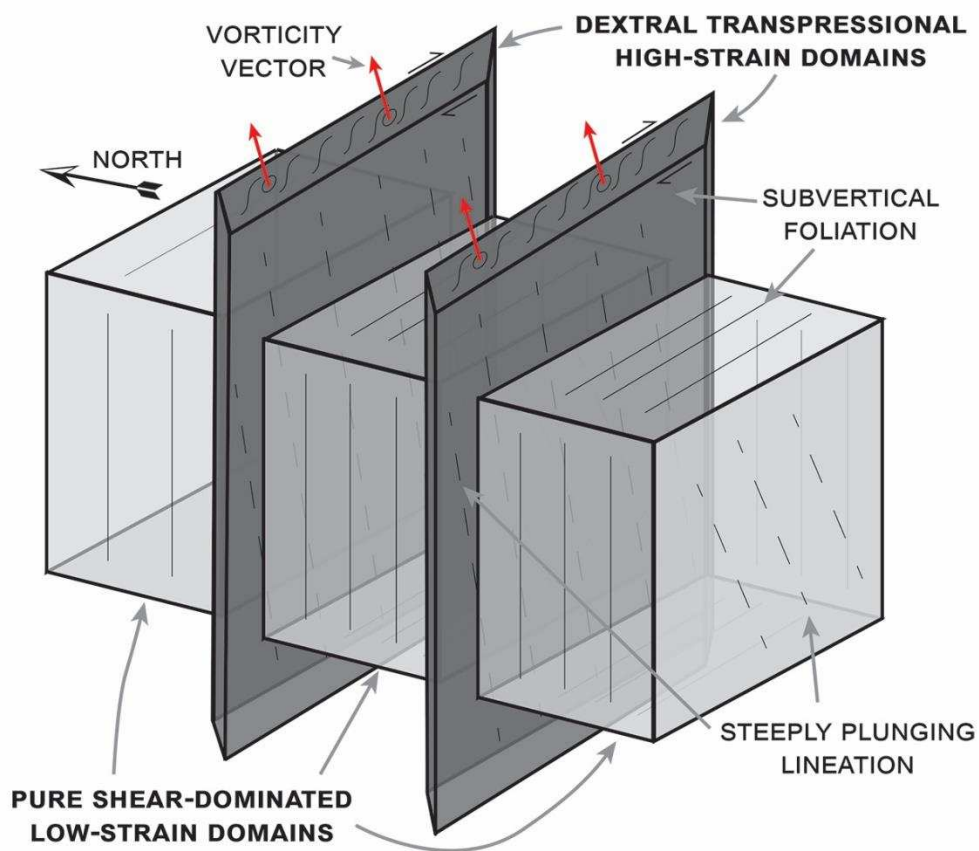


Figure 4.11 – Schematic diagram illustrating the inferred pattern of strain in the Kirkland Lake area. Alternating zones of low-strain, recording predominantly pure shear separate zones of high-strain, recording localized dextral transpression in a pure shear-dominated regime (red arrows indicate the orientation of the vorticity vector). The orientation of foliation and lineation are schematically illustrated.

The fact that D_3 high-strain zones show a moderately to steeply northeast-plunging lineation and dextral shear sense indicators (Z-fold, S-C fabrics, and σ -clasts) on horizontal erosional surfaces, suggests that the maximum stretching direction was subparallel to L_3 lineations, at high angle with the shear direction and closer to the vorticity vector (Fig. 4.11). Similar fabric relationships are well-documented along the LLCdz in Ontario and Quebec (Dimroth et al., 1983; Robert, 1989; Robin and Cruden, 1994; Wilkinson et al., 1999; Ispolatov et al., 2008; Lafrance, 2015; Bedeaux et al., 2017) and elsewhere in the Superior Province, such as along the boundary between the Wawa and Quetico subprovinces to the west (Hudleston et al., 1988; Czeck and Hudleston, 2003). A subvertical foliation with a subhorizontal shear direction and a steeply-plunging stretching direction suggests a pure shear-dominated

transpressional strain regime with a relatively low (e.g., ~0.1-0.5) kinematic vorticity number (W_k ; Fossen and Tikoff, 1993; Czeck and Hudleston, 2003). If W_k would have been high, the lineation in the high-strain zones would have been closer to the shear direction. In the low-strain zones no significant simple shear occurred, and L_3 is parallel to that in the high-strain zones. Thus, strain in the low-strain zones is interpreted as a result of predominantly pure shear with a moderately- to steeply-plunging stretching direction. Partitioning of the simple shear component into high-strain zones and distribution of the pure shear component over a wider zone including low-strain domains (Fig. 4.11) has also been recognized by Lin et al. (1998) in the Roper Lake shear zone in the Canadian Appalachians. The reason may be that simple shear is a weakening process while pure shear is a hardening process (Lin et al., 1998, and references therein). Based on the results of our mapping, it is unclear how these high-strain zones are interconnected. Some of the shear zones form northeast-trending zones that link the east-northeast trending zones (e.g., the Murdock Creek deformation zone; Fig. 4.9), but it is also likely that these zones form lozenge shaped domains that are interconnected in the subsurface (e.g., Hudleston, 1999).

4.6 Implications

While the known deposits within the studied segment of the LLCdz are primarily associated with the Main Break, each of the major brittle-ductile high-strain zones identified in this study is host to gold occurrences (Fig. 4.3). The relationship between high-strain zones and the upflow of potentially gold-bearing hydrothermal fluids suggests that orogenic gold in the Kirkland Lake district may be distributed in a much broader area north of the LLCdz than previously known, along a series of heterogeneously distributed structures (Fig. 4.12). This is similar to the across-strike architecture of the Val d'Or district of Quebec, where spaced (~500 m), higher-order fault zones occur that have been interpreted to have controlled the localization of ductile deformation as well as the dispersion of fluids during gold mineralization in a 30 km by 15 km vein field (Robert, 1994; Robert et al., 1995). While these studies defined the distribution of high-strain, they include no description of the characteristics of structure in the intervening low-strain zones. The distributed high-strain zones identified in this study may similarly represent a hydrothermal system beyond the LLCdz and Main Break. Exploration should focus on the high-strain zones that are localized along earlier brittle faults in the Kirkland Lake district (Fig. 4.12) and elsewhere in the southern Abitibi greenstone belt. Given the large vertical continuity of known mineralization in the Main Break (>2.5 km; Todd, 1928; Thomson et al., 1950; Charlewood, 1964; Kerrich and Watson, 1983; Watson, 1984; Still, 2001; Ispolatov et al., 2008), it is recommended that these zones be investigated in detail at depth. Brittle-ductile

zones dipping steeply towards the north-northwest or south-southeast with a strike of 025° to 035° as constrained by geophysical anomalies and/or drill core would present the most favorable targets. This study shows how more detailed structural syntheses of the across-strike architecture of major, regional fault segments can highlight new exploration targets in brownfield areas of the southern Abitibi greenstone belt, but also elsewhere in similar settings of any age.

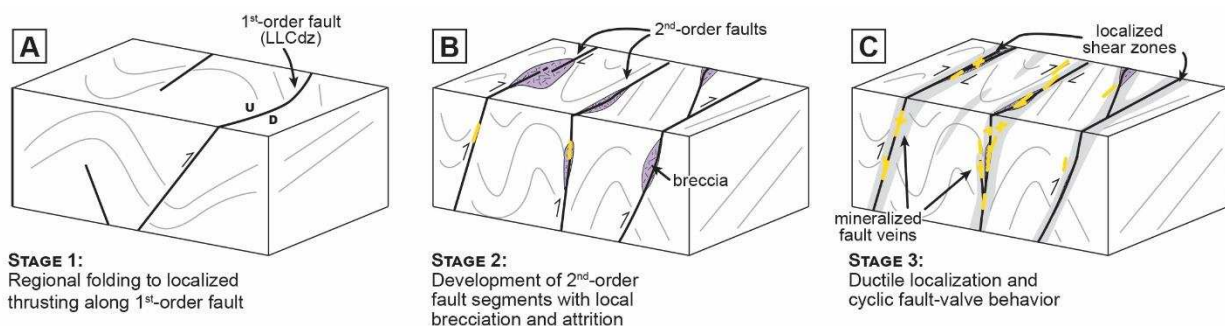


Figure 4.12 – Schematic conceptual diagrams illustrating the across-strike architectural evolution of the Larder Lake-Cadillac deformation zone (LLCdz) in Kirkland Lake. In stage 1, distributed folding gives way to localized thrusting along the 1st-order fault (the LLCdz). In stage 2, the initial formation and linkage of 2nd-order faults occurs with related brecciation and attrition processes. In stage 3, ductile strain is localized along zones of prior brittle deformation and is associated with intermittent fault-valve behavior and the emplacement of gold-bearing veins.

4.7 References

- Ayer, J., Amelin, Y., Corfu, F., Kamo, S., Ketchum, J., Kwok, K., Trowell, N., 2002. Evolution of the southern Abitibi greenstone belt based on U-Pb geochronology: Autochthonous volcanic construction followed by plutonism, regional deformation and sedimentation. *Precambrian Research* 115, 63–95.
- Ayer, J.A., Thurston, P.C., Bateman, R., Dubé, B., Gibson, H.L., Hamilton, M.A., Hathway, B., Hocker, S.M., Houlié, M.G., Hudak, G., Ispolatov, V.O., Lafrance, B., Leshner, C.M., MacDonald, P.J., Péloquin, A.S., Piercey, S.J., Reed, L.E., Thomson, P.H., 2005. Overview of results from the Greenstone Architecture Project: Discover Abitibi Initiative. Ontario Geological Survey Open File Report 6154, 146 p.
- Bateman, R., Bierlein, F.P., 2007. On Kalgoorlie (Australia), Timmins–Porcupine (Canada), and factors in intense gold mineralisation. *Ore Geology Reviews* 32, 187–206.
- Bedeaux, P., Pilote, P., Daigneault, R., Rafini, S., 2017. Synthesis of the structural evolution and associated gold mineralization of the Cadillac fault, Abitibi, Canada. *Ore Geology Reviews* 82, 49–69.
- Bleeker, W., 2012. Lode gold deposits in ancient deformed and metamorphosed terranes: The role of extension in the formation of Timiskaming basins and large gold deposits, Abitibi

- greenstone belt—a discussion. Ontario Geological Survey Open File Report 6280, 47-1–47-12.
- Böhlke, J.K., 1989. Comparison of metasomatic reactions between a common CO₂-rich vein fluid and diverse wall rocks; intensive variables, mass transfers, and Au mineralization at Alleghany, California. *Economic Geology* 84, 291–327.
- Cameron, E.M., 1993. Precambrian gold: Perspectives from top and bottom of shear zones. *Canadian Mineralogist* 31, 917–944.
- Charlewood, G.H., 1964. Geology of deep developments on the main ore zone at Kirkland Lake. Ontario Department of Mines Geological Circular 11, 49 p.
- Colvine, A.C., Fyon, J.A., Heather, K.B., Marmont, S., Smith, P.M., Troop, D.G., 1988. Archean Lode Gold Deposits in Ontario. Ontario Geological Survey Miscellaneous Paper 139, 136 p.
- Corfu, F., 1993. The evolution of the southern Abitibi greenstone belt in light of precise U-Pb geochronology. *Economic Geology* 88, 1323–1340.
- Corfu, F., Jackson, S.J., Sutcliffe, R.H., 1991. U-Pb ages and tectonic significance of Late Archean alkalic magmatism and nonmarine sedimentation, Timiskaming Group, southern Abitibi belt, Ontario. *Canadian Journal of Earth Sciences* 28, 489–503.
- Cox, S.C., Craw, D., Chamberlain, C.P. 1997. Structure and fluid migration in a late Cenozoic duplex system forming the Main Divide in the central Southern Alps, New Zealand. *New Zealand Journal of Geology and Geophysics* 40, 359–373.
- Craw, D. 1992. Fluid evolution, fluid immiscibility and gold deposition during Cretaceous-Recent tectonics and uplift of the Otago and Alpine Schist, New Zealand. *Chemical Geology* 98, 221–236.
- Craw, D., Begbie, M., MacKenzie, D., 2006. Structural controls on Tertiary orogenic gold mineralization during initiation of a mountain belt, New Zealand. *Mineralium Deposita* 41, 645–659.
- Czeck, D.M., Hudleston, P.J., 2003. Testing models for obliquely plunging lineations in transpression: A natural example and theoretical discussion. *Journal of Structural Geology* 25, 959–982.
- Daigneault, R., Mueller, W.U., Chown, E.H., 2002. Oblique Archean subduction: Accretion and exhumation of an oceanic arc during dextral transpression, Southern Volcanic Zone, Abitibi subprovince, Canada. *Precambrian Research* 115, 261–290.
- Dimroth, E., Imreh, L., Rocheleau, M., Goulet, N., 1982. Evolution of the south-central part of the Archean Abitibi belt, Quebec. Part I: Stratigraphy and paleogeographic model. *Canadian Journal of Earth Sciences*, 19, 1729–1758.
- Dimroth, E., Imreh, L., Goulet, N., Rocheleau, M., 1983. Evolution of the south-central segment of the Archean Abitibi Belt, Quebec. Part II: Tectonic evolution and geomechanical model. *Canadian Journal of Earth Sciences* 20, 1355–1373.

- Frieman, B.M., Kuiper, Y.D., Monecke, T., Kelly, N.M., 2017. Precambrian geology and new structural data, Kirkland Lake area, Ontario. Geological Survey of Canada Open File 8245, 8 p.
- Fossen, H., Tikoff, B., 1993. The deformation matrix for simultaneous simple shearing, pure shearing and volume change, and its application to transpression–transtension tectonics. *Journal of Structural Geology* 15, 413–422.
- Goldfarb, R.J., Miller, L.D., Leach, D.L., Snee, L.W., 1997. Gold deposits in metamorphic rocks of Alaska: *Economic Geology Monograph* 9, 151–190.
- Goldfarb, R.J., Groves, D.I., Gardoll, S., 2001. Orogenic gold and geologic time; a global synthesis. *Ore Geology Reviews* 18, 1–75.
- Goldfarb, R.J., Hart, C.J.R., Marsh, E.E., 2008. Orogenic gold and the evolution of the Cordilleran orogeny. *Arizona Geological Society Digest* 22, 311–323.
- Groves, D.I., Goldfarb, R.J., Gebre-Mariam, M., Hagemann, S.G., Robert, F., 1998. Orogenic gold deposits: A proposed classification in the context of their crustal distribution and relationship to other gold deposit types. *Ore Geology Reviews* 13, 7–27.
- Hattori, K., Hodgson, C.J., 1990. Gold-related geology in the Kirkland Lake and Timmins camps, Ontario. *International Association on the Genesis of Ore Deposits Symposium, 8th*, Ottawa, Canada, *Field Trip Guidebook* 5, 57 p.
- Hewitt, D.F., 1963. The Timiskaming Series of the Kirkland Lake area. *Canadian Mineralogist* 7, 497–523.
- Hodgson, C.J., 1989. The structure of shear-related, vein-type gold deposits: A review. *Ore Geology Reviews* 4, 231–273.
- Hudleston, P.J., 1999. Strain compatibility and shear zones: is there a problem? *Journal of Structural Geology* 21, 923–932.
- Hudleston, P.J., Schultz-Ela, D., Southwick, D.L., 1988. Transpression in an Archean greenstone belt, northern Minnesota. *Canadian Journal of Earth Sciences* 25, 1060–1068.
- Hyde, R.S., 1980. Sedimentary facies in the Archean Timiskaming Group and their tectonic implications, Abitibi greenstone belt, northeastern Ontario, Canada. *Precambrian Research* 12, 161–195.
- Ispolatov, V.O., Lafrance, B., Dubé, B., Hamilton, M., Creaser, R., 2005. *Geology, Structure, and Gold Mineralization, Kirkland Lake and Larder Lake Areas: Discover Abitibi Initiative*. Ontario Geological Survey Open File Report 6159, 170 p.
- Ispolatov, V., Lafrance, B., Dubé, B., Creaser, R., Hamilton, M., 2008. Geologic and structural setting of gold mineralization in the Kirkland Lake-Larder Lake gold belt, Ontario. *Economic Geology* 103, 1309–1340.
- Jackson, S.L., Cruden, A.R., White, D., Milkereit, B., 1995. A seismic-reflection-based regional cross section of the southern Abitibi greenstone belt. *Canadian Journal of Earth Sciences* 32, 135–148.

- Kerrich, R., Watson, G.P., 1984, The Macassa mine Archean lode gold deposit, Kirkland Lake, Ontario: Geology, patterns of alteration, and hydrothermal regimes. *Economic Geology* 79, 1104–1130.
- Lafrance, B., 2015. Geology of the orogenic Cheminis gold deposit along the Larder Lake-Cadillac deformation zone, Ontario. *Canadian Journal of Earth Sciences* 52, 1093–1108.
- Lin, S., Jiang, D., Williams, P.F., 1998. Transpression (or transtension) zones of triclinic symmetry: Natural example and theoretical modelling. *Geological Society of London Special Publication* 135, 41–57.
- MacLean, A., 1944. Township of Lebel, District of Timiskaming, Ontario. Ontario Department of Mines, Map 53a, scale 1:12 000.
- Monecke, T., Mercier-Langevin, P., Dubé, B., Frieman, B.M., 2017. Geology of the Abitibi greenstone belt. *Reviews in Economic Geology* 19, 7–49.
- Mueller, W., Donaldson, J.A., Doucet, P., 1994. Volcanism and tectonoplutonic influences on sedimentation in the Archean Kirkland Lake basin, Abitibi greenstone belt, Canada. *Precambrian Research* 68, 201–230.
- Phillips, G.N., Powell, R., 2010. Formation of gold deposits: A metamorphic devolatilization model. *Journal of Metamorphic Geology* 28, 689–718.
- Poulsen, K.H., 2017. The Larder Lake-Cadillac Break and its gold districts. *Reviews in Economic Geology* 19, 133–167.
- Robert, F., 1989. Internal structure of the Cadillac tectonic zone southeast of Val d'Or, Abitibi greenstone belt, Quebec. *Canadian Journal of Earth Sciences* 26, 2661–2675.
- Robert, F., 1994. Vein fields in gold districts: The example of Val d'Or, southeastern Abitibi subprovince, Quebec. *Geological Survey of Canada Current Research 1994-C*, 295–302.
- Robert, F., Poulsen, K.H., 2001. Vein formation and deformation in greenstone gold deposits. *Reviews in Economic Geology* 14, 111–155.
- Robert, F., Boullier, A.-M., Firdaous, K., 1995. Gold-quartz veins in metamorphic terranes and their bearing on the role of fluids in faulting. *Journal of Geophysical Research* 100, 12861–12879.
- Robert, F., Poulsen, K.H., Cassidy, K.F., Hodgson, C.J., 2005. Gold metallogeny of the Superior and Yilgarn cratons. *Economic Geology 100th Anniversary Volume*, 1001–1033.
- Robin, P.Y.F., Cruden, A.R., 1994. Strain and vorticity patterns in ideally ductile transpression zones. *Journal of Structural Geology* 16, 447–466.
- Rupert, R.J., Lovell, H.L., 1970. Bernhardt and Morrisette Townships, Timiskaming District, Ontario. Ontario Geological Survey, 2000 Series Map M.2193, scale 1:31 680.
- Sibson, R.H., Robert, F., Poulsen, K.H., 1988. High-angle reverse faults, fluid-pressure cycling, and mesothermal gold-quartz deposits. *Geology*, 16, 551–555.

- Still, A.C., 2001. Structural setting and controls of gold mineralization at the Macassa mine, Kirkland Lake, Ontario. Unpublished M.Sc. thesis, Kingston, ON, Queen's University, 151 p.
- Thomson, J.E., 1945. Township of Teck, district of Timiskaming, Ontario. Ontario Department of Mines, Map No. 1945-1, scale 1:12,000.
- Thomson, J.E., 1946. The Keewatin-Timiskaming unconformity in the Kirkland Lake district. *Transactions of the Royal Society of Canada IV*, 113–124.
- Thomson, J.E., 1948. Regional structure of the Kirkland Lake-Larder Lake area. *Structural Geology of Canadian Ore Deposits, A Symposium arranged by a Committee of the Geology Division, Canadian Institute of Mining and Metallurgy*, 627–632.
- Thomson, J.E., Charlewood, G.H., Griffin, K., Hawley, J.E., Hopkins, H., MacIntosh, C.G., Ogrizio, S.P., Perry, O.S., Ward, W., 1950. Geology of the main ore zone at Kirkland Lake. Ontario Department of Mines Annual Report 57, 196 p.
- Thurston, P.C., Ayer, J.A., Goutier, J., Hamilton, M.A., 2008. Depositional gaps in Abitibi greenstone belt stratigraphy: A key to exploration for syngenetic mineralization. *Economic Geology* 103, 1097–1134.
- Todd, E.W., 1928. Kirkland Lake gold area (a detailed study of the Central zone and vicinity). Ontario Department of Mines Annual Report 37, 1–176.
- Watson, G.P., 1984. Ore types and fluid regimes: Macassa gold mine, Kirkland Lake. Unpublished Ph.D. thesis, London, ON, University of Western Ontario, 341 p.
- Wilkinson, L., Cruden, A.R., Krogh, T.E., 1999. Timing and kinematics of post-Timiskaming deformation within the Larder Lake-Cadillac deformation zone, southwest Abitibi greenstone belt, Ontario, Canada. *Canadian Journal of Earth Sciences* 36, 627–647.

CHAPTER 5

FORMATION AND EVOLUTION OF GOLD-BEARING SPLAYS OF CRUSTAL-SCALE FAULT ZONES: A CASE STUDY OF THE KIRANA DEFORMATION ZONE IN THE KIRKLAND LAKE AREA OF ONTARIO, CANADA

Detailed structural analysis was conducted on the Kirana deformation zone (Kdz), a higher-order, gold-bearing splay of the Larder Lake-Cadillac deformation zone (LLCdz) in the Kirkland Lake area of Ontario, in order to investigate its regional significance, structural history, and potential for gold. The earliest formed structures along the Kdz are local quartz-carbonate veins and dilational breccia domains. Particle size distribution analysis of the breccia domains resulted in relatively low D-values of 0.93-1.71. In general, higher D-values were observed in texturally evolved breccia from the fault core, while lower D-values correspond to fractured wall rock in the damage zone. Breccia in both the fault core and damage zone are interpreted as fluid-assisted, 'implosion'-style breccia that formed at dilational sites during early fault slip, perhaps at a dilational jog or asperity. The dilational fracture networks are filled with quartz-rich material, suggesting that silica-rich fault fluids were associated with the brecciation event. However, despite this inferred coseismic fluid migration, no gold mineralization is documented in association with the early breccia-forming event. Following fault-related brecciation, the Kdz accommodated ductile shear at greenschist facies metamorphic conditions, which was localized along the fault zone. The shear zones show a subvertical ENE-trending foliation with a moderately to steeply NE-plunging mineral lineation and dextral shear sense indicators on horizontal erosional surfaces. The shear zones are interpreted to reflect NW-SE shortening and dextral transpression. Pervasive carbonate and sericite-rich assemblages that are texturally associated with shear zone fabrics indicate syn-kinematic fluid flow, similar to other shear zone-hosted gold deposits along the LLCdz. Observed native gold within the fault core of the Kdz display textural relationships that suggest mineralization was syn- to post-ductile shear, similar to other structurally-controlled deposits along the LLCdz. Following ductile shear, abundant quartz-carbonate shear veins with disseminated alteration halos formed, indicating renewed brittle deformation. Mutually crosscutting vein sets are common, representing cyclic emplacement (fault-valve behavior). Kinematic analysis of the shear veins indicates that they formed during NNW-SSE shortening, similar to the ductile shortening direction. Thus, the Kdz records progressive brittle-ductile deformation where strain and hydrothermal fluids were localized along pre-existing structures, and gold was deposited during the later ductile and brittle phases of deformation. A key observation is that the deformation zone is localized along

brecciated domains. Where such breccia zones exist, it is possible that later ductile-brittle structures exist in the area that are now known to be prospective for gold.

5.1 Introduction

Higher-order structures associated with crustal-scale fault zones are some of the primary hosts for orogenic gold in mountain belts, both ancient and modern (Goldfarb et al., 2001). Prominent Phanerozoic examples include the Mother Lode belt of California (Goldfarb et al., 2008) and the Macraes district of New Zealand (MacKenzie et al., 2017), while Archean examples include the mining districts of the Timmins-Porcupine camp and the Golden Mile deposits in the Superior and Yilgarn cratons, respectively (Robert et al., 2005; Bateman and Bierlein, 2007). Regardless of age, gold mineralization in these higher-order structural networks is related to coupled deformation and fluid flow processes that are controlled by a primary, crustal-scale fault zone (Fig. 5.1A; Groves et al., 1998; Cox et al., 2001). These structures transport potentially gold-bearing fluids derived from metamorphic devolatilization reactions (Phillips and Powell, 2010) from the middle to lower crust to sites of deposition in the middle to upper crust (Groves et al., 1998). Fluid migration is thought to occur due to the build-up of fluid pressure in the deep fluid reservoirs that induces fault failure events, a process that is termed fault-valve behavior (Sibson et al. 1988; Robert and Poulsen, 2001). Depositional sites may be along the primary, crustal-scale fault (Groves et al., 1998; Lafrance, 2015), but may also occur in distributed, higher-order fault networks that can occur as far as 2-10 km from the first-order fault (Fig. 5.1B; Colvine et al., 1988; Robert, 1994; Robert et al., 1995; Groves et al., 1998; Cox et al., 2001). Thus, understanding the deformational history of these higher-order structures may help predict where gold deposits are likely to occur. In particular, the role of early brittle deformation in the localization of later ductile shear, fluid flow, and gold mineralization is explored in this contribution.

A world-class example of an orogenic gold deposit hosted in a higher-order structure is the 'Main Break' in the Kirkland Lake area of Ontario (Figs. 5.2 and 5.3; Todd, 1928; Thomson et al., 1950; Charlewood, 1964; Kerrich and Watson, 1983; Watson, 1984; Still, 2001; Ispolatov et al., 2008). This deposit has yielded over 30 Moz of gold and occurs in association with the crustal-scale Larder Lake-Cadillac deformation zone (LLCdz; Fig. 5.3). Based on across-strike investigations of the LLCdz in the Kirkland Lake area (Chapter 4), the Main Break is one of a series of higher-order structures distributed in >6 km area to the north of the first-order fault zone (Fig. 5.3). One of these higher-order structures, the Kirana deformation zone (Kdz),

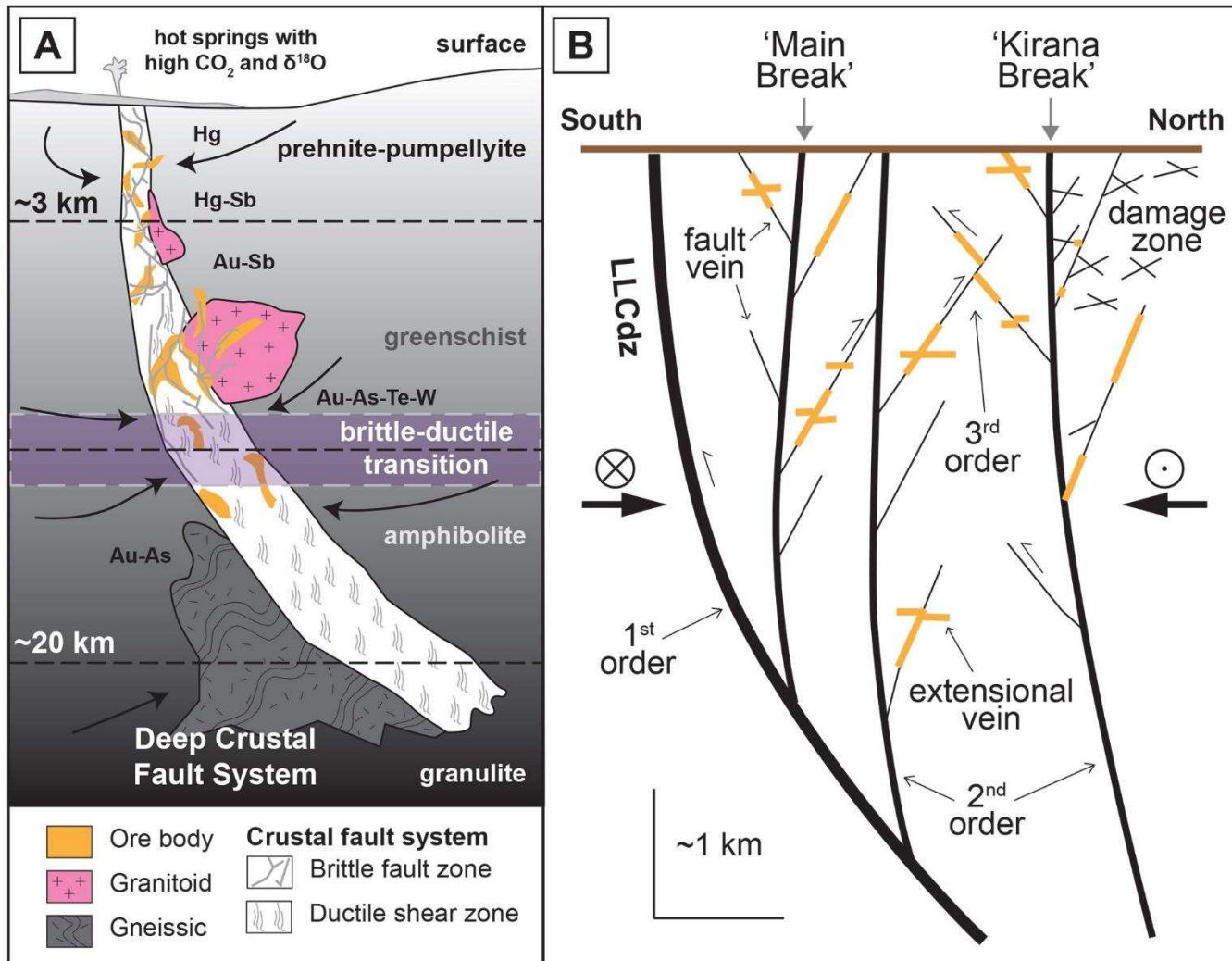


Figure 5.1 – Schematic illustrations of orogenic gold-bearing fault systems. (A) Schematic diagram illustrating the characteristics of crustal scale deformation zones with associated orogenic gold deposits. The vertical scale varies (modified from Groves et al., 1998). (B) Schematic illustration of the relationship between the primary, first-order fault zone (LLCdz – Larder Lake Cadillac deformation zone) and higher-order structures such as gold-bearing faults, shear zones, damage zones, and gold-bearing veins (modified from Robert et al., 1995).

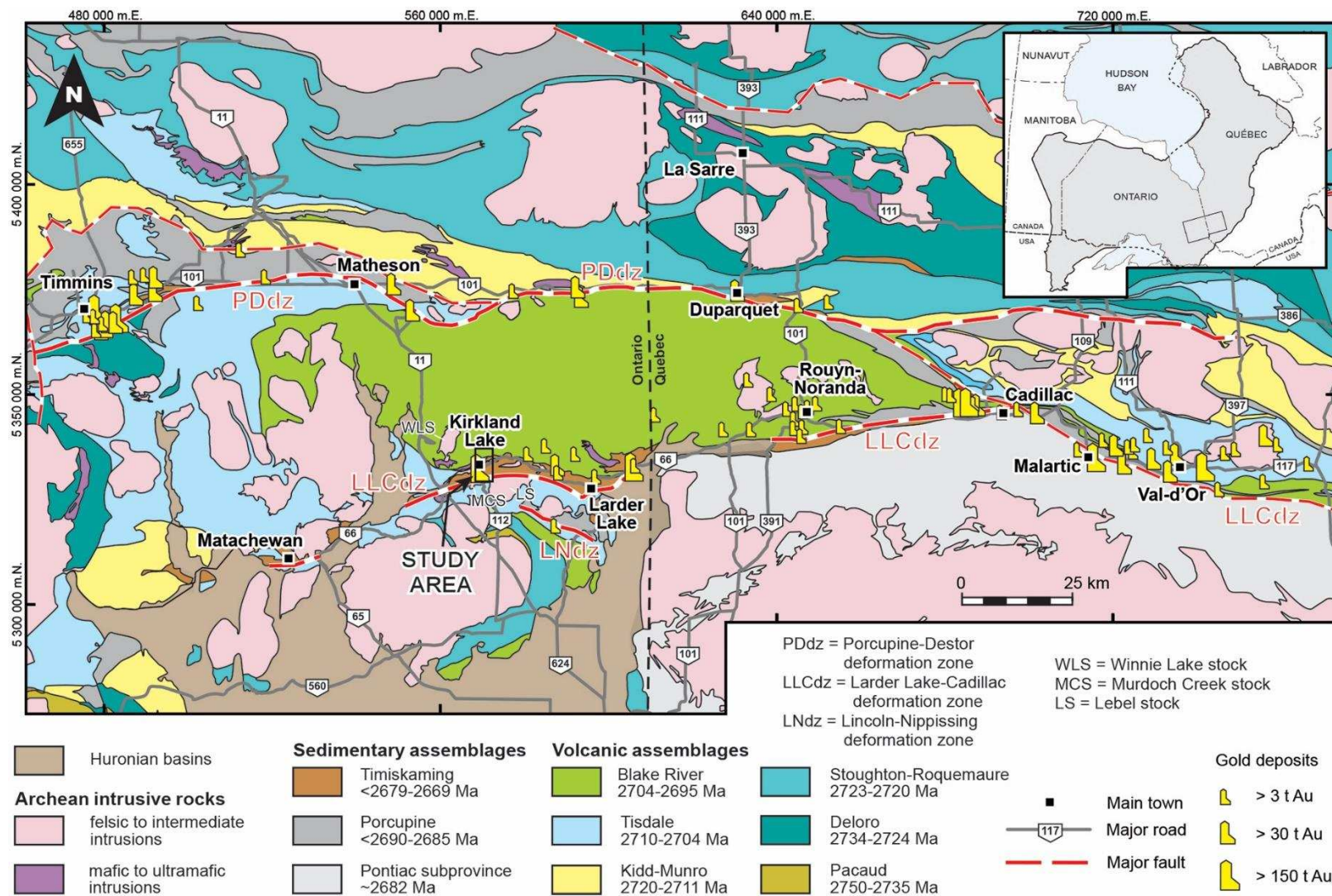


Figure 5.2 – Geological map of the south-central Abitibi subprovince. Map displays the distribution major crustal-scale fault zones, orogenic gold deposits, and the location of the Kirkland Lake study area (modified from Thurston et al., 2008 and Monecke et al., 2017)

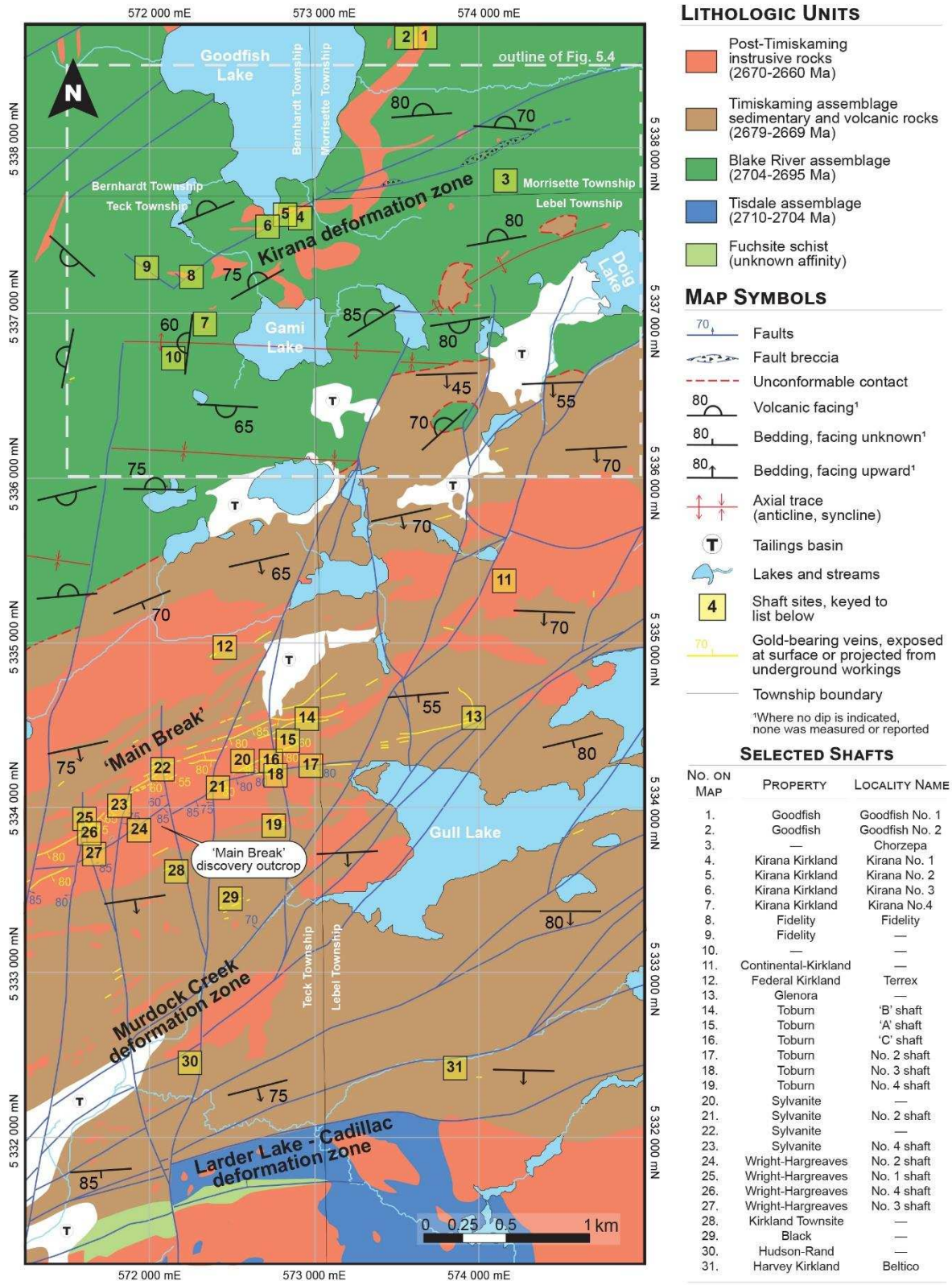


Figure 5.3 – Simplified geological map of the Kirkland Lake study area. Modified from Frieman et al. (2017). Location indicated in Fig. 5.2.

represents a little-studied, gold-bearing structure that is well exposed to the north of the LLCdz. While the structural history and relationships between gold and structures are well described in the LLCdz and Main Break (Todd, 1928; Thomson et al., 1950; Charlewood, 1964; Kerrich and Watson, 1983; Watson, 1984; Wilkinson et al., 1999; Still, 2001; Ispolatov et al., 2008; Poulsen, 2017), they are not for the Kdz. The Kdz preserves the early formational history of the fault, subsequent ductile shear zones, and late-formed brittle structures as a result of fault-valve behavior, all localized in the fault zone (Chapter 4). The exceptional preservation of the deformation history along the Kdz provides an opportunity to describe it in detail to gain insight into the mechanisms of brittle-ductile strain localization and associated gold mineralization. The goals of this study were, therefore, to (1) describe the structural evolution of the Kdz, (2) establish its relationships with the LLCdz, (3) investigate how brittle-ductile deformation processes facilitated localization of progressive ductile and brittle strain, and hydrothermal fluid flow that resulted in gold mineralization, and (4) investigate the potential for other prospective higher-order deformation zones. This was accomplished through new mapping, microstructural and petrographic investigations, quantitative analysis of early fault-related breccia, kinematic analysis of overprinting ductile shear fabrics, and kinematic analysis of late quartz-carbonate shear veins.

5.2 Geologic setting

The Kdz is a higher-order fault that occurs ~5 km to the north of the regionally extensive, crustal-scale LLCdz in the Kirkland Lake area of Ontario (Figs. 5.3 and 5.4). The LLCdz is a broadly E-trending fault zone that extends for 100s of km along strike and hosts gold deposits that contain over 100 Moz of gold along its length (Fig. 5.2; Monecke et al., 2017). The LLCdz extends at least as far as 15 km depth (Jackson et al., 1995) and is a long-lived structure that was a locus of strain throughout regional deformation from ~2695 Ma to ~2665 Ma (Robert, 1989; Dimroth et al., 1982, 1983; Wilkinson et al., 1999; Lafrance, 2015; Ispolatov et al., 2008; Bedeaux et al., 2017). In Kirkland Lake, a series of spaced (500-1000 m), higher-order, brittle-ductile deformation zones and associated gold occurrences are distributed in a broad, >6 km zone to the north of the LLCdz (Fig. 5.3; Chapter 4). These include the 'Main Break' and Kdz (Fig. 5.3; Chapter 4). The Main Break forms a continuous zone of parallel and/or branching faults, fault veins, and shear zones that extends for ~5 km along strike and to a depth of >2.5 km from which over 30 Moz of gold has been recovered (Fig. 5.3; Todd, 1928; Thomson et al., 1950; Charlewood, 1964; Kerrich and Watson, 1983; Watson, 1984; Still, 2001; Ispolatov et al., 2008).

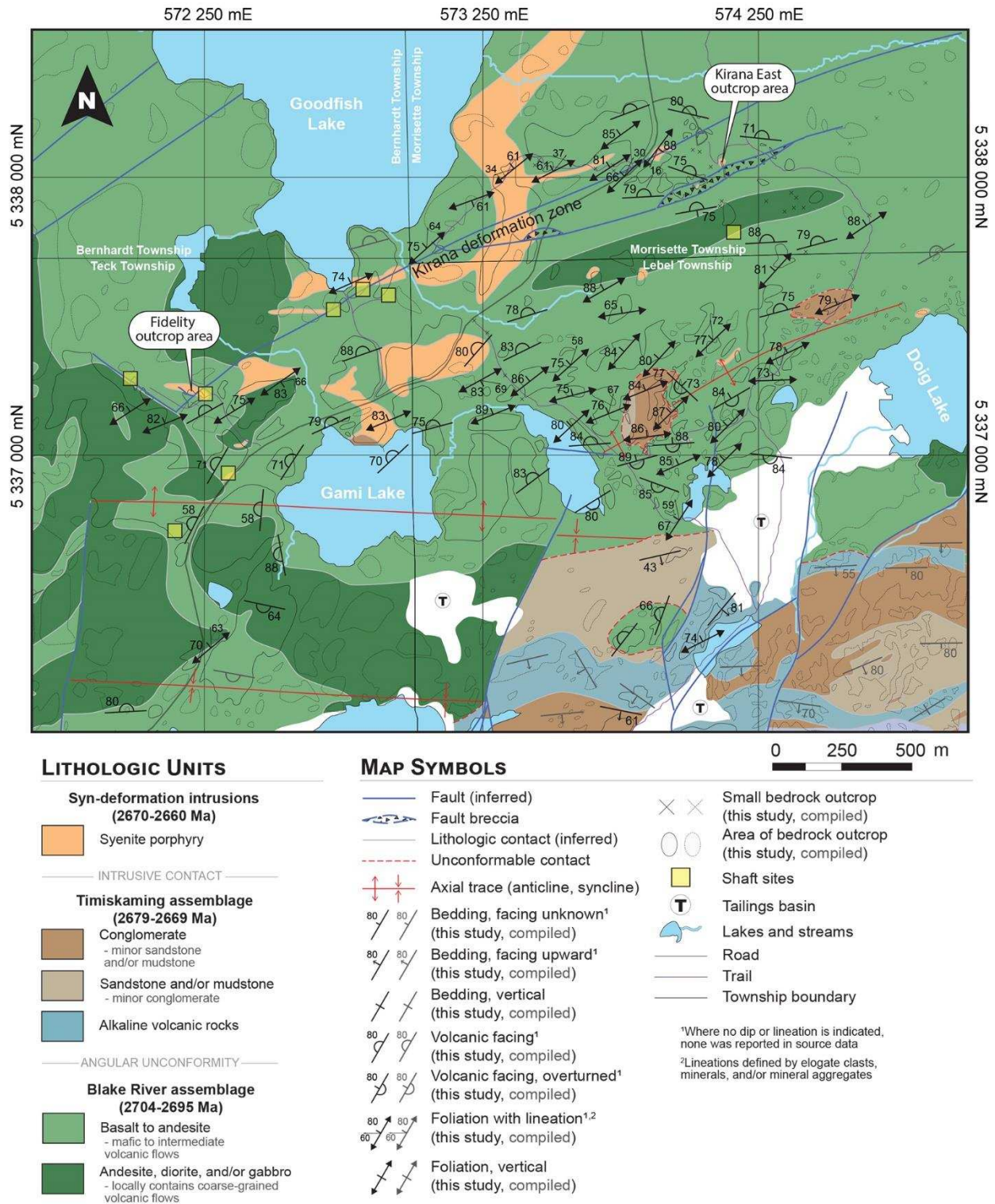


Figure 5.4 – Geologic map of the Kirana deformation zone with new structural data. The location of the Fidelity and Kirana East outcrops discussed in the text are indicated.

In the Kirkland Lake area, the LLCdz and higher-order deformation zones are hosted by older volcanic greenstone successions and younger broadly syn-deformational sedimentary and igneous rocks (Fig. 5.3). The ~2710-2704 Ma Tisdale assemblage consists of interstratified tholeiitic basalt and komatiite, while the ~2704-2695 Ma Blake River assemblage consists of tholeiitic to calc-alkaline basalt with minor rhyolite and andesite (Ayer et al., 2002). The Tisdale and Blake River assemblages represent km-thick, composite volcanic successions that were emplaced in a submarine environment during primary igneous construction of the Abitibi greenstone belt (Ayer et al., 2002). The younger, primarily sedimentary rocks are part of the ~2679-2669 Ma Timiskaming assemblage (Fig. 5.3; Ayer et al., 2002). The Timiskaming assemblage forms a 3-4 km-thick package of conglomerate, sandstone, and mudstone units that are intercalated with alkaline volcanic rocks (Hyde, 1980; Mueller et al., 1994). These were deposited in a fault-controlled basin associated with the LLCdz in a subaerial, alluvial-fluvial to lacustrine or shallow marine environment (Hyde, 1980; Mueller et al., 1994). While fault-bounded to the south, the Timiskaming assemblage is in unconformable contact with the Blake River assemblage to the north (Fig. 5.3; Thomson, 1946; Chapter 4). Younger, ~2670-2660 Ma intrusive rocks are locally abundant, particularly in the vicinity of higher-order deformation zones such as the Main Break and Kdz (Fig. 5.3; Corfu et al., 1991; Corfu, 1993; Wilkinson et al., 1999; Ayer et al., 2002, 2005). These consist of mafic (augite) syenite, syenite, and porphyritic syenite (Hattori and Hodgson, 1990). The porphyritic syenite rocks are the youngest of the intrusive rocks since they form sill to dike-like intrusions that cross-cut both the mafic (augite) syenite and syenite intrusions (Ispolatov et al., 2008).

Three major deformation events have been recognized in the study area as a result of progressive N-S shortening to dextral transpression (Wilkinson et al., 1999; Ispolatov et al., 2008). Upright folds in the Tisdale and Blake River assemblages, D_1 , occurred prior to the deposition of the Timiskaming assemblage (Wilkinson et al., 1999; Poulsen, 2017; Chapter 4). Following the deposition of the Timiskaming assemblage, N-S shortening during D_2 deformation resulted in tilting of the assemblage into a south-facing monocline (Fig. 5.3). D_2 is associated with an E-trending, subvertical foliation (S_2) that is poorly preserved in the study area (Ispolatov et al., 2008). D_2 deformation also resulted in thrust displacements along the LLCdz that, based on juxtaposition of the older Tisdale assemblage in the south over the younger Timiskaming assemblage in the north, has been interpreted as north directed (Thomson, 1948; Wilkinson et al., 1999; Lafrance 2015). A transition to NW-SE shortening and dextral transpression, D_3 , resulted in the formation of reverse to oblique-reverse faults and localized shear zones (Ispolatov et al., 2008; Chapter 4). Fault zones are defined by the occurrence of quartz-

carbonate veins and discrete slip surfaces with observable offsets that locally display gouge, cataclasite, and/or breccia zones. Shear zones are characterized by the occurrence of a subvertical, NE-trending penetrative foliation with an associated moderately to steeply NE-plunging mineral lineation and abundant dextral shear sense indicators (S-C fabrics, σ -clasts, and Z-folds) on horizontal erosional surfaces (Robin and Cruden, 1994; Wilkinson et al., 1999; Ispolatov et al., 2008; Chapter 4). Higher-order fault zones such as the Main Break or Kdz predominately record D₃ brittle-ductile structures, although direct timing constraints are lacking and these may, in part, represent reactivated structures that formed during D₂ (Frieman et al., 2017; Chapter 4). The Kdz displays brittle-ductile structures including fault-related breccia and veins, shear zones, and overprinting small-scale faults and shear veins that relate to D₃ transpression (Chapter 4), which are investigated in detail in this work.

5.3 Fault-associated brecciation and vein forming processes

This section summarizes two types of fault-associated processes recorded in the Kdz, which are fluid-assisted processes (Jébrak, 1997; Clark et al., 2006), and attrition or comminution processes (Engelder, 1974; Keulen et al., 2007). While attrition or comminution processes result from grinding along fault-slip surfaces, fluid-assisted breccia forms as a result of the build-up of hydrothermal fluid pressures to supra-hydrostatic conditions. There are two primary types of fluid-assisted breccia. One is associated with fault veins or vein arrays (Jébrak, 1997) and the other is dilational or 'implosion'-style breccia in fault jogs (cf. Sibson, 1985).

Fluid-assisted breccia commonly occurs above intrusive bodies in epithermal deposits where thermal gradients drive fluid flow (Simmons et al., 2005; Micklethwaite, 2009) or in orogenic gold deposits where fault-valve behavior drives periodic vein formation events (Sibson et al., 1988; Robert and Poulsen, 2001). In either case, veins may represent a single or multiple emplacement events. If multiply reactivated, they may display banding, laminated structures, and/or crack-seal textures (Hodgson, 1989). If there was a component of displacement across the vein during emplacement, shear veins can form. These represent a subset of veins that can be recognized based on the presence of fibrous or elongate crystals that precipitate at a small angle to the fault vein margin and, through crack-seal processes, build-up asymmetric steps that can be used to infer fault slip directions (Twiss, 1990; Passchier and Trouw, 2005).

In addition to discrete fault veins and arrays, fluid-assisted dilational or 'implosion'-style brecciation is common to fault zones where fault jogs or asperities create dilational sites during displacement (Fig. 5.5A; Sibson, 1985, 1986; Harris et al., 1991). During rupture, the near-instantaneous creation of void space drives extreme fluid pressure gradients that, if they exceed the tensile strength of the wall rock, produce dynamic off-fault fracture networks in which fluids

are catastrophically injected (Sibson, 1985; 1986; Pavlis et al., 1993). These types of fault-associated breccia domains can be identified by in-situ fragmentation textures such as crackle, mosaic, or 'jigsaw' patterns and typically have high dilation ratios expressed by an abundance of matrix relative to clasts (Jébrak, 1997).

Attrition or comminution breccia forms due to fracturing and grinding along principal fault-slip surfaces (Fig. 5.5A). Thus, the size and shape of attrition products evolve toward smaller particle sizes with time due to progressive displacement that drives particle interaction and wear-abrasion (Jébrak, 1997; Billi et al., 2003; Storti et al., 2003; Billi and Storti, 2004; Billi, 2005; Keulen et al., 2007). Attrition products predominantly evolve by intra- to trans-granular cracking, frictional grain boundary sliding, and grain rotation processes (Engelder, 1974; Jébrak, 1997; Billi et al., 2003; Billi, 2005; Keulen et al., 2007). Attrition products commonly display low to negligible amounts of dilation and may develop planar fabrics due to shortening within the fault zone, contrasting strength of particles, and/or preferential clast orientations (Jébrak, 1997).

5.4 Analysis of fault products by particle size distributions

Particle size distributions (PSDs) have been widely applied in natural fault systems as a means to quantify the self-similarity of fractured and fragmented rocks and to develop micromechanical models for fault zone development (Fig. 5.5; Engelder, 1974; Allégre et al., 1982; Turcotte, 1986; Sammis et al., 1987; Blenkinsop, 1991; Hattori and Yamamoto, 1999; Billi et al., 2003; Billi and Storti, 2004; Billi, 2005; Keulen et al., 2007; Luther et al., 2013; Melosh et al., 2014). A PSD for a sample is created by plotting the cumulative number of particles against their size in log-log space (Fig. 5.5B). The log-linear portion of the resultant curve is fit with an exponential equation:

$$N(S) = S^{-D} \quad (5.1)$$

Where S is the clast size, $N(S)$ is the number of clasts above size S , and D is the slope of the best fit line that approximates log-linear segments of the curve (i.e., the D -value). Commonly, only the central portion of the resultant curve is linear, as the upper and lower clast sizes are underrepresented due to observational or sampling limitations (Blenkinsop, 1991). D -values can be determined for 3D volumes or 2D areas. The mathematical relationship between these results is: $D_{3D} = D_{2D} + 1$ (Mandelbrot, 1982). Typically one D -value is obtained for a sample population, although two or more log-linear segments with distinct slopes have been observed (Keulen et al., 2007; Melosh et al., 2014). The mechanical significance of multiple log-linear segments in PSDs is poorly understood. Multiple D -values in a sample population may reflect an attrition limit wherein smaller particles become harder to break down by mechanical

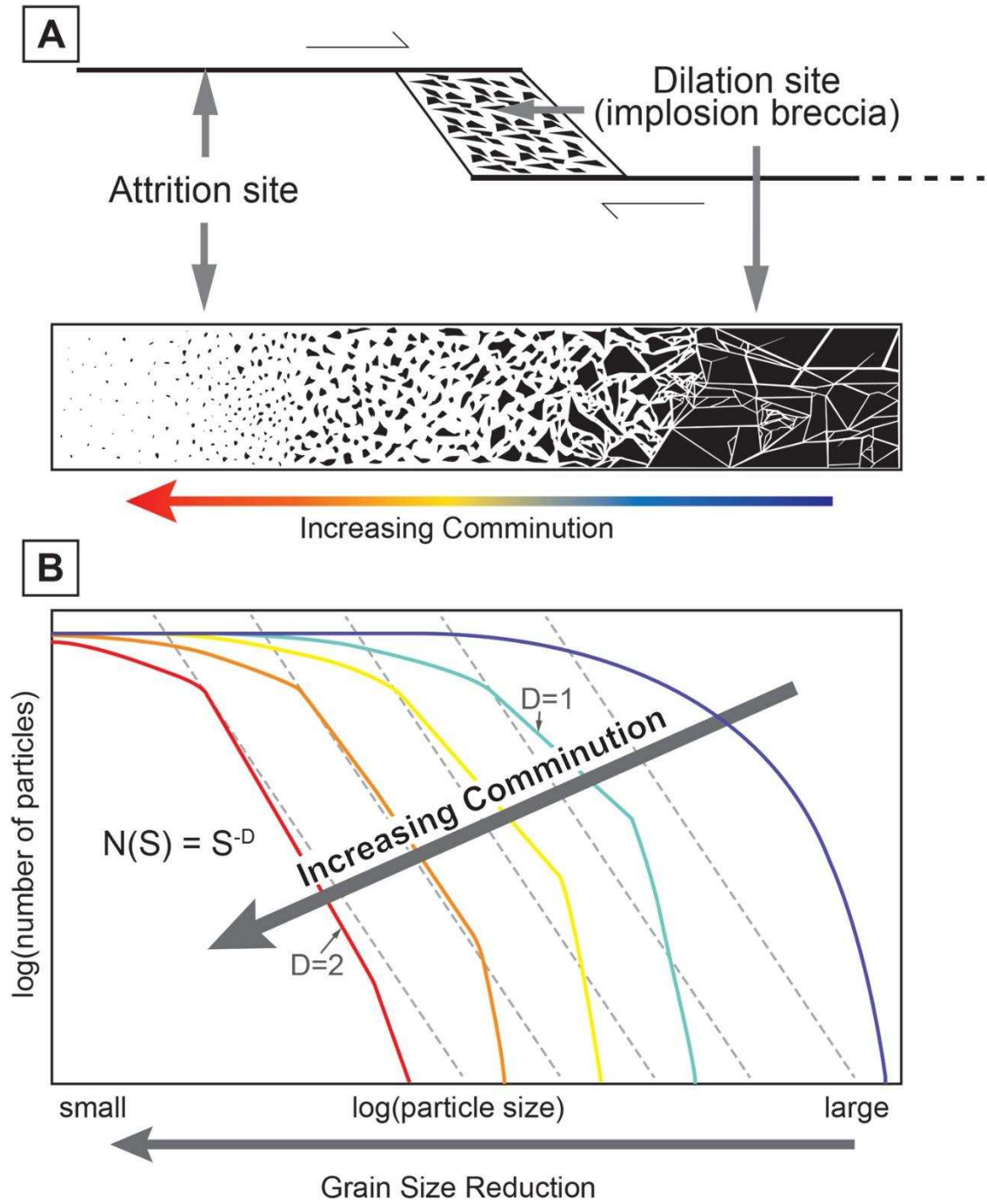


Figure 5.5 – Schematic illustrations of the relationship between fault breccia and particle size distribution. (A) Schematic illustration of the distribution and associated textural characteristics of attrition and dilational breccia products produced along a dextral fault step-over (modified from Melosh et al., 2014). (B) Schematic model of the evolution of hypothetical particle size distributions (PSDs) (solid lines) with increasing comminution plotted with reference D-values labeled based on the mathematical relationship included on the left (see text for explanation of variables). The PSD curve colors correspond to the colors and associated textures illustrated in (A) (modified from Blenkinsop and Fernandes, 2000, and Melosh et al., 2014).

processes, while larger particles can still evolve by attrition (Keulen et al., 2007). Alternatively, multiple D-values have also been attributed to pre-existing mineralogical or textural heterogeneity that imparts a geometric control (Melosh et al., 2014). In some cases, PSDs are not log-linear and cannot be approximated by a power-law relationship as described above (Blenkinsop and Fernandes, 2000; Melosh et al., 2014). In isolation, D-values can yield ambiguous results. Therefore, they are combined with observations from field and thin-section analysis to interpret fault processes (Melosh et al., 2014).

D-values quantify the cumulative number of particles and the relative abundance of clast sizes within a size fraction. A greater abundance of smaller versus larger grains within the log-linear portion of the size fraction results in a steeper slope and a higher D-value. Because cataclasis results in progressive particle size reduction, it is to be expected that gouge or cataclasite will contain a larger proportion of fine particles and, thus, have a higher D-value than initially fragmented breccia (Fig. 5.5B). Typical D-values (2D) for natural or experimentally deformed samples are ~1.0-2.0 (Storti et al., 2003; Billi and Storti, 2004; Billi, 2005; Keulen et al., 2007). Attrition dominated samples, such as (ultra)cataclasite or gouge rocks, have yielded D-values (2D) that cluster around ~1.6-1.7 (Sammis et al., 1987; Biegel et al., 1989; Marone and Scholz, 1989), although values as high as 2.5 have been documented (Keulen et al., 2007 and references therein). Changes in D-values from damage zone to fault core material (e.g., from 1.0 to 2.0) within a given set of fault samples have been interpreted to reflect preferential fragmentation of larger particles due to progressive fault slip (Blenkinsop, 1991; Billi and Storti, 2004; Billi, 2005). Fractured granite samples have yielded an average D-value of ~1.2 (Keulen et al., 2007) and fluid-assisted breccia samples have yielded similarly low D-values of ~1.0-1.4 (Blenkinsop, 1991; Jébrak, 1997; Clark et al., 2006). In these cases, lower D-values have been attributed to regular fracture spacing and/or less overall attrition and particle wear due to high associated fluid pressures (Marone and Schultz, 1989; Jébrak, 1997).

5.5 Methods

To constrain the structural development of the Kdz we conducted (1) km- to m-scale mapping, (2) microstructural and petrographic characterization, (3) quantification of fault-related breccia by PSD analysis, and (4) kinematic small-scale faults or shear veins by movement plane analysis.

5.5.1 Field mapping

Field mapping was conducted during the 2013-2015 field seasons and resulted in a series of new outcrop- to km-scale maps. The lithologic distribution of the study area was derived from map compilations in portions of the Teck (Thomson, 1945; Ispolatov et al., 2005),

Lebel (MacLean, 1944; Ispolatov et al., 2005), Bernhardt (Rupert and Lovell, 1970), and Morrisette (Rupert and Lovell, 1970) townships (Fig. 5.3). A new 1:2500 scale map for the Kdz was produced (Fig. 5.4).

5.5.2 Microstructural and petrographic characterization

To establish the paragenetic history of deformed, metamorphosed, and altered samples from the Kdz, oriented, polished thin-sections were analyzed by optical and scanning electron microscopy (SEM) techniques. SEM analyses included high-resolution field emission SEM (FE-SEM) imaging as well as automated mineralogy SEM scans. These were both performed in the Colorado School of Mines Department of Geology and Geological Engineering Electron Microscopy Laboratory. The automated mineralogy SEM analyses were performed on a TESCAN-VEGA-3 Model LMU VP-SEM platform and were initiated using the control program TIMA3. Four energy dispersive X-ray (EDX) spectrometers acquired spectra from each particle with a beam stepping interval (i.e., spacing between acquisition points) of 1 μm for bright phase search scans and 20 μm for mineralogical scans, an accelerating voltage of 25 keV, and a beam intensity of 14. Interactions between the beam and the sample were modeled through Monte Carlo simulation. The EDX spectra were compared with spectra held in a look-up table allowing an assignment to be made of a composition at each acquisition point. The assignment makes no distinction between mineral species and amorphous grains of similar composition. Results were output by the TIMA software as a spreadsheet giving the area percent of each composition in the look-up table. This procedure allows a compositional map to be generated. Composition assignments were grouped appropriately. Supplementary back scattered electron (BSE) and secondary electron (SE) imaging of selected areas was performed using a TESCAN MIRA3 FE-SEM that was operated at high vacuum, 15 kV, and a beam current of 11 nA.

5.5.3 Particle size distribution analysis

Five samples of breccia with a range of breccia textures including crackle, mosaic, and chaotic textures were selected for particle size distribution (PSD) analysis (Fig. 5.6). D-values reported in this study are 2D having been derived from high-resolution images of thin-sections, oriented hand samples, or outcrop exposures. For each sample, clasts were manually outlined on scaled, high-resolution photos using vector graphics software. The resultant black and white images (Fig. 5.6) were quantified using the freely available ImageJ software suite (Schneider et al., 2012). In ImageJ, the 2D area of each clast was determined and, to allow for comparison, converted to equivalent (circular) diameters. The cumulative number of particles greater than a given size fraction were plotted versus the measured 'equivalent (circular) diameters' in log-log

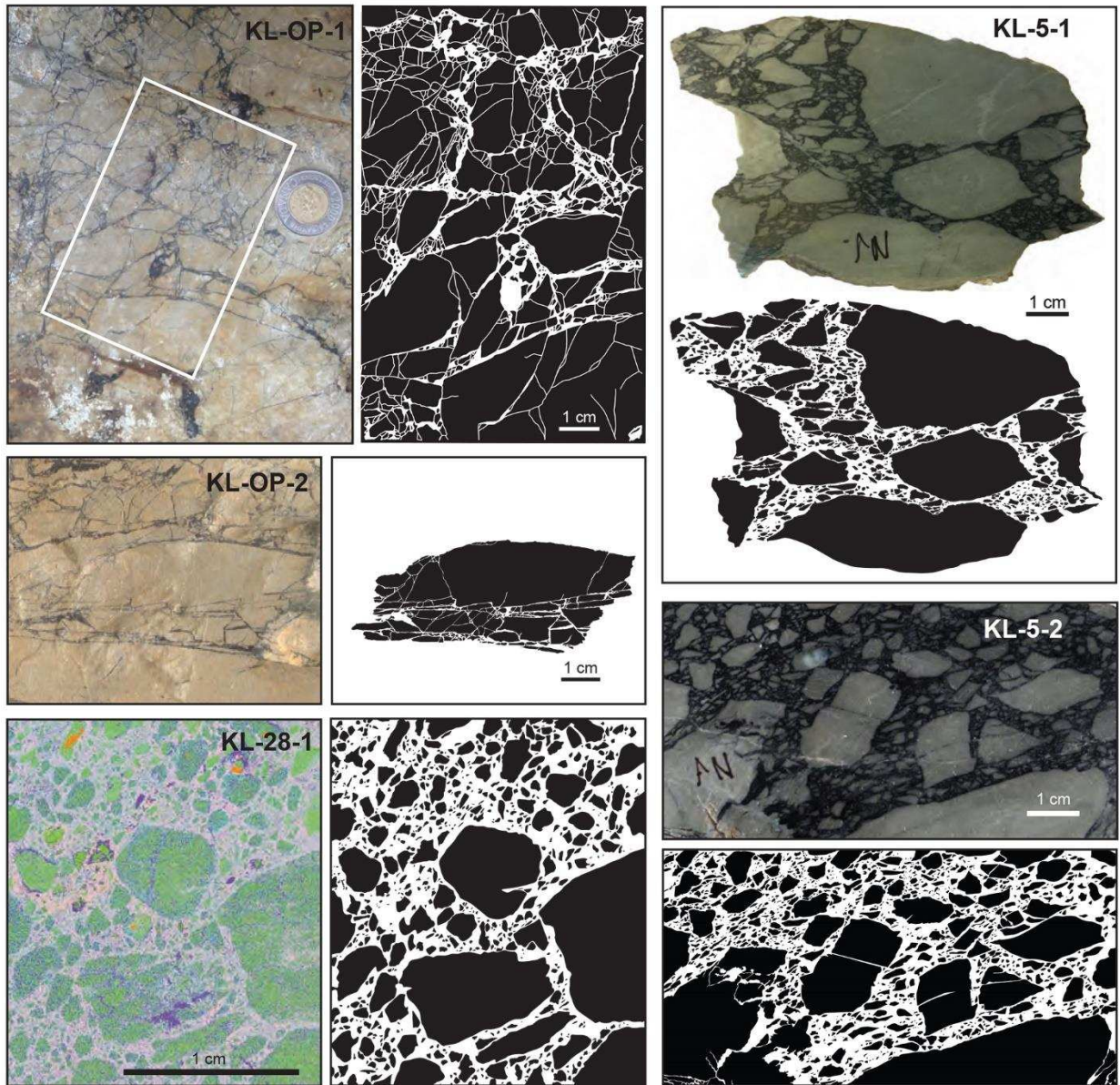


Figure 5.6 – Outline drawings of the breccia samples from the Kirana East outcrop area used for particle size distribution analysis. All samples are parallel to a horizontal spatial reference frame. The sample numbers refer to the locations labeled on Figure 5.12.

space (see section 5.8). Best fit curves for manually selected log-linear portions and associated D-values were calculated using Microsoft Excel.

5.5.4 Kinematic analysis of small-scale faults and shear veins

Kinematic analysis of small-scale faults and shear veins was conducted using movement plane (M-plane) geometries in Orient 3.0.1 (Fig. 5.7; Vollmer, 2015). M-plane analysis is a well-established method for constraining the stress directions and kinematics associated with fault displacements (Angelier, 1979; Marshak and Mitra, 1988; Twiss and Unruh, 1998; Marrett and Allmendinger, 1990; Twiss and Moores, 2007). The method is based on Andersonian theory of fault behavior and requires the orientation of a fault plane, a displacement vector inferred from slip lineations, and a motion sense from asymmetric structures such as slickenfiber steps (Fig. 5.7; Twiss, 1990; Passchier and Trouw, 2005). These structures are used to define the M-plane by fitting a plane that contains both the pole to the fault plane and the slip lineation (Fig. 5.7). Based on the directional displacement vector and movement sense, incremental shortening and extension axes (P- and T-axis, respectively) are defined at $\pm 45^\circ$ along the M-plane from its intersection with the fault plane and slip lineation (Fig. 5.7). Orient calculates individual shortening and extension axes for each fault and directional slip lineation pair entered. A population of P- and T-axes can be collectively analyzed using moment tensor analysis to produce a 'beachball' solution diagram (Marrett and Allmendinger, 1990; Vollmer, 2015).

5.6 Results of the km- to outcrop-scale mapping

Mapping and compilation results indicate that the Kdz is a continuous, >3 km, ENE-trending zone of brittle-ductile deformation (Figs. 5.3 and 5.4). The Kdz is interpreted to dip steeply towards the north based on underground workings (Burrows and Hopkins, 1916) and the local orientation of faults and shear zone fabrics (Fig. 5.8A; Frieman et al., 2017). It is largely hosted by volcanic rocks of the Blake River assemblage, but also affects post-Timiskaming assemblage porphyritic syenite intrusions (Fig. 5.4).

In the west, the Kdz is well exposed in a large area (100s of m²) of stripped bedrock exposure named the Fidelity outcrop (Fig. 5.4). At this location, the Kdz forms a wide, >15 m shear zone that displays pervasive carbonate alteration (Fig. 5.9A). The foliation is NE-trending, subvertical and shows a moderately- to steeply-plunging mineral lineation (Fig. 5.8), and dextral shear sense indicators on horizontal erosional surfaces, including S-C fabrics and σ -clasts. The shear zone affects both mafic volcanic and porphyritic intrusive rocks, locally forming asymmetric lozenge shaped domains of each lithology bounded by foliation surfaces (Fig. 5.9B). Shear fabrics also overprint pods of breccia developed in the mafic volcanic rocks (Fig. 5.10A), however, brecciation of the intrusive rocks was not observed.

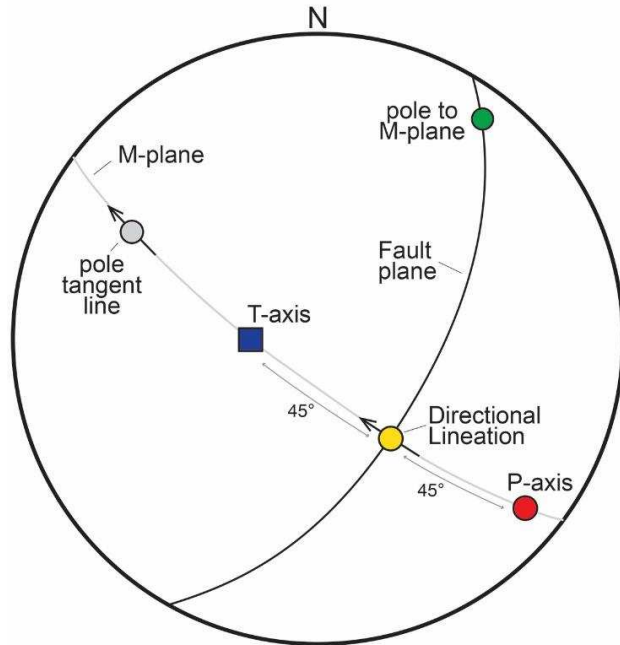


Figure 5.7 – Schematic diagram illustrating movement plane kinematic analysis. Lower-hemisphere equal-area projection of a reverse fault, with a slip lineation (yellow), pole to fault plane (grey), the movement plane, or M-plane (dashed grey), and its pole or M-axis (green; intermediate). The P-axis (red; shortening) and T-axis (blue; extensional) bisect the angle between the fault plane and its pole along the M-plane. Arrows are tangent lines that show the displacement sense of the hanging wall with respect to the footwall.

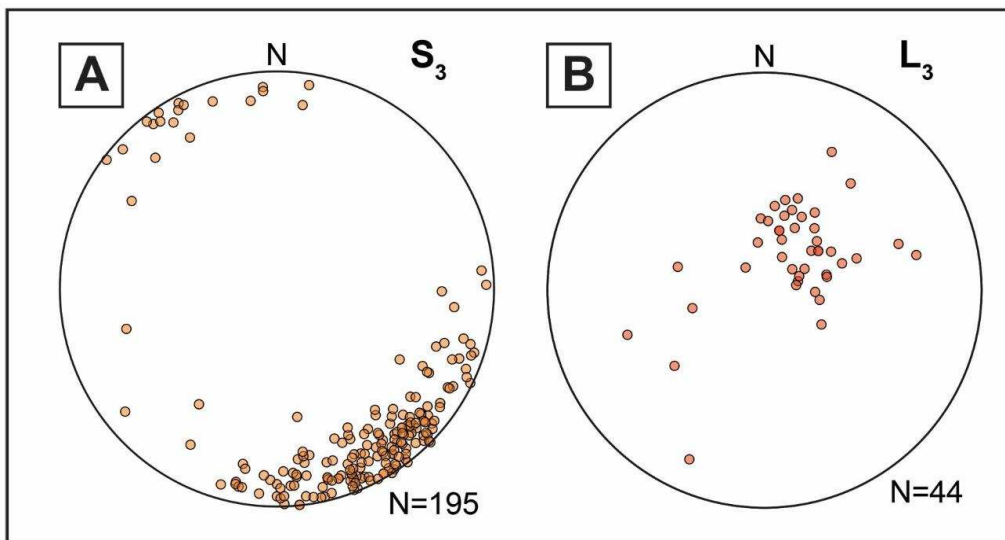


Figure 5.8 – S_3/L_3 structural orientation data. Poles to foliation (A) and lineation (B) data for ductile fabrics developed along the Kirana deformation zone shown as equal-area lower-hemisphere projections.

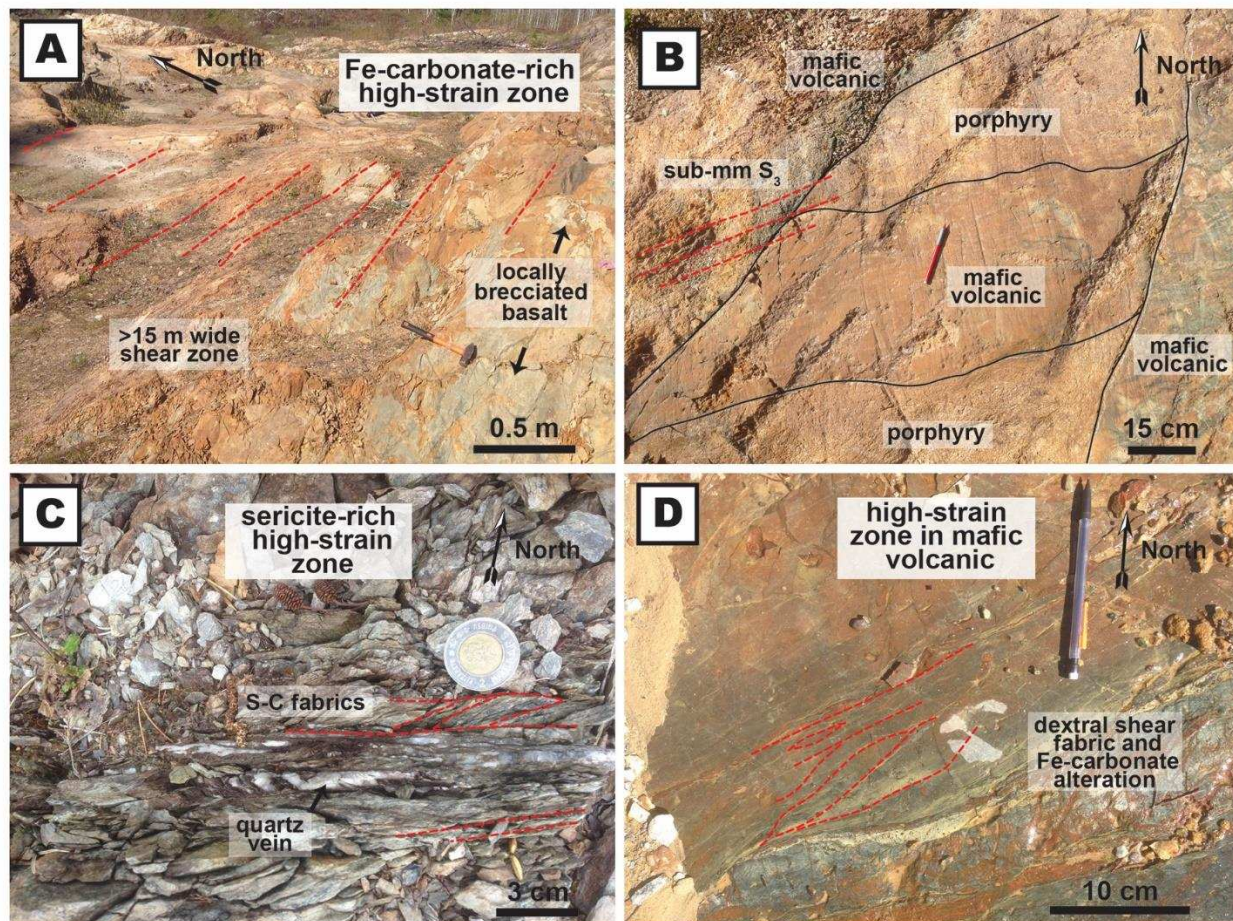


Figure 5.9 – Field photos of ductile structures observed along the Kirana deformation zone. (A) A broad, >15 m wide zone ductile shear with intense carbonate alteration at the Fidelity outcrop. (B) Sheared basalt and porphyritic intrusive rocks at the Fidelity outcrop. (C) A sericite-rich mylonite zone at the Kirana East outcrop displaying dextral S-C fabrics and local quartz veins. (D) An example of a mylonitic dextral shear zone developed in mafic volcanic rocks adjacent to the Kirana East outcrop. Outcrop locations shown in Fig. 5.4.

Several generations of quartz-carbonate veins are observed. Earlier formed veins are strongly foliated and are parallel to the local foliation (Fig. 5.11A). These form composite fault veins and are associated with carbonate alteration halos. Late veins are nearly undeformed and commonly occur as shallowly- to moderately-dipping conjugate vein sets (Fig. 5.11B). Carbonate alteration halos are also associated with both the early and late vein sets.

Towards the east, the Kdz is mapped as two distinct fault/shear zone splays (Fig. 5.4). The northern splay is defined by a ~5-10 m wide shear zone that largely occurs in massive, fine-grained mafic volcanic rocks. The southern splay is defined by zones of breccia, ductile shear, and/or intensely carbonate-altered rocks. The fault core and damage zone of the Kdz are well

exposed at the Kirana East outcrop (Fig. 5.4). There, the fault zone is also overprinted by m-scale mylonite to ultramylonite zones (Fig. 5.9C, D), which are themselves overprinted by abundant small-scale faults, shear veins, and disseminated alteration minerals. Thus, the Kirana East outcrop preserves many of the key structures and crosscutting relationships that are ideal to establish the history of the Kdz. It is described and discussed in detail below.

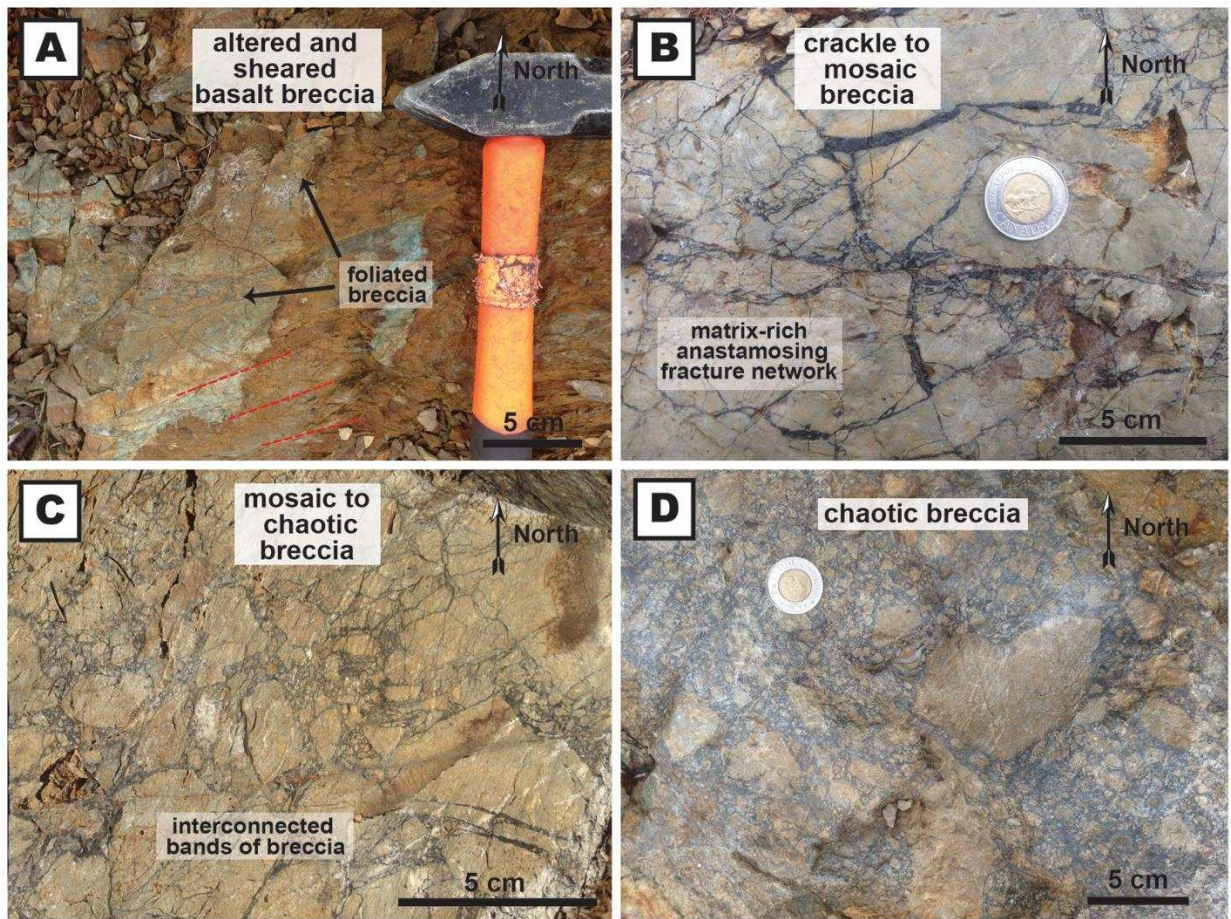


Figure 5.10 – Field photos of brittle deformation textures observed along the Kirana deformation zone (Kdz). (A) Pillow basalt from the Fidelity outcrop that displays intense alteration and penetrative foliation that overprints locally formed breccia bodies. (B) An example of crackle to mosaic breccia from within the damage zone of the Kdz exposed at the Kirana East outcrop, displaying anastomosing, matrix-rich primary fracture networks. (C) Pervasive zones of mosaic to chaotic breccia at the Kirana East outcrop. (D) Carbonate-altered chaotic breccia from the fault core of the Kdz exposed at the Kirana East outcrop. Outcrop locations shown in Fig. 5.4.

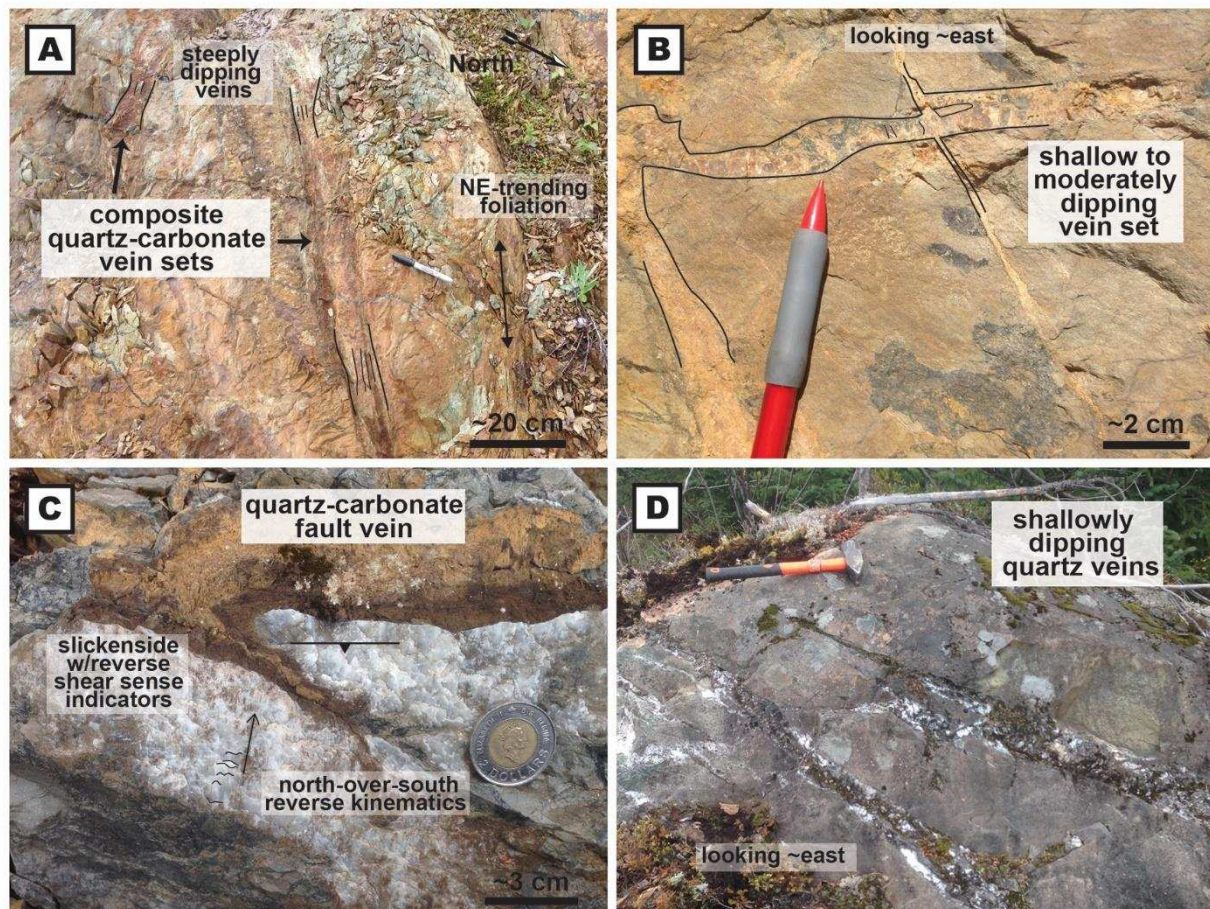


Fig. 5.11 – Field photos of quartz vein morphologies commonly observed along the Kirana deformation zone. (A) Early steeply-dipping and NE-trending composite quartz-carbonate vein sets that are overprinted by penetrative fabric observed at the Fidelity outcrop. (B) Relatively late, shallowly- to moderately-dipping, conjugate vein set that is texturally associated with alteration of the host wall rock and displays little to no post-emplacment deformation observed at the Fidelity outcrop. (C) Example of a quartz-carbonate shear vein observed at the Kirana East outcrop with well-developed linear slickensides with asymmetric steps that indicate north-over-south displacement that was included in M-plane analysis. (D) Shallowly-dipping quartz vein array that occurs within ~100m of the Kirana East outcrop. Outcrop locations shown in Fig. 5.4.

5.6.1 The Kirana East outcrop

The Kirana East outcrop is a ~10 m by ~70 m area of stripped bedrock outcrop (Fig. 5.4). The outcrop area was mapped in detail (1:50; Fig. 5.12) and oriented hand samples were collected for petrographic and textural characterization. Below, the outcrop area is described from north to south and then the observed structures are described in detail from oldest to youngest.

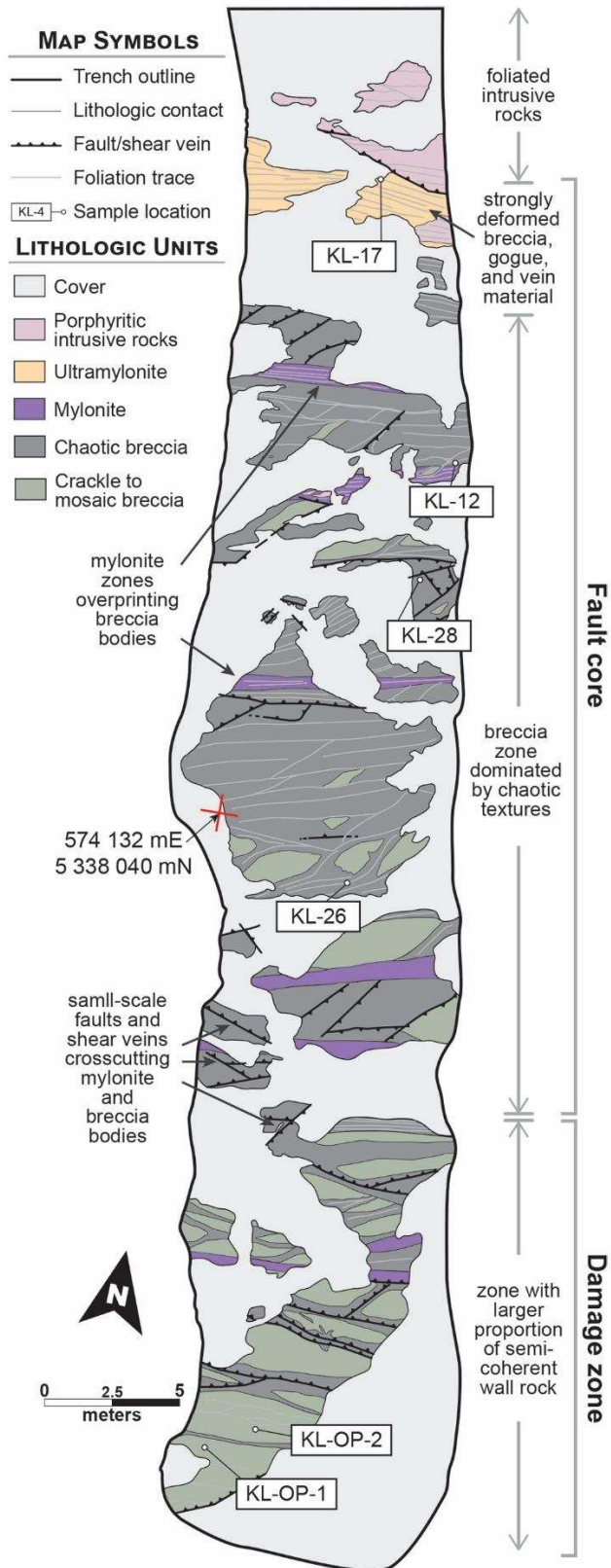


Fig. 5.12 – Detailed geological map of the Kirana East outcrop. See Fig. 5.4 for the outcrop location. The location of oriented samples discussed in text are indicated.

The northern portion of the outcrop area exposes ~15 m of porphyritic intrusive rocks. These contain anastomosing networks of penetrative foliation defined by mm-scale sericite or chlorite-rich domains (Figs. 5.12 and 5.13B). The intrusive rocks display no evidence for brecciation. The remaining ~55 m exposes variably deformed, grey volcanic rocks (Fig. 5.10B-D). The volcanic rocks are massive, fine-grained, and contain distinctive mm-scale quartz phenocrysts. Thus, the protolith is interpreted to be a rhyolite (Fig. 5.13A). The porphyritic intrusive rocks and rhyolitic unit are separated by a ~4 m ultramylonite zone that contains strongly deformed and foliated breccia, fault gouge, and quartz-carbonate vein material (Figs. 5.11C and 5.12). The original width of the mylonitized gouge zone is unknown as it is truncated by the porphyritic intrusive rocks to the north.

Chaotic breccia domains dominate the central portion of the outcrop area defining a ~30 m breccia zone of the fault core (Fig. 5.11D). In the breccia zone, asymmetric, m-scale pods of crackle to mosaic breccia are bounded by zones of chaotic breccia (Fig. 5.12). The chaotic breccia zones contain clasts that are subrounded to subangular in shape (Fig. 5.11D), indicating higher degrees of particle interaction and wear abrasion. The contact between mosaic and chaotic breccia is most commonly transitional, making discrete boundaries difficult to define.

Crackle to mosaic breccia domains are most abundant in the southern ~20 m of the outcrop (Figs. 5.11B, C and 5.12). There, larger proportions of semi-coherent wall rock are observed defining the damage zone of the Kdz (Fig. 5.12). Matrix filled primary fracture networks preserved in the crackle breccia form anastomosing, interconnected, and branching networks that are <1 mm to >1cm in width (Fig. 5.11B). Primary fracture networks largely have planar geometries, but also form irregular, lobate shapes at fracture intersections or in strain shadows adjacent to larger clasts (Fig. 5.11B).

Throughout the fault core and damage zone, breccia domains form anastomosing, broadly ENE-trending, interconnected arrays of matrix supported breccia. Clasts are entirely comprised of Blake River assemblage wall rock and no 'exotic' clasts were observed. Clasts display sharp boundaries with the matrix, have cusped to irregular margins, and angular to subangular shapes (Figs. 5.6 and 5.10B, C). Wall rock clasts display a wide range of sizes including m-scale blocks to sub-mm fragments within matrix vein networks. The breccia matrix is comprised of black quartz-rich material (Figs. 5.6 and 5.10C-D).

Breccia domains are crosscut by m-scale mylonitic shear zones (Fig. 5.12). These are defined by a penetrative foliation with sub-mm-scale spacing and sericite, chlorite, or carbonate-rich domains (Fig. 5.9C, D). The foliation in these zones is subvertical to steeply N-dipping and

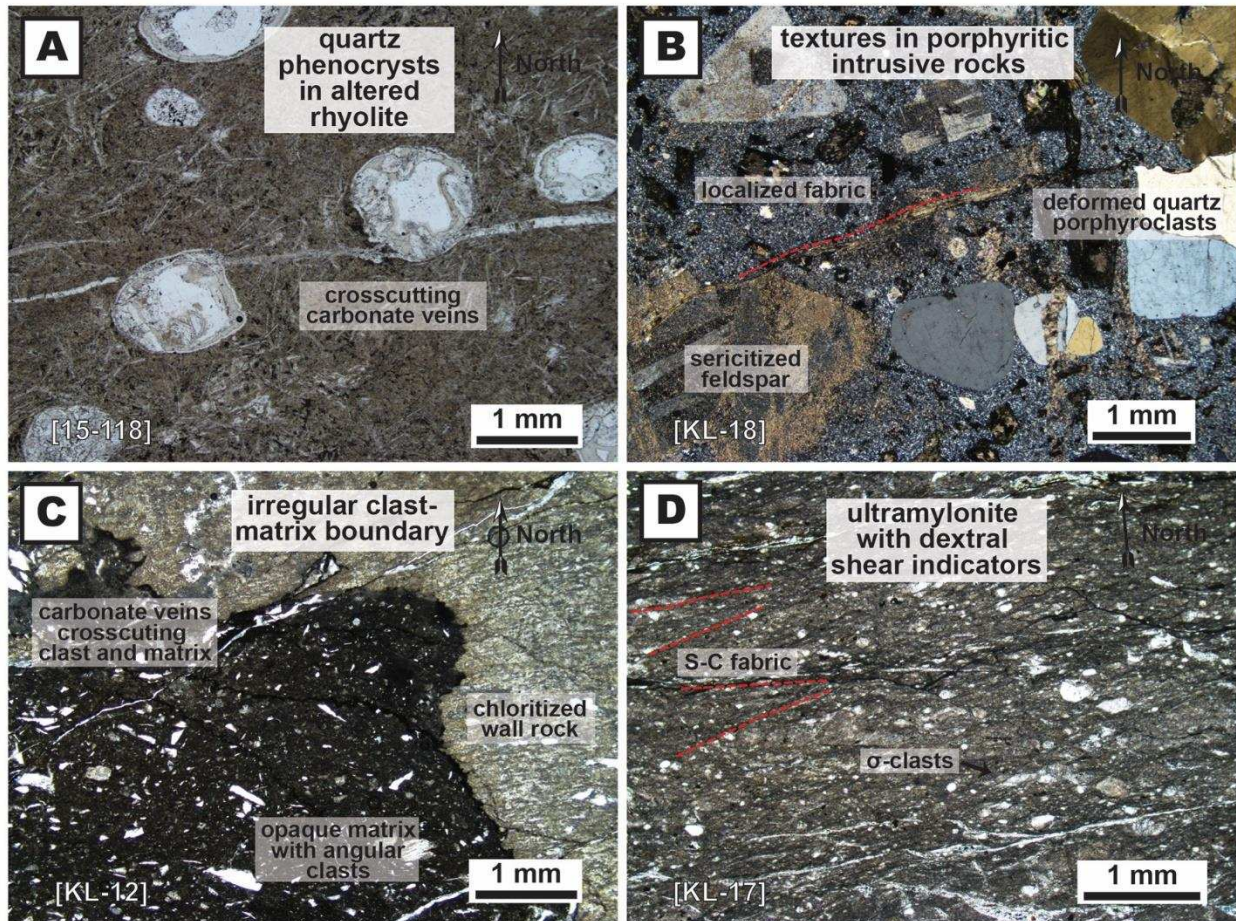


Figure 5.13 – Photomicrographs of samples from the Kirana deformation zone. (A) Plane polarized light photomicrograph displaying quartz phenocrysts in altered rhyolitic wall rock along the Kirana deformation zone. (B) Photomicrograph in crossed polarized light displaying localized fabric, sericite alteration of K-feldspar, and deformed quartz porphyroclasts in the porphyritic intrusive rocks of the Kirana East outcrop. (C) Plane polarized light photomicrograph displaying an irregular boundary between chloritized wall rock and opaque, clast-rich matrix material from the Kirana East outcrop. Note: carbonate veins cross-cut wall rock, matrix material, and their contact. (D) Plane polarized light photomicrograph of ultramylonite sample from near the Kirana East outcrop displaying dextral shear sense indicators such as S-C fabrics and σ -clasts. Outcrop locations shown in Fig. 5.4.

contains a moderately to steeply NE-plunging stretching lineation defined by aligned mineral grains or aggregates (Fig. 5.8). Dextral shear sense indicators such as S-C fabrics are common on horizontal erosional surfaces (Fig. 5.9C, D). In the areas between the mylonitic zones, the foliation is a weak spaced (at least cm-scale) cleavage that is associated with flattening of the breccia clasts.

Small-scale faults and quartz-carbonate shear veins crosscut the mylonite zones and breccia domains of the fault core and damage zone (Figs. 5.11C and 5.12). These are

shallowly- to steeply-dipping with variable strikes and are randomly distributed throughout the outcrop (Fig. 5.12) and are also common within ~100-200 m of the Kirana East outcrop (Fig. 5.11D). Exposed small-scale faults and shear veins form prominent erosional surfaces that display well-developed fibrous slickensides and asymmetric steps (Fig. 5.11C). Displacements inferred from these structures predominantly indicate reverse to oblique-reverse, S-side-up or N-side-up motions (e.g., Fig. 5.11C). Where possible, the orientation of the small-scale faults and shear veins, fibrous slickenside lineations, and the displacement sense were documented for M-plane analysis (see section 5.9).

5.7 Petrographic and microstructural observations

The following sections summarize the petrographic and microstructural observations made from oriented thin sections of Kdz samples. First, the microstructural characteristics of the Kirana East breccia samples are discussed. Then, the microstructural observations from (ultra)mylonite and foliated intrusive samples are presented.

5.7.1 Microstructural characteristics of breccia samples

The wall rock fragments in the Kirana East breccia samples consist of chlorite, quartz, albite, and minor amounts of plagioclase, rutile, muscovite, kaolinite, and apatite (Figs. 5.13C, 5.14, 5.15, and 5.16). Chlorite is modally abundant in the clast domains (~45-55%), but is a lesser component (10-15%) in the matrix domains (Figs. 5.14, 5.15, and A.6). Chlorite overprints both clast and matrix domains (Fig. 5.14). In some locations, chlorite grains are aligned, defining penetrative S_3 fabrics, while in other locations they form randomly oriented static overgrowths (Fig. 5.14). Disseminated albite is modally abundant in both clast and matrix material of all samples (~10-30%; Fig. 5.15).

Carbonate (calcite and/or ankerite) is abundant in most samples (modally ~5-20%; Fig. A.6), occurring as disseminations and veinlets or conjugate veinlet sets. Carbonate \pm quartz veinlets crosscut both breccia clast and matrix material (Figs. 5.14 and 5.15). Albite- and chlorite-rich domains form rims on the veinlet margins (Figs. 5.15 and 5.16A, B). Some samples display veinlets in the breccia matrix material, while adjacent wall rock clasts contain disseminated carbonate (Fig. 5.14). Veinlet emplacement was cyclic based on the occurrence of successive, mutually crosscutting relationships (Fig. 5.14). Sulfide minerals commonly occur in textural association with the veinlets as well as disseminated carbonate or albite (Fig. 5.15). Pyrite and chalcopyrite are common, while lesser amounts galena and sphalerite were observed.

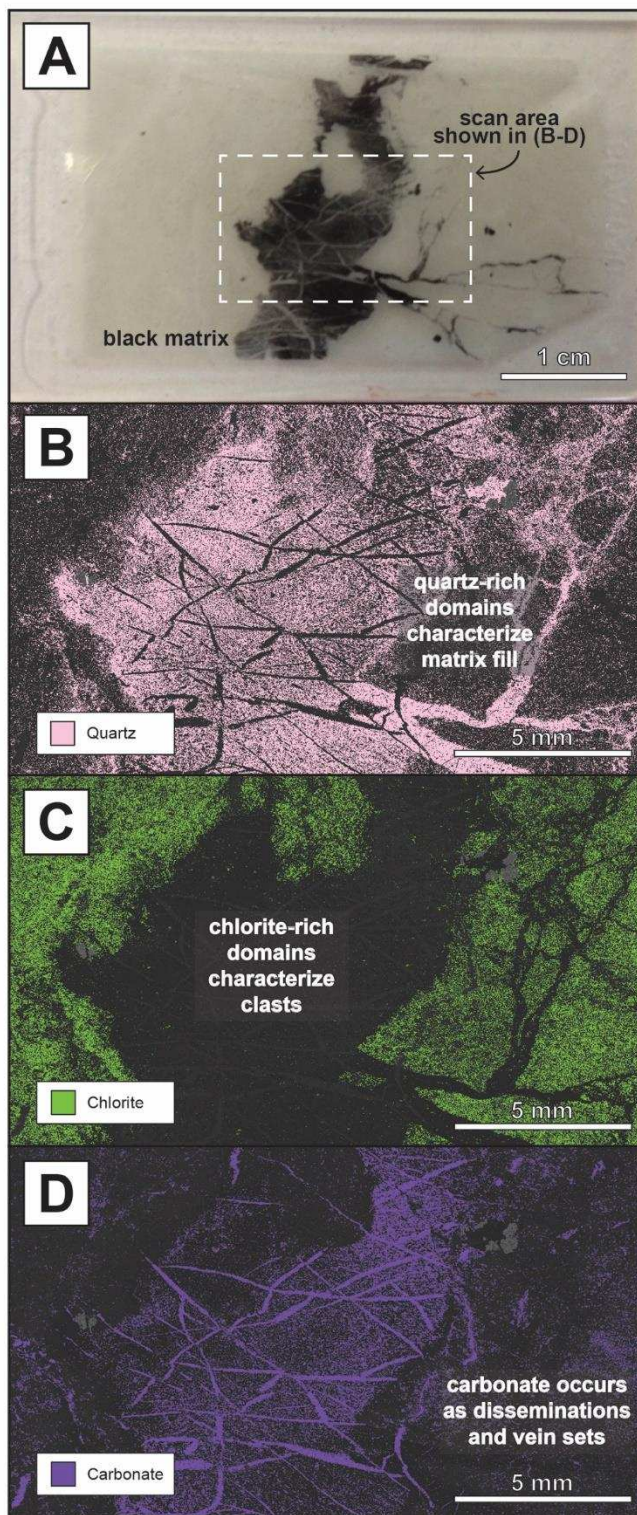


Figure 5.14 – Mineralogical characteristics of sample KL-12. (A) Thin-section scan of sample KL-12 (Fig. 5.12) displaying a thick (~1 cm) black breccia matrix vein. (B-D) Back-scattered electron images with overlays of the distribution of quartz (B), chlorite (C), and carbonate (D) phases from the automated mineralogical SEM analysis.

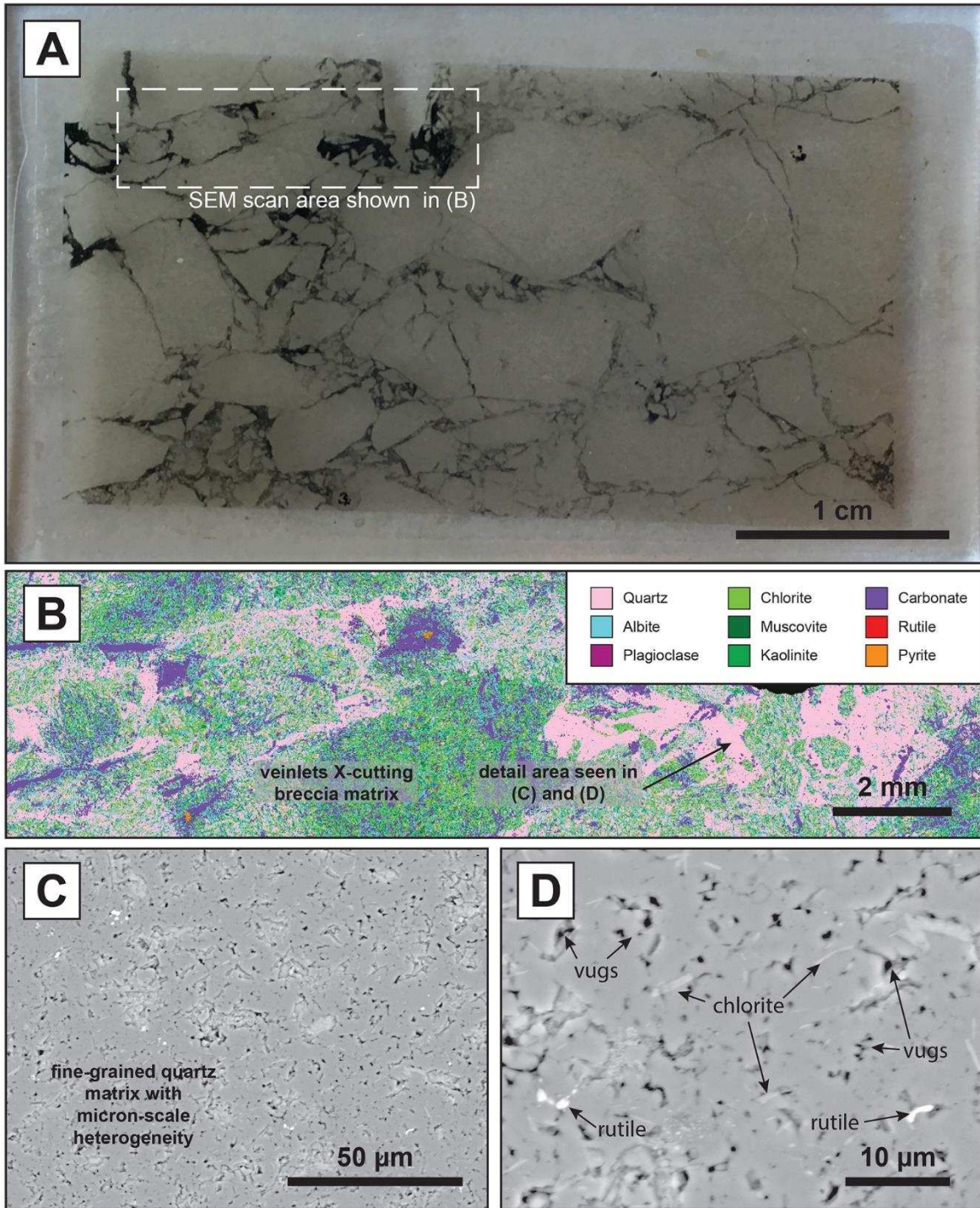


Figure 5.15 – Microstructural characteristics of sample KL-26. (A) Thin-section scan of sample KL-26 (Fig. 5.12) consisting of crackle to mosaic breccia that contains abundant matrix filled primary fracture networks. (B) Results of automated mineralogical SEM scan for the area indicated in (A) displaying quartz-rich breccia matrix domains, chlorite-rich clasts, and overprinting carbonate and albite alteration. (C-D) High-resolution, back-scattered electron images of the quartz-rich breccia matrix displaying abundant micrometer-scale heterogeneity defined by the presence of small ($\sim 1 \mu\text{m}$) vugs, chlorite, and rutile.

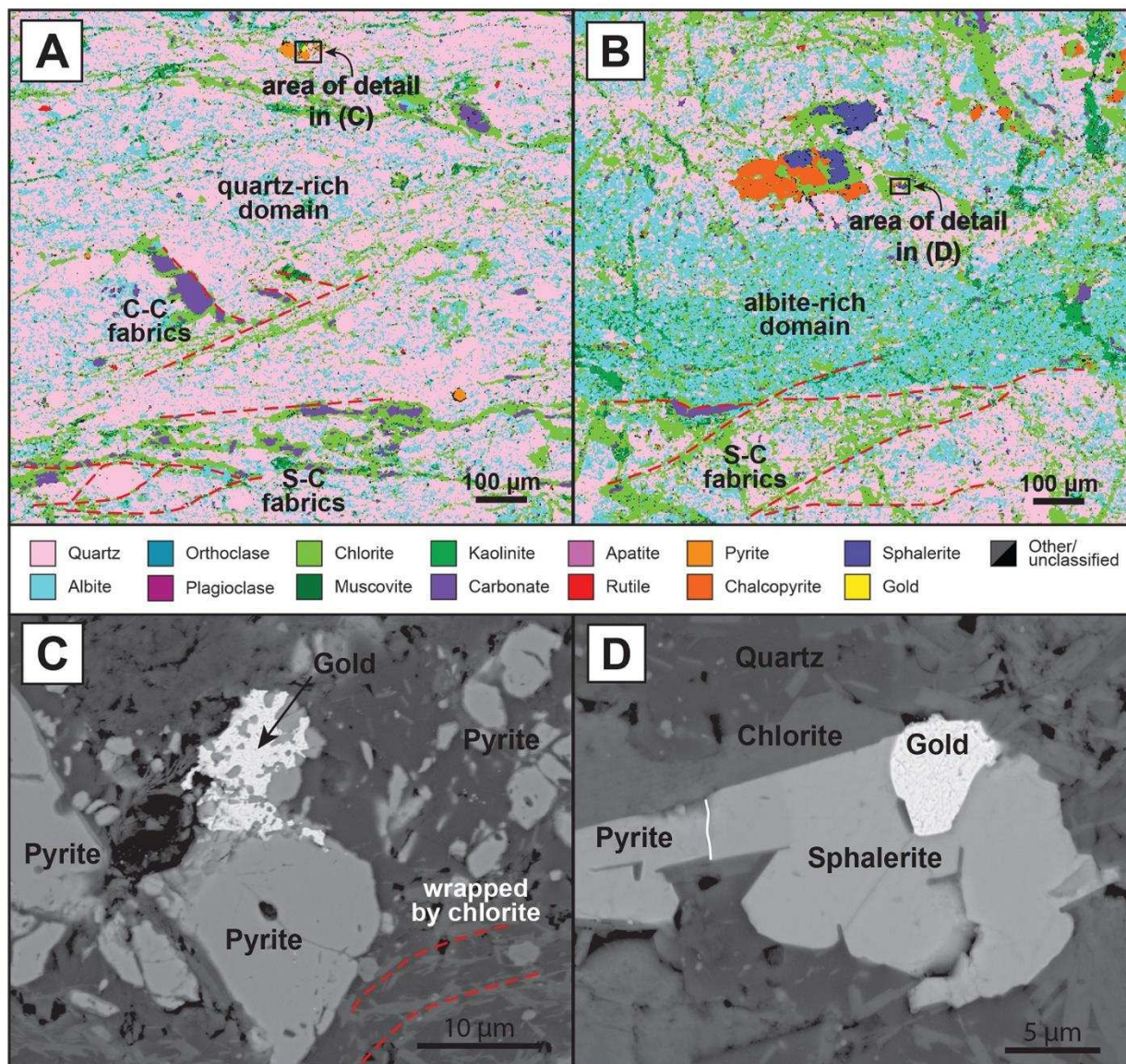


Figure 5.16 – Mineralogical and microstructural characteristics of sample KL-17. (A-B) Results of the automated mineralogical SEM scans of selected areas of sample KL-17 (Fig. 5.12) displaying a fine-grained (10-100 μm) quartz and albite matrix, aligned chlorite domains, asymmetric pods and veinlets of carbonate, sulfides, and associated gold. (C-D) High-resolution back-scattered electron images of the gold occurrences shown in (A-B), in association with pyrite and sphalerite.

In thin-section, the breccia matrix and clasts display sharp, but irregular boundaries (Fig. 5.13C). Fine-grained (<0.5 mm) matrix supported breccia clasts of quartz and chloritized wall rock that display angular shapes occur within matrix filled fractures (Fig. 5.13C). The breccia matrix material is black and opaque, making optical characterization difficult (Fig. 5.13C). Automated mineralogical SEM scans, conducted at 20 μm step-size, indicate that the matrix material primarily consists quartz (Figs. 5.14 and 5.15). However, high-resolution (>1000X), FE-SEM imaging of the least altered matrix material reveals micrometer-scale, textural and mineralogical heterogeneity (Fig. 5.15C, D). In addition to fine-grained quartz, homogeneously distributed vugs, chlorite, and rutile were observed (Fig. 5.15D). The vugs are \sim 1-5 μm in diameter with angular, polygonal boundaries bounded by statically recrystallized quartz (Fig. 5.15D). Chlorite occurs as randomly oriented, elongate crystals that are <1-5 microns wide, while rutile forms circular to lobate micron-scale disseminations (Fig. 5.15D).

5.7.2 Kirana East (ultra)mylonite samples

Ultramylonite from the fault core of the Kdz (KL-17) is chlorite-rich and displays a matrix composed of fine-grained (\sim 10-100 μm), dynamically recrystallized quartz or albite (Figs. 5.13D and 5.16A, B). Porphyroclasts of quartz and albite consisting of individual grains or aggregates form asymmetric σ -clasts bounded by fabric forming chlorite. Dextral S-C and C-C' shear sense indicators defined by aligned chlorite-rich domains are common (Fig. 5.16A, B). Chlorite also rims carbonate pods or veinlets (Fig. 5.16A, B).

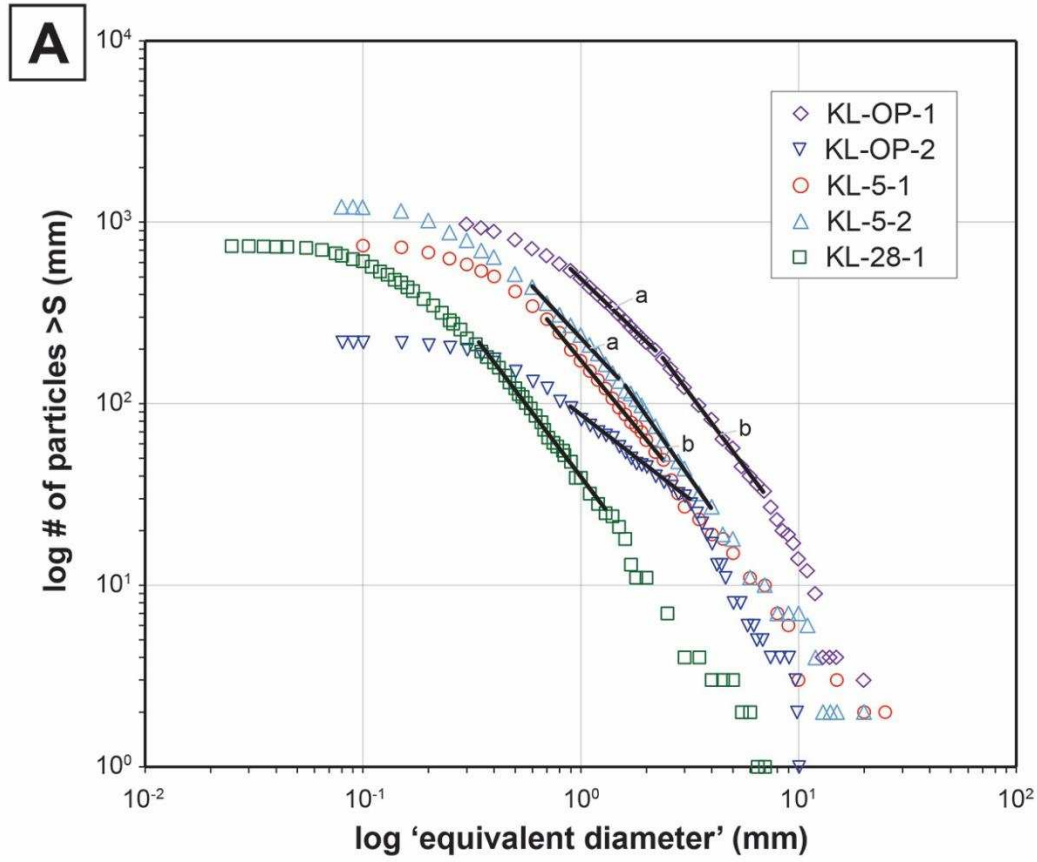
Native gold grains occur in association with sulfide minerals such as sphalerite, pyrite, and chalcopyrite (Fig. 5.16C, D). These are fine-grained (\sim 5-10 μm) and were only identified within the mylonitized fault core material (KL-17; Fig. 5.12). The gold-associated sulfides lie within the mylonitic fabric and are wrapped by fine-grained, fabric-forming chlorite (Fig. 5.16C).

5.7.3 Foliated intrusive rocks

In thin-section, the porphyritic intrusive rocks display abundant mm-scale quartz and K-feldspar phenocrysts with a fine-grained quartz- and plagioclase-rich groundmass (Fig. 5.13B). Quartz phenocrysts are commonly microfractured and display intracrystalline deformation textures, while K-feldspar phenocrysts are sericitized. Micro-scale foliation is defined by aligned, fine-grained sericite that crosscuts larger porphyroclasts of quartz or feldspar.

5.8 Particle size distributions of Kirana East breccia samples

All samples analyzed yielded log-linear distributions in their PSDs with D-values ranging from 0.93 to 1.71 (Fig. 5.17). The crackle to mosaic breccia samples yielded lower D-values of 0.93, 1.15, and 1.60, while the mosaic to chaotic breccia samples yielded higher D-values of 1.28, 1.46, 1.58, and 1.71 (Fig. 5.17B). Of these results, two samples (KL-OP-1 and KL-5-2)



	Sample #	D-value	R ²	Range of N for best fit	N
crackle breccia	KL-OP-1	(a) 1.15	0.9989	345	1157
		(b) 1.60	0.9981	143	
	KL-OP-2	0.93	0.9961	67	218
mosiac to chaotic breccia	KL-5-1	1.46	0.9992	243	747
	KL-5-2	(a) 1.28	0.9959	305	1214
		(b) 1.71	0.9958	91	
	KL-28-1	1.58	0.9948	178	737

Figure 5.17 – Results of the particle size distribution analysis. (A) Log-log plot of the number of particles >size (S) in each sample versus particle diameter for the samples analyzed in this study. (B) D-value results for the log-linear portions of the curves identified in (A) with a table showing D-values, R² fit, range of N for best curves, and total number of particles (N) in each sample population. See text for explanation.

yielded two distinct log-linear segments in their PSDs, which are separated by distinct breaks in slope (Fig. 5.17A). In these samples, a smaller grain size population, from ~0.7 to ~2-3 mm, corresponds to D-values of 1.15 and 1.28 for KL-OP-1 and KL-5-2, respectively (Fig. 5.17B). Conversely, a coarser grain size fraction, from ~2-3 to ~8 mm, defines log-linear trends that correspond to higher D-values of 1.60 and 1.71 for KL-OP-1 and KL-5-2, respectively (Fig. 5.17B).

5.9 Results of small-scale faults and shear veins kinematic analysis

The orientation data used for M-plane analysis are displayed in Figure 5.18 as pole tangent line diagrams. These display the pole to the fault/shear plane with the displacement vector of the hanging wall with respect to the foot wall (see Fig. 5.7 for a more detailed explanation). Data from two individual field localities, the Fidelity (Fig. 5.18A) and Kirana East (Fig. 18B) outcrops, are plotted separately. These data are also shown combined with additional data collected from throughout the Kdz study area (Fig. 5.18C).

M-plane calculations for these data correspond to variably oriented, moderately- to steeply-plunging or subvertical extensional axes and distributed clusters of shortening axes that are shallowly-plunging or subhorizontal (Fig. 5.18). The largest proportion of shortening axes plunge to the N-NNE or S-SSE, although a subordinate proportion plunge to the WSW or ENE. Eigenvector analysis of these data yielded 'beachball' solutions consistent with NNW-SSE shortening (Fig. 5.18).

5.10 Discussion and structural synthesis

New mapping and structural analysis indicates that the Kdz is a gold-bearing, brittle-ductile deformation zone that has similar characteristics and a similar structural history as the well-studied and well-mineralized Main Break (Frieman et al., 2017; Chapter 4). Field observations indicate that the early structural history of the Kdz is dominated by brittle processes, characterized by the formation of variably developed breccia domains. Ductile shear at greenschist facies conditions followed, localized along the breccia domains of the fault zone. Subsequent renewed brittle deformation resulted in the formation of abundant small-scale faults and shear veins within the Kdz and adjacent domains. The details of this structural evolution are discussed below in the order in which they formed. This structural evolution is further compared to other well-studied deformation zones along the LLCdz in order to place the deformation history into a regional context.

5.10.1 Early fault behavior and breccia-forming processes

The breccia domains along the Kdz (Figs. 5.10 and 5.12) are overprinted by all other phases of deformation, alteration, metamorphism, and mineralization, and therefore are the

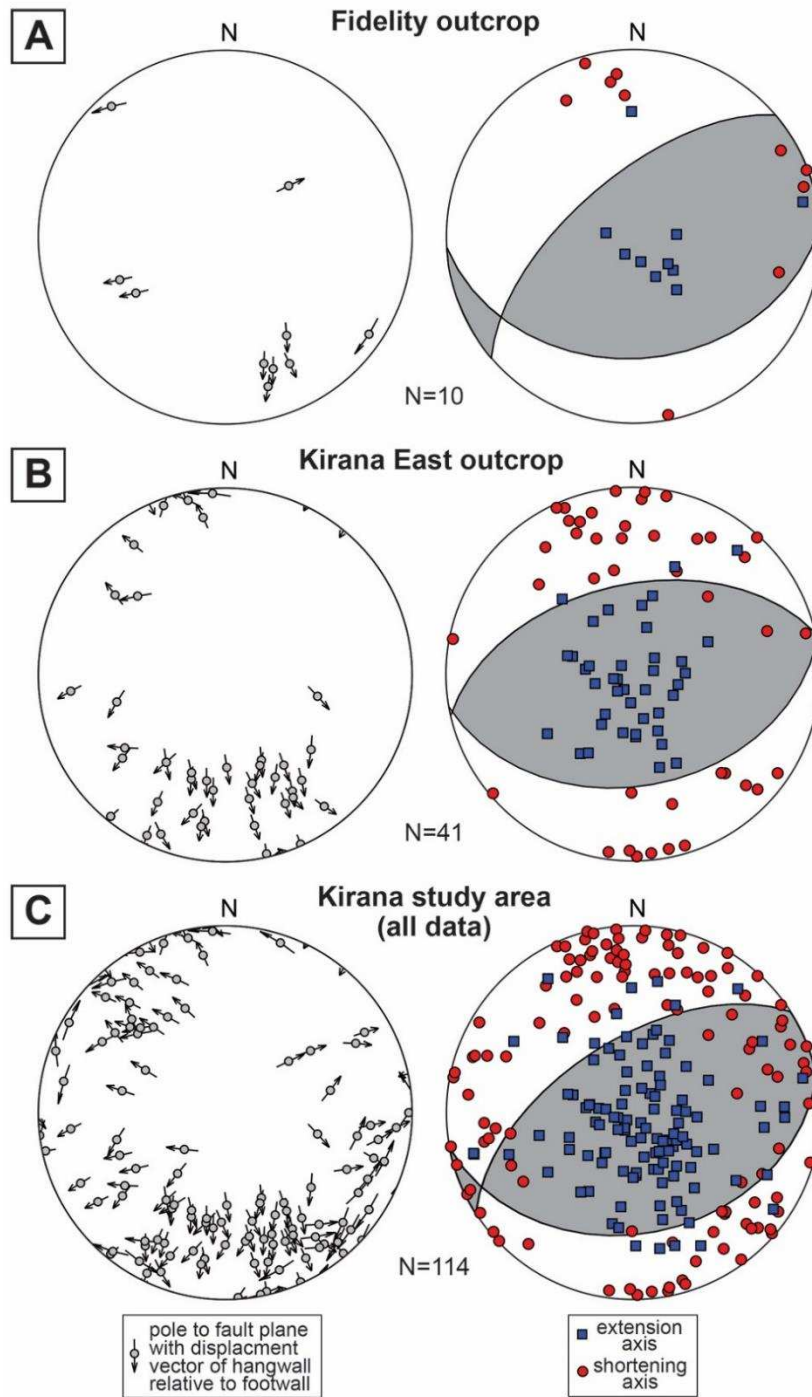


Figure 5.18 – Orientation data and kinematic analysis of small-scale faults and shear veins. Results from the Fidelity (A) and Kirana East (B) outcrops (Fig. 5.4), and the entire Kirana deformation zone study area (C). Pole-tangent slip diagrams (left column) display the displacement sense of the hanging wall with respect to the footwall projected onto the pole to the fault plane. Plots of the instantaneous extension and shortening axes and resultant 'beachball' solution diagrams (right column) calculated from the populations of instantaneous extension (blue squares) and shortening (red circles) axes shown by eigenvector analysis. Grey corresponds to zones of extension and white to zones of shortening.

earliest structures. Breccia clasts consist solely of altered and metamorphosed rhyolitic wall rock, indicating that no significant transport occurred along the fault. Breccia is abundant along the Kdz, but best exposed at the Kirana East outcrop in both fault core and damage zone (Figs. 5.10 and 5.12). PSD analysis of breccia from the fault core and damage zone yielded fractal dimensions (D-values) of 0.93-1.71 (Fig. 5.17). The lowest values (0.93-1.28) correspond to samples where the primary fracture networks were identified (i.e., crackle domains) in the damage zone to the Kdz (Fig. 5.12). These D-values are relatively low when compared to comminution products (1.6-1.7; Storti et al., 2003; Keulen et al., 2007), but are similar to D-values from dynamic off-fault breccia formed in zones of dilation along faults (1-1.5; Blenkinsop, 1991; Jébrak, 1997; Melosh et al., 2014). Thus the field observations and PSD analysis support the interpretation that the primary fracture networks reflect a fluid-assisted, dilational mechanism of brecciation (Fig. 5.2A; Sibson, 1985; 1986; Pavlis et al., 1993). In contrast, higher observed D-values (1.46-1.71) largely correspond to more evolved, chaotic breccia textures from the fault core of the Kdz (Figs. 5.6, 5.10D, and 5.12). The chaotic breccia domains display no geometric fit between the clasts and contain abundant subangular to subrounded clasts, suggesting they record greater proportions of particle wear abrasion as indicated by the generally higher D-values.

In comparison, a similar evolution of D-values documented between damage zone and fault core material has been reported from the strike-slip, Mattinata Fault zone of southern Italy (Billi, 2005). There, breccia from the damage zone yielded D-values of ~ 1.0 , while more evolved breccia in the fault core yielded values of ~ 2.0 (Billi, 2005). The transition of ~ 1.0 to ~ 2.0 was interpreted as progressive incorporation of the damage zone material by surface abrasion processes in the fault core during progressive fault displacement (Billi, 2005). It is possible that our samples have recorded a similar evolution. Initial fragmentation in the wall rock may have resulted from a fluid-assisted, dilational breccia, while material was progressively added to the fault core by further abrasion (Fig. 5.19).

Two of the samples (KL-OP-1 and KL5-2) display two distinct log-linear segments in their PSDs (Fig. 5.17). Sample KL-OP-1 is a crackle breccia from the damage zone, while sample KL-5-2 is a chaotic breccia from the fault core (Fig. 5.17). In both samples, a smaller grain size fraction (~ 0.7 -3 mm) corresponds to lower D-values (1.15 and 1.28), while a coarser grain size (~ 3 -8 mm) corresponds to higher D-values (1.60 and 1.71; Fig. 5.17). These trends are similar to those reported by Keulen et al. (2007) who attributed multiple D-values in a given sample to a grinding limit, where grain size reduction by attrition processes becomes more difficult below a certain grain size. This suggests that there is a grain size threshold (~ 3 mm in

samples) above which it is relatively easy for clasts to become smaller and below which it is harder to further reduce the grain size. Sample KL-OP-1 is a crackle breccia that retains the primary fracture network, with no indication for attrition, and a grinding limit does not apply. In general, fractures in the damage zone are <5 mm in width (e.g., Fig. 5.6), limiting the maximum size of grains that could have been mobilized by fluid-assisted processes within those fractures. Therefore, in sample KL-OP-1, the lower D-value in the smaller grain size fraction in our samples may reflect more similarly sized clasts in the fracture networks, while the higher D-values reflect a larger proportion of small versus large clasts within the fractured wall rock. The fact that two D-values are documented in both crackle (KL-OP-1) and chaotic breccia samples (KL-5-2), suggests that this bimodal fractal distribution may have been preserved through progressive breccia evolution. However, given sufficient attrition, it is likely that the PSD would homogenize to a single D-value (Fig. 5.19).

Based on outcrop- to micro-scale observations and the results of the PSD analysis, we interpret that early brecciation resulted from a dilational, fluid-assisted process associated with fault slip. The breccia textures we observed are similar to dilational, 'implosion'-style breccia that form at fault step-overs (e.g., Sibson, 1985; 1986; Pavlis et al., 1993), suggesting that the initial Kdz involved a dilational jog or asperity. This process resulted in the emplacement of quartz-rich matrix material, reflecting significant coseismic fluid flow. The dilational brecciation resulted in grain-size reduction through breccia-forming processes that likely mechanically weakened the Kdz.

The quartz-rich matrix networks observed in breccia domains of the Kdz are interpreted to reflect the emplacement of silica-rich fluids during early brecciation. These matrix networks contain mineralogical and textural heterogeneity that includes micrometer-scale chlorite, rutile, and vugs. Enigmatically, the matrix networks display banding, zoning, or other precipitation and crystallization textures, which are typically of hydrothermally precipitated quartz (Hodgson, 1989; see section 5.3). Precipitation and/or crystallization textures may be difficult to observe due to the high vug density that makes the matrix material optically opaque. The significance of the vugs is enigmatic. They may have formed by a secondary process such as volume reduction due to a phase transition from opal-A to alpha quartz (Herdianita et al., 2000; Lynne et al., 2005). However, this interpretation is speculative and further investigation is required to firmly establish their significance.

5.10.2 Early fault veins and intrusion of porphyritic rocks

At the Fidelity outcrop area an early generation of fault veins was observed. These display composite structures and banding textures interpreted to represent multiple reactivation

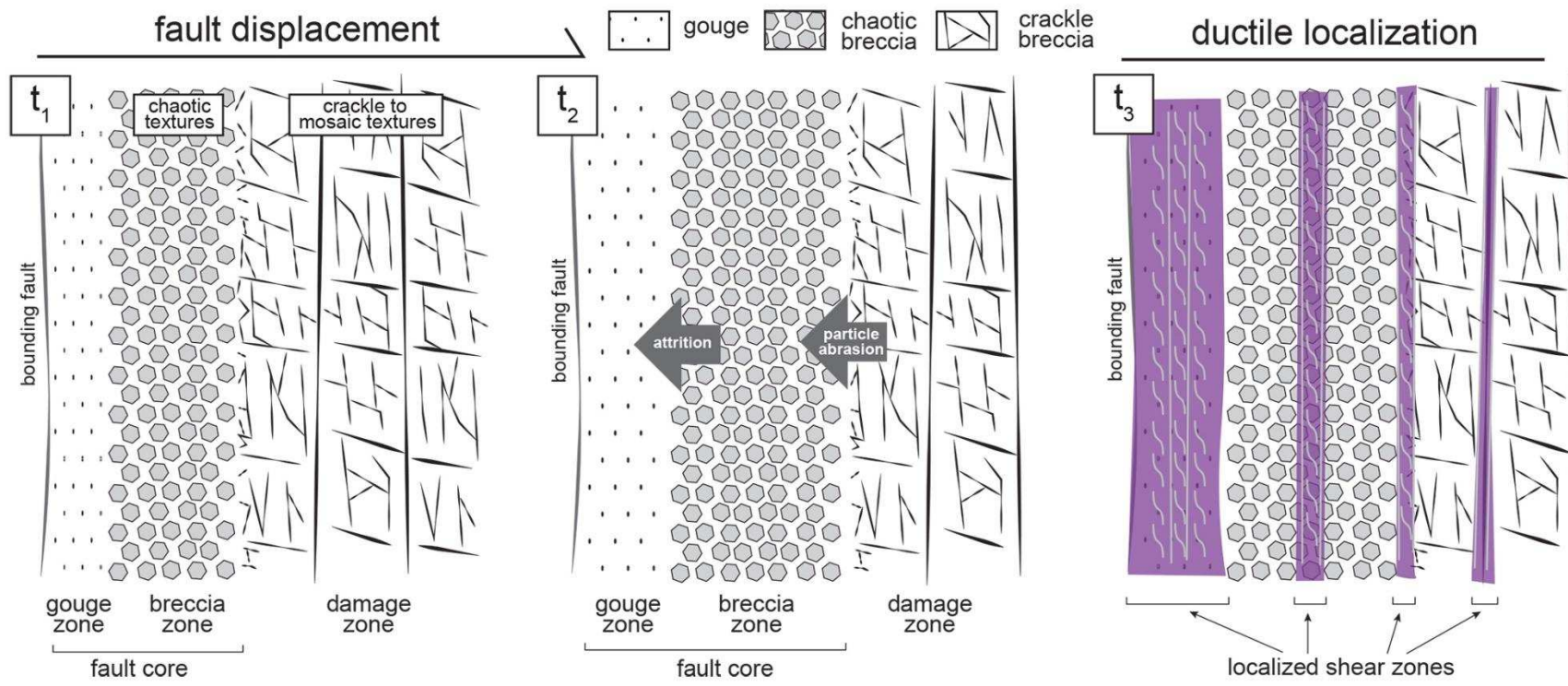


Figure 5.19 – Schematic illustration of the relationship between the observed breccia textures and the fault core and associated damage zone of the Kirana deformation zone during progressive displacement through time (t_1 to t_2) and subsequent ductile localization (t_3). Growth of the fault core is schematically shown by addition of material to the breccia zone and gouge zone through particle abrasion and attrition processes, respectively (after Billi, 2005). Ductile localization is schematically shown to preferentially develop within favorable zones of the fault core and damage zone.

events. These veins are steeply dipping, strike to the SW, and are strongly overprinted by D_3 shear zones (Fig. 5.11A). The temporal relationship of these veins to early dilational breccia is unknown, since early veins with similar orientations and textural characteristics are not preserved at the Kirana East outcrop. However, since both are overprinted by ductile shear zones, it is likely that early vein emplacement at the Fidelity outcrop was broadly coeval with early brecciation observed at the Kirana East outcrop.

Porphyritic intrusive rocks along the Kdz display no evidence for brecciation, crosscut the fault core of the Kdz, and are overprinted by ductile shear zones (Figs. 5.9B, 5.12, and 5.13B). Thus, they were likely emplaced after initial brecciation, but prior to ductile shear. The age of these intrusions are unconstrained along the Kdz. Directly to the south on the northern shore of Gami Lake (Fig. 5.4), compositionally and texturally similar intrusions crosscut the Timiskaming assemblage. This suggests that the intrusive rocks along the Kdz are post-Timiskaming in age (i.e., <2679-2669 Ma). Towards the west, the Winnie Lake stock (Fig. 5.2) yielded an ID-TIMS U-Pb zircon crystallization age of 2677 ± 3 Ma (Corfu, 1993). Similarly, porphyritic syenite intrusions of the Murdoch Creek and Lebel stocks (Fig. 5.2) that occur to the south of the LLCdz and are foliated by S_3 yielded ID-TIMS U-Pb zircon crystallization ages of 2672 ± 2 Ma and 2673 ± 2 Ma, respectively (Wilkinson et al., 1999). Based on similar compositions, crosscutting relationships, overprinting fabrics, it is inferred that the porphyritic intrusions along the Kdz are ~2675-2665 Ma in age, and that early fault processes are older and ductile shear was younger.

5.10.3 Ductile shear

After initial dilational brecciation, early fault vein development, and the emplacement of porphyritic intrusive rocks, deformation along the Kdz was characterized by widespread ductile shear related to D_3 deformation (Frieman et al., 2017; Chapter 4). The foliation in the shear zones (S_3) is predominately steeply-NNW-dipping and contains a moderately- to steeply-ENE-plunging lineation, and dextral shear sense indicators on horizontal erosional surfaces and in oriented thin-sections (Figs. 5.8 and 5.9C, D). Based on these fabric relationships the shear zones are interpreted to have formed as a result of NW-SE shortening that resulted in localized dextral transpressive strain with a steeply inclined extensional direction (Frieman et al., 2017; Chapter 4).

At the Fidelity outcrop, shear zones are >15 m wide (Fig. 5.9A), while towards the east, shear zones are <5 m wide (Figs. 5.9C and 5.12). Ductile fabrics commonly occur in chlorite-rich domains, indicating that greenschist facies metamorphism accompanied ductile shear. Alteration assemblages such as carbonate or sericite also occur along the same foliation planes

(Fig. 5.9) suggesting that either deformation occurred in the presence carbonic or potassic fluids, or that these assemblages formed during later alteration by retrograde processes. Albite rims on aligned chlorite grains (Fig. 5.15) and in dynamically recrystallized matrix material in the mylonitic samples (Fig. 5.16A, B), which supports the interpretation that infiltration of sodic fluids was syn-kinematic. A similar history of syn-kinematic alteration by sodic and carbonic fluids has been documented within the LLCdz and Main Break to the south (Kerrich and Watson, 1984; Wilkinson et al., 1999; Ispolatov et al., 2008; Poulsen, 2017). Furthermore, at the Cheminis deposit, to the NE of Larder Lake (Fig. 5.2), alteration assemblages include chlorite, sericite, carbonate, and albite regardless of host rock composition (Lafrance, 2015). This suggest that hydrothermal fluids with similar carbonic/sodic compositions were migrating along the LLCdz and secondary structures elsewhere in the region.

D₃ deformation along the Kdz is interpreted to have been coeval with brittle-ductile localization in the LLCdz and other higher-order structures such as the Main Break (Wilkinson et al., 1999; Ispolatov et al., 2008; Frieman et al., 2017; Chapter 4). The maximum age of D₃ deformation is ~2675-2665 Ma, which is the crystallization age of porphyritic intrusions that are faulted and foliated by D₃ structures (Corfu, 1993; Wilkinson et al., 1999). Furthermore, S₃ fabric forming titanite from the Murdock Creek stock along the LLCdz yielded a 2665 ± 4 Ma U-Pb ID-TIMS age (Fig. 5.2), which we interpret as the timing of D₃ ductile localization along the Kdz.

5.10.4 Renewed brittle deformation

After a period of ductile shear at greenschist facies conditions, renewed brittle deformation occurred along the Kdz. This phase of deformation is represented by the widespread formation of small-scale faults and quartz-carbonate shear veins (Figs. 5.9B-D, 5.12, and 5.18) within a 100-200 m wide corridor along the Kdz (Figs. 5.9D and 5.18; Section 5.9). Mutually crosscutting vein sets (Fig. 5.12 and 5.14) indicate cyclic formation. Chlorite along vein margins and disseminated carbonate and albite alteration halos (Fig. 5.15B) indicate that renewed brittle deformation occurred at greenschist facies conditions and that carbonic and sodic fluids were present.

Kinematic analysis of these small-scale faults and shear veins indicate NW-SE to NNW-SSE shortening (Fig. 5.18). M-plane analysis of these structures yielded variably oriented, shallow to subhorizontal shortening axes and consistently subvertical to steeply inclined extensional axes (Fig. 5.18), generally consistent with those for the preceding ductile strain.

The reason for the transition of ductile to brittle deformation is unclear. Ductile transpression may have resulted in extrusion of rocks along the Kdz to a shallower depth. However, greenschist facies assemblages associated with both the ductile shear zones and

later small-scale faults and veins suggest they both formed at or near the brittle-ductile transition. Alternatively, an influx of fluids and/or build-up of pressure in interconnected fluid reservoirs, may have caused the change from ductile to brittle behavior (cf. Sibson et al., 1988; Robert and Poulsen, 2001). Because composite fault veins sets are strongly overprinted by D_3 shear zones at the Fidelity outcrop area (Fig. 5.9A) and subsequent the late veins related to the renewed phase of brittle deformation (Fig. 5.9B-C), fault-valve behavior may have been intermittent, occurring both prior to and after ductile shear along the Kdz.

5.10.5 Timing of gold mineralization

Gold mineralization is documented within the fault core of the Kdz at the Fidelity outcrop area (Burrows and Hopkins, 1916) and at the Kirana East outcrop area (this study). Native gold occurs in association with (e.g. in strain shadows of) pyrite and sphalerite (Fig. 5.16) that are aligned with S_3 fabrics and rimmed by or weakly wrapped by fabric-forming chlorite (Fig. 5.16C, D). Therefore, gold mineralization occurred syn- to post- D_3 deformation within the Kdz. This is consistent with the timing of mineralization in Main Break to the south, where mineralized D_3 fault veins and breccia are foliated by S_3 shear fabrics (Ispolatov et al., 2008), and other structurally controlled deposits along the LLCdz, such as at Kerr Addison in Ontario (Hodgson et al., 1991; Smith et al., 1993) and the Malarctic (DeSouza et al., 2017) and Val D'Or (Robert et al., 1995) districts in Quebec (Fig. 5.2). In contrast, gold mineralization in other deposits hosted within the LLCdz or immediate splays in Ontario, such as the Upper Canada, Ankoï, McBean, and Cheminis deposits, is interpreted to have been coeval with D_2 deformation (Ispolatov et al., 2008; Lafrance, 2015). This suggests that the upflow of gold-bearing hydrothermal fluids occurred during and after both D_2 and D_3 deformation along different segments of the LLCdz.

5.11 Implications

Early brittle processes along the Kdz resulted in dilational breccia networks in its damage zone. These likely formed during fault slip at the location of dilational zones such as at fault step-overs or asperities along the Kdz (e.g., Sibson, 1985; 1986). The dilational fracture networks are filled with a quartz-rich material, probably as a result of coseismically emplaced silica-rich fluids, which makes them favorable sites for economic mineralization (Sibson, 1987; Micklethwaite and Cox, 2004; Weatherley and Henley, 2013). However, no mineralization is documented in association with the dilational breccia zones. This may be because the fault-related fluids did not contain significant gold, and/or because of the rapid sealing of the primary fracture networks by the silica-rich fluids, limiting the post-seismic infiltration of later mineralizing fluids (Cox et al., 2001). Furthermore, if the fault-related fluids were not sourced from deep fluid

reservoirs and/or contained a large meteoric water component they would have been unlikely to contain significant gold.

Early fault-related breccia processes created favorable sites for subsequent ductile shear due to grain size reduction and creation of rheological heterogeneity. Ductile shear at greenschist facies conditions likely resulted in further weakening of the fault zone by additional grain size reduction through dynamic recrystallization and other strain softening processes (e.g., Wilkinson et al., 1999). This behavior likely helped to maintain the Kdz as an active fluid conduit and eventually resulted in syn- to post-ductile shear gold mineralization. Ductile shear zones are overprinted by abundant quartz-carbonate shear veins that are interpreted to have resulted from fault-valve behavior, suggesting that the Kdz continued to accommodate significant fluid flow. Thus, a mixture of progressive brittle-ductile processes contributed to long-lived fluid localization along the Kdz, making it a favorable structure for economic gold mineralization.

In summary, the Kdz records a mixed history of brittle-ductile deformation that provides insight into the structural development of gold-bearing splays of crustal-scale fault zones. Based on comparisons to the regional structural framework, deformation and gold mineralization within the Kdz was broadly coeval with mineralization in the Main Break to the south and in other deposits along the LLCdz to the east. While no mineralization is associated with the early dilational breccia zones, they formed a zone of weakness localizing subsequent strain and fluid flow that facilitated gold mineralization. Mineralization is documented within a relatively narrow zone within the fault core of the Kdz. However, breccia domains occur in much broader zones. These may provide an indicator towards the core of gold-bearing structures, especially if they display a later history of ductile shear, fluid infiltration, and/or fault valve behavior.

5.12 References

- Allegre, C., Le Mouel, J., Provost, A., 1982. Scaling rules in rock fracture and possible implications for earthquake prediction. *Nature* 297, 47–49.
- Angelier, J., 1979. Determination of the mean principal directions of stresses for a given fault population. *Tectonophysics* 56, T17–T26.
- Ayer, J., Amelin, Y., Corfu, F., Kamo, S., Ketchum, J., Kwok, K., Trowell, N., 2002. Evolution of the southern Abitibi greenstone belt based on U-Pb geochronology: Autochthonous volcanic construction followed by plutonism, regional deformation and sedimentation. *Precambrian Research* 115, 63–95. doi:10.1016/S0301-9268(02)00006-2
- Ayer, J.A., Thurston, P.C., Bateman, R., Dubé, B., Gibson, H.L., Hamilton, M.A., Hathway, B., Hocker, S.M., Houlié, M.G., Hudak, G., Ispolatov, V.O., Lafrance, B., Leshner, C.M., MacDonald, P.J., Pélouquin, A.S., Piercey, S.J., Reed, L.E., Thomson, P.H., 2005. Overview of results from the greenstone architecture project: Discover Abitibi Initiative. Open File Report 6154, 146 p.

- Bateman, R., Bierlein, F.P., 2007. On Kalgoorlie (Australia), Timmins–Porcupine (Canada), and factors in intense gold mineralisation. *Ore Geology Reviews* 32, 187–206.
- Bedeaux, P., Pilote, P., Daigneault, R., Rafini, S., 2017. Synthesis of the structural evolution and associated gold mineralization of the Cadillac fault, Abitibi, Canada. *Ore Geology Reviews* 82, 49–69.
- Biegel, R.L., Sammis, C.G., Dieterich, J.H., 1989. The frictional properties of a simulated gouge having a fractal particle distribution. *Journal of Structural Geology* 11, 827–846.
- Billi, A., 2005. Grain size distribution and thickness of breccia and gouge zones from thin (<1m) strike-slip fault cores in limestone. *Journal of Structural Geology* 27, 1823–1837.
- Billi, A., Storti, F., 2004. Fractal distribution of particle size in carbonate cataclastic rocks from the core of a regional strike-slip fault zone. *Tectonophysics* 384, 115–128.
- Billi, A., Salvini, F., Storti, F., 2003. The damage zone-fault core transition in carbonate rocks: implications for fault growth, structure and permeability. *Journal of Structural Geology* 25, 1779–1794.
- Blenkinsop, T., 1991. Cataclasis and processes of particle size reduction. *Pure and Applied Geophysics* 136, 59–86.
- Blenkinsop, T., Fernandes, T., 2000. Fractal characterization of particle size distributions in chromitites from the Great Dyke, Zimbabwe. *Pure and Applied Geophysics* 157, 505–522.
- Burrows, A.G., Hopkins, P.E., 1916. Goodfish Lake gold area. Ontario Department of Mines Bulletin 29, 21–24.
- Charlewood, G.H., 1964. Geology of deep developments on the main ore zone at Kirkland Lake. Ontario Department of Mines Geological Circular 11, 49 p.
- Clark, C., Mumm, A.S., Collins, A.S., 2006. A coupled micro-and macrostructural approach to the analysis of fluid induced brecciation, Curnamona Province, South Australia. *Journal of Structural Geology* 28, 745–761.
- Colvine, A.C., Fyon, J.A., Heather, K.B., Marmont, S., Smith, P.M., Troop, D.G., 1988. Archean Lode Gold Deposits in Ontario. Ontario Geological Survey Miscellaneous Paper 139, 136 p.
- Corfu, F., 1993. The evolution of the southern Abitibi greenstone belt in light of precise U-Pb geochronology. *Economic Geology* 88, 1323–1340.
- Corfu, F., Jackson, S.J., Sutcliffe, R.H., 1991. U-Pb ages and tectonic significance of Late Archean alkalic magmatism and nonmarine sedimentation, Timiskaming Group, southern Abitibi belt, Ontario. *Canadian Journal of Earth Sciences* 28, 489–503.
- Cox, S.F., Knackstedt, M.A., Braun, J., 2001. Principles of structural control on permeability and fluid flow in hydrothermal systems. *Reviews in Economic Geology* 14, 1–27.
- De Souza, S., Dubé, B., McNicoll, V.J., Dupuis, C., Mercier-Langevin, P., Creaser, R.A., Kjarsgaard, I.M., 2017. Geology and hydrothermal alteration of the world-class Canadian

- Malartic gold deposit: Genesis of an Archean stockwork-disseminated gold deposit in the Abitibi greenstone belt. *Reviews in Economic Geology* 19, 263–291.
- Dimroth, E., Imreh, L., Rocheleau, M., Goulet, N., 1982. Evolution of the south-central part of the Archean Abitibi belt, Quebec. Part I: Stratigraphy and paleogeographic model. *Canadian Journal of Earth Sciences*, 19, 1729–1758.
- Dimroth, E., Imreh, L., Goulet, N., Rocheleau, M., 1983, Evolution of the south-central segment of the Archean Abitibi Belt, Quebec. Part II: Tectonic evolution and geomechanical model. *Canadian Journal of Earth Sciences* 20, 1355–1373.
- Engelder, T., 1974. Cataclasis and the generation of fault gouge. *Bulletin of the Geological Society of America* 85, 1515-1522.
- Frieman, B.M., Kuiper, Y.D., Monecke, T., Kelly, N.M., 2017. Precambrian geology and new structural data, Kirkland Lake area, Ontario. Geological Survey of Canada Open File 8245, 8 p.
- Goldfarb, R.J., Groves, D.I., Gardoll, S., 2001. Orogenic gold and geologic time: A global synthesis. *Ore Geology Reviews* 19, 1–75.
- Goldfarb, R.J., Hart, C.J.R., Marsh, E.E., 2008. Orogenic gold and the evolution of the Cordilleran orogeny. *Arizona Geological Society Digest* 22, 311–323.
- Groves, D.I., Goldfarb, R.J., Gebre-Mariam, M., Hagemann, S.G., Robert, F., 1998. Orogenic gold deposits: A proposed classification in the context of their crustal distribution and relationship to other gold deposit types. *Ore Geology Reviews* 13, 7–27.
- Harris, R.A., Archuleta, R.J., Day, S.M., 1991. Fault steps and the dynamic rupture process: 2-D numerical simulations of a spontaneously propagating shear fracture. *Geophysical Research Letters* 18, 893–896.
- Hattori, I., Yamamoto, H., 1999. Rock fragmentation and particle size in crushed zones by faulting. *Journal of Geology* 107, 209–222.
- Hattori, K., Hodgson, C.J., 1990. Gold-related geology in the Kirkland Lake and Timmins camps, Ontario. *International Association on the Genesis of Ore Deposits Symposium*, 8th, Ottawa, Canada, Field Trip Guidebook 5, 57 p.
- Herdianita, N.R., Browne, P.R.L., Rodgers, K.A., Campbell, K.A., 2000. Mineralogical and textural changes accompanying ageing of silica sinter. *Mineralium Deposita* 35, 48–62.
- Hodgson, C.J., 1989. The structure of shear-related, vein-type gold deposits: A review. *Ore Geology Reviews* 4, 231–273.
- Hodgson, C.J., Hamilton, J.V., Guimond, R.P. 1991. Relationship between gold deposits and the tectonic framework of the Abitibi Greenstone Belt in the Kirkland Lake – Larder Lake area. Ontario Geological Survey Open File Report 5782, 60 p.
- Hyde, R.S., 1980. Sedimentary facies in the Archean Timiskaming Group and their tectonic implications, Abitibi greenstone belt, northeastern Ontario, Canada. *Precambrian Research* 12, 161–195.

- Ispolatov, V.O., Lafrance, B., Dubé, B., Hamilton, M., Creaser, R., 2005. Geology, Structure, and Gold Mineralization, Kirkland Lake and Larder Lake Areas: Discover Abitibi Initiative. Ontario Geological Survey Open File Report 6159, 170 p.
- Ispolatov, V., Lafrance, B., Dubé, B., Creaser, R., Hamilton, M., 2008. Geologic and structural setting of gold mineralization in the Kirkland Lake-Larder Lake gold belt, Ontario. *Economic Geology* 103, 1309–1340.
- Jackson, S.L., Cruden, A.R., White, D., Milkereit, B., 1995. A seismic-reflection-based regional cross section of the southern Abitibi greenstone belt. *Canadian Journal of Earth Sciences* 32, 135–148.
- Jébrak, M., 1997. Hydrothermal breccias in vein-type ore deposits: a review of mechanisms, morphology and size distribution. *Ore Geology Reviews* 12, 111–134.
- Kerrich, R., Watson, G.P., 1984. The Macassa mine Archean lode gold deposit, Kirkland Lake, Ontario: Geology, patterns of alteration, and hydrothermal regimes. *Economic Geology* 79, 1104–1130.
- Keulen, N., Heilbronner, R., Stünitz, H., Boullier, A.-M., Ito, H., 2007. Grain size distributions of fault rocks: A comparison between experimentally and naturally deformed granitoids. *Journal of Structural Geology* 29, 1282–1300.
- Lafrance, B., 2015. Geology of the orogenic Cheminis gold deposit along the Larder Lake-Cadillac deformation zone, Ontario. *Canadian Journal of Earth Sciences* 52, 1093–1108.
- Luther, A., Axen, G., Selverstone, J., 2013. Particle-size distributions of low-angle normal fault breccias: Implications for slip mechanisms on weak faults. *Journal of Structural Geology* 55, 50–61.
- Lynne, B.Y., Campbell, K.A., Moore, J.N., Browne, P.R.L., 2005. Diagenesis of 1900-year-old siliceous sinter (opal-A to quartz) at Opal Mound, Roosevelt Hot Springs, Utah, U.S.A. *Sedimentary Geology* 179, 249–278.
- MacKenzie, D., Farmer, L., Moore, J., Craw, D., 2017. Contrasting coeval paragenesis of gold and scheelite in an orogenic hydrothermal system, Macraes mine, New Zealand., *Ore Geology Reviews* 80, 645–657.
- MacLean, A., 1944. Township of Lebel, District of Timiskaming, Ontario. Ontario Department of Mines, Map 53a, scale 1:12 000.
- Mandelbrot, B.B., 1982. *The Fractal Geometry of Nature*. Freeman and Co., New York.
- Marone, C., Scholz, C., 1989. Particle-size distribution and microstructures within simulated fault gouge. *Journal of Structural Geology* 11, 799–814.
- Marrett, R., Allmendinger, R.W., 1990. Kinematic analysis of fault-slip data. *Journal of Structural Geology* 12, 973–986.
- Marshak, S., Mitra, G., 1988. *Basic methods of structural geology*. Prentice Hall, 446 p.

- Melosh, B.L., Rowe, C.D., Smit, L., Groenewald, C., Lambert, C.W., Macey, P., 2014 Snap, Crackle, Pop: Dilational fault breccias record seismic slip below the brittle–ductile transition. *Earth and Planetary Science Letters* 403, 432–445.
- Micklethwaite, S., 2009. Mechanisms of faulting and permeability enhancement during epithermal mineralisation: Cracow goldfield, Australia. *Journal of Structural Geology* 31, 288–300.
- Micklethwaite, S., Cox, S.F., 2004. Fault-segment rupture, aftershock-zone fluid flow, and mineralization. *Geology* 32, 813–816. doi:10.1130/G20559.1
- Monecke, T., Mercier-Langevin, P., Dubé, B., Frieman, B.M., 2017. Geology of the Abitibi greenstone belt. *Reviews in Economic Geology* 19, 7–49.
- Mueller, W., Donaldson, J.A., Doucet, P., 1994. Volcanism and tectonoplutonic influences on sedimentation in the Archean Kirkland Lake basin, Abitibi greenstone belt, Canada. *Precambrian Research* 68, 201–230.
- Passchier, C.W., Trouw, R.A.J., 2005. *Microtectonics*, second ed. Springer Verlag, Berlin.
- Pavlis, T.L., Serpa, L.F., Keener, C., 1993. Role of seismogenic processes in fault-rock development—an example from Death Valley, California. *Geology* 21, 267–270.
- Phillips, G.N., Powell, R., 2010. Formation of gold deposits: A metamorphic devolatilization model. *Journal of Metamorphic Geology* 28, 689–718.
- Poulsen, K.H., 2017. The Larder Lake-Cadillac Break and its gold districts. *Reviews in Economic Geology* 19, 133–167.
- Robert, F., 1989. Internal structure of the Cadillac tectonic zone southeast of Val d'Or, Abitibi greenstone belt, Quebec. *Canadian Journal of Earth Sciences* 26, 2661–2675.
- Robert, F., 1994. Vein fields in gold districts: The example of Val d'Or, southeastern Abitibi subprovince, Quebec. *Geological Survey of Canada Current Research 1994-C*, 295–302.
- Robert, F., Poulsen, K.H., 2001. Vein formation and deformation in greenstone gold deposits. *Society of Economic Geologists Reviews* 14, 111–155.
- Robert, F., Boullier, A.M., Firdaous, K., 1995. Gold–quartz veins in metamorphic terranes and their bearing on the role of fluids in faulting. *Journal of Geophysical Research* 100, 12861–12881.
- Robert, F., Poulsen, K.H., Cassidy, K.F., Hodgson, C.J., 2005. Gold metallogeny of the Superior and Yilgarn cratons. *Economic Geology 100th Anniversary Volume*, 1001–1033.
- Robin, P.Y.F., Cruden, A.R., 1994. Strain and vorticity patterns in ideally ductile transpression zones. *Journal of Structural Geology* 16, 447–466.
- Rupert, R.J., Lovell, H.L., 1970. Bernhardt and Morrisette Townships, Timiskaming District, Ontario. *Ontario Geological Survey, 2000 Series Map M.2193*, scale 1:31 680.
- Sammis, C., King, G., Biegel, R., 1987. The kinematics of gouge deformation. *Pure and Applied Geophysics* 125, 777–812.

- Schneider, C.A., Rasband, W.S., Eliceiri, K.W., 2012. NIH image to ImageJ: 25 years of image analysis. *Nature Methods* 9, 671–674.
- Sibson, R., 1985. Stopping of earthquake ruptures at dilational fault jogs. *Nature* 316, 248–251.
- Sibson, R., 1986. Brecciation processes in fault zones: inferences from earthquake rupturing. *Pure and Applied Geophysics* 124, 159–175.
- Sibson, R.H., 1987. Earthquake rupturing as a mineralizing agent in hydrothermal systems. *Geology* 15, 701–704.
- Sibson, R.H., Robert, F., Poulsen, K.H., 1988. High-angle reverse faults, fluid pressure cycling, and mesothermal gold deposits. *Geology* 16, 551–555.
- Simmons, S.F., White, N.C., John, D.A., 2005. Geological characteristics of epithermal precious and base metal deposits. *Economic Geology 100th Anniversary Volume*, 485–522.
- Smith, J.P., Spooner, E.T.C., Broughton, D.W., Ploeger, F.R. 1993. Archean Au-Ag-(W) quartz vein/disseminated mineralisation within the Larder Lake – Cadillac Break, Kerr Addison – Chesterville system, North East Ontario, Canada. Ontario Geological Survey Open File Report 5831, 309 p.
- Still, A.C., 2001. Structural setting and controls of gold mineralization at the Macassa mine, Kirkland Lake, Ontario. Unpublished M.Sc. thesis, Kingston, ON, Queen’s University, 151 p.
- Storti, F., Billi, A., Salvini, F., 2003. Particle size distributions in natural carbonate fault rocks: insights for non-self-similar cataclasis. *Earth and Planetary Science Letters* 206, 173–186.
- Thomson, J.E., 1945. Township of Teck, district of Timiskaming, Ontario. Ontario Department of Mines, Map No. 1945-1, scale 1:12,000.
- Thomson, J.E., 1946. The Keewatin-Timiskaming unconformity in the Kirkland Lake district. *Transactions of the Royal Society of Canada* IV, 113–124.
- Thomson, J.E., 1948. Regional structure of the Kirkland Lake-Larder Lake area. *Structural Geology of Canadian Ore Deposits, A Symposium arranged by a Committee of the Geology Division, Canadian Institute of Mining and Metallurgy*, 627–632.
- Thomson, J.E., Charlewood, G.H., Griffin, K., Hawley, J.E., Hopkins, H., MacIntosh, C.G., Ogryzlo, S.P., Perry, O.S., Ward, W., 1950. Geology of the main ore zone at Kirkland Lake. Ontario Department of Mines Annual Report 57, 54–188.
- Thurston, P.C., Ayer, J.A., Goutier, J., Hamilton, M.A., 2008. Depositional gaps in Abitibi greenstone belt stratigraphy: A key to exploration for syngenetic mineralization. *Economic Geology* 103, 1097–1134.
- Todd, E.W., 1928. Kirkland Lake gold area (a detailed study of the Central zone and vicinity). Ontario Department of Mines Annual Report 37, 1–176.
- Turcotte, D.L., 1986. Fractals and fragmentation. *Journal of Geophysical Research* 91, 1921–1926.

- Twiss, R.J., 1990. Curved slickenfibers; a new brittle shear sense indicator with application to a sheared serpentinite. *Journal of Structural Geology* 11, 471–481.
- Twiss, R.J., Unruh, J.R., 1998. Analysis of fault slip inversions: do they constrain stress or strain rate? *Journal of Geophysical Research* 103, 12205–12222.
- Twiss, R.J., Moores, E.M., 2007. *Structural geology*, 2nd edition. W.H. Freeman, New York, 736 p.
- Vollmer, F.W., 2015. Orient 3.0.1: Spherical projection and orientation data analysis software. www.frederickvollmer.com.
- Watson, G.P., 1984. Ore types and fluid regimes: Macassa gold mine, Kirkland Lake. Unpublished Ph.D. thesis, London, ON, University of Western Ontario, 341 p.
- Weatherley, D.K., Henley, R.W., 2013. Flash vaporization during earthquakes evidenced by gold deposits. *Nature Geoscience* 6, 294–298.
- Wilkinson, L., Cruden, A.R., Krogh, T.E., 1999. Timing and kinematics of post-Timiskaming deformation within the Larder Lake-Cadillac deformation zone, southwest Abitibi greenstone belt, Ontario, Canada. *Canadian Journal of Earth Sciences* 36, 627–647.

CHAPTER 6

GENERAL CONCLUSIONS

This thesis provides insight into Archean geodynamics and crustal growth processes, the amalgamation history of the southern Superior Province, and the across-strike architecture and deformation history of gold-bearing, crustal-scale fault systems in the Neoproterozoic south-central Abitibi subprovince. Conclusions from each of the chapters in this thesis are summarized below.

6.1 Investigations into the U-Pb LA-ICP-MS age patterns of detrital zircon grains from graywacke of successor basins (Chapter 2)

Approximately 2100 U-Pb LA-ICP-MS analyses of detrital zircon grains were acquired from graywacke of the syn-orogenic Porcupine assemblage (six samples), Pontiac subprovince (2 samples), and Timiskaming assemblage (eight samples) successor basins. Sedimentary rocks of the Porcupine assemblage were deposited at ~2690-2685 Ma, the Timiskaming assemblage at ~2679-2669 Ma, and Pontiac subprovince basins at ~2685-2682 Ma (Ayer et al., 2002; Davis, 2002). Statistical analysis reveals that all samples are dominated by Neoproterozoic grains (80-95% of the total population), suggesting a predominance of local sources. However, statistical differences in the proportion of Mesoproterozoic grains were observed. Porcupine assemblage samples contain ~5% Mesoproterozoic zircon, while Pontiac subprovince and Timiskaming assemblage samples contain ~18% and ~13% Mesoproterozoic zircon, respectively. Since no Mesoproterozoic rocks are documented in the Abitibi or Pontiac subprovinces, these grains must have been derived from a developing hinterland during regional amalgamation. The higher proportion of Mesoproterozoic zircon in the younger Timiskaming assemblage relative to the older Porcupine assemblage suggests that detritus from the hinterland was more prevalent during the late stages of collision, probably as a result of progressive uplift and denudation of the hinterland. Comparison to ~1500 published U-Pb zircon ages for the southern Superior Province indicates that the hinterland was to the northwest and was, in part, comprised of the Winnipeg River, Marmion, and Opatoca subprovinces. Thus, the detrital zircon age patterns of successor basins from the Abitibi and Pontiac subprovinces record detrital transport across subprovince or terrane boundaries and progressive hinterland emergence. These observations, in conjunction with the progressive southward younging of contractional deformation, successor basin formation, and felsic plutonism in the southern Superior Province, are most consistent with a modern-style collisional or accretionary orogenic model.

6.2 Multi-isotope U-Pb and Lu-Hf LA-ICP-MS analysis of detrital zircon from successor basins of the Abitibi and Pontiac subprovinces (Chapter 3)

In order to gain insight into crustal growth processes and coupled crust-mantle evolution during Meso- to Neoproterozoic construction of the southern Superior Province, Lu-Hf LA-ICP-MS detrital zircon analyses of grains from the successor basin samples were conducted at the locations of the U-Pb within the detrital zircon grains. The resultant data set includes ~1800 paired U-Pb and Lu-Hf isotopic analyses. This data set represents one of the most comprehensive multi-isotope detrital zircon data sets for the region. These results provided constraints on the isotopic character of magmatic source domains and were used to further assess the provenance of the successor basins, providing an indication of the configuration of terranes during regional amalgamations at the time of ~2690-2670 Ma successor basin formation. The majority of the results (~96%) yielded ϵ_{Hf} values of +1 to +10 in the ~3000-2675 Ma age range. These data plot along projections from modern MORB depleted mantle (mMORB-DM; Griffin et al., 2002) compositions into the Archean, suggesting they were derived from a modern-style depleted mantle reservoir. The subordinate results, comprising ~4% of the data set, either yielded CHUR-like or lower ϵ_{Hf} values, or values $>+10$. These results were interpreted to reflect derivation from sources that experienced multi-stage melt histories, reworking after short-lived crustal residence times, and/or mixing with magmas derived from or local melting of older crust.

Comparisons to published U-Pb and Lu-Hf zircon data for the southern Superior Province suggest that likely source regions include the Winnipeg River, Marmion, and Quetico subprovinces, supporting the interpretations made solely from the U-Pb age patterns. Since mMORB-DM-like compositions predominate our results and sources are interpreted to include domains from across a wide region of the southern Superior Province, it is suggested that a modern-style depleted upper mantle reservoir was not only well-established, but prevalent in the mantle below each of these areas during their construction. The development of this reservoir likely occurred by pre-3000 Ma geodynamic processes. The strong mMORB-DM signature is inconsistent with non-tectonic processes, such as mantle overturn and stagnant lid behavior, because they predict that crustal growth by mantle upwelling results in a primitive mantle signature. It is suggested that the U-Pb and Lu-Hf data are most consistent with coupled crust-mantle evolution that strongly resembles those in modern-style plate tectonic environments.

6.3 Across-strike architecture of the Larder Lake-Cadillac deformation zone in the Kirkland Lake area of Ontario (Chapter 4)

The regional, crustal-scale Larder Lake-Cadillac deformation zone (LLCdz) of Ontario and Quebec, Canada, was the site of strain localization during regional amalgamations and

hosts numerous orogenic gold deposits along its length (Monecke et al., 2017). Deposits are hosted directly within the first-order fault, but also occur within higher-order structural networks that can form broad, 2-10 km distributed fault zones (Robert, 1994; Robert et al., 1995). One such example is the world-class 30 Moz deposit hosted in the higher-order Main Break in the Kirkland Lake area of Ontario (Ispolatov et al., 2008). This study revealed that ductile high-strain zones are spaced (every ~500-1000 m) in a >6 km area to the north of the LLCdz. The high-strain zones are characterized by a penetrative east-northeast-trending, subvertical foliation with a moderately- to steeply-northeast-plunging stretching lineation, and dextral shear sense indicators on horizontal erosional surfaces. These fabric relationships are interpreted to reflect a pure shear-dominated (i.e., a low kinematic vorticity number) dextral transpressional strain regime with a steeply inclined extension direction. The high-strain zones are spatially associated with earlier formed fault zones, and form the location for carbonate alteration and gold occurrences. The ductile high-strain zones separate zones of low strain where primary sedimentary and igneous structures are well preserved. The foliation is weakly developed and subparallel to that in the high-strain domains, and alteration is generally weak, except where directly adjacent to the high-strain zones. The low-strain domains show no shear sense indicators and are interpreted as predominantly pure-shear domains that formed coevally with the high-strain zones.

The spatial association between ductile high-strain, earlier formed faults, carbonate altered rock, and gold occurrences suggests that each of the observed brittle-ductile deformation zones were conduits for locally mineralizing fluids during D_3 deformation. This is similar to the pattern of mineralization observed in the Val D'Or district of Quebec (Robert, 1994; Robert et al., 1995). Based on these results, higher-order structures to the north of the Main Break may undiscovered deposits in the Kirkland Lake area. Exploration by geophysics or drilling in these areas should target steeply-dipping, NE-trending deformation zones.

6.4 The Kirana deformation zone (Chapter 5)

The Kirana deformation zone (Kdz) is a gold-bearing, higher-order splay of the crustal-scale Larder Lake-Cadillac deformation zone (LLCdz) located in the Kirkland Lake area of Ontario (Chapter 4), which uniquely preserves structural relationships from early brittle fault behavior to later ductile and brittle deformation. The earliest structures are breccia domains and quartz-carbonate fault veins. Brecciated domains are well exposed at the Kirana East outcrop where chaotic breccia is present in the fault core and crackle breccia in the damage zone of the Kdz. Exploded 'jigsaw' textures are common, suggesting that the early development of the Kdz records dilational fault processes. Particle size distribution analysis of the breccia domains that

yielded relatively low D-values of 0.93-1.71, supporting the interpretation that they formed by a fluid-assisted, dilational origin. These results are consistent with an early history of 'implosion'-style brecciation along the Kdz, perhaps at a dilational jog or asperity. The dilational fracture networks are filled with quartz-rich material, suggesting that silica-rich fluids were coseismically emplaced during the early fault-slip events. However, no gold mineralization is documented in association with the breccia textures, potentially due to a lack of significant gold in the fault fluids at this time. After early fault development, widespread ductile shear at greenschist facies metamorphic conditions occurred along the Kdz. The ductile shear fabrics are characterized by subvertical dips, NE-trends, and dextral shear sense indicators on horizontal surfaces. These fabric relationships are interpreted to reflect NW-SE shortening and localized dextral transpressive strain. The sheared rocks are intensely carbonate altered and fabrics are defined by sericite- or chlorite-rich domains, suggesting they record syn-kinematic fluid infiltration. Native gold grains in the mylonitized fault core of the Kdz display textural relationships indicative of syn- to post-shear mineralization. The alteration assemblages and timing relationships recorded in the Kdz are similar to the Main Break to the south and other structurally-controlled deposits farther east along the LLCdz in Ontario and Quebec. The shear zones are crosscut by abundant small-scale faults and quartz-carbonate shear veins, indicating that a period of renewed brittle deformation followed ductile strain. These are associated with disseminated alteration halos of carbonate, albite, and sulfide minerals, indicating continued fluid flow during this phase of deformation. Mutually crosscutting vein sets are common and are interpreted to reflect cyclic emplacement driven by fault-valve behavior. Kinematic analysis of the shear veins indicates that they formed during NNW-SSE shortening, similar to the shortening direction during ductile deformation. Thus, this study constrains a series of progressive brittle-ductile deformation events, each of which facilitated further localization of strain and hydrothermal fluid flow. The early history of fault-related brecciation is interpreted to have played a major role in controlling the location of subsequent shear strain and gold mineralization. Thus, identification of such breccia zones may be used as an indicator for identification of prospective splays of crustal-scale faults in similar setting of all ages.

6.5 References

Ayer, J., Amelin, Y., Corfu, F., Kamo, S., Ketchum, J., Kwok, K., Trowell, N., 2002. Evolution of the southern Abitibi greenstone belt based on U-Pb geochronology: Autochthonous volcanic construction followed by plutonism, regional deformation and sedimentation. *Precambrian Research* 115, 63–95. doi:10.1016/S0301-9268(02)00006-2

- Davis, D.W., 2002. U-Pb geochronology of Archean metasedimentary rocks in the Pontiac and Abitibi subprovinces, Quebec, constraints on timing, provenance and regional tectonics. *Precambrian Research* 115, 97–117. doi:10.1016/S0301-9268(02)00007-4
- Griffin, W.L., Wang, X., Jackson, S.E., Pearson, N.J., O'Reilly, S.Y., Xu, X., Zhou, X., 2002. Zircon chemistry and magma mixing, SE China: in-situ analysis of Hf isotopes, Tonglu and Pingtan igneous complexes. *Lithos* 61, 237–269.
- Ispolatov, V., Lafrance, B., Dubé, B., Creaser, R., Hamilton, M., 2008. Geologic and structural setting of gold mineralization in the Kirkland Lake-Larder Lake gold belt, Ontario. *Economic Geology* 103, 1309–1340.
- Monecke, T., Mercier-Langevin, P., Dubé, B., Frieman, B.M., 2017. Geology of the Abitibi greenstone belt. *Reviews in Economic Geology* 19, 7–49.
- Robert, F., 1994. Vein fields in gold districts: The example of Val d'Or, southeastern Abitibi subprovince, Quebec. *Geological Survey of Canada Current Research 1994-C*, 295–302.
- Robert, F., Boullier, A.-M., Firdaous, K., 1995. Gold-quartz veins in metamorphic terranes and their bearing on the role of fluids in faulting. *Journal of Geophysical Research* 100, 12861–12879.

APPENDIX A

ADDITIONAL FIELD MAPS AND OBSERVATIONS

One additional compilation map, several new 1:500-1:2000 scale maps and field observations in the general area of Kirkland Lake, Ontario, Canada, and results of automated mineralogy scanning electron microscope analyses, not presented in the thesis are included below.

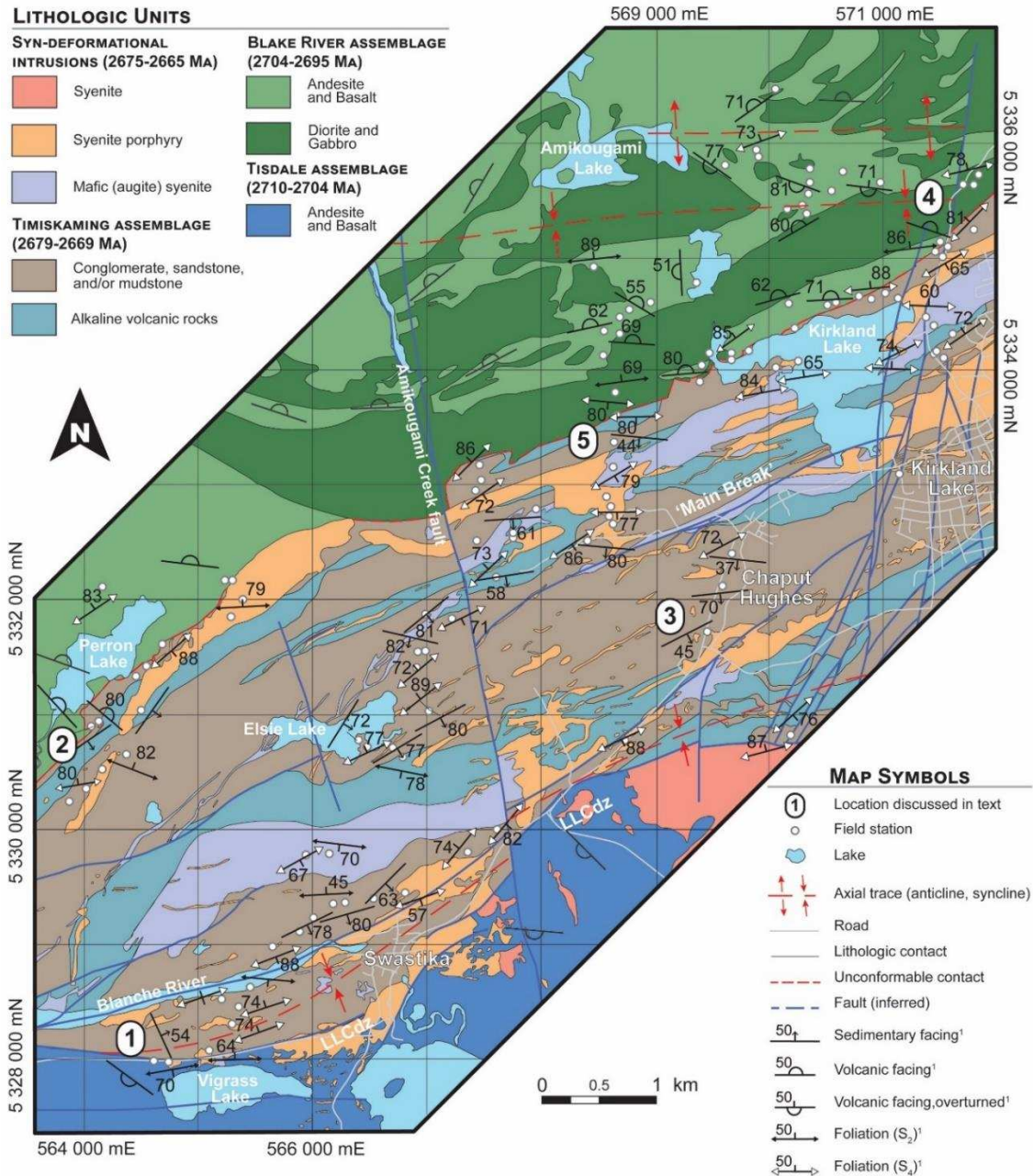


Figure A.1 – Geological map of the western Kirkland Lake area, Ontario (modified from Thomson, 1945).

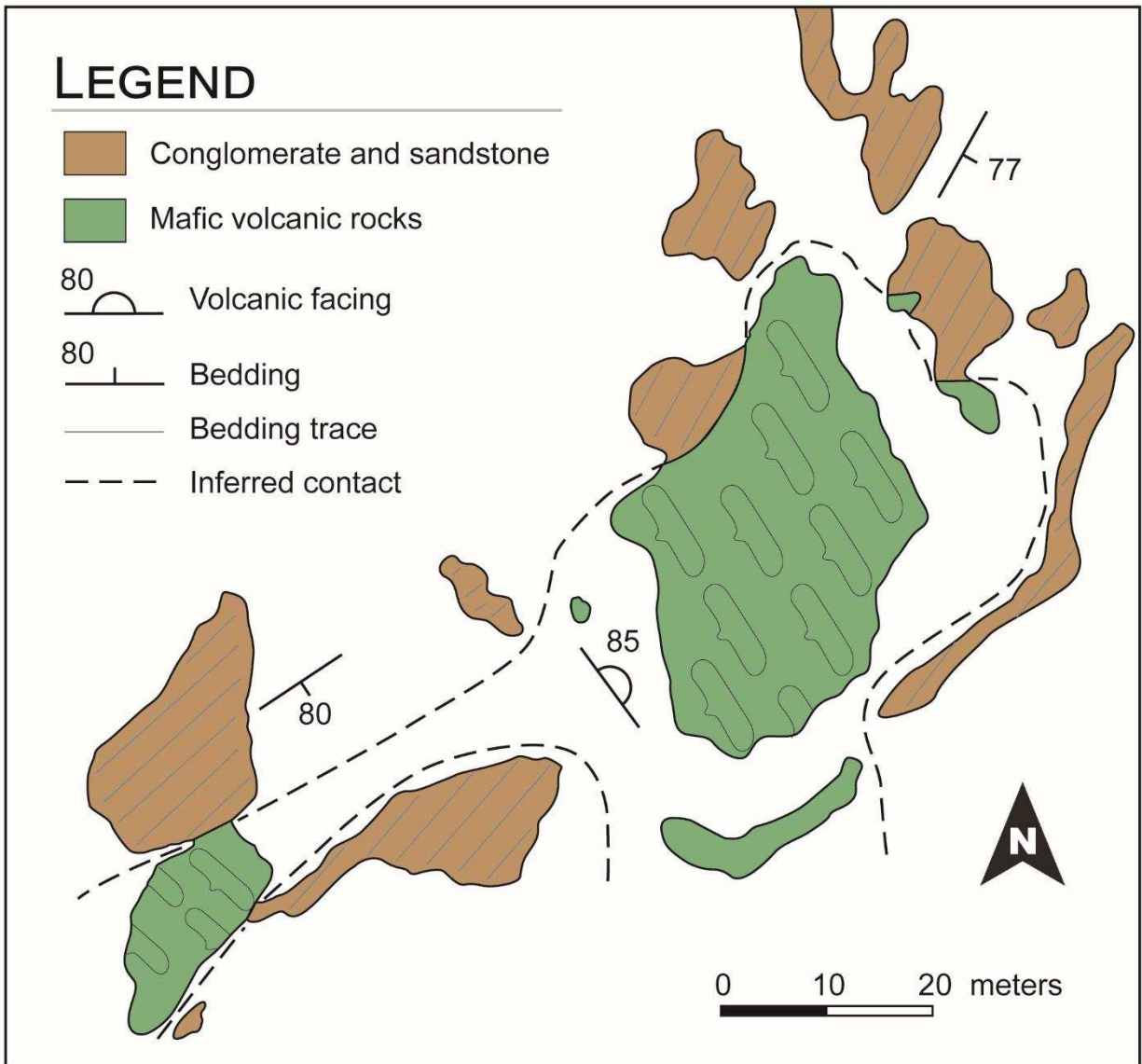


Figure A.2 – Geological map of the Blake River assemblage – Timiskaming assemblage Timiskaming unconformity at Perron Lake. The outcrop occurs ~7 km to the west of Kirkland Lake (location #2 in Fig. A.1; after Thomson, 1946).

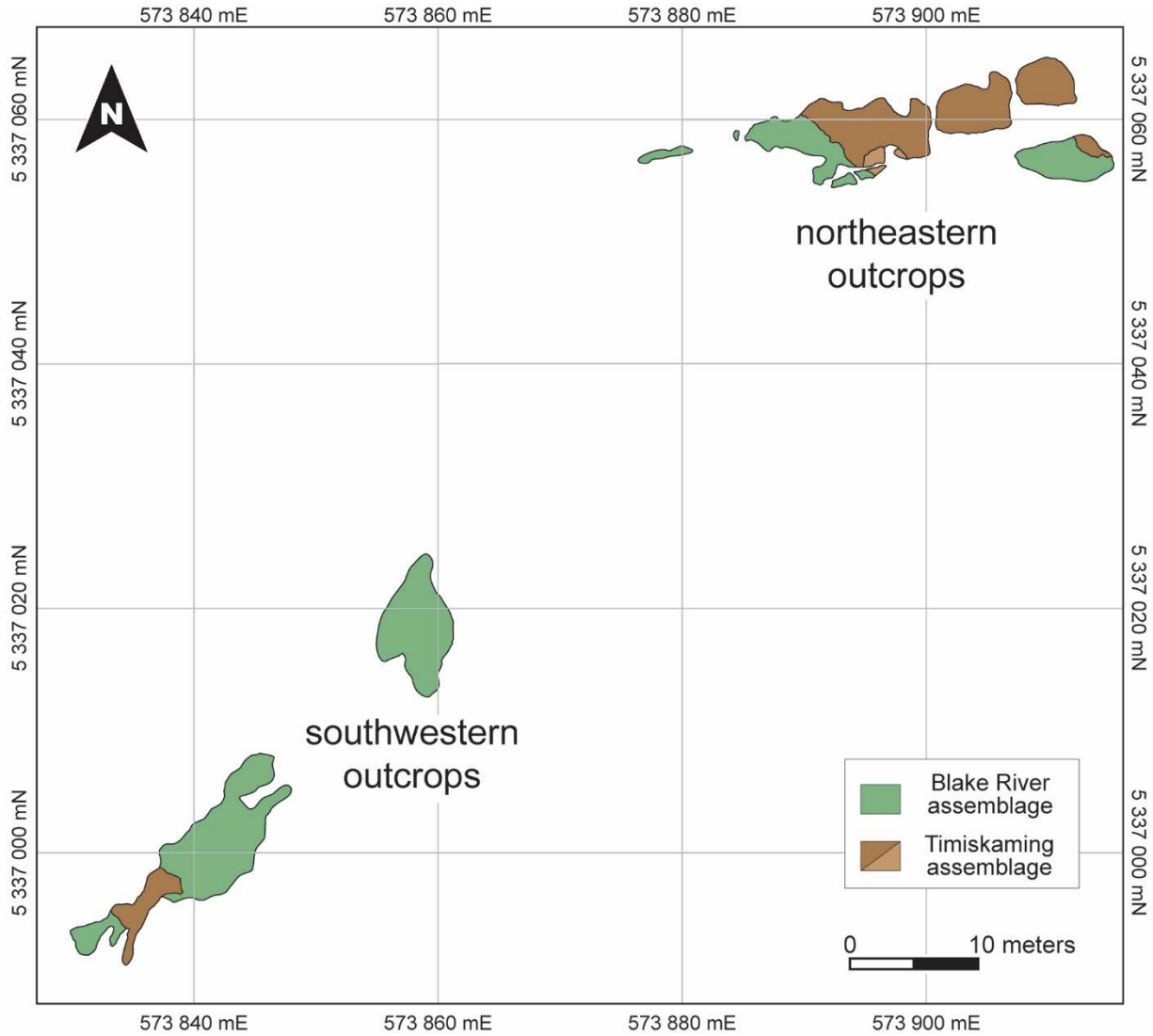


Figure A.3 – Distribution of outcrops associated with the Blake River assemblage – Timiskaming assemblage unconformity in the north of Kirkland Lake. The outcrops occur ~2 km to the north of Kirkland Lake. Northeastern and southwestern outcrops refer to detailed maps in Fig. A.4.

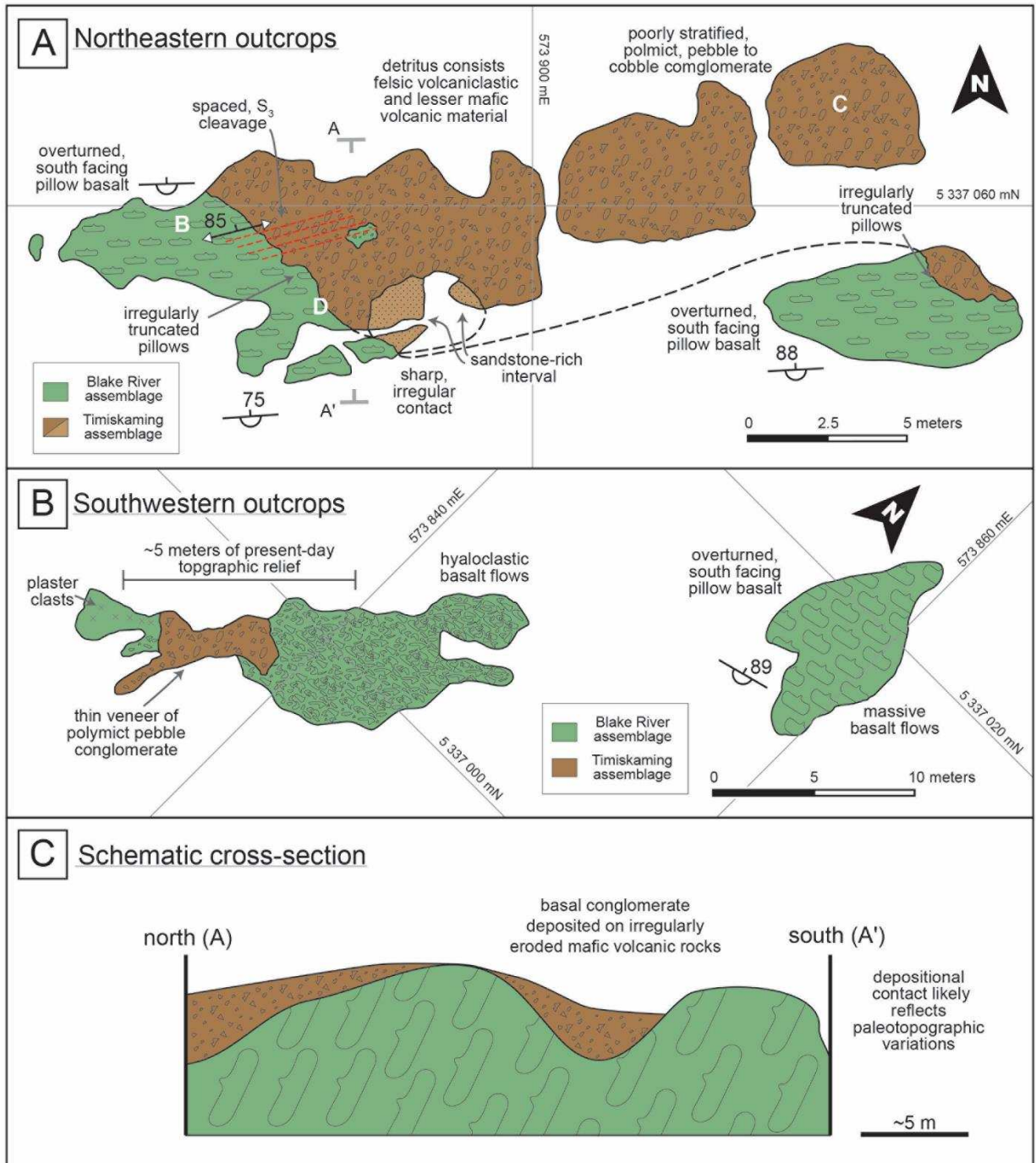


Figure A.4 – Results of the outcrop-scale mapping conducted at the Blake River assemblage – Timiskaming assemblage in the north of Kirkland Lake. The unconformity occurs ~2km to the north of Kirkland Lake near Doig Lake. Letters refer to the location of photographs shown in Fig. A.5.

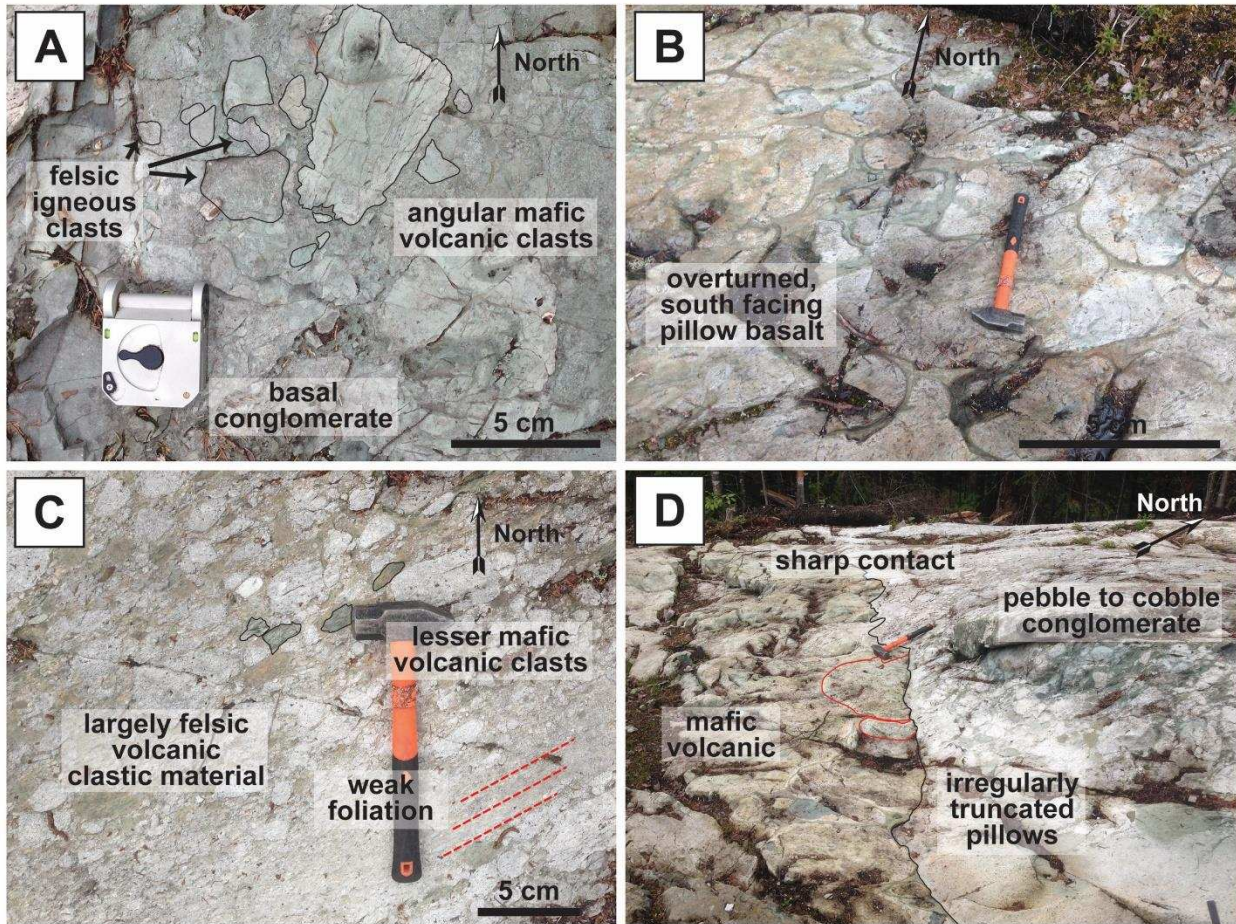


Figure A.5 – Field photos of the Blake River assemblage – Timiskaming assemblage unconformity in the north of Kirkland Lake. The unconformity occurs near Doig Lake ~2 km to the north of Kirkland Lake. The hammer is 38 cm in length. The location of the photographs displayed in B-D are shown in Fig. A.4A.

Phase	Breccia samples			Clast subdomains		Ultramylonite	
	15-61	KL-12	KL-28.2	15-61	KL-12	KL-17 (area 1)	KL-17 (area 2)
Albite	8.41	12.69	24.91	10.88	21.42	30.31	33.35
Apatite	0.01	0.01	-	0.07	0.02	0.03	-
Carbonate	4.45	21.03	15.62	6.48	3.52	5.54	2.99
Chalcopyrite	0.01	0.01	0.01	0.01	0.01	-	0.51
Chlorite	28.5	20.93	24.3	45.87	54.26	14.33	22.7
Kaolinite	2.03	1.78	4.89	2.92	6.06	3.38	4.51
Muscovite	0.24	0.42	0.28	0.39	1.21	1.29	1.99
Orthoclase	-	-	-	-	-	0.01	-
Plagioclase	0.02	0.03	0.12	0.02	0.03	0.05	0.09
Pyrite	0.07	0.33	0.27	0.01	-	0.04	-
Quartz	55.52	41.97	28.45	32.22	12.25	44.24	32.8
Sphalerite	-	-	-	-	-	-	0.22
Rutile	0.25	0.23	0.29	0.34	0.49	0.16	0.06
Other/ Unclassified	0.49	0.56	0.84	0.79	0.74	0.63	0.77
Total	100	100	100	100	100	100	100

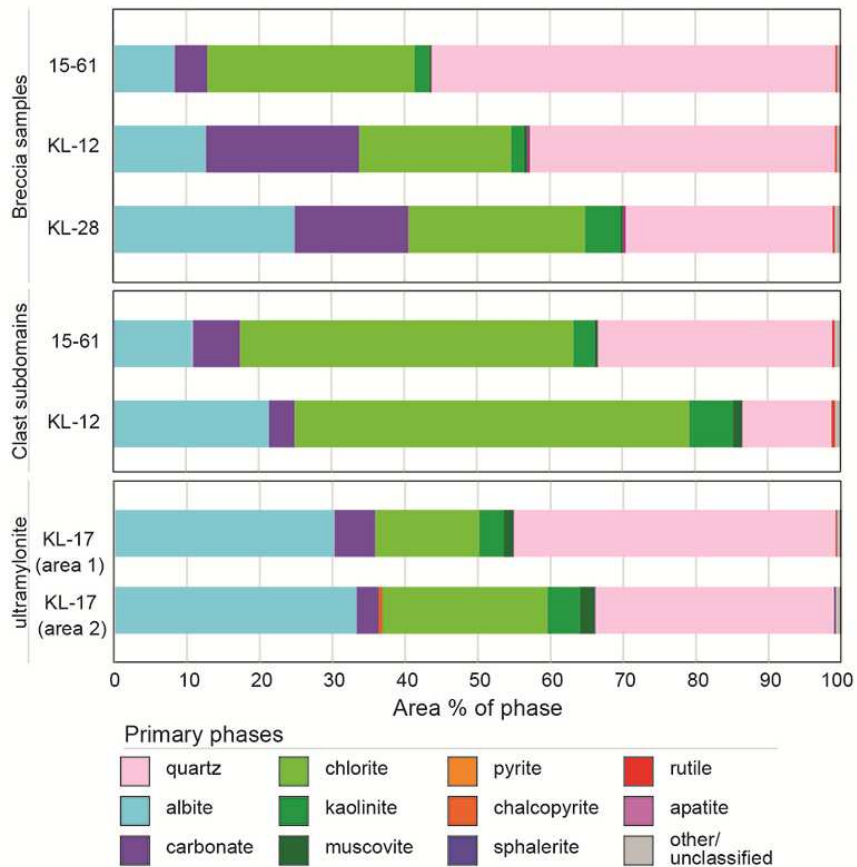


Figure A.6 – Modal mineralogy of Kirana East breccia samples. Results of automated mineralogy scanning electron microscopy of samples from the Kirana East outcrop (Chapter 5).

A.1 References

Thomson, J.E., 1945. Township of Teck, district of Timiskaming, Ontario. Ontario Department of Mines, Map No. 1945-1, scale 1:12,000.

Thomson, J.E., 1946. The Keewatin-Timiskaming unconformity in the Kirkland Lake district. Transactions of the Royal Society of Canada IV, 113–124.

APPENDIX B

SUPPLEMENTAL ELECTRONIC FILES

A list of the supplemental electronic material that supports the thesis work conducted in the south-central Abitibi subprovince is included below. The files include imagery of zircon grain mounts, compilations of previously published U-Pb zircon geochronology, data tables from the multi-isotope, U-Pb and Lu-Hf LA-ICP-MS analysis, structural orientation data, extended abstracts and posters presented at various conferences, and a copy Frieman et al. (2017) that contains a 1:10 000 map of the Kirkland Lake area of Ontario. The files are included either as zip, pdf, or excel files.

File Name	Content description
Table LA-ICP-MS U-Pb data.xlsx	Excel spreadsheet of U-Pb LA-ICP-MS data (Chapter 2)
Table Detrital Hf data.xlsx	Excel spreadsheet of Lu-Hf LA-ICP-MS data (Chapter 3)
Zircon Imagery and Extra Plots.zip	Optical and SEM images of zircon grains (Chapters 2 and 3)
Tables of Compiled U-Pb Zircon.zip	Zip file of compiled zircon geochronology (Chapter 2)
Frieman_Structure Data_2014-15.xlsx	Excel spreadsheet of structural orientation data (Chapters 4 and 5)
Abstracts and Posters.zip	Zip file containing extended abstracts and posters
Frieman et al., 2017; GSC of_8245.pdf	GSC report containing a 1:10 000 scale map of the Kirkland Lake area of Ontario, Canada (Chapters 4 and 5)

B.1 References

Frieman, B.M., Kuiper, Y.D., Monecke, T., Kelly, N.M., 2017. Precambrian geology and new structural data, Kirkland Lake area, Ontario. Geological Survey of Canada, Open File 8245, 8 p. <https://doi.org/10.4095/304206>